Enhancing Chemical and Biochemical Transformations in Dynamic Thin Films Under Flow

by

Jessica M. Phillips

Thesis
Submitted to Flinders University
for the degree of

Doctor of Philosophy in Chemistry

College of Science and Engineering

Febuary 2021

Table of Contents

Abstract

There have been significant efforts into improving efficiency, reducing waste and enhancing quality and control in the research and manufacturing of active pharmaceutical ingredients (APIs), natural products, value-added chemicals, and materials, in order to reduce costs while increasing the sustainability of the manufacturing processes.

Recently, applying continuous-flow technologies to the synthesis of valuable compounds has become widespread, particularly in academia. Although the pharmaceutical industry still heavily relies on multipurpose batch or semi-batch reactors, interest is rising towards continuous flow production of synthetic molecules, including highly functionalised and chiral compounds. Furthermore, the industry has typically focused on classical synthetic chemistry and small molecules. However, in recent decades there has been a move towards incorporating bioprocesses and biotechnology for organic synthesis and for the creation of biological agents for therapeutic purposes.

This dissertation focuses on the use of continuous-flow and microfluidics for the improvement of chemical and biochemical processes in the vortex fluidic device (VFD). First, PdNPs were immobilised within cellulose paper using a fast and effective reduction of palladium acetate with hydrogen gas after 90 seconds. The Pd-cellulose catalyst was applied in the VFD for scalable and efficient continuous flow hydrogenation reactions at ambient temperature and pressure. High catalyst stability and re-usability is demonstrated along with the chemoselective and scalable synthesis of industrially important fine chemicals.

The research was extended further to the rapid covalent immobilisation of enzymes through APTES-gluteraldehyde functionalization of cellulose paper. The stable and re-usable

enzyme-cellulose catalyst can be easily and efficiently used in the VFD for continuous-flow biocatalysis with comparable rates to batch. The method was further applied to the continuous-flow synthesis of a valuable chiral terpene, aristolochene, through the immobilisation of aristolochene synthase from *Aspergillus terreus*.

Immobilisation of biomolecules were explored for applications beyond biocatalysis. A bladder cancer biomarker, DJ-1, was immobilised onto nickel affinity resin through a fused histidine-tag, coating the inner surface of the VFD tube, for continuous-flow phage-displayed antibody fragment and peptide selections. Using this system, Fab and peptide binders were isolated for high affinity and specificity for DJ-1, from two highly diverse libraries.

The mechanical energy of the VFD was further explored for accelerating enzymatic catalysis of protenaise K in extracting DNA from formalin-fixed American lobster tissue. Through optimization, the optimal VFD rotational speed was identified for recovery of PCR-amplified DNA; 500+ base pairs were sequenced from the organism, with shorter amplicon lengths more consistently obtained.

Overall the work has established methods for employing catalysis, biocatalysis, immobilisation, and biotechnology in thin-films in the VFD for process enhancement for chemical and biochemical applications.

Declaration

I certify that this thesis does not incorporate without acknowledgment any material previously submitted for a degree or diploma in any university; and that to the best of my knowledge and belief it does not contain any material previously published or written by another person except where due reference is made in the text.

This thesis contains published work, some of which has been co-authored. The details of the work and where it appears in the thesis are outlined below.

Chapter 2 - **Phillips, J. M.,** Ahamed, M., Duan, X., Lamb, R. N., Qu, X., Zheng, K., Zou, J., Chalker, J. M., Raston, C.L. Chemoselective and continuous flow hydrogenations in thin film using a palladium nanoparticle catalyst embedded in cellulose paper. *ACS Appl. Bio Mater*., **2019**, *2*, 488– 494.
Author Contributions: JMP, JMC and CLR designed the research, JMP undertook all the research, XD undertook XPS analysis, XQ and KZ undertook HRTEM analysis, JMP, MA, XD, JZ, JMC, CLR finalised the manuscript.

Chapter 5 - Totoiu, C. A., **Phillips**, **J. M.,** Reese, A. T., Majumdar, S., Girguis, P. R., Raston, L., Weiss, G. A. Vortex fluidics-mediated DNA rescue from formalin-fixed museum specimens. *PLoS ONE*, **2020**, *15*(1).
Author Contributions: CAT, JMP and GAW designed the research, CAT and JMP undertook all the research, CAT, JMP, SM, ATR, PRG, CLR, and GAW finalised the manuscript. The chapter was re-written by JMP.

_____

Jessica M. Phillips

Date: _____

Acknowledgement

It is a very exciting moment when it comes to writing this part of my dissertation. To me, it is a symbolic moment that my PhD journey has come to an end and I am ready to begin a whole new chapter of my life. I would like to take this opportunity to acknowledge and express my sincere gratitude to all of those who helped and supported me physically or mentally, towards the completion of my research throughout the years.

I am truly grateful to have Prof. Colin L. Raston as my supervisor. From the time he agreed to take me as his student and throughout my three and a half years PhD, he has provided me with invaluable guidance and support. I appreciate the confidence he has had in me and his willingness to share his wisdom. It has inspired me to keep going. There are no words that could fully express my deepest respect and gratitude to Prof. Colin L. Raston.

Thank you to Prof. Gregory Weiss for giving me the amazing opportunity to visit and work in his laboratory at UCI. I learnt so many valuable skills and lessons under his supervision, which was invaluable. His guidance and belief in me has allowed me to gain confidence in my ability as a scientist. Thank you to Dr. Sudipta Majumdar. I consider him one of my greatest mentors. I have learnt so much from him, and am so grateful for his patience, guidance and belief in me also, Thank you!

My research would not be successful without the generous help and support of all collaborators. Thank you to Christian Totoiu, my main collaborator in the DNA extraction research and the person who first helped me intergrate into the Weiss lab. Thank you to Emily Sanders and Alicia Santos for your support with phage display and selections. Thank you to Dr. Xiaofei Duan and Prof. Robert N. Lamb for XPS analysis, and Xianlin Qu, Kun Zheng, Jin Zou for HRTEM analysis. I thank all my colleagues in the Raston research group and the Weiss research group for being great support.

I would like to acknowledge my funding sources, which allowed me to focus solelyon my research without financial pressure. I was awarded the Flinders University Research Scholarship (FURS), now the Research Training Program (RTP) scholarship, which provided a stipend and full tuition waiver for my 3.5 years candidature.

Thank you to my fiancé, Clinton Kalweit, for mentally supporting me through out my PhD experience and for making it through our time apart while I was conducting my 12 months of research in California. Thank you to my best friends and roommates, Diandra Sferruzzi and Nick Langley, for taking us in and allowing us a place to live during my travels to and from the US. It has made the last 1.5 years so much easier on us. Lastly, my deepest gratitude to my family, Mum and Dad, you have raised me with love and support to be strong and independent. I am proud to say I have amazing parents and I love you both so much.

I may have missed out some names, once again, thank you everyone. I truly appreciated the opportunity to experience this enriching PhD journey.

Jessica M. Phillips
Flinders University
March 2020

List of Publications

1. **Phillips, J. M**., Ahamed, M., Duan, X., Lamb, R. N., Qu, X., Zheng, K., Zou, J., Chalker, J. M., Raston, C.L. Chemoselective and continuous flow hydrogenations in thin film using a palladium nanoparticle catalyst embedded in cellulose paper, *ACS Appl. Bio Mater*., **2019**, *2*, 488–494.

2. Totoiu, C. A., **Phillips**, **J. M.,** Reese, A. T., Majumdar, S., Girguis, P. R., Raston, C. L., Weiss, G. A. Vortex fluidics-mediated DNA rescue from formalin-fixed museum specimens. *PLoS ONE*, **2020**, *15*(1).

List of Figures

List of Tables

List of Acronyms

2YT	2 x yeast extract
ADS	Amorpha-4,11-diene synthase
AP	Alkaline phosphatase
AS	Aristolochene synthase
API	Active pharmaceutical ingredient
APTES	(Aminopropyl)triethoxylsilane
BME	*beta*-mercaptoethanol
BSA	Bovine serum albumin
CD	Circular dichroism
CDR	Complementarity-determining region
CFU	Colony-forming units
CH1	Heavy chain constant region 1
CL	Light chain constant region
DJ-1	Protein deglycase 1
DCM	Dichloromethane
DNA	deoxyribonucleic acid
dATP	Deoxyadenosine triphosphate
ddH_2O	Milli-Q purified water
dNTP	Deoxynucleoside triphosphate
dsDNA	double stranded DNA
DTT	Dithiothreitol
E. coli	*Escherichia coli*
EDX	Energy-dispersive X-ray
EDTA	Ethylenediaminetetraacetic acid
eGFP	Green fluorescent protein
ELISA	Enzyme-linked immunosorbent assay
Fab	Antigen-binding region
FTIR	Fourier-transform infrared spectroscopy
GC	Gas chromatography
HEWL	Hen egg white lysozyme
HG	Hemoglobin

HSA	Human serum albumin
HRTEM	High resolution transmission electron microscopy
ICP-MS	Inductively coupled plasma mass spectrometry
IDA	Iminodiacetic acid
IMAC	Immobilized metal affinity chromatography
IPTG	Isopropyl B-D-1-thiogalactopyranoside
kDa	Kilodaltons
LB	Lysogeny broth
LIC	Ligation independant cloning
MeOH	Methanol
MOI	Multiplicity of infection
MRPL	Mega random peptide library
MS	Mass spectrometry
Ni	Nickel
NPs	Nanoparticles
NEB	New England Biolabs
NMR	Nuclear magnetic resonance
NTA	Nitrilotriacetic acid
NMP22	Nuclear matrix protein 22
P3	Major coat protein 3
P8	Major coat protein 8
Pd	Palladium
PBS	Phosphate buffered saline
PBS-T	PBS + 0.05 % Tween 20
PCR	Polymerase chain reaction
PEG	Polyethylene glycol
PAGE	Polyacrylamide gel electrophoresis
PNPP	*para*-Nitrophenol phosphate
ProK	Proteinase K
Pd(OAc)2	Palladium acetate
qPCR	quantitative PCR
rpm	Revolutions per minute
RT	Room temperature

SDS	Sodium dodecyl sulphate
SEC	Size-exclusion chromatography
SEM	Scanning electron microscopy
TMB	1,3,5-trimethylbenzene
tNMP22	truncated NMP22
Tris	Trisaminomethane
TSE	Tris-Sucrose-EDTA
UV-Vis	Ultraviolet-visible spectroscopy
VFD	Vortex fluidic device
VH	Heavy chain variable region
VL	Light chain variable region
XPS	X-ray photoelectron spectroscopy
XRD	X-ray diffraction

Chapter 1: Introduction

1.1. Improved Methodology for Pharmaceutical and Value-Added Compounds

There have been significant efforts into improving efficiency, reducing waste and enhancing quality and control in the research and manufacturing of active pharmaceutical ingredients (APIs), natural products, value-added chemicals, and materials, in order to reduce costs while increasing the sustainability of the manufacturing processes [1].

APIs are typically structurally complex organic molecules that have precise arrangements of chemical groups [2]. They are produced using sequences of organic reactions, commonly six to ten chemical steps, that increase in complexity, starting with commercially available materials [2]. Each step is commonly run in a separate batch reactor where each step requires specific operations: combining reagents under certain conditions, to quench the reaction, and separate, isolate and purify compounds formed at intermediate stages. These complex syntheses often involve highly hazardous reactions such as exothermic reactions, reactions that require the use of high temperatures and pressures, and hazardous or toxic reagents or intermediates [3]. It is reported that the pharmaceutical industry produces approximately 25-100kg of waste for every one kg of product in a synthesis involving 6-8 steps, significantly more than other chemical industries [1]. Therefore, there is great need for pharmaceutical manufacturers to move towards greener methods, to use less toxic reagents and solvents, and to minimise the waste generated. This has the added benefit of reducing costs, including the cost of energy usage.

The application of technology, such as catalysis, biocatalysis, and continuous-flow has been an increasing interest for more sustainable, efficient, economical and safer processing

(Figure 1.1). Recently, the growth in continuous-flow technologies to the synthesis of valuable compounds has become widespread, particularly in academia. Although the pharmaceutical industry still heavily relies on batch or semi-batch reactors, much industry is moving towards continuous flow manufacturing of synthetic molecules, including highly functionalised and chiral compounds, and natural products [4]. Furthermore, the industry has typically focused on classical synthetic chemistry and small molecules. However, in recent decades there has been a move towards incorporating bioprocesses and biotechnology for the organic synthesis and for the creation of biological agents for therapeutical purposes [5, 6]. However, for the growth of continuous flow technologies to continue there needs to be further enhancement and further development, as will be discussed in this chapter.

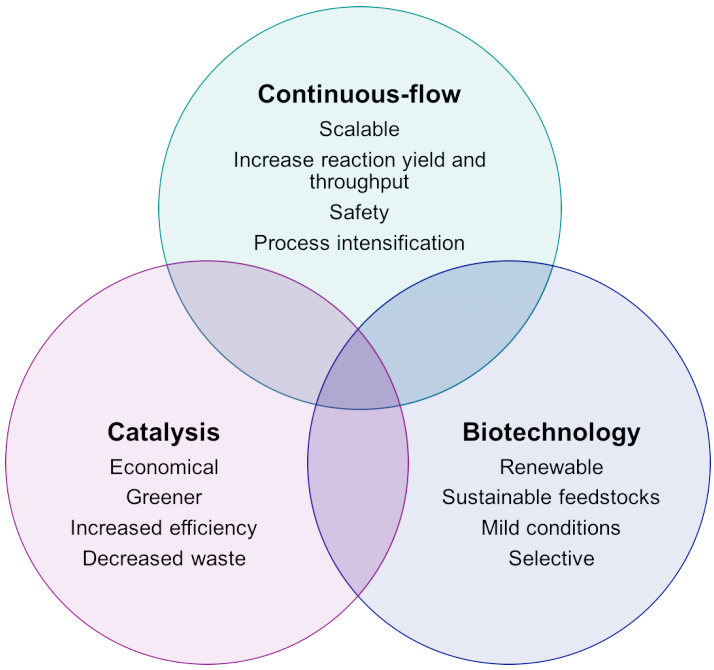

Figure 1.1. Improving chemical processes by incorporating and improving upon catalysis, continuous-flow, and biotechnology.

1.2. Continuous-Flow Technology

The rapid progress of continuous-flow techniques allows for the scalable continuous-preparation of complex materials, such as fine chemicals, APIs, natural products, agrochemicals, polymers, and controlled nanomaterials. Continuous-flow processing is typically performed within microfluidic devices. Microfluidic devices can be divided into chip based, tubular or centrifugal micro-reactors. This technology has many advantages, and as a result its application has dramatically grown in academia and manufacturing industries.

The high surface to volume ratio within channel based micro-reactors offers for the rapid change in reaction temperatures through the application or removal of heat [7]. This allows for the use of novel thermal systems not accessible using conventional batch apparatus. The low reaction volumes within these systems is advantageous, in respect to both reaction safety, and also in allowing for accurate reaction parameter control, which can afford an abundance of information from small quantities of reagents and catalysts. These metrics also allow for reduced reaction time, enhanced chemical selectivity and yields [8]. Further benefits in terms of green chemistry metrics include reduced solvent waste, energy saving, improved atom efficiency, as a result of precise reaction control, and the ability to incorporate in-line analysis to monitor a reaction more thoroughly, and just in time production, avoiding the storage of large volumes of product [9, 10].

The construction of these continuous flow reactors is often modular and are assembled from several specialised yet easily integrated components for accompanying operations such as micro-mixing, heating and cooling, extraction, separation, pervaporation, in-line concentration, solid handling, and crystallization [10]. This allows for simple automation and continuous operation, as well as enables chemists to perform potentially hazardous and otherwise forbidden reactions in a safer and more reliable manner. Continuous-flow technology

also allows for the easy integration of light sources such light-emitting diodes (LED), continuous fluorescence lamps and powerful UV lamps, for performing photochemical reactions. Organic photochemistry is a powerful tool that generate molecules with high structural complexity, simplicity, sustainably, and under mild conditions [11, 12]. Continuous-flow allows for efficient and uniform radiation in a thin film or narrow channel, scale-up without alterations to reaction parameters and short residency times, meaning less time for decomposition of reaction components due to over-radiation.

Continuous flow processing platforms permit in-line analysis and data generation. The ability to monitor a reaction using in-line spectroscopic techniques can allow analysis of product composition and identity in real time [13]. Real time data generation increases throughput and efficiency, with fewer modifications required, reduced costs, and reduced potential for exposure or release of toxic or hazardous materials to the environment [10]. Furthermore, large utilisation of process analytical technology ensures product quality and reduces the burden for final produce testing.

Continuous-flow allows for the use of multiple systems in parallel, termed numbering-up or scaling out. This removes the financial risk associated with failing to scale a process due to changes that can occur in the thermal and mass transportation properties of a reactor or its inability to conduct the reaction safely [14]. Multiple-step continuous-flow platforms are essentially multiple reactors connected to create a single flow sequence. Utilising multi-step continuous-flow synthesis of APIs, natural products, and commodity chemicals is growing in interest, however there are few examples generated as such under continuous-flow.

Several reviews have been published on examples of continuous-flow synthesis of APIs [1, 14-18]. Some of the seminal advancements that have occurred in recent years include the synthesis of ibuprofen by McQuade and co-workers, where three difficult transformations were incorporated into a single flow system, yielding ibuprofen in 51% yield, for a residency time

of 10 minutes at 9mg/min [19]. In 2015 the Jamison group improved this synthesis by removing triflic acid from the process, which provided a more economical oxidative rearrangement. This synthesis of ibuprofen afforded 83 % yield at 8.09 g/h and required only 3 minutes of residency time (Figure 1.2A) [20]. In this synthesis, it is important to note some features which highlight the advantage of using continuous-flow. Firstly, the reactor coil used is constructed from affordable components, which provided an economical alternative to the expensive commercially available continuous-flow reactors. Secondly, soluble metal salts were removed *in-situ* by feeding the continuous-flow stream through a Zaiput membrane separator, which prepared the intermediate for subsequent steps.

The synthesis of artemisinin, a valuable API used for antimalarial treatment, was also translated into continuous-flow for the purpose of reaction scale-up and on demand compound production (Figure 1.2B) [21, 22]. The complexity of this molecule meant there was no commercially viable route to the scale up. In addition, performing this synthesis in continuous-flow allowed for the efficient and safe generation of singlet oxygen, a highly reactive species, crucial in the synthesis of artemisinin from dihydroartemisinic acid. This was achieved via a photochemical *ene* reaction, using 60 high-powered LEDs to create a high proton flux. This represents another important advantage of synthesis in continuous-flow, notably the high surface to volume ratio of liquid traveling through the system which allows for more uniform light exposure and penetration, unlike in a round bottom flask. This system resulted in the production of artemisinin in 65% yield and 97% conversion, at 8.33g/h, with a residency time of 11.5 minutes.

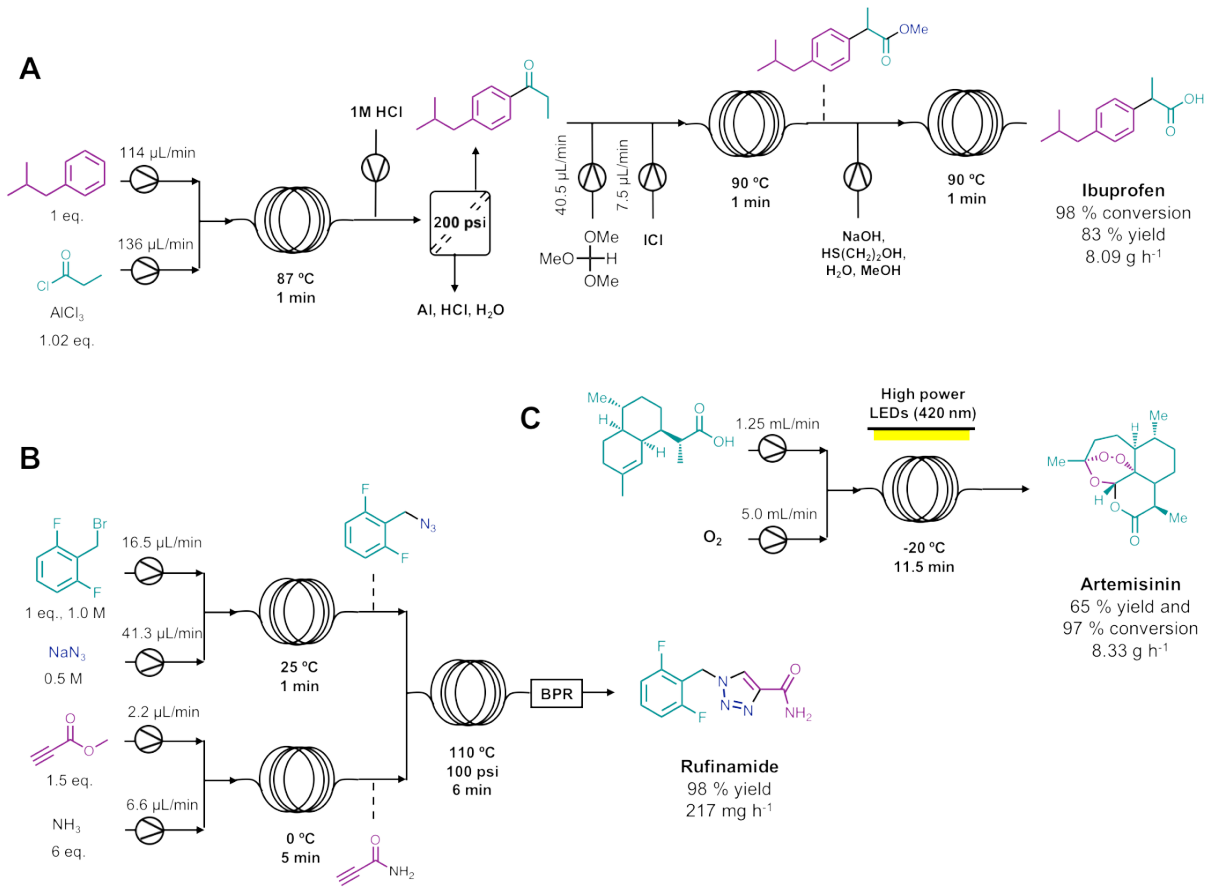

Figure 1.2. The continuous-flow syntheses of ibuprofen, artemisinin and rufinamide. (A) Ibuprofen was synthesized by Friedel–Crafts acylation, followed by a 1,2-aryl oxidative migration, and saponification. A membrane separator was used for in-line work-up and the need for triflic acid was avoided. This system resulted in a yield of 83% with an overall reactor throughput of 8.09g/h [20]. (B) Artemisinin was synthesized from dihydroartemisinic by a photochemical *ene* reaction using singlet oxygen, resulting in a 97% and 65% conversion and yield, respectively, at 8.33g/h [21]. (C) Rufinamide was synthesized using a three-step sequence, first azide and amide intermediates are generated in separate reactor coils, followed by a azide-alkyne cycloaddition, with an overall yield of 92% [24].

Jamison and colleagues reported on the continuous-flow synthesis of the antiepileptic API, rufinamide (Figure 1.2C) [23]. The reaction involved the S_N2 substitution of 2,6-difluorobenzyl bromide with sodium azide in one reaction coil, and the amidation of methyl

propiolate with an aqueous ammonium solution in another reaction coil, cooled to 0°C. As demonstrated in this case, the application of continuous-flow can be used to minimize the hazardous handling of organic azides, which can be prone to detonation upon exposure to slight heat, pressure or light. Following this, the two reaction streams were mixed and heated to 110°C in a copper reactor maintained at 100psi using a back pressure regulator. After 6 min residence time, rufinamide was obtained with an overall yield of 92%, with a productivity of 217mg h^{-1}. This type of copper coil has been applied to a variety of other chemical transformations, including macrocyclisation of linear peptoids, Ullman reactions, Pd-free Sonogashira couplings, and decarboxylation reactions [24].

Continuous-flow chemistry has developed from an innovative synthesis concept for improving chemical synthesis to a powerful and widely applicable tool that can enable the efficient multistep synthesis of many APIs. Current evaluations suggest an increase in the industrial application of continuous-flow manufacturing of pharmaceutical ingredients of 5 to 30% over the next years [22].

Although there are numerous advantages to continuous flow processing, it presents disadvantages relative to batch processing. For the average laboratory, batch processing is easy to set-up and run quickly, which can be important for early stage drug development. Batch processing provides the necessary few grams to kilograms of an API for initial animal studies and pre-clinical trials, however presents a disadvantages when metric tons are required in future manufacturing requirements. Furthermore, integrating continuous flow systems can be a higher investment for production facilities and tight controls on input quality often requires increased analytical support. Inline precipitation can also pose a problem in conventional continuous flow processing.

Other drawbacks exist when incorporating in-line catalysts, including catalyst fouling, which can reduce the reliability of the process through inconsistencies and impurities. It is clear

that in order for the growth to continue there needs to be further enhancement and further development in continuous flow technologies and the need for easy and economical access and integration of these technologies.

1.2.1. Catalyst Immobilisation

The replacement of stoichiometric reagents for synthetic transformation by catalytic routes is an integral part of the movement towards the development of safer, greener and more economic chemical processes [25]. Chemical catalysts and biocatalysts are essential in improving reaction efficiency and reaction conditions, increasing productivity and yield, and achieving the necessary stereoselectivity. Over the years, several methods have been developed for the immobilising catalysts onto solid supports, generally based on adsorption, encapsulation, covalent or ionic bonding, (Figure 1.3) [26].

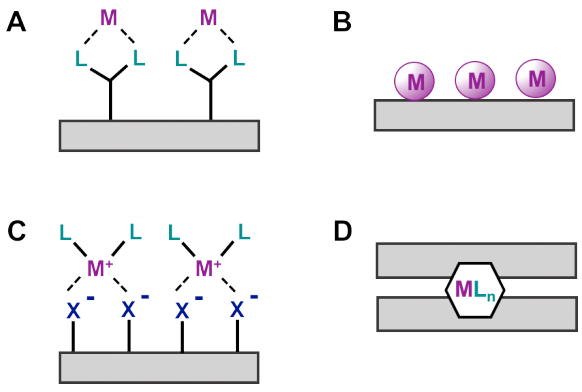

Figure 1.3. Most common immobilisation techniques for metal catalysts. (A) Covalent bonding, (B) adsorption, (C) ionic bonding, and (D) encapsulation [26]. M = metal, L = ligand, X^- = surface ion.

Companies, contract manufacturers, and other researchers are progressing this area for producing fine-chemicals, pharmaceutical intermediates and APIs [25]. However, the discovery, development and implementation of new scalable catalytic methodologies suitable for complex pharmaceutical intermediates poses a synthetic chemical challenge [27].

1.2.2. Catalysis in Continuous-Flow

Combining continuous-flow micro-reactors and heterogeneous catalysis permits cleaner, safer, and scalable methods for carrying out a variety of catalytic reactions sustainably [28]. One of the major features of micro-reactors that benefits heterogeneous catalysis is the high surface area-to-volume ratio, which is significantly larger then in traditional chemical reactors. The large interfacial area between different phases, such as liquid-liquid, gas-liquid, and gas-liquid-solid, is achieved. This combined with additional features of microfluidic reactors, such as improved heat and mass transfer properties, allows for higher efficiency, safety and selectivity in heterogeneous catalysis.

Heterogeneous catalysts in microfluidic devices are most commonly carried out using; (a) Packed-bed micro-reactors, where the catalyst is tethered to a solid support material, either polymeric or inorganic, randomly assembled within a device; (b) monolithic, which consists of network of meso- and microporous channels obtained from the copolymerisation of the catalysts and another monomer inside the device; and (c) wall-coated, where the catalyst is immobilised into the inner walls of a reactor (Figure 1.4) [28, 29].

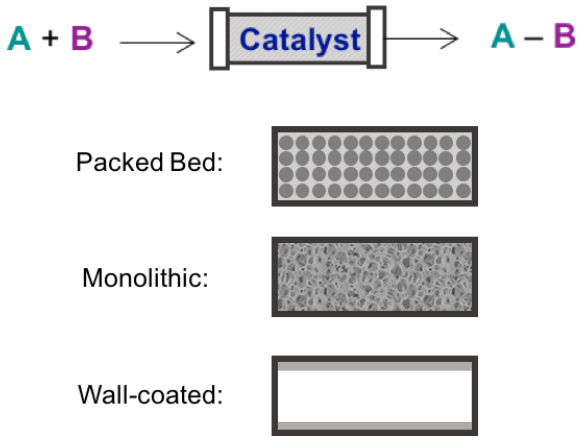

Figure 1.4. Schematic representation of the common types of immobilised catalysts used in continuous-flow.

Metal, organometallic, organic, and enzymatic catalysts can be immobilised, for use in packed bed reactors, onto either polymeric, commercially available resins or custom made polymers, or inorganic materials, such as silica, alumina, Fe_2O_3, zeolite or ceria. This approach allows for high catalyst loading, relatively easy characterization and quantification, and easy fabrication of the catalytic device by filling the channels with the catalytic material [30]. Alternatively, monolithic micro-reactors are constructed with polymeric or inorganic networks of meso- and microporous channels obtained from the copolymerisation of the catalysts and another monomer inside the device [31, 32]. These reactors have several advantages over conventional packed bed reactors, including a tolerance for higher flow rates, efficient mass transfer through the pores, allowing higher back pressures and productivity. However, there are drawbacks which include pore clogging, non-uniformity of radical permeability, and reduced access of the catalytic sites. The third most common reactor type, wall-coated micro-reactors, substantially minimise mass transfer resistance, and does not lead to pressure drops blockages of micro-channels [33, 34]. Despite this, catalyst loadings are lower compared to packed bed and monolithic approaches.

Kobayashi and colleagues reported the first example of a fully continuous synthesis of an API using only immobilised catalysts [27]. Both enantiomers of Rolipram were synthesised in 50 % yield and high enantiomeric excess (>99%) at 42mg/h, using a system comprised of four columns packed with specific heterogeneous catalysts (Figure 1.5). Initially, they applied a silica-supported amine to catalyse the nitroaldol reaction of aldehyde and nitromethane. The resulting nitroalkene was mixed with malonate, followed by removal of water by passing the solution through molecular sieves in a packed bed. A small reactor coil is then applied to precool the solution before feeding into two columns containing a chiral calcium catalyst, previously developed my Kobayashi and co-workers. This catalyst comprised of a chiral pybox ligand immobilised on polystyrene and mixed with $CaCl_2.2H_2O$ and celite. This catalyst achieved an asymmetric Michael-type addition. Following this, the hydrogenation of the nitro group was achieved over a palladium catalyst supported on carbon and polysilane (Pd@DMPSi-C) resulted in the ©-lactam. After separation of the excess H_2 in a receiving unit, the crude mixture was combined with water and *o*-xylene in a packed bed of celite. Lastly, the ©-lactam underwent hydrolysis and decarboxylation using a silica-supported carboxylic acid catalyst in a packed bed reactor, to produce (*S*)-rolipram. Furthermore, switching the second packed column with the opposite enantiomer catalysts resulted in the opposite enantiomer of rolipram. This modular and flexible synthesis was demonstrated on a laboratory scale, producing gram quantities of the drug per day and demonstrated stable operation for at least a week. Furthermore, chiral metal complexes or enzymes are particularly important due to the demand for enantio-pure intermediates in the fine chemical and pharmaceutical industries [35]. Therefore, simple asymmetric processes which can be scaled up, are stable, recyclable and are not too costly, are required [36]. This can be achieved by the immobilisation of effective and robust catalytic systems in continuous flow reactors [37]. Several reviews exist on continuous-flow synthesis using heterogeneous catalysts [28, 32, 38, 39].

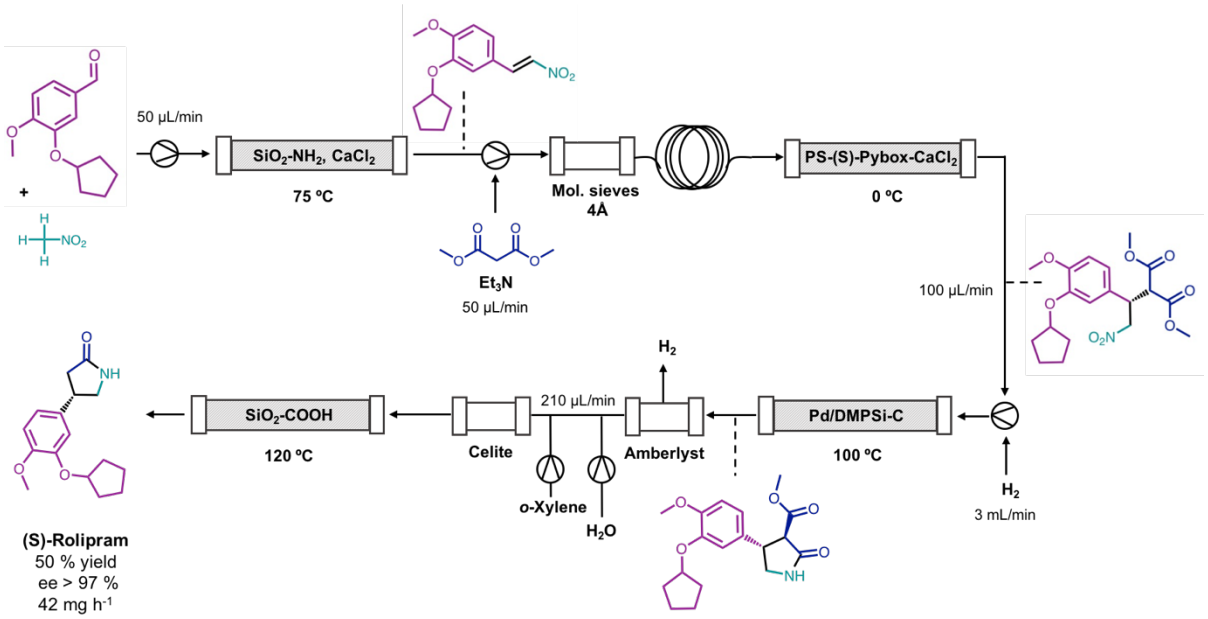

Figure 1.5. Continuous-flow synthesis of (S)-Rolipram. Each step of the synthesis; condensation and dehydration, stereoselective Michael addition, hydrogenation, and hydrolysis and decarboxylation; are performed using four packed bed reactors each containing a heterogeneous catalyst. Both enantiomers can be synthesised by switching the enantiomer of the heterogeneous catalyst used [27].

1.2.3. Immobilisation of Biocatalysts

Biocatalysis is a powerful tool for constructing complex molecules. Enzymes offer an attractive advantage over traditional small molecule catalysts, such as high selectivity, low catalysts loadings, and the ability to optimise their performance through protein engineering [40]. A number of enzyme-based processes have been commercialised for production of valuable products since biocatalysis was introduced [41, 42].

Biocatalytic reactions can be performed using enzymes in whole cells or purified. Whole-cell enzymes have advantages including reduced cost compared to using purified

enzymes, the reaction doesn't need to be supplemented with expensive co-factors which are contained within the cell, and the reaction is performed in its native environment [43, 44]. However, unless the protein is secreted from the cell or displayed on the membrane surface the substrate [45] must enter the cell for the reaction to take place, this is limited by membrane penetration of the substrate and the product, making reactions slower [46, 47]. Toxic by-products can also result from undesirable metabolic pathways that can take place within the cell. Lastly, the process is more complicated, and thus research and development for a specific molecular target can take longer.

Enzymes can be isolated from the cell by bacterial expression, cell lysis to release the protein and purification through chromatography or precipitation [48-50]. Biocatalysis using purified protein results in very specific reactions, reducing by-product formation. However, this makes the enzyme specific for particular substrates [51]. In addition, the substrate only needs to access to the active site of the enzyme without needing to pass through cell membranes. However, the process of purification can be time consuming and expensive, and in many cases the protein is not correctly folded, effecting its solubility and activity. Purified enzymes can also require specific environments and additional co-factors for high activity and can be unstable outside of the cell.

Despite great potential of enzymes, their application in the industry has been hampered mostly due to undesirable properties of the system, such as lack of stability, catalytic efficiency, and specificity. In recent years, advances in biotechnology and protein engineering have been achieved to attempt to overcome these drawbacks. These technologies have allowed enzymes to be produced at more acceptable prices and to manipulate them so they exhibit desired properties with regard to substrate specificity, promiscuity, selectivity, stability, activity, and optimal pH [52-54].

Another avenue for increasing the application and efficiency of enzymes is through

immobilisation to solid supports [55-60]. There are several advantages to enzyme immobilisation such as the ability to recover and reuse them, which is particularly beneficial for enzymes which are only available in small quantities. Retention of the enzyme also simplifies the lengthy purification process. Enzyme immobilisation has also been shown, in some cases, to increase stability, reactivity and selectivity [61].

Properties that should be considered when choosing an immobilisation support are large surface area, hydrophilic/hydrophobic character, sufficient functional groups for attachment, water insolubility, chemical and thermal stability, mechanical strength, rigidity, resistance to microbial degradation, and easy of regeneration. Enzymes can be immobilised onto synthetic organic polymers, biopolymers or inorganic polymers by adsorption, covalent attachment, affinity immobilisation, entrapment and carrier-free immobilisation by cross-linking (Figure 1.6) [55, 56, 60], as detailed below:

A. Covalent immobilisation relies on chemical bonds between a solid support and surface-exposed amino acids on the protein or cell (Figure 1.6A). The major benefits of covalent attachment are the potential to improve catalyst lifespan due to a reduction in leaching. However, not all proteins are suitable for covalent immobilisation.

B. Adsorption of enzymes onto a solid support relies on hydrophobic, salt bridge, van der Waals, or hydrogen interactions (Figure 1.6B). Methods of adsorption is easier to perform and can be used to avoid enzyme denaturation through alteration of the protein. However, the lifetime and efficiency can be lower in comparison to covalent attachment methods.

C. Affinity immobilisation relies on creating a bio-affinity bond between an activated support and a specific group on an enzyme's surface, under specific conditions. An example is the immobilisation of enzymes onto nickel nitrilotriacetic acid (Ni-NTA) resin, which is most commonly used for protein purification. Protein can be expressed

with a poly-histidine tag which have an affinity for the resin under neutral conditions. The protein can then be released from the resin by adding a high concentration of imidazole or lowering the pH (Figure 1.6C).

D. Entrapment immobilisation is achieved by synthesizing the support, typically acrylamide, silica sol-gel or hydrogel, in the presence of the enzyme where the enzyme is trapped within the support (Figure 1.6D). Additional covalent attachment is often required, as only physical entrapment typically lead to enzyme or cell leakage.

E. Immobilisation through cross-linking enzymes is achieved through attachment of surface amino functional groups with a bifunctional cross-linker (Figure 1.6E). Cross-linked enzyme crystals (CLECs) are enzymes crosslinked to crystals by adding a bifunctional reagent, commonly glutaraldehyde, and are typically robust and highly active, with the particle size being easily controlled [62]. Cross-linked enzyme aggregates (CLEAS) are simpler, less expensive and based on the precipitation of the enzymes to for aggregates of protein molecules, held together by non-covalent bonding without disruption of their tertiary structure [63, 64].

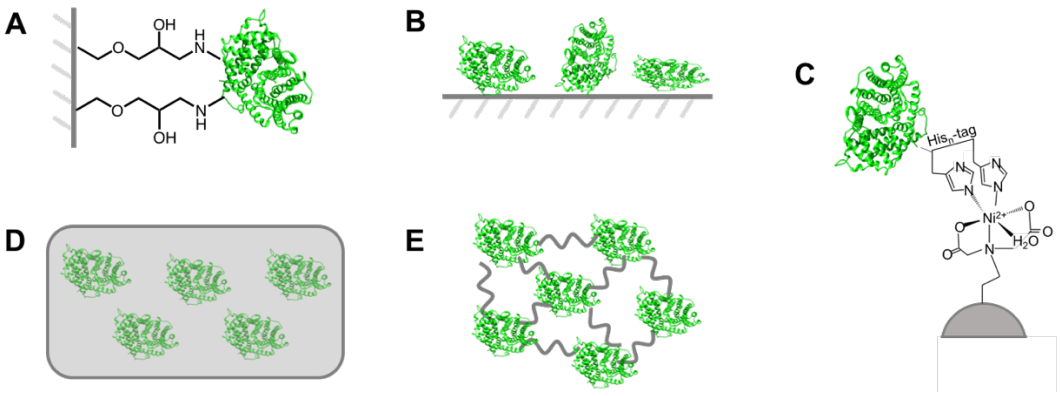

Figure 1.6. Enzyme Immobilisation techniques. (A) Covalent attachment. (B) Physical adsorption. (C) Affinity Immobilisation. (D) Encapsulation. (E) Cross-linking. A-C are examples of immobilisation to a support carrier [55].

Immobilisation of an enzyme to a support should provide an active and stable biocatalyst. The cost of carrier, fixing agents and overall immobilisation process should also be considered when choosing an immobilisation method. As discussed with catalyst immobilisation in general, the mass transfer limitations that can occur when immobilising enzymes to a solid support can be overcome by the application of continuous-flow.

1.2.4. Biocatalysis in Continuous-Flow

Merging enzyme immobilisation and continuous-flow is a growing area of interest in both academia and the industry. As discussed earlier in this chapter enzyme immobilisation has been shown to increase stability, selectivity and improve reaction rates [61]. Furthermore, some enzymes are only available in small quantities, and therefore, attaching the enzyme to a solid support allows it to be recycled, thereby decreasing the amount required [51, 65]. Additional advantages of biocatalysis in continuous-flow include reduction in enzyme inhibition by continuous removal of products, simpler downstream processing when using immobilised biocatalysts, and improved throughput [66].

Immobilisation of lipases have been extensively explored for application in continuous-flow, due to their commercial availability, promiscuity, stability under a wide range of conditions and organic solvents [67-69]. Lipase B from *Candida anartica* (Novozyme 435) has been applied to amidation [70, 71], esterification [70, 72-74], hydrolysis [75, 76] and oxidation [77] reactions under continuous-flow. An example is the synthesis of pseudo-ceramides, active compounds in pharmaceuticals and cosmetics, using Novozyme 435 [71]. Maugeri et al. demonstrated the chemoenzymatic two-step continuous-process, starting with the amidation of 3-amino-1,2-propanediol using stearic acid in 92% yield, followed by the esterification of the remaining hydroxyl groups with myristic acid in 54% yield (Figure 1.7). This system operated

for three weeks without loss of yield in the first step.

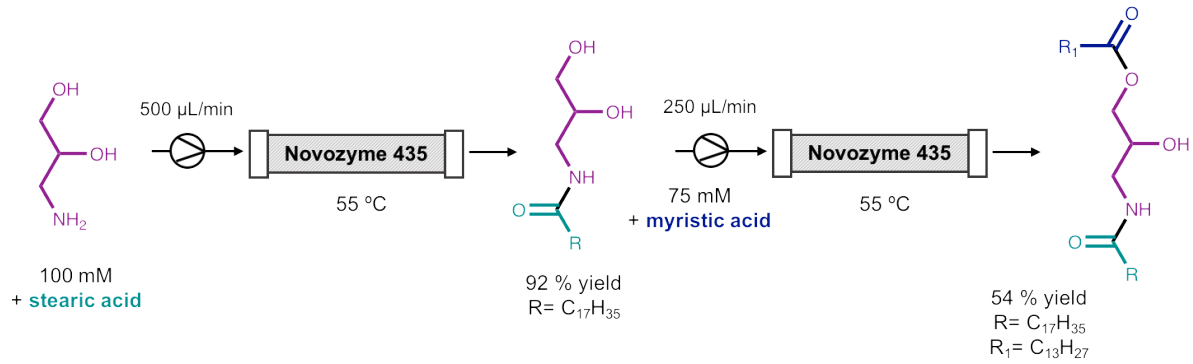

Figure 1.7. Continuous-flow synthesis of ceramides through the amidation and esterification of 3-amino-1,2-propanediol using Novozyme 435 [71].

Several examples have been explored for the continuous-flow synthesis of pharmaceutical motifs and valuable compounds using immobilised enzymes [51, 66].]- Transaminases are the most commonly used enzymes for the synthesis of chiral amines from corresponding carbonyls, with their immobilisation implemented in industry, including in the landmark production of sitagliptin by Merck [78-79]. Several examples of immobilised transaminases under continuous flow have been described [80-83]. One example is the synthesis of enantiopure amines by Paradisi and co-workers using an immobilised transaminase, integrated with a two-step in situ product removal process (Figure 1.8A) [83]. A transaminase from *Halmonas elongata* (HEWT), displaying broad substrate scope, thermal and pH tolerance, and stability in high salt concentrations and organic solvents, was applied to the synthesis of a panel of amines in continuous-flow. The his-tagged enzyme was covalently immobilised onto a metal derivitised epoxy resin, with high enrichment, however, with a significant loss of activity. The desired amine was isolated from the ketone by-product using an in-line purification protocol, consisting of basification of the reaction stream, followed by extraction with ethyl acetate. The system gave high conversions and reduced the total reaction time, from hours to minutes relative to batch processing.

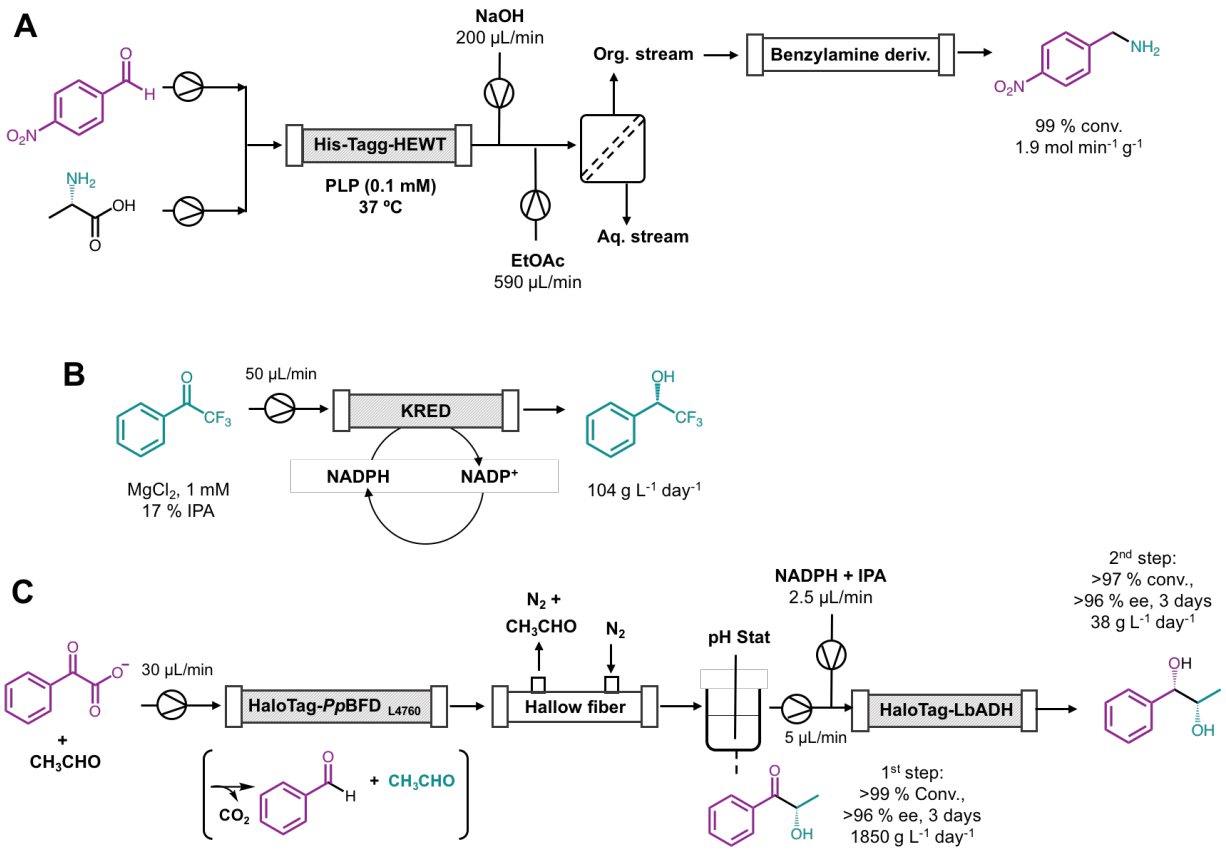

Figure 1.8. Continuous-flow biocatalysis using immobilised enzymes. (A) Synthesis of enantiopure amines using an immobilisation transaminase, integrated with a two-step *in situ* product removal process [83]. (B) Co-immobilisation of a ketoreducatse (KRED) and co-factor, NADPH, on an agarose-based cation carrier [84]. (C) Two-enzyme continuous-flow system for the synthesis of chiral diastereomeric 1,2-diols, using HaloTag fusion immobilisation [85].

The requirement of expensive co-factors, which are difficult to recycle, places economic limitations on process feasibility on an industrial scale. Therefore, pairing cofactor recycling systems has been proposed as an efficient approach for continuous-flow applications [51, 66, 86]. Lôpez-Gallego and co-workers recently reported an approach for the immobilisation and recycling of enzyme and cofactor [87]. A commercially available KRED

was co-immobilized with its cofactor, NADPH, onto a commercially available agarose-based cationic carrier with a monolayer of tertiary amines. KRED was strongly bound to the support, whereas, NADPH was immobilised through ionic absorption, establishing an association/dissociation equilibrium. The catalytic system was loaded into a packed-bed reactor and applied to the continuous-flow synthesis of (S)-(trifluoromethyl)benzyl alcohol in the presence of $MgCl_2$ and 17% isopropanol, yielding 104g $L^{-1}day^{-1}$, with a flow rate of 50L min^{-1} (Figure 1.8B).

Although the majority of continuous-flow catalysis have been single-enzymatic step transformations, implementing multienzyme or chemoenzymatic cascade reactions in continuous-flow is a growing area of interest [88]. Pohl and co-workers reported the two-step enzyme cascade reaction for the continuous synthesis of (1S,2S)-1-phenylpropane-1,2-diol, using direct HaloTag fusion immobilisation of (PpBFD) and alcohol dehydrogenase (LbADH) (Figure 1.8C) [85]. The first step involved the decarboxylation of benzylformate *in situ* to the aceylation of resulting benzaldehyde by HaloTag-*Pp*BFD L476Q (4mg bound to 360mg of wet HaloLink resin). The excess acetaldehyde was removed from solution by membrane- supported stripping using a hollow fiber module and a reversed nitrogen flow. The pH was adjusted to 7.0 using a pH-stat prior to the second step. Here a column containing immobilised HaloTag-LbADH (16mg in 20cm column) selectively reduced (S)-2-hydroxy-1- phenylpropane-1-one to the desired diol with a conversion of >97%. The cofactor, NADPH, was regenerated from NADP+ in 10% v/v 2-propanol. The two enzymes displayed activity for at a minimum of 3 days, before a significant drop in activity was observed for *Pp*BFD.

1.2.5. Additional Biotechnology in Continuous-Flow

In the past two decades, the development and sale of biotherapeutics has grown rapidly, with the dominant product class in the pharmaceutical market being biologic drugs [89]. This demand has led to a push in the biopharmaceutical industry to develop innovative, flexible and cost-effective manufacturing processes. As described above, process intensification through translating to continuous manufacturing from batch production has been extensively explored for small molecules. However, its application for the manufacture of biologics manufacturing has been slow. Recently, interest in continuous bioprocessing for creating more efficient processes is growing, as it enables standardization, faster processing and more reliable product formation [89].

Microfluidic devices have been used to study cellular microenvironments of bacterial, yeast, and mammalian cells [90-92]. Continuous culturing of cells is the process in which cells are maintained in the exponential growth phase by the regular addition of fresh medium and removal of cell suspension from the bioreactor [93]. Culturing adherent cells in microfluidic devices allows for control over the microenvironment of the cells, nutrient supply, removal of product, and waste product biomolecules, and can regulate cell-cell and cell-matrix interactions, which all effect cell growth, viability, and metabolism [90]. Long-term culturing of adherent cells in microfluidic bioreactors has been explored by several research groups for protein and mAbs production [94-96]. These groups applied different agents for improved adhesion and viability of cells, such as fibronectin [95] and poly-D-lysine [96]. Additionally, Green et al. tested the effect of microchannel geometries and thicknesses and the influence of flow rate on the efficiency and viability of cell culturing in continuous-flow [94].

Numerous unit operations for downstream processing of biopharmaceuticals and biotechnology products used in batch mode were originally designed for continuous processing

[99]. Downstream processing of protein and antibody expression incorporates all process steps from cell harvest to the final purified product. Efforts for continuous centrifugation, filtration, homogenization and lysis, precipitation/crystallisation, extraction, refolding, and chromatography, have been described [99, 100]. Notably, the most commonly used continuous process is continuous chromatography for product purification. Chromatographic techniques are typically continuous-flow in their individual steps. However, they are moving towards multiple steps in a continuous flow sequence. For example, Sanofi manufactured a continuous three step antibody purification, involving protein capture, cation exchange or mixed-mode ligand, and flow-through anion exchange [101]. Unlike batch processing, all columns are run continuously without holds or adjustments.

Microfluidic continuous-flow devices have been extensively applied to the fabrication of nano- and micro-materials for biomedical applications [102] including cell encapsulation, tissue engineering (microfiber) or 3D cell culture, separation of biological materials, and materials for bioimaging and biomolecular detection. Microfluidic devices have been applied for preparing particles for preventing drug degradation, enhancing cellular uptake, and controlling drug release. These devices allow for a simple and consistent method for synthesising uniform-sized nanoparticles, with improved release profiles, prepared from different materials such as PLGA, PEG, polycaprolactone (PCL), chitosan, and copolymers.

Antibody-drug conjugates (ADCs) are a unique and rapidly developing class of targeted therapeutics. There is need for robust processing methods that permit selective and efficient functionalisation of antibodies for addition of linkers and spacer groups for conjugation. However, conventional bioconjugation conditions result in heterogeneity and inconsistent drug to antibody ratios. Sebeika et al. utilised a continuous-flow micro-reactor for functionalisation of proteins and antibodies for the exploring ADCs [103]. The efficiency in mixing and heating

within the system offers the ability to accelerate reaction times and increase tagging with BSA and infliximab (Remicade®).

Increased application of microfluidic devices for process intensification of more bioprocesses has potential for a diversity of molecular targets, and future work is warranted. Currently, a majority of the industrial manufactured products use the traditional batch mode of processing, involving isolating each operation from the next. This is despite that such operations are inefficient and the industry is trending toward continuous bioprocessing for more efficiency and greater yield of product. Additional drivers include better process control, improved process robustness and reduced operational and capital expenditure.

1.3. Vortex Fluidic Device

A less developed area of microfluidics involves centrifugally generated films formed by passing liquids over rotating surfaces, most commonly in spinning disk reactors (SDR) [104, 105], rotating tube processors (RTP) [105, 106] and in the vortex fluidic device (VFD) [107-111]. The VFD is a variant of the rotating tube processing and has been found to be a more versatile processing platform. The vortex fluidic device (VFD) processes liquids as a dynamic thin film, ≥ 200 ∝m thick, resulting from the rapid rotation of an angled glass tube (Figure 1.9) [112]. The VFD can operate in the so-called confined mode, where a specified small finite volume of liquid is placed in the rapidly rotating tube (2mL or less for the typically 20mm diameter VFD), or the continuous-flow mode, where liquids are fed into the base of the tube, through jet feeds, with the liquid travelling up the inner surface of the glass tube, and exiting at the top of the tube. For both types of operation of the tube, the tunable tilt angle of the tube is 45°. The interaction between the liquid and the glass tube generates intense micro-mixing,

shear stress and unique complex fluid dynamics [113]. These physical properties of the liquid in the tube are governed by a number of parameters including the diameter of the tube, its rotational speed and tilt angle of the glass tube, flow rate of the liquid, fluid viscosity and density, and the hydrophobicity and texturing of the tube's inner surface [107, 114, 115].

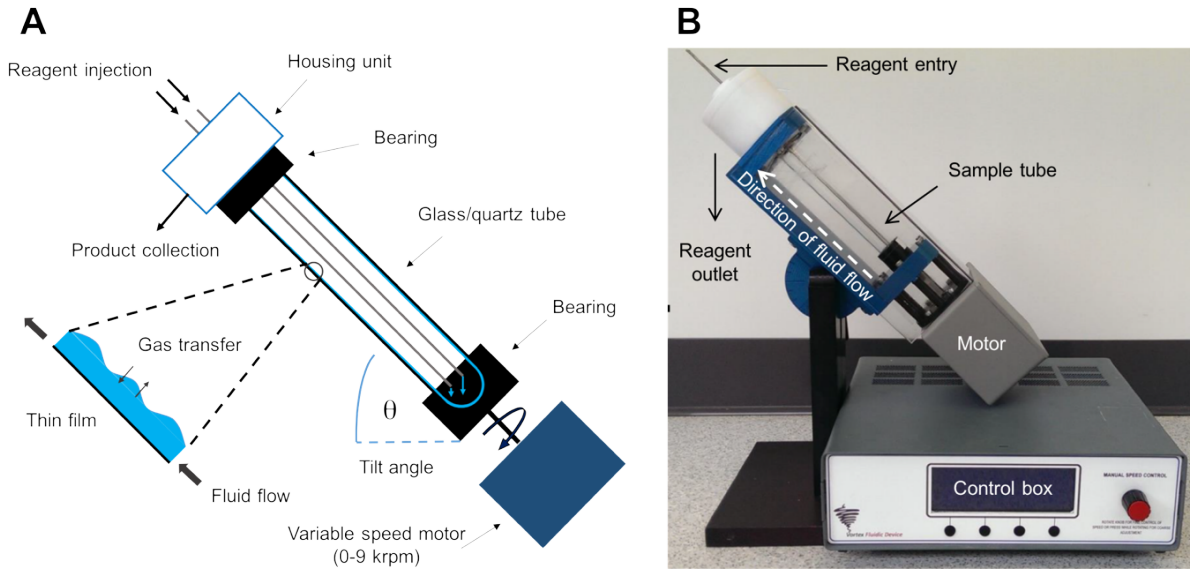

Figure 1.9. The vortex fluidic device (VFD). (A) A schematic of the VFD, (B) a photograph of the VFD. (A) Reproduced with permission [116]. Copyright 2019, American Chemical Society.

Thin film VFD microfluidics is distinctly different relative to conventional channel based microfluidics discussed above, with the fluid flow moving away from laminar flow characteristics of channel based-systems, into pro-turbulence. The oscillating film thickness in the VFD at $< 90°$ drives the formation of Faraday waves. Faraday waves are nonlinear standing waves that appear on liquids enclosed by vibrating vessel, and are characterised by pressure fluctuations that induce eddies [117]. At rotational speeds $\geq$ 6k rpm and at a tilt angle of 45°, in a 20mm OD tube, these eddies strike the surface of the tube resulting in higher shear stress

[118]. At rotational speeds between 3.8k rpm and 4.5k rpm the interplay between Faraday-wave double helical flow and circular flow result in high localised mixing.

Additional features of the VFD are that it does not suffer from clogging unlike conventional microfluidics and commercially available flow chemistry apparatus, which can also require significant capital outlay. The VFD, however, is inexpensive to construct, is simple to operate and can be set up within minutes (plug-and-play) compared to several hours or days for channel based microfluidics, allowing scaling-up through parallel processing. In addition, VFD is modular, with interchangeable attachments for field effects and/or real time monitoring for *in situ* reaction optimisation.

The benefits of the VFD have been extensively applied for a number of different chemical transformations [107]. Micromixing, mass transfer and vibrational effects in dynamic thin films provide the ability to control and accelerate organic transformations [107]. Reactions in round bottom flasks have poor mixing and heat transfer, particularly at larger scales, making scaling up reactions difficult. Alternatively, processing in the dynamic thin film in the VFD allow for these difficulties to be overcome. For example, VFD-mediated reactions can result in gaining control of kinetic over thermodynamic products. This is demonstrated by the chemoselective Michael addition reaction favoured in the VFD over Schiff-base formation in batch [114, 119]. Kinetic control was also possible in synthesising macrocyclic resorcin[4]arenes and pyrogalo[4]arenes [120].

The high heat transfer experienced in thin-film allows processing of exothermic reactions, including acylation reactions using acyl chlorides [121] and epoxidation of hydrophobic alkenes using hydrogen peroxide [122]. These reactions, when performed in batch, typically result in low yields, reagent degradation and safety concerns. The high mass transfer can also lead to more efficient delivery of gases into the thin film in comparison to

batch, for example oxygen, as demonstrated by the significant increase in yield for aerobic oxidations [122].

The ability of the VFD to facilitate continuous-flow chemistry allows for the exploration of chemical synthesis, including the production of amides [123], biodiesel [124, 125], esters [115], tri-alkylpyridines [114, 119], photoredox products [126, 127], three-component reactions, such as Ugi-type three component reaction and an A^3 coupling reaction [127]. Continuous-flow in the VFD enables multi-step reactions (Figure 1.10). This can be achieved by either connecting multiple VFD systems with one transformation per tube, where the outflow from one is fed into the next, or by performing multiple transformations in a single VFD, with multiple jet-feeds set up at different points along the tube. This concept has been demonstrated using the three-step synthesis of ⟨-aminophosphonates [121] and the API, lidocaine [123] (Figure 1.10C).

The large surface area exposure of the liquid in the VFD tube allows for the integration of light sources for performing photochemical reactions, for example the use of green LED lights for photoredox acceleration and increased yields [126, 127], and the photolytic reduction of graphene oxide using UV light [128]. The VFD also allows for external energy input in the form of thermal, laser irradiation and non-thermal plasma [129]. Integrating the VFD with a pulsed laser is effective in forming metal nanoparticles [130] and their composites [131].

The VFD has been widely used for fabrication and manipulation of 2D materials, including exfoliating graphite and boron nitride [110], fabricating single walled nanotube toroids [132], carbon dots (Cdots, ≈6nm) from multi-walled carbon nanotubes [133], and the lateral slicing of carbon nanotubes [112, 134] (Figure 1.10). The VFD has also been utilised for decorating phosphonic acid calix[8]arene functionalized graphene with well dispersed palladium nanoparticles [135], and for decorating carbon nano-onions with platinum or palladium nanoparticles [136, 137]. Other materials that have been fabricated in the VFD are

calcium carbonate polymorphs [138, 139], protein-based nanoparticles [140], tunable fluorescent polyethylenimine nanoparticles for cellular imaging [141], and hydrogels for drug delivery [142].

Biochemical transformations can be accelerated and controlled within the VFD (Figure 1.10). VFD-mediated folding of four proteins, including hen egg white lysozyme (HEWL) and cAMP-dependant protein kinase A (PKA) has been demonstrated, resulting in a 100 fold decrease in reaction time and a 10^3 fold decrease for larger, more complex protein, caveolin-1 [109, 144]. It is hypothesised that the Faraday wave pressure effects, which develop at 5k rpm, drive the hydrophobic collapse. This fluid dynamic effect lead to the investigation of enzyme acceleration for biocatalysis. Acceleration of enzymatic catalysis occurs at rotational speeds between 5K and 9k rpm in the VFD with a 45° tilt angle [108]. Hypothesis attributes the enzymatic acceleration results to firstly, the intense micro-mixing and high mass transfer experienced in the thin film, caused by periodic changes in film thickness. Secondly, changing zones of high and low pressure, resulting in Faraday waves, within the reaction mixture. The pressure oscillations and high mass transfer in the VFD could increase substrate accessibility and removal from the enzyme active site.

Immobilisation of enzymes in the VFD has previously been explored through functionalisation of the borosilicate glass surface for non-covalent and covalent attachment [145], and by affinity immobilisation onto Ni-NTA resin [143] for biocatalysis. Bioconjugation and special segregation of fused his_n-tagged proteins to Ni-NTA resin allowed for a ten-minute protein purification from cell lysate, and the sequential biocatalytic reaction using the immobilised, purified enzyme. Spatial segregation of enzymes allows the potential for multi-step enzymatic transformations.

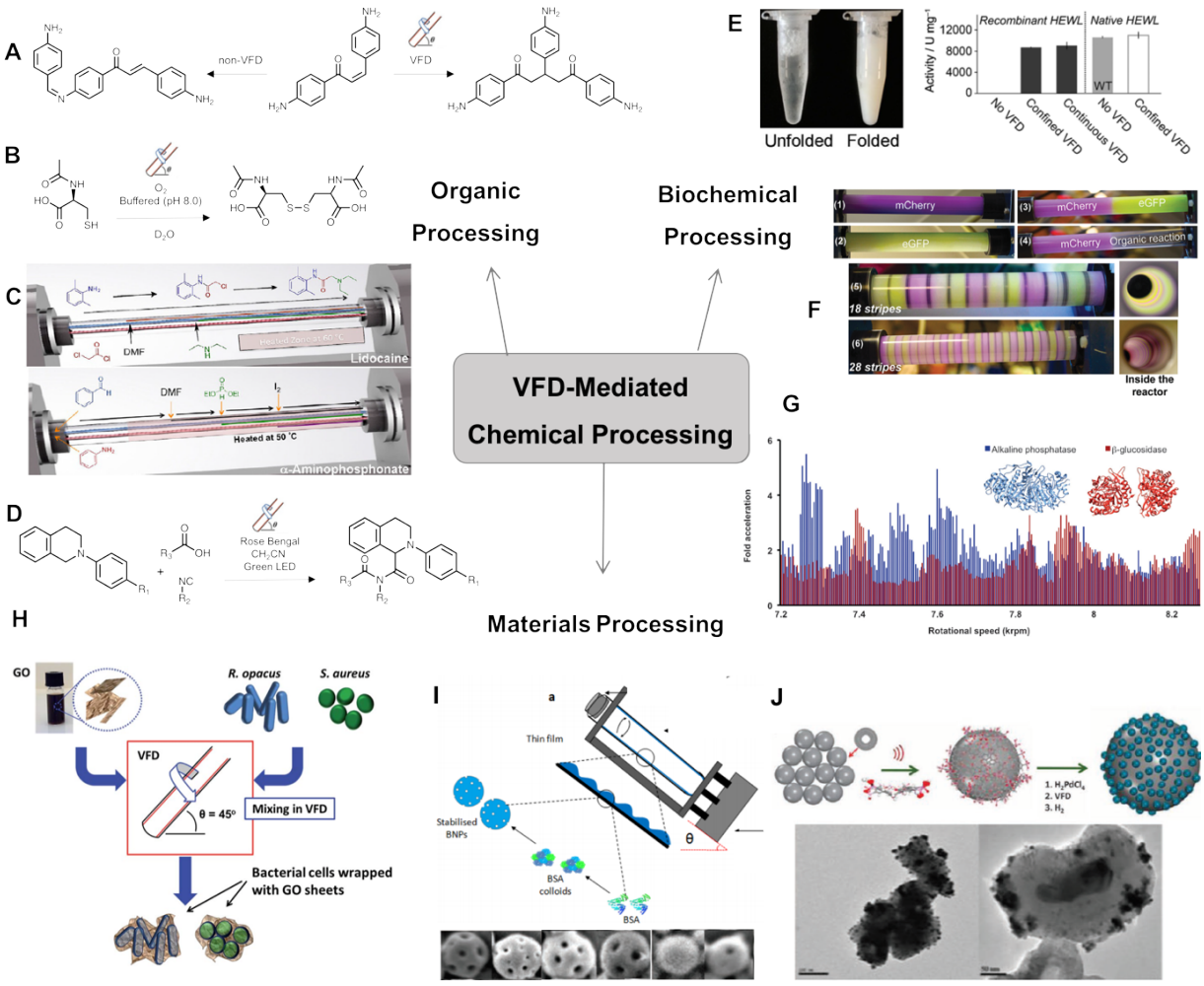

Figure 1.10. An overview of VFD-mediated chemical transformations reproduced from the literature [107]. Organic transformation including (A) the VFD favoured Michael-addition product over the non-VFD Schiffs base product [119], (B) aerobic oxidation [122], (C) assembly line synthesis of lidocaine, top, and ⟨–amino-phosphonates, bottom, using spatially segregated transformations and in situ solvent exchange [121, 123], and (D) photochemical three component Ugi-type reaction [127]. Biochemical processing including, (E) the refolding of hen egg white lysozyme (HEWL) [109], (F) immobilisation of mCherry and eGFP to the inner surface of the tube through bioconjugation of protein fused his_n-tags to metal affinity chromatography (IMAC) resin [143], and (G) acceleration of alkaline phosphatase and ®-glucosidase activity [108]. Materials processing including (H)

encapsulation of *staphylococcus auras* and *rhodococcus opacus* graphene oxide sheets [112], (I) fabrication of macroporous bovine serum albumin nanoparticles with controllable diameter and morphology [140], and (J) decorating carbon nano-onions with Pd nanoparticles [137]. (C top) Reproduced with permission [120]. Copyright 2015, Wiley-VCH. (C bottom & E) Reproduced with permission [123, 109]. Copyright 2015, Wiley-VCH. (F) Reproduced with permission [143]. Copyright 2017, Wiley-VCH. (G) Reproduced with permission [108]. Copyright 2018, Wiley-VCH. (H) Reproduced with permission [112]. Copyright 2011, Royal Society of Chemistry. (I) Reproduced with permission [140]. Copyright 2018, American Chemical Society. (J) Reproduced with permission [137]. Copyright 2012, American Chemical Society.

1.4. Research Objectives

Overall, the VFD has been utilised for enhancing several organic, biochemical, and materials processing. Based on this seminal work, research objective were devised. In this thesis methods for for inorganic and bio- catalyst immobilisation in the VFD will be developed which will lead to the efficient and scalable chemical and biochemical processing, expanding the toolbox of the VFD for the production of valuable compounds.

Immobilisation of biomolecules in the VFD will be applied for biotechnological applications beyond biocatalysis. The development of a continuous-flow phage selection method will be developed, which features the immobilisation of biomarker antigens. A valuable monoclonal antibody and peptide, which is specific to a bladder cancer biomarker will be developed. These binders have the potential for use in bladder cancer diagnostics.

This thesis will also explore the use of mechanical energy in the VFD for enzyme acceleration for the extraction of DNA from formalin fixed museum samples.

Overal, this thesis attempted to extend the VFD for developing greener, less laborious scientific techniques and application and establish methods for employing catalysis, biocatalysis, immobilisation, and biotechnology in thin-films in the VFD for process enhancement of chemical and biochemical transformations.

1.5. References

[1] Gupta, P., Mahajan, A., Green chemistry approaches as sustainable alternatives to conventional strategies in the pharmaceutical industry. *RSC Adv*., **2015**, *5*, 26686-26705.

[2] Hawkins, J. M., Streamlining drug synthesis. Nature, **2015**, *520*, 302-303.

[3] Movsisyan, M., Delbeke, E. I. P., Berton, J. K. E. T., Battilocchio, C., Ley, S. V., Stevens, C. V. Taming hazardous chemistry by continuous flow technology. *Chem. Soc. Rev*., **2016**, *45*, 4892-4928.

[4] Pastre, J. C., Browne, D. L., Ley, S. V. Flow chemistry syntheses of natural products. *Chem. Soc. Rev*. **2013**, *42*, 8849–8869.

[5] Walsh, G. Biopharmceutical benchmarks 2018. *Nat. Biotechnol*. **2018**, *36*, 1136-1145.

[6] Badenhorst, C. P. S., Bornscheuer, U. T. Getting Momentum: From Biocatalysis to Advanced Synthetic Biology, *Trends Biochem. Sci*. **2018**, *43*, 180-198.

[7] Wiles, C.W., P., Continuous Flow Reactors, a Tool for the Modern Synthetic Chemist. *Eur. J. Org. Chem*., **2008**, 10, 1655-1671.

[8] Elvira, K. S. S., Wootton, R. C. R., deMello, A. J. The past, present and potential for microfluidic reactor technology in chemical synthesis. *Nat. Chem*., **2013**. *5*, 905-915.

[9] Sheldon, R. A., Woodley, J. M. Role of Biocatalysis in Sustainable Chemistry. *Chem. Rev*. **2018**, *118*, 801-838.

[10] Rogers, L. Jensen. K. F. Continuous manufacturing – the Green Chemistry promise? *Green Chem*., **2019**, *21*, 3481–3498.

[11] Politano, F., Oksdath-Mansilla, G. Light on the Horizon: Current Research and Future

Perspectives in Flow Photochemistry. *Org. Process Res. Dev*. **2018**, *22*, 1045−1062.

[12] Di Filippo, M., Bracken, C., Baumann, M. Continuous Flow Photochemistry for the Preparation of Bioactive Molecules. *Molecules*, **2020**, *25*, 356, 1-12.

[13] Baumann, M. Integrating continuous flow synthesis with in-line analysis and data generation. *Org. Biomol. Chem*., **2018**, *16*, 5946–5954.

[14] Britton, J., Raston, C. L. Multistep reactions in continuous flow. *Chem. Soc. Rev*. **2017**, *46*, 1250-1271.

[15] Gutmann, B. Cantillo, D., Kappe, C. O. Continuous-Flow Technology—A Tool for the Safe Manufacturing of Active Pharmaceutical Ingredients. *Angew. Chem. Int. Ed*., **2015**, *54*, 6688-6728.

[16] Baumann, M., Baxendale, I. R. The synthesis of active pharmaceutical ingredients (APIs) using continuous flow chemistry. *Beilstein J. Org. Chem*. **2015**, *11*, 1194−1219.

[17] Porta, R., Benaglia, M., Puglisi, A. Flow chemistry: recent developments in the synthesis of pharmaceutical products. *Org. Process Res. Dev*. **2016**, *20*, 2−25.

[18] Baumann, M., Moody, T. S., Smyth, M., Wharry, S. A Perspective on Continuous Flow Chemistry in the Pharmaceutical Industry. *Org. Process Res. Dev*. **2020**, Accepted article.

[19] Bogdan, A.R., Poe, S. L., Kubis, D. C., Broadwater, S. J., McQuade, D. T. The Continuous-Flow Synthesis of Ibuprofen. *Angew. Chem. Int. Ed*., **2009**, *48*, 8547-8550.

[20] Snead, D. R. J., Jamison, T. F. A Three-Minute Synthesis and Purification of Ibuprofen: Pushing the Limits of Continuous-Flow Processing. *Angew. Chem. Int. Ed*., **2015**, *54*, 983-987.

[21] Kopetzki, D., Lévesque, F., Seeberger, P. H., A Continuous-Flow Process for the Synthesis of Artemisinin. *Chem. Eur. J*., **2013**, *19*, 5450-5456.

[22] Baumann, M., Baxendale, I. R. The synthesis of active pharmaceutical ingredients (APIs) using continuous flow chemistry. *Beilstein J. Org. Chem*. **2015**, *11*, 1194−1219.

[23] Zhang, P., Russell, M. G., Jamison, T. F. Continuous Flow Total Synthesis of Rufinamide. *Org. Process Res. Dev*. **2014**, *18*, 1567-1570.

[24] Zhang, Y., Jamison, T. F., Patel, S., Mainolfi, N. Continuous Flow Coupling and Decarboxylation Reactions Promoted by Copper Tubing. *Org. Lett*. **2011**, *13*, 280−283.

[25] Dunn, P.J.H., K. K. M.; Krische, M. J.; Williams, M. T., *Sustainable Catalysis: Challenges and Practices for the Pharmaceutical and Fine Chemical Industries*. 2013: John Wiley and Sons.

[26] Cantillo, D., Kappe, C. O. Immobilized Transition Metals as Catalysts for Cross-Couplings in Continuous Flow—A Critical Assessment of the Reaction Mechanism and Metal Leaching. *Chem. Cat. Chem*., **2014**, *6*, 3286-3305.

[27] Tsubogo, T., Oyamada., H., Kobayashi, S. Multistep continuous-flow synthesis of (R)- and (S)-rolipram using heterogeneous catalysts. *Nature*, **2015**, *520*, 329-332.

[28] Munirathinam, R., Huskens, J., Verboom, W. Supported Catalysis in Continuous-Flow Microreactors. *Adv. Synth. Catal*. **2015**, *357*, 1093 –1123.

[29] Plutschack, M. B., Pieber, B., Gilmore, K., Seeberger, P. H. The Hitchhiker's Guide to Flow Chemistry. *Chem. Rev*. **2017**, *117*, 11796−11893.

[30] Karim, A., Bravo, J., Gorm, D., Conant, T., Datye, A. Catalytic Microstructured Reactors. *Catal. Today*, **2005**, *110*, 86–91.

[31] Sachse, A., Galarneau, A., Coq, B., Fajula, F. Monolithic flow microreactors improve fine chemicals synthesis. *New J. Chem*. **2011**, *35*, 259–264.

[32] Kirschning, A., Solo-denko, W., Mennecke, K. Combining Enabling Techniques in Organic Synthesis: Continuous Flow Processes with Heterogenized Catalysts. *Chem. Eur. J*. **2006**, *12*, 5972– 5990.

[33] Kiwi-Minsker, L., Renken, A. Microstructured reactors for catalytic reactions. *Catal. Today*, **2005**, *110*, 2–14.

[34] Lopes, J. P., Alves, M. A., Oliveira, M. S. N., Cardoso, S. S. S., Rodrigues, A. E. Regime mapping and the role of the intermediate region in wall-coated microreactors. *Chem. Eng. Sci.* **2013**, *94*, 166–184.

[35] Kirschning, A., Jas, G. Applications of Immobilized Catalysts in Continuous Flow Processes. *Top. Curr. Chem*., **2004**, *242*, 209-239.

[36] Zhao, D., Ding. K. Recent Advances in Asymmetric Catalysis in Flow. *ACS Catal*. **2013**, *3*, 928−944.

[37] Hartwig, J., Metternich, J. B., Nikbin, N., Kirschning, A., Ley, S. V. Continuous flow chemistry: a discovery tool for new chemical reactivity patterns. *Org. Biomol. Chem*., **2014**, *12*, 3611-3615.

[38] Frost, C. G., Mutton, L. Heterogeneous catalytic synthesis using microreactor technology. *Green Chem*. **2010**, *12*, 1687–1703.

[39] Tsubogo, T., Ishiwata, T., Kobayashi, S. Asymmetric carbon–carbon bond formation under continuous-flow conditions with chiral heterogeneous catalysts. *Angew. Chem. Int. Ed*. **2013**, *52*, 6590–6604.

[40] Sandoval, B. A., hyster, T. K. Emerging strategies for expanding the toolbox of enzymes in biocatalysis. *Curr. Opin. Chem. Biol*. **2020**, *55*, 45-51.

[41] DiCosimo, R., McAuliffe, J., Pouloseb, A. J., Bohlmann, G. Industrial use of immobilized enzymes. *Chem. Soc. Rev*. **2013**, *42*, 6437-6474.

[42] Choi, J. M., Han, S. S., Kim, H. S. Industrial applications of enzyme biocatalysis: Current status and future aspects. *Biotech. Adv*. **2015**, *33*, 1443-1454.

[43] Lin, M., Tao, Y. Whole-cell biocatalysts by design. *Microb Cell Fact*. **2017**, *16*, 106, 1-12

[44] Lam, C. M. C., Sua´rez Diez, M., Godinho, M., dos Santos, V. A. P. M. Programmable bacterial catalysis - Designing cells for biosynthesis of value-added compounds. *FEBS Lett*. **2012**, *586*, 2184-90.

[45] Schüürmann, J., Quehl, P., Festel, G., Jose, J. Bacterial whole-cell biocatalysts by surface display of enzymes: toward industrial application. *Appl Microbiol Biotechnol*. **2014**, *98*, 8031-8046.

[46] Fukuda, H., Hama, S., Tamalampudi, S., Noda, B. Whole-cell biocatalysts for biodiesel fuel production. *Trends Biotechnol*. **2008**, *26*, 668–673.

[47] Chen, R. R. Permeability issues in whole-cell bioprocesses and cellular membrane engineering. *Appl. Microbiol. Biotechnol*. **2007**, *74*, 730–738.

[48] Baneyx, F. Recombinant protein expression in Escherichia coli. *Curr. Opin. Biotechnol*., **1999**, *10*, 411–421.

[49] Overton, T. W. Recombinant protein production in bacterial hosts. *Drug Discovery Today*, **2014**, *19*, 590–601.

[50] Terpe, K. Overview of bacterial expression systems for heterologous protein production: from molecular and biochemical fundamentals to commercial systems. *Appl. Microbiol. Biotechnol*., **2006**, *72*, 211-222.

[51] Britton, J., Majumdar, S., Weiss, G. A. Continuous flow biocatalysis. *Chem. Soc. Rev*. **2018**, *47*, 5891-5918.

[52] Bornscheuer, U. T., Kazlauskas, R. J. Catalytic promiscuity in biocatalysis: using old enzymes to form new bonds and follow new pathways. *Angew Chem. Int. Ed.* **2004**, *43*, 6032–6040.

[53] Renata, H., Wang, Z.J., Arnold, F.H. Expanding the enzyme universe: accessing non-natural reactions by mechanism guided directed evolution. *Angew Chem. Int. Ed.* **2015**, *54*, 3351–3367.

[54] Arnold, F. H. Directed evolution: bringing new chemistry to life. *Angew Chem. Int. Ed*. **2018**, *57*, 4143–4148.

[55] Sheldon, R. A. and Pelt, S. V. Enzyme immobilisation in biocatalysis: why, what and how. *Chem. Soc. Rev.* **2013**. *42*, 6223-6235.

[56] Liese, A., Hilterhaus, L. Evaluation of immobilized enzymes for industrial applications. *Chem. Soc. Rev*., **2013**, *42*, 6236–6249.

[57] Hartmann, M., Kostrov, X. Immobilization of enzymes on porous silicas – benefits and challenges. *Chem. Soc. Rev*., **2013**, *42*, 6277–6289.

[58] Sheldon, R. A. Enzyme Immobilization: The Quest for Optimum Performance. *Adv. Synth. Catal*., **2007**, *349*, 1289–1307.

[59] Magner E. Immobilisation of enzymes on mesoporous silicate materials. *Chem. Soc. Rev*., **2013**, *42*, 6213–6222.

[60] Secundo, F. Conformational changes of enzymes upon immobilisation. *Chem. Soc. Rev*., **2013**, *42*, 6250–6261.

[61] Rodrigues, R. C., Ortiz, C., Berenguer-Murcia, A., Torres, R. Fernandez-Lafuente, R. Modifying enzyme activity and selectivity by immobilization. *Chem. Soc. Rev*., **2013**, *42*, 6290–6307.

[62] Roy, J. J., Abraham, T. E. Strategies in making cross-linked enzyme crystals. *Chem. Rev.*, **2004**, *104*, 3705–3721.

[63] Sheldon, R. A. Characteristic features and biotechnological applications of cross-linked enzyme aggregates (CLEAs). *Appl. Microbiol. Biotechnol*., **2011**, *92*, 467–477

[64] Sheldon, R. A. Cross-Linked Enzyme Aggregates as Industrial Biocatalysts. *Org. Process Res. Dev*., **2011**, *15*, 213–223.

[65] Romero-Fernández, M., Paradisi, F. Protein immobilization technology for flow biocatalysis. *Curr. Opin. Chem. Biol.* **2020**, *55*, 1-8.

[66] Thompson, M. P, Peñafiel, I., Cosgrove, S. C., Turner, N. J. Biocatalysis Using Immobilized Enzymes in Continuous Flow for the Synthesis of Fine Chemicals. *Org. Process Res. Dev*. **2019**, *23*, 9−18.

[67] Kumar, A., Dhar, K., Kanwar, S. S., Arora, P. K. Lipase catalysis in organic solvents: advantages and applications. *Biol. Proced. Online*, **2016**, *18*, 2.

[68] Kamal, M. Z., Yedavalli, P., Deshmukh, M. V., Rao, N. M. Lipase in aqueous-polar organic solvents: Activity, structure, and stability. *Protein Sci*., **2013**, *22*, 904–915.

[69] Adlercreutz, P. Immobilisation and application of lipases in organic media. *Chem. Soc. Rev*., **2013**, *42*, 6406–6436.

[70] Porcar, R., Sans, V., Rı´os-Lombardı´a, N., Gotor-Ferna´ndez, V., Gotor, V., Burguete, M. I., Garcı´a-Verdugo, E., Luis, S. V. Stereoselective Chemoenzymatic Synthesis of Enantiopure 2-(1*H*-imidazol-yl)cycloalkanols under Continuous Flow Conditions. *ACS Catal*., **2012**, *2*, 1976–1983.

[71] Le Joubioux, F., Bridiau, N., Sanekli, M., Graber, M. Maugard, T. J. Continuous lipase-catalyzed production of pseudo-ceramides in a packed-bed bioreactor. *Mol. Catal. B: Enzym*., **2014**, *109*, 143–153.

[72] Sa´nchez, A., del Rı´o, J. L., Valero, F., Lafuente, J., Faus, I., Sola, C. Continuous enantioselective esterification of *trans*-2-phenyl-1-cyclohexanol using a new *Candida rugosa* lipase in a packed bed bioreactor. *J. Biotechnol*., **2000**, *84*, 1–12.

[73] Woodcock, L. L., Wiles, C., Greenway, G. M., Watts, P., Wells, A., Eyley, S. Enzymatic synthesis of a series of alkyl esters using novozyme 435 in a packed-bed, miniaturized, continuous flow reactor. *Biocatal. Biotransform.*, **2008**, *26*, 466–472.

[74] Wang, J., Gu, S.-S., Cui, H.-S., Wu, X.-Y., Wu, F.-A. A novel continuous flow biosynthesis of caffeic acid phenethyl ester from alkyl caffeate and phenethanol in a packed bed microreactor. *Bioresour. Technol*., **2014**, *158*, 39–47.

[75] Brahma, A., Musio, B., Ismayilova, U., Nikbin, N., Kamptmann, S. B., Siegert, P., Jeromin, G. E., Let, S. V., Pohl, M. An Orthogonal Biocatalytic Approach for the Safe Generation and Use of HCN in a Multistep Continuous Preparation of Chiral *O*-Acetylcyanohydrins. *Synlett*, **2015**, 262–266.

[76] Saranya, P., Ramani, K., Sekaran, G. Biocatalytic approach on the treatment of edible oil refinery wastewater. *RSC Adv*., **2014**, *4*, 10680–10692.

[77] Wiles, C., Hammond, M. J., Watts, P. The development and evaluation of a continuous flow process for the lipase-mediated oxidation of alkenes. *Beilstein J. Org. Chem*., **2009**, *5*, 27.

[78] Savile, C. K., Janey, J. M., Mundorff, E. C., Moore, J. C., Tam, S., Jarvis, W. R., Colbeck, J. C., Krebber, A., Fleitz, F. J., Brands, J., Devine, P. N., Huisman, G. W., Hughes, G. J. Biocatalytic Asymmetric Synthesis of Chiral Amines from Ketones Applied to Sitagliptin Manufacture. *Science*, **2010**, *329*, 305−309.

[79] Truppo, M. D., Strotman, H., Hughes, G. Development of an Immobilized Transaminase Capable of Operating in Organic Solvent. *ChemCatChem*, **2012**, *4*, 1071−1074.

[80] van den Biggelaar, L., Soumillion, P., Debecker, D. Enantioselective Transamination in Continuous Flow Mode with Transaminase Immobilized in a Macrocellular Silica Monolith. *Catalysts*, **2017**, *7*, 54.

[81] Andrade, L. H., Kroutil, W., Jamison, T. F. Continuous Flow Synthesis of Chiral Amines in Organic Solvents: Immobilization of E. Coli Cells Containing Both ω-Transaminase and PLP. *Org. Lett.* **2014**, *16*, 6092−6095.

[82] Bajić, M., Plazl, I., Stloukal, R., Žnidaršič-Plazl, P. Development of a Miniaturized Packed Bed Reactor with ω-Transaminase Immobilized in LentiKats®. *Process Biochem*. **2017**, *52*, 63−72.

[83] Planchestainer, M., Contente, M. L., Cassidy, J., Molinari, F., Tamborini, L., Paradisi, F. Continuous Flow Biocatalysis: Production and in-Line Purification of Amines by Immobilised Transaminase from Halomonas Elongata. *Green Chem*. **2017**, *19*, 372−375.

[84] Benítez-Mateos, A. I., San Sebastian, E., Ríos-Lombardía, N., Morís, F., González-Sabín, J., López-Gallego, F. Asymmetric Reduction of Prochiral Ketones by Using Self-Sufficient Heterogeneous Biocatalysts Based on NADPH Dependent Ketoreductases. *Chem. Eur. J*. **2017**, *23*, 16843−16852.

[85] Döbber, J., Gerlach, T., Offermann, H., Rother, D., Pohl, M. Closing the Gap for Efficient Immobilization of Biocatalysts in Continuous Processes: HaloTag TM Fusion Enzymes for a Continuous Enzymatic Cascade towards a Vicinal Chiral Diol. *Green Chem*. **2018**, *20*, 544−552.

[86] Hartley, C. J., Williams, C. C., Scoble, J. A., Churches, Q. I., North, A., French1, N. G., Neb, T., Coia, G., Warden, A. C., Simpson, G., Frazer, A. R., Jensen, C. N., Turner, N. J., Scott, C. Engineered enzymes that retain and regenerate their cofactors enable continuous-flow biocatalysis. *Nat Catal.* **2019**, *2*, 1006–1015.

[87] Benítez-Mateos, A. I., San Sebastian, E., Ríos-Lombardía, N., Morís, F., González-Sabín, J., López-Gallego, F. Asymmetric Reduction of Prochiral Ketones by Using Self-Sufficient Heterogeneous Biocatalysts Based on NADPH Dependent Ketoreductases. *Chem. Eur. J*. **2017**, *23*, 16843−16852.

[88] Schrittwieser, J. H., Velikogne, S., Hall, M., Kroutil, W. Artificial Biocatalytic Linear Cascades for Preparation of Organic Molecules. *Chem. Rev*. **2018**, *118*, 270−348.

[89] Walsh, G. Biopharmceutical benchmarks 2018. *Nat. Biotechnol*. **2018**, *36*, 1136-1145.

[90] Hajba, L., Guttman, A. Continuous-Flow-Based Microfluidic Systems for Therapeutic Monoclonal Antibody Production and Organ-on-a-Chip Drug Testing. *J. Flow Chem*. **2017**, *7*, 118-123.

[91] Marques, M. P. C., Szita, N. Bioprocess microfluidics: applying microfluidic devices for bioprocessing. *Curr. Opin. Chem. Eng*. **2017**, *18*, 61–68.

[92] Tapia, F., Vázquez-Ramirez, D., Genzel, Y., Reichl, U. Bioreactors for high cell density and continuous multi-stage cultivations: options for process intensification in cell culture-based viral vaccine production. *Appl Microbiol Biotechnol*. **2016**, *100*, 2121–2132.

[93] Hanaa M. Hegab, Ahmed ElMekawy, A., Stakenborg, T. Review of microfluidic microbioreactor technology for high-throughput submerged microbiological cultivation. *Biomicrofluidics,* **2013**, *7*, 021502.

[94] Green J. V., Kniazeva T., Abedi M., Sokhey D. S., Taslim M. E., Murthy S. K. Effect of channel geometry on cell adhesion in microfluidic devices. Lab Chip, **2009**, 9, 677–685.

[95] Garza-Garcia, L. D., Garcia-Lopez, E., Camacho-Leon, S., Rocha-Pizana, M. D., Lopez-Pacheco, F., Lopez-Meza, J., Araiz-Hernandez, D., Tapia-Mejia, E. J., Trujillo-de Santiago, G., Rodriguez-Gonzalez, C. A., Alvarez, M. M. Continuous flow micro-bioreactors for the production of biopharmaceuticals: the effect of geometry, surface texture, and flow rate. *Lab Chip*, **2014**, *14*, 1320–1329.

[96] Penaherrera, A., Payes, C., Sierra-Rodero, M., Vega, M., Rosero, G., Lerner, B., Helguera, G., Perez, M. S. Evaluation of cell culture in microfluidic chips for application in monoclonal antibody production. *Microelectron. Eng*. **2016**, *158*, 126129.

[99] Penaherrera, A., Payes, C., Sierra-Rodero, M., Vega, M., Rosero, G., Lerner, B., Helguera, G., Perez, M. S. Evaluation of cell culture in microfluidic chips for application in monoclonal antibody production. *Microelectron. Eng*. **2016**, *158*, 126129.

[100] Rathore, A., Kateja, N., Agarwal, H., Sharma, A. K. Continuous Processing for the Production of Biopharmaceuticals. *Biopharm. Int*. **2016**, *29*, 14–19.

[101] Mothes, B., Pezzini, J., Schroeder-Tittmann, K., Villain, L. Accelerated, Seamless Antibody Purification Process Intensification with Continuous Disposable Technology. *BioProc. Int*. **2016**, *14*, 34-58.

[102] Luo, X., Su, P., Zhang, W., Raston, C. L. Microfluidic Devices in Fabricating Nano or Micromaterials for Biomedical Applications. *Adv. Mater. Technol*. **2019**, *4*, 1900488.

[103] Meaghan M. Sebeika, Nicholas G. Gedeon, Sara Sadler, Nicholas L. Kern, Devan J. Wilkins, David E. Bell and Graham B. Jones, Protein and Antibody Functionalization Using Continuous Flow Microreactor Technology. *J. Flow Chem*. **2015**, *5*, 151–154.

[104] Brechtelsbauer, C., Lewis, N., Oxley, P., Ricard, F., Ramshaw, C. Evaluation of a spinning disc reactor for continuous processing, *Org. Proc. Res. Dev*. **2001**, **5**, 65-68.

[105] Chen, X., Smith, N. M., Iyer, K. S., Raston, C. L. Controlling nanomaterial synthesis, chemical reactions and self-assembly in dynamic thin films, *Chem. Soc. Rev*., **2014**, *43*, 1387-1399.

[106] Lodha, H., Jachuck R., Singaram, S. S. Intensified biodiesel production using a rotating tube reactor, *Energy Fuels,* **2012***, 26*, 7037-7040.

[107] Britton, J., Stubbs, K. A., Weiss, G. A. & Raston, C. L. Vortex Fluidic Chemical Transformations, *Chem. Eur. J.,* **2017**, *23*, 13270-13278.

[108] Britton, J., Meneghini, L. M., Raston, C. L. & Weiss, G. A. Accelerating Enzymatic Catalysis Using Vortex Fluidics, *Angew. Chem. Int Ed.,* **2016**, *55*, 11387-11391.

[109] Yuan, T. Z. et al. Shear-Stress-Mediated Refolding of Proteins from Aggregates and Inclusion Bodies. *ChemBioChem*, **2016**, *16*, 393-396.

[110] T M D. Alharbi, T. M. D., Vimalanathan, K., Lawrance, W. D. & Raston, C. L. Controlled slicing of single walled carbon nanotubes under continuous flow, *Carbon,* **2018,** *140*, 428-432.

[110] Chen, X., Dobson, J. F. & Raston, C. L. Vortex fluidic exfoliation of graphite and boron

nitride. *Chem. Commun.,* **2012***, 48*, 3703–3705.

[111] Wahid, M. H. et al. Microencapsulation of bacterial strains in graphene oxide nano-sheets using vortex fluidics. *RSC Advances*, **2015**, *5*, 37424-37430.

[112] Vimalanathan, K., Gascooke, J. R., Suarez-Martinez, I., Marks, N. A., Kumari, H., Garvey, C. J., Atwood, J. L., Lawrance, W. D., Raston, C. L. Fluid dynamic lateral slicing of high tensile strength carbon nanotubes. *Sci. Rep*. **2016**, *6*, 22865.

[113] Britton, J., Dalziel, S. B., Raston, C. L. The synthesis of di-carboxylate esters using continuous flow vortex fluidics. *Green Chem*. **2016**, *18*, 2193–2200.

[114] Yasmin, L., Chen, X., Stubbs, K. A., Raston, C. L. Optimising a vortex fluidic device for controlling chemical reactivity and selectivity. *Sci. Rep*. **2013**, *3*, 2282.

[115] Britton, J., Dalziel, S. B., Raston, C. L. Continuous flow Fischer esterifications harnessing vibrational-coupled thin film fluidics. *RSC Adv*. **2015**, *5*, 1655–1660.

[116] Phillips, J. M., Ahamed, M., Duan, X., Lamb, R. N., Qu, X., Zheng, K., Zou, J., Chalker, J. M., Raston, C.L. Chemoselective and continuous flow hydrogenations in thin film using a palladium nanoparticle catalyst embedded in cellulose paper, *ACS Appl. Bio Mater*., **2019**, *2*, 488–494.

[117] Périnet, N., Gutiérrez, P., Urra, H., Mujica, N., & Gordillo, L. Streaming patterns in Faraday waves, *J. Fluid Mech.* **2017**, *819*, 285-310.

[118] Alsulami, I. K., Alharbi, T. M. D., Harvey, D. P., Gibson, C. T. & Raston, C. L. Controlling the growth of fullerene C_{60} cones under continuous flow, *Chem. Commun*. **2018**, *54*, 7896-7899.

[119] Yasmin, L., Eggers, P. K., Skelton, B. W., Stubbs, K. A., Raston, C. L. Thin film microfluidic synthesis of fluorescent highly substituted pyridines. *Green Chem*. **2014**, *16*, 3450–3453.

[120] Yasmin, L., Coyle, T., Stubbs, K. A., Raston, C. L. Stereospecific synthesis of resorcin[4]arenes and pyrogallol[4]arenes in dynamic thin films. *Chem. Commun*. **2013**, *49*, 10932–10934.

[121] Britton, J., Castle, J. W., Weiss, G. A., Raston, C. L. Harnessing Thin-Film Continuous-Flow Assembly Lines. *Chem. Eur. J.* **2016**, *22*, 10773 – 10776.

[122] Pye, S. J., Dalgarno, S. J., Chalker, J. M., Raston, C. L. Organic oxidations promoted in vortex driven thin films under continuous flow, *Green Chem.*, **2018**, *20*, 118 – 124.

[123] Britton, J., Chalker, J. M., Raston, C. L. Rapid Vortex Fluidics: Continuous Flow Synthesis of Amides and Local Anesthetic Lidocaine. *Chem. Eur. J.* **2015**, *21*, 10660 –10665.

[124] Britton, J., Raston, C. L. Rapid high conversion of high free fatty acid feedstock into biodiesel using continuous flow vortex fluidics. *RSC Adv*. **2015**, *5*, 2276–2280.

[125] Britton, J., Raston, C. L. Continuous flow vortex fluidic production of biodiesel. *RSC Adv*. **2014**, *4*, 49850–49854.

[126] Gandy, M. N., Raston, C. L., Stubbs, K. A. Towards aryl C–N bond formation in dynamic thin films. *Org. Biomol. Chem*. **2014**, *12*, 4594–4597.

[127] Ho, L. A., Raston, C. L., Stubbs, K. A. Angled Vortex Fluidic Mediated Multicomponent Photocatalytic and Transition Metal-Catalyzed Reactions. *Chem. Eur. J.* **2018**, *24*, 8869 –8874.

[128] Alharbi, T. M. D., Alghamdi, A. R. M., Vimalanathan, K., Raston, C. L. Continuous flow photolytic reduction of graphene oxide, *Chem. Comm.*, **2019**, *55*, 11438-11441.

[129] Jones, D. B., Raston, C. L. Improving oxidation efficiency through plasma coupled thin film processing. *RSC Adv*. **2017**, *7*, 47111-47115.

[130] Luo, X., Al-Antaki, A. H. M., Alharbi, T. M. D., Hutchison, W. D., Zou, Y. C., Zou, J., Sheehan, A., Zhang, W., Raston, C. L. Laser-Ablated Vortex Fluidic-Mediated Synthesis of Superparamagnetic Magnetite Nanoparticles in Water Under Flow. *ACS Omega*, **2018**, *3*, 11172-11178.

[131] Al-antaki, A. H. M., Luo, X., Duan, A., Lamb, R. N., Eroglu, E., Hutchison, W., Zou, Y. C., Zou, J., Raston, C. L. Continuous flow synthesis of phosphate binding h-BN@magnetite hybrid material. *RSC Adv*. **2018**, *8*, 40829-40835.

[132] Vimalanathan, K., Chen, X., Raston C. L., Shear induced fabrication of intertwined single walled carbon nanotube rings. *Chem. Commun*. **2014**, *50*, 11295-11298.

[133] Luo, X., Al-Antaki, A. H. M., Vimalanathan, K., Moffatt, J., Zheng, K., Zou, Y., Zou, J., Duan, X., Lamb, R. N., Wang, S., Li, Q., Zhang, W., Raston, C. L. Laser irradiated vortex fluidic mediated synthesis of luminescent carbon nanodots under continuous flow. *React. Chem. Eng*. **2018**, *3*, 164-170.

[134] Alharbi, T. M.D., Vimalanathan, K., Lawrance, W. D., Raston, C. L. Vortex fluidic mediated transformation of graphite into highly conducting graphene scrolls. *Nanoscale Adv.* **2019**, *1,* 2495-2501.

[135] Chen, X., Yasin, F. M., Eggers, P. K., Boulos, R. A., Duan, X., Lamb, R. N., Iyer, K. S., Raston, C. L. Non-covalently modified graphene supported ultrafine nanoparticles of palladium for hydrogen gas sensing. *RSC Adv*. **2013**, *3*, 3213-3217.

[136] Goh, Y. A., Chen, X., Yasin, F. M., Eggers, P. K., Boulos, R. A., Wang, X., Chua, H. T., Raston, C. L. Shear flow assisted decoration of carbon nano-onions with platinum nanoparticles. *Chem. Commun*. **2013**, *49*, 5171-5173.

[137]Yasin, F. M., Boulos, R. A., Hong, B. Y., Cornejo, A., Iyer, K. S., Gao, L., Chua, H. T., Raston, C. L. Microfluidic size selective growth of palladium nano-particles on carbon nano-onions. *Chem. Commun*. **2012**, *48*, 10102-10104.

[138] Peng, W., Chen, X., Zhu, S., Guo, C., Raston, C. L. Room temperature vortex fluidic synthesis of monodispersed amorphous proto-vaterite. *Chem. Commun*. **2014**, *50*, 11764–11767.

[139] Boulos, R. A., Zhang, F., Tjandra, E. S., Martin, A. D., Spagnoli, D., Raston, C. L. Spinning up the polymorphs of calcium carbonate. *Sci. Rep*. **2014**, *4*, 3616, 1-6.

[140] Luo, X., Al-Antaki, A. H. M., Harvey, D. P., Ruan, Y., He, S., Zhang, W., Raston, C. L. Vortex Fluidic Mediated Synthesis of Macroporous Bovine Serum Albumin-Based Microspheres. *ACS Appl. Mater. Interfaces,* **2018**, *10*, 27224-27232.

[141] Luo, X., Al-Antaki, A. H. M., Pye, S., Meech, R., Zhang, W., Raston, C. L. High-Shear-Imparted Tunable Fluorescence in Polyethylenimines. *ChemPhotoChem*, **2018**, *2*, 343-248.

[142] Tong, C. L., Stroeher, U. H., Brown, M. H., Raston, C. L. Continuous flow vortex fluidic synthesis of silica xerogel as a delivery vehicle for curcumin. *RSC Adv*. **2015**, *5*, 7953-7958.

[143] Britton, J., Dyer, R. P., Majumdar, S., Raston, C. L., Weiss, G. A. Ten-Minute Protein Purification and Surface Tethering for Continuous-Flow Biocatalysis. *Angew. Chem. Int. Ed*. **2017**, *56*, 2296-2301.

[144] Britton, J., Smith, J.N., Raston, C.L., Weiss, G.A. Protein folding using a vortex fluidic device. *Methods Mol. Biol.* **2017,** 1586, 211-220.

[145] Britton, J., Raston, C. L., Weiss, G. A. Rapid protein immobilization for thin film continuous flow biocatalysis. *Chem. Commun*., **2016**, *52*, 10159-10162.

Chapter 2: Chemoselective and Continuous-Flow Hydrogenations in Thin Film using a Palladium Nanoparticle Catalyst Embedded in Cellulose Paper

---

This chapter is adapted with permission from: Phillips, J. M., Ahamed, M., Duan, X., Lamb, R. N., Qu, X., Zheng, K., Zou, J., Chalker, J. M., Raston, C.L. Chemoselective and continuous flow hydrogenations in thin film using a palladium nanoparticle catalyst embedded in cellulose paper, *ACS Appl. Bio Mater.*, **2019**, *2*, 488–494.

2.1. Abstract

Cellulose immobilised palladium (0) nanoparticles (PdNPs) were prepared for the use in scalable catalytic reactions in flow. Preparation of the catalyst is remarkably simple and fast, where a palladium acetate solution is drop-cast onto cellulose paper and then exposed to one atmosphere of hydrogen for a mere 90 seconds to produce embedded Pd(0) nanoparticles. This catalyst system is efficient in the hydrogenation of alkenes, nitroarenes, ketones and enamides, with products formed in high yield, under ambient pressure and temperature. The system is also effective for transfer hydrogenation using ammonium formate as an alternative hydrogen source. High catalyst stability and re-usability is demonstrated along with the chemoselective and scalable synthesis of industrially important fine chemicals, including the bio-based molecule cyrene.

2.2. Introduction

Catalytic transformations are essential in the synthesis of fine chemicals, pharmaceuticals, and other valuable materials [1]. However, efficient catalytic systems need

to be stable, readily accessible, and reusable when scaling up a synthesis. Heterogeneous catalytic systems have a number of advantages over homogeneous systems in terms of economy and sustainability, including the ease of separation and recyclability [2]. These catalytic systems also do not often require complex ligands and phase transfer reagents [2]. Heterogeneous catalysts based on metal nanoparticles have been extensively explored because of their high surface to volume ratio and unique reactivity and catalytic performance [3, 4]. However, heterogeneous catalysis has potential challenges to overcome, including low mass transfer and increased catalyst fouling, leading to deactivation and catalyst leaching [4]. Technologies for enhancing organic synthesis which combine heterogeneous catalysis with flow chemistry have also attracted considerable interest, driven by the advantages of process intensification and the development of greener, safer and economical chemical manufacture [2, 5-8].

This research reports on an operationally simple synthesis of palladium nanoparticles (PdNPs) on a cellulose paper for use as an immobilized catalyst in a vortex fluidic device (VFD). The VFD is a microfluidic platform useful in organic, biochemical, and materials chemistry [9, 10]. The VFD can operate under continuous flow mode where reagents are delivered to the base of a rapidly rotating glass tube (up to 9k rpm) or delivered along the tube for multistep synthesis. Reagents are then forced up the tube as dynamic thin films that facilitate mass transfer of both gases and liquids, heat dissipation, and mixing [9, 10]. Given these features, it was anticipated that immobilizing metal catalysts in the VFD tube would confer an important new capability to this reactor. For this purpose, cellulose, a renewable and biodegradable agro-resource, was targeted as the support for PdNP because of its low-cost, accessibility, flexibility, high surface area and compatibility with a diverse range of solvents [11]. However, current methods for preparing PdNPs on cellulose typically prescribe a combination of higher temperature or pressure, additives, and long preparation and reduction times [12-15]. Here, a simple and rapid preparation of cellulose paper impregnated with

palladium nanoparticles (PdNP@cellulose) for application in hydrogenation reactions under ambient pressure and temperature is disclosed. Hydrogenations using a Pd catalyst have been used in continuous flow, but they typically require higher pressures, back pressure regulators and complex catalyst synthesis [16-21].

2.3. Results and Discussion

2.3.1. Preparation of the PdNP@Cellulose

To prepare the PdNP@cellulose catalyst, the cellulose paper (20-25μm pore size, 0.2mm thickness) was first cut into a 50 × 140mm rectangle so that it could be rolled into a cylinder and inserted into the VFD tube which is usually 20mm in diameter (Figure 2.1B). A 1.3mL solution of palladium acetate in dichloromethane (34mM in Pd) was then evenly drop-casted onto the cellulose paper using a pipette and the solvent evaporated in open air (Figure 2.1A and 2.1C). Prepared in this way, the paper contains 0.64μmol Pd/cm^2. To provoke the reduction of the immobilized Pd(II) to Pd(0), the cellulose-supported palladium was exposed to one atmosphere of hydrogen gas. Within 90 seconds, the cellulose paper changed from yellow to black, suggesting an efficient reduction to elemental palladium embedded in the cellulose (Figure 2.1A, 2.1D). The reduction of $Pd(OAc)_2$ to Pd(0) has been previously reported on non-cellulose supports, including at room temperature using H_2 as a reducing agent [21-23]. In contrast, our preparation is faster and operationally simple, and only a small amount of organic solvent is required, which could be recovered for larger scale catalyst preparations. Furthermore, the PdNP@cellulose composites can be simply rolled up and inserted into the VFD for convenient use, and no modification of the glass tubes is required, which greatly increases their life span. The PdNP@cellulose, when wet with the desired solvent, adheres to

the surface of the glass tube, and when rotating in the VFD the high centrifugal forces leads to no movement of the paper during processing. The catalyst 'bed' size can also be modified by simply cutting the paper to the desired dimensions.

Scanning electron microscopy (SEM) was used to ascertain the overall morphology of the material (Figure 2.1F) and the presence of homogenously dispersed palladium was confirmed using X-ray energy dispersive spectroscopy (EDX) elemental mapping (Figure S2.5). The PdNPs were not distinguishable using SEM, and accordingly high resolution transmission electron microscopy (TEM) was used, which revealed the presence of crystalline particles of Pd, of uniform size, 5-8nm in diameter (Figure 2.1G and 1H). This is consistent with a ~7nm diameter of the particles determined using X-ray diffraction data (XRD) (Figure S2.7). X-ray photoelectron spectroscopy (XPS) gave $3d_{5/2}$ and $3d_{3/2}$ binding energies for Pd at 335.3 and 340.6eV, respectively, in accordance with the reduction of $Pd(OAc)_2$ to Pd(0) (Figure 2.1I). In addition, the XPS had C and O peaks, as expected for cellulose and was devoid of peaks corresponding to chlorine, and thus any DCM present in the composite material is minimal (Figure 2.1I). Other methods of palladium reduction (wet hydrogenation or thermal annealing at 150°C) were also investigated, which interestingly resulted in larger particles of PdNPs, less uniform in size (Figures S2.3-S2.4). Given the uniformity and high surface area of the PdNPs prepared by reduction with hydrogen gas, the PdNP@cellulose in Figures 2.1 was used for all experiments on its application in synthesis.

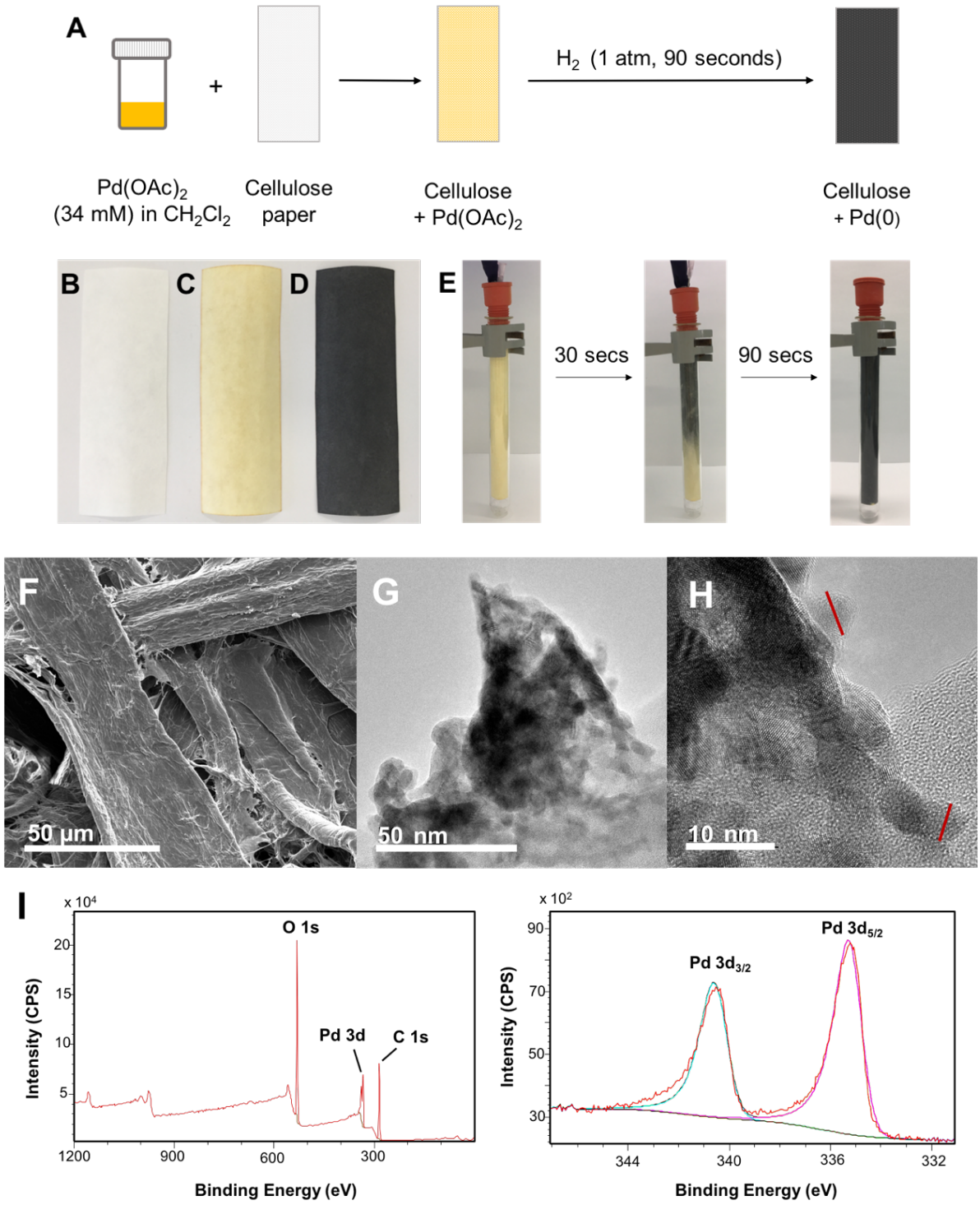

Figure 2.1. Schematic for the preparation of cellulose supported PdNPs (A), images of cellulose paper (B), cellulose supported $Pd(OAc)_2$ (C), PdNP@cellulose post reduction (D), and time lapse of the reaction after 0 seconds (E). SEM image (F) TEM image (G) and high-resolution TEM image (H), XPS spectra (I) of PdNP@cellulose after reduction of $Pd(OAc)_2$ with H_2. A video of the catalyst reduction is provided as supplementary information.

2.3.2. Catalyst Application in Hydrogenation Reactions

The catalytic activity of PdNP@cellulose (5-8nm Pd(0) particles) was explored in hydrogenation reactions in the VFD (Table 2.1). The substrate scope was initially explored under confined mode of operation of the device in which the reaction is run in a sealed VFD tube [24]. Accordingly, the substrate (0.3mmol) in ethanol (1.5mL) was added to the reaction tube lined with PdNP@cellulose (15mol% catalyst loading), and then the tube was sealed and filled with one atmosphere of hydrogen gas. Processing at 7k rpm and a 45° tilt angle [25-27] for 20 minutes at room temperature produced quantitative yields for the reduction of cinnamic acid (**1**), 4-nitrophenol (**3**), and *N*-(1-phenylvinyl)acetamide (**5**) (Table 2.1, Entries 1-3). The specific optical rotation of **6** established that it was formed as a racemic mixture, an important test given the chiral nature of cellulose paper. Future exploration should be performed using chiral chromatography to ascertain if there is any minor asymmetric induction. Hydrogenation of the ketone in benzophenone (**7**) provided alcohol **8** in a moderate yield (Entry 4) and indicated that the utility of the catalyst system is not limited to the hydrogenation of olefins. The reduction of these compounds constituted an important first test given the value of these compounds in the pharmaceutical and fine chemical industry [1, 28].

The chemoselective hydrogenation of the olefin in isophorone (**9**) provided dihydroisophorone (**10**), again in quantitative yield (Table 2.1 Entry 5). Compound **10** is a common solvent in paints and coatings so this transformation provides access to an industrially important compound. Notably, previous reports of the reduction of **9** suffered in conversion and selectivity, with competing reduction of the carbonyl moiety [29]. Where high selectivity and conversions have been achieved previously, high pressures and temperatures were required which represents an energy penalty [18].

Table 2.1. Hydrogenation reaction substrate scope under confined mode.

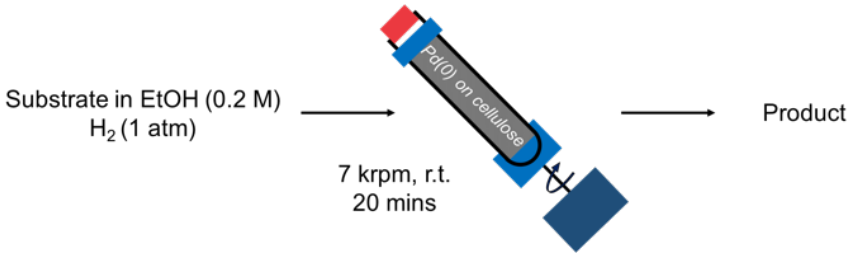

Entry	Substrate	Product	Conversion (%)
1	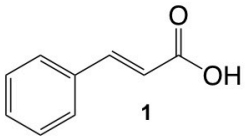 1	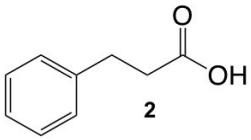 2	100
2	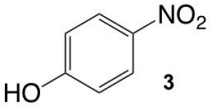 3	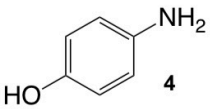 4	100
3	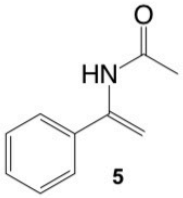 5	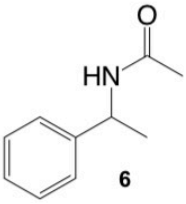 6	100
4	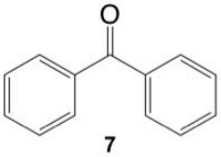 7	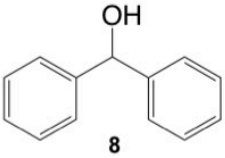 8	52
5	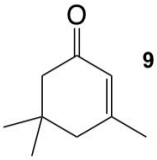 9	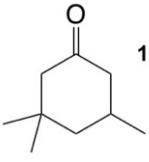 10	93
6	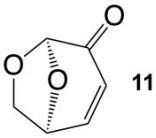 11	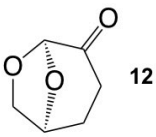 12	100

In further exploring the utility of the PdNP@cellulose, hydrogenations were then carried out under continuous flow. A solution of **9** dissolved in EtOH (0.2M) was added at 0.3mL/min through a jet feed to the base of a VFD tube containing PdNP@cellulose paper, rotating at 7k rpm at a 45° tilt angle. In a second jet feed, a steady stream of H_2 gas was delivered to the base of the tube (~1atm). It is important to note that the liquid flows through the cellulose paper (Figure S2.37). The flow rate of 0.3mL/min provided the best conversions while minimizing solvent evaporation (Table S2.1). Under these conditions, a conversion of 53% was achieved for the chemoselective hydrogenation of **9** to **10** (Table 2.2A, Entry 1). This conversion can be improved by increasing the residence time, for instance by recycling the product back through the VFD. Indeed, a conversion of 93% was achieved after three cycles through the VFD (Entry 3), generating more than one gram of this useful product. The ability to recycle presents another benefit of continuous flow. This can be achieved by continuously pumping the product back through the same device for smaller scale processing or into a second device as part of a parallel array of VFDs for larger industrial scale processing.

Chemoselective hydrogenation of (-)-levoglucosenone (**11**) was also explored. This compound is derived directly from cellulose and when selectively reduced it provides cyrene (**12**), a renewable, bio-based molecule which has promise as a dipolar aprotic solvent [30, 31]. The conversion of levoglucoseone to cyrene was achieved in 100% in the confined mode (Table 2.1, Entry 6). When transitioning to continuous flow mode, a 90% conversion was achieved under ambient temperature and pressure, with no **14** detected (Table 2.2B, Entry 4). The use of a longer tube (38cm) in a modified VFD containing a longer length of PdNP@cellulose bed (36.5cm) increased residence time and resulted in full conversion on a gram scale of **11** to **12**. In this system the product is collected in ethanol, with the only post-production step being the evaporation of ethanol, which can then be condensed and reused. Notably, when **11** was reacted neat, a moderate 52% conversion to **12** was observed (Table 2.2B, Entry 6).

Table 2.2. Continuous flow chemoselective hydrogenation of **9** (A), and 11 (B).

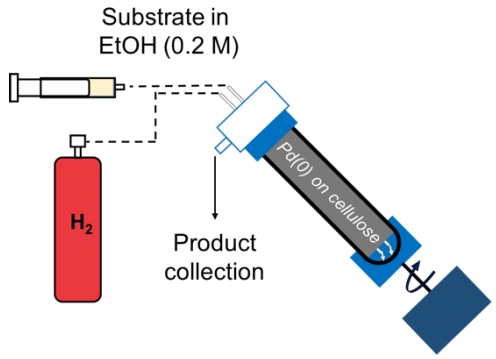

A

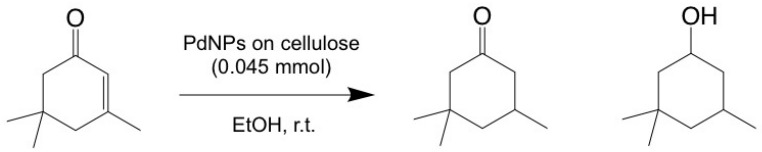

9 **10** **13**

Entry[a]	Catalyst Bed Length (cm)	Cycle	Conversion (%) 10	13
1	14	1	53	-
2	14	2	80	-
3	14	3	93	-

B

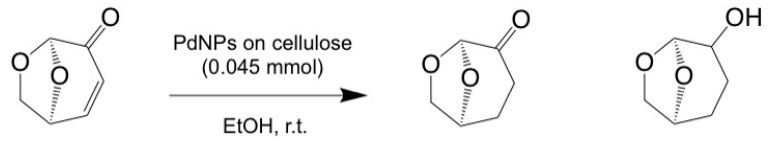

11 **12** **14**

Entry[b]	Catalyst Bed Length (cm)	Cycle	Conversion (%) 12	14
4	14	1	90	-
5	37	1	100	-
6	37	1	52[c]	-

[a] reaction performed at room temperature, 0.3ml/min flow rate, 7k rpm rotational speed, 45° tilt angle. [b] 0.5ml/min flow rate used, [c] reaction performed neat

Previously reported batch hydrogenation of levoglucosenone requires a number of days to reach full conversion at atmospheric pressure with a cumbersome catalyst separation post-reaction [30]. In contrast, reduction using the PdNP@cellulose in the VFD requires just a few minutes and does not require a separation step, greatly reducing the energy required and waste generated, making it a sustainable option for application in industry.

2.3.3. Catalyst Application in Transfer Hydrogenation Reactions

It is important to note that the continuous flow system is not fully enclosed, which is potentially hazardous. Transfer hydrogenation is a safer and more flexible alternative. Accordingly, a number of hydrogen sources were explored as an alternative to hydrogen gas, including tetrahydroxydiboron, formic acid, and ammonium formate. Preliminary experiments found ammonium formate to be a suitable candidate (Table S2.3). Ammonium formate is regarded as a greener hydrogen source as its by-products are CO_2 and NH_3.

Table 2.3. Transfer Hydrogenation Substrate Scope.

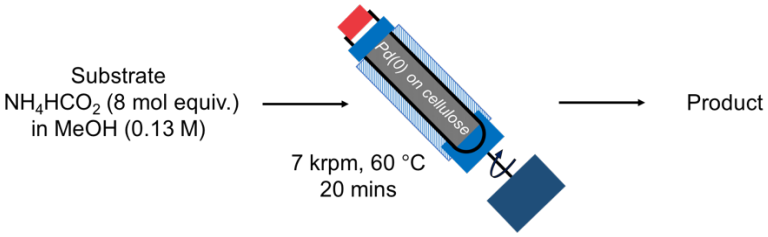

Entry	Substrate	Product	Conversion (%)
1	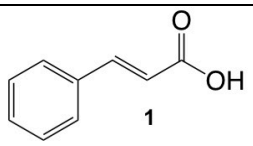 1	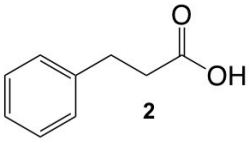 2	100
2	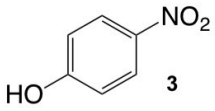 3	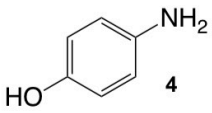 4	92
3	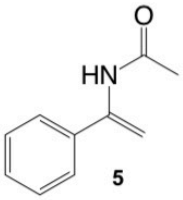 5	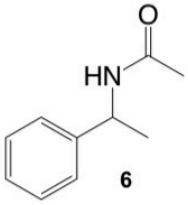 6	100
4	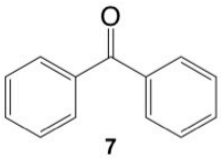 7	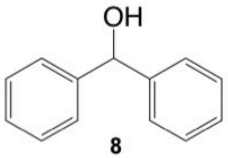 8	20
5	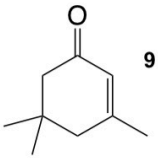 9	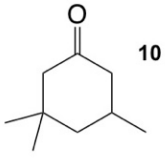 10	-
6	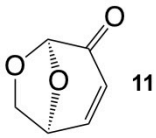 11	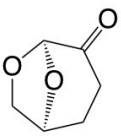 12	100[a]

[a] reaction performed at room temperature

The substrate scope was explored using ammonium formate, where similar conversions were achieved compared to using hydrogen gas, provided the reaction mixture was heated to 60°C (Table 2.3). Chemoselective hydrogenation was also achieved in the confined mode for the hydrogenation of **11** to **12**, at room temperature (Entry 5). However, when translated into continuous flow, hydrogenation at the ketone as well as the ring double bond prevailed (Figure S2.26 and S2.27). The transfer hydrogenation of **1** was also explored for translation into continuous flow (Table 4). Similar to results found using hydrogen gas, a moderate conversion was obtained for the first cycle transfer hydrogenation using ammonium formate at room temperature (Entry 1). However, recycling back through the VFD increased the conversion, with an 89% conversion was achieved on the third cycle (Entry 3). Heating the reaction did not increase conversion (Entry 4).

Previously reported continuous flow hydrogenation systems, using conventional devices, exhibit higher throughput however these systems use high pressure (16-28atm) and higher temperatures (50- 120°C) resulting in a significantly higher energy penalty. This system allows for hydrogenation at ambient pressure and temperature, leading to reduced energy penalty and simpler processing [17-19].

Table 2.4. Continuous flow transfer hydrogenation of **1**

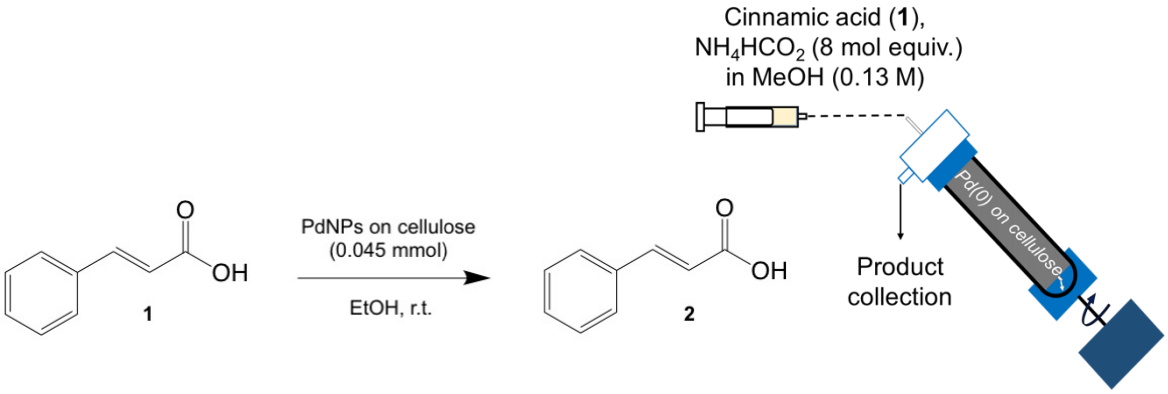

Entry	Temperature (°C)	Cycle	Conversion (%)
1	r.t.	1	35
2	r.t.	2	63
3	r.t.	3	89
4	60	1	34

2.3.4. Catalyst Recycling

Reuse of PdNP@cellulose as a catalyst was investigated under confined mode of operation of the VFD, focusing on the hydrogenation of **1**. After each reaction, the tube containing PdNP@cellulose paper was washed with ethanol three times and used for the next reaction without further treatment. It has been established that PdNP@cellulose paper can be used ten times without loss in any significant catalytic activity (Figure 2.2, Table S2.4, Figure S2.31), and without the need for any complicated post-VFD treatment. Further characterization using SEM, HRTEM, XPS, and XRD showed no change in morphology, chemistry and particle size after 10 re-uses (Figure 2.3 and Figure S2.32-2.36). For catalyst re-use, it is important that the catalyst has no change in morphology or deactivation. This is critical for use in the industry

in order to minimise the time, effort and cost of catalyst recycling and activation. Leaching of palladium was investigated, with fractions of solution collected during a continuous flow hydrogenation reaction and analysed using ICP-MS. Less than 0.1ppm palladium was found in each fraction (Table S2.5). This is an important finding because reducing the levels of palladium in a product to between 2-20ppm is crucial for it to be used in a pharmaceutical context [32].

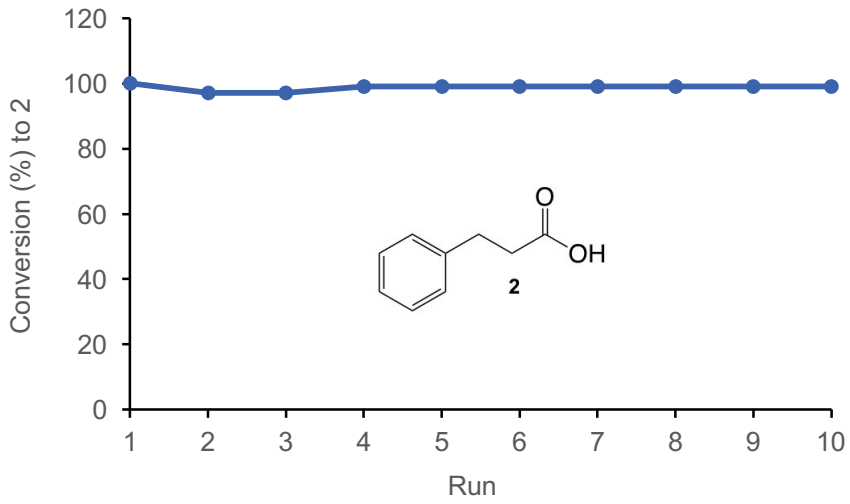

Figure 2.2. Recycling of PdNP@cellulose for confined mode hydrogenation of **1** (0.3 mmol) in EtOH (1.5 mL), with ambient pressure of hydrogen gas 7k rpm, 20 mins, at room temperature, where catalyst is washed with EtOH between runs.

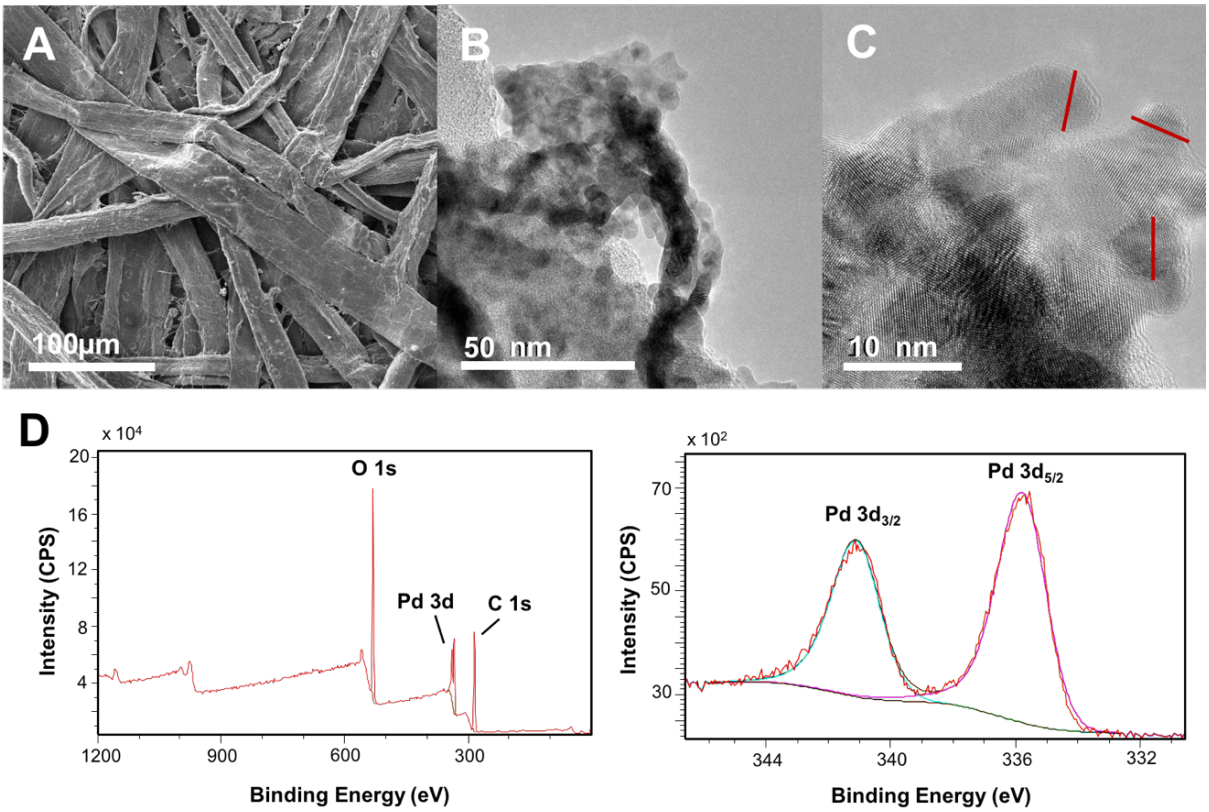

Figure 2.3. SEM image (A), TEM image (B) and high-resolution TEM image (C), XPS spectra (D) of PdNP@cellulose after ten re-uses in the hydrogenation of alkene **1.**

2.4. Conclusion

In summary, a robust, paper-based palladium catalyst for continuous flow hydrogenations has been developed. For any continuous flow reactor, readily available cartridges of transition metal catalysts are critical for a variety of chemical processes. This capability is now realized in the VFD by simply lining the walls of the reaction tube with a sheet of the PdNP@cellulose paper. This catalyst system is easily prepared within minutes and displays excellent catalytic activity and chemoselectivity for reductions in the confined and continuous flow modes of the VFD under ambient pressure and temperature, all important in reducing energy usage and the generation of waste. Industrially important compounds were prepared on a gram scale using this system, where high atom economy, low toxicity and safer

processing is displayed, especially when compared to the conventional vessels and other microfluidic devices which often require high pressures and temperatures. In addition, the VFD is a modular, "plug and play" device that is cheap and easily transportable. This allows for just-in-time production, resulting in reduced storage requirements and improved safety of handling. Effective continuously flow transfer hydrogenation using ammonium formate as the reducing agents was also demonstrated. The PdNP@cellulose paper can be reused with no loss in catalytic activity after 10 recycles and leaching of palladium is minimal. Overall the findings showcase the versatility, efficiency, and robustness of the cellulose paper impregnated with PdNPs for scalable organic processing. Further exploration of this catalyst and reactor system in the continuous synthesis of valuable fine chemicals and pharmaceuticals is anticipated.

2.5. Experimental

2.5.1. Preparation of Palladium Catalyst

Palladium acetate, ($Pd(OAc)_2$ (10mg, 0.045mmol)), was dissolved in dichloromethane (DCM, 1.3mL) (See Figure 2.1). The solution was evenly deposited onto cellulose paper (supplied from Machenerey-Nagel, grade MN617, 20-25 μm pore size, 0.2 mm thickness, cut to 50mm x 140mm size) using a Pasteur pipette and the DCM allowed to evaporate at room temperature for five minutes (Figure 2.1). The $Pd(OAc)_2$ doped cellulose paper was inserted into a 20mm VFD tube, sealed and purged with N_2. The $Pd(OAc)_2$ was reduced by a steady stream of H_2 until the paper had turned black with no yellow colouration visible. The tube was purged with N_2 as to avoid the Pd(0) from potentially reacting with oxygen in the air.

2.5.2. Characterisation of PdNP@cellulose

SEM imaging was performed on a FEI Quanta 450 High Resolution Field Emission SEM, with a voltage of 5kV, and working distance of 10mm. Prior to SEM imaging samples were coated with Pt (10nm) using a Quorumtech K757X sputter coater to avoid charging of the cellulose fibers.

Analysis of XPS samples was performed using a Kratos Axis ULTRA instrument (Thermo Scientific, UK). The XPS measurements were acquired using a Kratos Axis ULTRA X-ray photoelectron spectrometer incorporating a 165mm hemispherical electron energy analyser. The incident radiation was Monochromatic Al Kα X-rays (1486.6 eV) at 150W (15kV, 15mA). Survey scans were taken at an analyser pass energy of 160 eV and multiplex high resolution scans at 20eV. Scanned area is approximately 0.8mm x 0.3mm and the depth is less than 10nm (volume is approx. 2400 cubic microns). Survey scans were carried out over a binding energy range of 1200-0eV with a step size of 1.0eV and a dwell time of 100ms. Narrow high-resolution scans were run with a step size of 0.05eV and a dwell time of 250ms. Base pressure in the analysis chamber was 1.0×10^{-9}torr and during sample analysis 1.0×10^{-8}torr. The spectra was processed using CasaXPS software. C *1s* at 285.0eV was used as the reference peak for calibration.

2.5.3. Confined Mode VFD Hydrogenation Reactions

The catalytic hydrogenation of various substrates for as prepared PdNP@cellulose paper in the VFD was determined using the confined mode of operation of the device. Substrate (0.3mmol) was dissolved in ethanol (1.2mL) and transferred to a 20mm O.D. VFD tube containing PdNP@cellulose paper. The tube was sealed with a rubber stopper, and flushed with N_2. Following this, H_2 gas was added to the VFD tube via a balloon inserted using a syringe, with

a second syringe in place to flush out nitrogen. The exit needle and balloon were removed sequentially before the balloon was completely deflated to provide an atmosphere of hydrogen gas in the VFD reaction tube. After the balloon and syringe were removed the VFD was operated at 7k rpm for 20 mins, with the tube set at 45^{o} tilt angle. After flushing the reaction with N_2 the reaction mixture was removed from the tube and the PdNP@cellulose paper washed with ethanol. All organic liquid was combined and concentrated under vacuum. The reaction conversion was determined using ^{1}H NMR spectroscopy.

2.5.4. Continuous Flow VFD Hydrogenation Reactions

A solution of substrate (1.33mmol) in ethanol (10 ml, 0.13M) was injected via syringe pump, at varying flow rates, into the base of the VFD tube, operating at 7k rpm with a 45° tilt angle. In another jet feed of the VFD, a stream of H_2 gas was introduced so that the flow rate was no more than 0.5L/min. The percentage conversion was detected using ^{1}H NMR spectroscopy.

2.5.5. Confined Mode VFD Transfer Hydrogenation Reactions

Substrate (0.3 mmol), and ammonium formate (2.4mmol, 8 mol equiv.) were dissolved in a methanol (1.5mL) and transferred to a 20 mm O.D. VFD tube containing PdNP@cellulose paper. The tube was sealed with a rubber stopper. The VFD was operated at 7k rpm for 20 mins with the tube inclined at 45^{o} tilt angle. The reaction mixture was removed from the tube and the PdNP@cellulose paper washed with solvent. All organic liquid was combined and concentrated under vacuum. The reaction conversion was determined using ^{1}H NMR spectroscopy.

2.5.6. Continuous Flow VFD Transfer Hydrogenation Reactions

A solution of cinnamic acid (540mg, 3.6mmol), ammonium formate (1.0g, 15.8mmol) in ethanol (10mL, 0.13M) was injected via syringe pump at 0.5mL/min, into the base of the VFD tube, operating at 7k rpm with a 45° tilt angle. A percentage conversion of 35% was detected using ^{1}H NMR spectroscopy (Table S2.3). The reaction solution was taken to 10mL with ethanol and additional ammonium formate (15.8 mmol) dissolved. The solution was fed through the VFD a second time to give a conversion of 63%. The process was repeated a third time to give a conversion of 89% (Figure S2.28).

2.6. Acknowledgments

This work is supported by the Australian Research Council, the Governments of South Australia, the Australian Microscopy & Microanalysis Research Facility and Flinders Analytical. Special thanks to Dr. Alex Duan and Prof. Robert N. Lamb for XPS analysis, Xianlin Qu, Kun Zheng, Prof. Jin Zou for HRTEM analysis, and Dr. Muneer Ahamed for guidance in publication writing.

2.7. References

[1] Busacca, C. A.; Fandrick, D. R.; Song, J. J.; Senanayake, C. H. The Growing Impact of Catalysis in the Pharmaceutical Industry. *Adv*. *Synth*. *Cat*. **2011**, *353*, 1825-1864.

[2] Anastas, P.; Eghbali, N. Green Chemistry: Principles and Practice. *Chem*. *Soc*. *Rev*. **2010**, *39*, 301–312.

[3] Xia, Y. N.; Yang, H.; Campbell, C. T. Nanoparticles for Heterogeneous Catalysis: New Mechanistic Insights. *Acc. Chem. Res*. **2013**, *46*, 1671−1672.

[4] Astruc, D.; Lu, F.; Aranzaes, J. R. Nanoparticles as Recyclable Catalysts: The Frontier between Homogeneous and Heterogeneous Catalysis. *Angew. Chem. Int. Ed*. **2005**, *44*, 7852−7872.

[5] Frost, C. G.; Mutton, L. Heterogeneous Catalytic Synthesis using Microreactor Technology. *Green Chem*., **2010**, *12*, 1687–1703.

[6] Tsubogo, T.; Ishiwata, T.; Kobayashi, S. Asymmetric Carbon-Carbon Bond Formation under Continuous-Flow Conditions with Chiral Heterogeneous Catalysts. *Angew. Chem. Int. Ed*., **2013**, *52*, 6590–6604.

[7] Munirathinam, R.; Huskens, J.; Verboom, W. Supported Catalysis in Continuous-Flow Microreactors. *Adv*. *Synth*. *Catal*., **2015**, *357*, 1093-1123.

[8] Gutmann, B.; Cantillo, D.; Kappe, C. O. Continuous-Flow Technology—a Tool for the Safe Manufacturing of Active Pharmaceutical Ingredients. *Angew. Chem., Int. Ed*. **2015**, *54*, 6688−6728.

[9] Britton, J.; Stubbs, K. A.; Weiss, G. A.; Raston, C. L. Vortex Fluidic Chemical Transformations. *Chem*. *Eur*. *J*., **2017**, *23*, 13270-13278.

[10] Pye, S. J.; Dalgarno, S. J.; Chalker, J. M.; Raston, C. L. Organic Oxidations Promoted in Vortex Driven Thin Films under Continuous Flow. *Green Chem*., **2018**, *20*, 118-124.

[11] Klemm, D.; Heublein, B.; Fink, H. P.; Bohn, A. Cellulose: Fascinating Biopolymer and Sustainable Raw Material. *Angew*. *Chem*., *Int*. *Ed*., **2005**, *44*, 3358–3393.

[12] Li, Y.; Xu, L.; Mao, Z.; Xu, H.; Zhong, Y.; Zhang, L.; Wang, B.; Sui, X. Cellulose Sponge Supported Palladium Nanoparticles as Recyclable Cross-Coupling Catalysts. *ACS Appl*. *Mater*. *Interfaces*. **2017**, *9*, 17155-17162.

[13] Cirtiu, C. M.; Dunlop-Brière, A. F.; Moores, A. Cellulose Nanocrystallites as an Efficient Support for Nanoparticles of Palladium: Application for Catalytic Hydrogenation and Heck Coupling under Mild Conditions. *Green Chem*., **2011**, *13*, 288-291.

[14] Xiao, J.; Lu, Z.; Li, Y. Carboxymethylcellulose-Supported Palladium Nanoparticles Generated in Situ from Palladium(II) Carboxymethylcellulose: An Efficient and Reusable Catalyst for Suzuki–Miyaura and Mizoroki–Heck Reactions. *Ind. Eng. Chem. Res.*, **2015**, *54*, 790-797.

[15] Kaushik, M.; Basu, K.; Benoit, C.; Cirtiu, C. M.; Vali, H.; Moores, A. Cellulose Nanocrystals as Chiral Inducers: Enantioselective Catalysis and Transmission Electron Microscopy 3D Characterization. *J. Am. Chem. Soc.* **2015**, *137*, 6124-6127.

[16] Hornung, C. H.; Nguyen, X.; Carafa, A.; Gardiner, J.; Urban, A.; Fraser, D.; Horne, M. D.; Gunarsegaram, D. R.; Tsanaktsidis, J. Use of Catalytic Static Mixers for Continuous Flow Gas−Liquid and Transfer Hydrogenations in Organic Synthesis. *Org. Process Res. Dev.* **2017**, *21*, 1311-1319.

[17] Mo, Y.; Imbrogno, J.; Zhang, H.; Jensen, K. F. Scalable Thin-Layer Membrane Reactor for Heterogeneous and Homogeneous Catalytic Gas–Liquid Reactions. Green Chem. 2018, 20, 3867-3874.

[18] Hitzler, M. G.; Smail, F. R.; Ross, S. K.; Poliakoff, M. Selective Catalytic Hydrogenation of Organic Compounds in Supercritical Fluids as a Continuous Process. *Org. Process Res. Dev.*, **1998**, *2*, 137-146.

[19] Jensen, R. K.; Thykier, N.; Enevoldsen, M. V.; Lindhardt, A. T. A High Mobility Reactor Unit for R&D Continuous Flow Transfer Hydrogenations. *Org. Process Res. Dev.*, **2017**, *21*, 370-376.

[20] Goszewska, I.; Giziński, D.; Zienkiewicz-Machnik, M.; Lisovytskiy, D.; Nikiforov, K.; Masternak, J.; Śrębowata, A.; Sá, J. A Novel Nano-Palladium Catalyst for Continuous-Flow Chemoselective Hydrogenation Reactions. *Catal. Commun.* **2017**, *94*, 65-68.

[21] Matsuyama, K.; Tanaka, S.; Kato, T.; Okuyama, T.; Muto, H.; Miyamoto, R.; Bai, H. Supercritical Fluid-Assisted Immobilization of Pd Nanoparticles in the Mesopores of Hierarchical Porous SiO2 for Catalytic Applications. *J. Supercrit. Fluids*, **2017**, *130*, 140-146.

[22] Tarnowicz, S.; Alsalahi, W.; Mieczyńska, E.; Trzeciak, A. M.; Heck Arylation of Allyl Alcohol Catalyzed by Pd(0) Nanoparticles. *Tetrahedron*, **2017**, *73*, 5605-5612.

[23] Groppo, E.; Agostini, G.; Borfecchia, E.; Wei, L.; Giannici, F.; Portale, G.; Longo, A.; Lamberti, C. Formation and Growth of Pd Nanoparticles Inside a Highly Cross-Linked Polystyrene Support: Role of the Reducing Agent. *J. Phys. Chem. C*, **2014**, *118*, 8406-8415.

[24] Yasmin, L.; Chen, X.; Stubbs, K. A.; Raston, C. L. Optimising a Vortex Fluidic Device for Controlling Chemical Reactivity and Selectivity. *Sci. Rep.,* **2013**, *3*(2282), 1-12.

[25] Britton, J.; Raston, C. L. Rapid High Conversion of High Free Fatty Acid Feedstock into Biodiesel using Continuous Flow Vortex Fluidics. *RSC Adv*. **2015**, *5*, 2276 – 2280.

[26] Britton, J.; Dalziel, S. B.; Raston C. L. Continuous Flow Fischer Esterifications Harnessing Vibrational-Coupled Thin Film Fluidics. *RSC Adv*. **2015**, 5, 1655 – 1660.

[27] Britton, J.; Raston, C. L. Continuous Flow Vortex Fluidic Production of Biodiesel. *RSC Adv*. **2014**, *4*, 49850 – 49854.

[28] Lawrence, S. A. *Amines: Synthesis, Properties and Applications*, Cambridge University Press: New York, **2004**.

[29] Cotrupe, D. P.; Wellman, W. E.; Burton, P. E. Method for Preparing Dihydroisophorone. Patent No. US 3446850, **1969**.

[30] Clark, J. H.; De bruyn, M.; Constantinou, A.; Moity, L.; McElroy, C. R.; Farmer, T. J.; Duncan, T.; Raverty, W.; Hunt, A. J.; Clark, J. H. Dihydrolevoglucosenone (Cyrene) as a Bio-Based Alternative for Dipolar Aprotic Solvents. *Chem. Comm*., **2014**, *50*, 9650-9652.

[31] Wilson, K. L.; Kennedy, A. R.; Murray, J.; Greatrex, B.; Jamieson, C.; Watson, A. J. Scope and Limitations of a DMF Bio-Alternative within Sonogashira Cross-Coupling and Cacchi-Type Annulation. *Beilstein J. Org. Chem*. **2016**, *12*, 2005-2011.

[32] EMA/CHMP/ICH/353369/2013, *Committee for Human Medicinal Productions: ICH guidline Q3D(R1) on elemental impurities*, European Medicines Agency: Science Medicines Health, Evaluation of Medicines for Human Use; 28 March 2013.

2.8. Supplementary Information

General Consideration

All NMR dta was collected on either a 600 or 400MHz Bruker advance spectrometer using $CDCl_3$ or DMSO-d_6 as the solvent, as specified. Spectra were acquired using a relaxation delay time of 2 seconds. All chemical shifts are presented in ppm using residual solvent as the internal standard. All solvents and reagents were used as received from commercial suppliers, except for *N*-(1-phenylethyl)acetamide which was synthesized from the method stated, using solvents and reagents as supplied from commercial source. Infrared (IR) spectra were recorded on a Perkin Elmer ATR Fourier Transform spectrometer as liquid films, or solid crystals. Absorption maxima (ν_{max}) are reported in wavenumbers (cm^{-1}).

The vortex fluidic device (VFD) modular in nature, thus this device can have many configurations. Unless otherwise specified, throughout this report the following specifications were used. The tube used was a borosilicate glass, 19cm long with a 20mm outer diameter (OD) and a 17mm internal diameter (ID). “Confined mode” refers to the mode of operation where a finite amount of reagent is reacted within the tube, “continuous flow” refers to mode of operation where reagents are delivered via stainless steal jet feed (2mm OD) to the base of the rotating tube, and reaction mixture is collected after exiting the tube. Liquid reagents were delivered using syringe pumps, with a borosilicate glass syringe and plunger, and stainless steel 17 G needles. The rotating tube was always operated at a 45˚ tilt angle (θ).

Thin layer chromatography (TLC) was carried out using aluminum backed sheets coated with 60F254 silica gel. Visualization of the silica plates was achieved using a UV lamp

(254nm). Flash column chromatography was carried out using 40-60mm silica gel, wet packed to a height of 15cm in a 30mm OD column.

GC-MS analysis was performed on an Agilent 7890 gas chromatograph coupled to an Agilent 5975C mass spectrometer and equipped with an Agilent 7693 auto-sampler and an Agilent DB-5MS UI 30m x 0.25mm column with 0.25μm film thickness. Carrier gas was helium at a flow rate of 1mL/min, inlet temperature was 280°C, oven program was 50°C for 4 min; 20°C/min to 290°C, MS interface temperature was 250°C, quadrapole temperature was 150°C, ion source temperature was 230°C and scan range was 43- 350m/z.

2.5.1. Alternative Preparations of Palladium Catalyst

Palladium acetate, ($Pd(OAc)_2$ (10mg, 0.045mmol)), was dissolved in dichloromethane (DCM, 1.3mL) (See Figure S2a). The solution was evenly deposited onto cellulose paper (supplied from Machenerey-Nagel, grade MN617, 20-25 μm pore size, 0.2mm thickness, cut to 50mm x 140mm size) using a Pasteur pipette and the DCM allowed to evaporate at room temperature for five minutes (Figure S2b).

Dry H_2 Reduction: The $Pd(OAc)_2$ doped cellulose paper was inserted into a 20 mm VFD tube, sealed and purged with N_2. The $Pd(OAc)_2$ was reduced by a steady stream of H_2 until the paper had turned black with no yellow colouration visible. The tube was purged with N_2 as to avoid the Pd(0) from potentially reacting with oxygen in the air.

Wet H_2 Reduction: The $Pd(OAc)_2$ doped cellulose paper was inserted into a 20mm VFD tube and dampened with distilled water. The tube was sealed and purged with N_2. The $Pd(OAc)_2$ was reduced by a steady stream of H_2 until the paper had turned black with no yellow

colouration visible. The tube was purged with N_2 as to avoid the now highly reactive Pd(0) from reacting with oxygen in the air in the presence of combustible cellulose.

Thermal Reduction: The $Pd(OAc)_2$ doped cellulose paper was placed in an oven at 150°C for 14h.

Scanning Electron Microscopy (SEM)

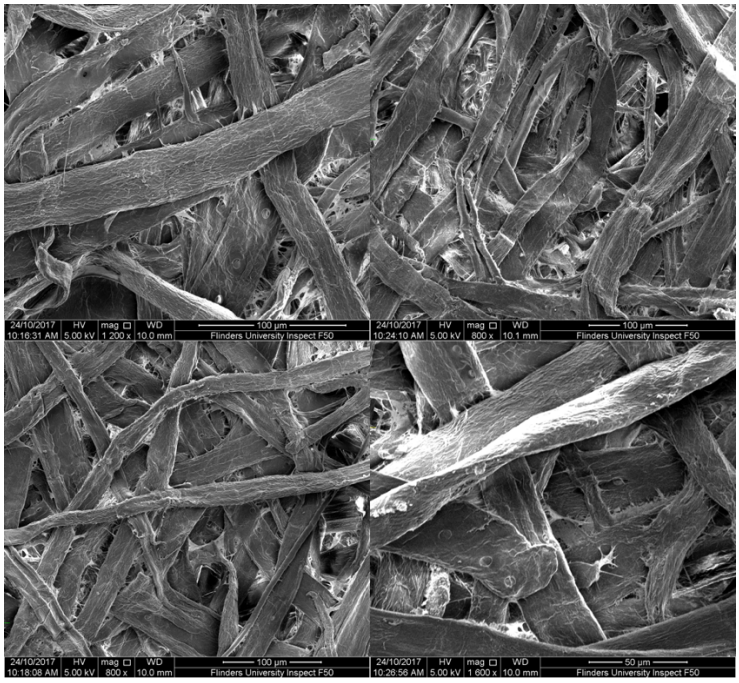

Figure S2.1. SEM images of as recieved cellulose paper, supplied from Machenerey-Nagel, grade MN617, 20-25µm pore size, 0.2 mm thickness, coated with a 10nm layer of Pt.

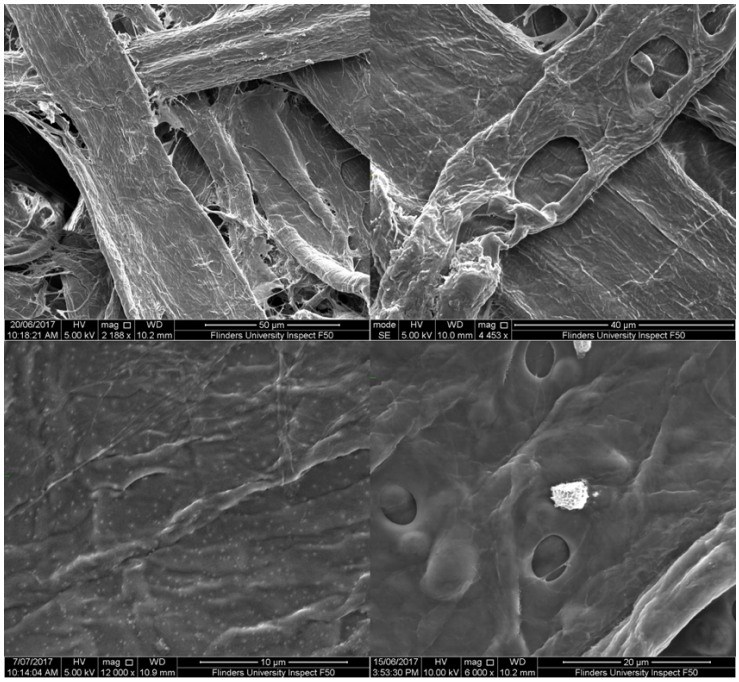

Figure S2.2. SEM images of cellulose paper soaked with $Pd(OAc)_2$ in methylene chloride, then dried, and treated with H_2 gas at ambient pressure and room temperature, coated with a 10nm layer of Pt.

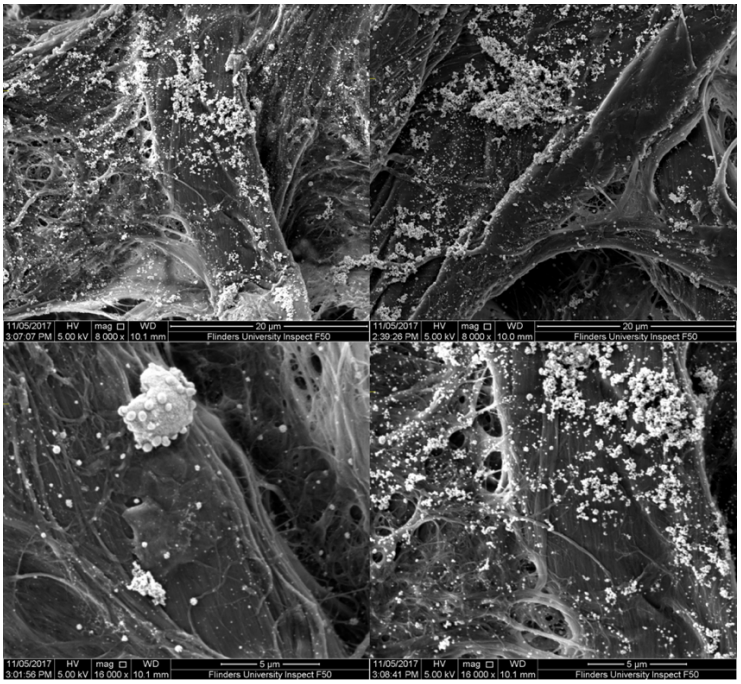

Figure S2.3. SEM images of cellulose paper soaked with $Pd(OAc)_2$ in methylene chloride and dried, then soaked with water and treated with H_2 gas at ambient pressure and room temperature, coated with a 10nm layer of Pt.

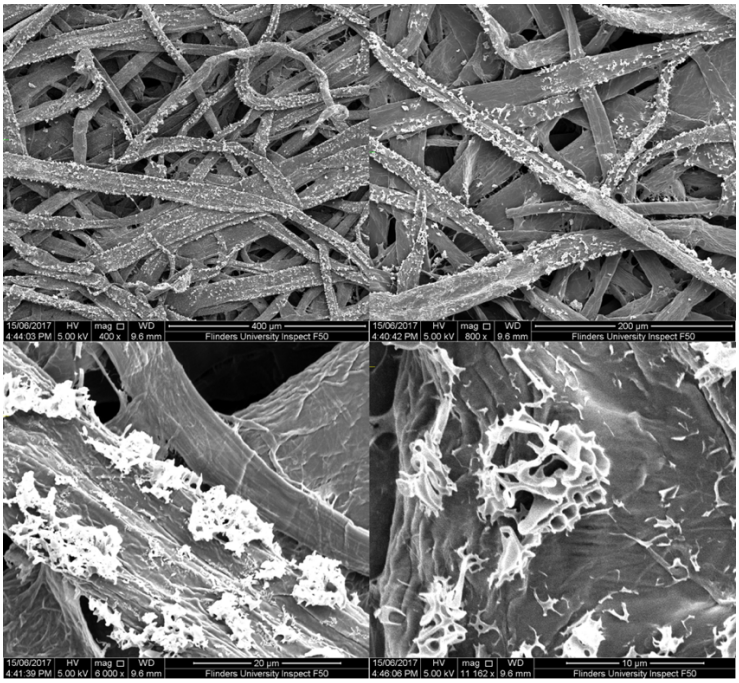

Figure S2.4. SEM images of PdNPs@cellulose formed by heating cellulose paper with impreganted $Pd(OAc)_2$ at 150°C for 14h, coated with a 10nm layer of Pt.

Energy Dispersive X-Ray (EDX) Analysis

This revealed the presence of palladium, as indicated by the detection of the Pd $L\alpha_1$, $L\beta_1$, and $L\beta_2$ X-ray emissions at 3 KeV.

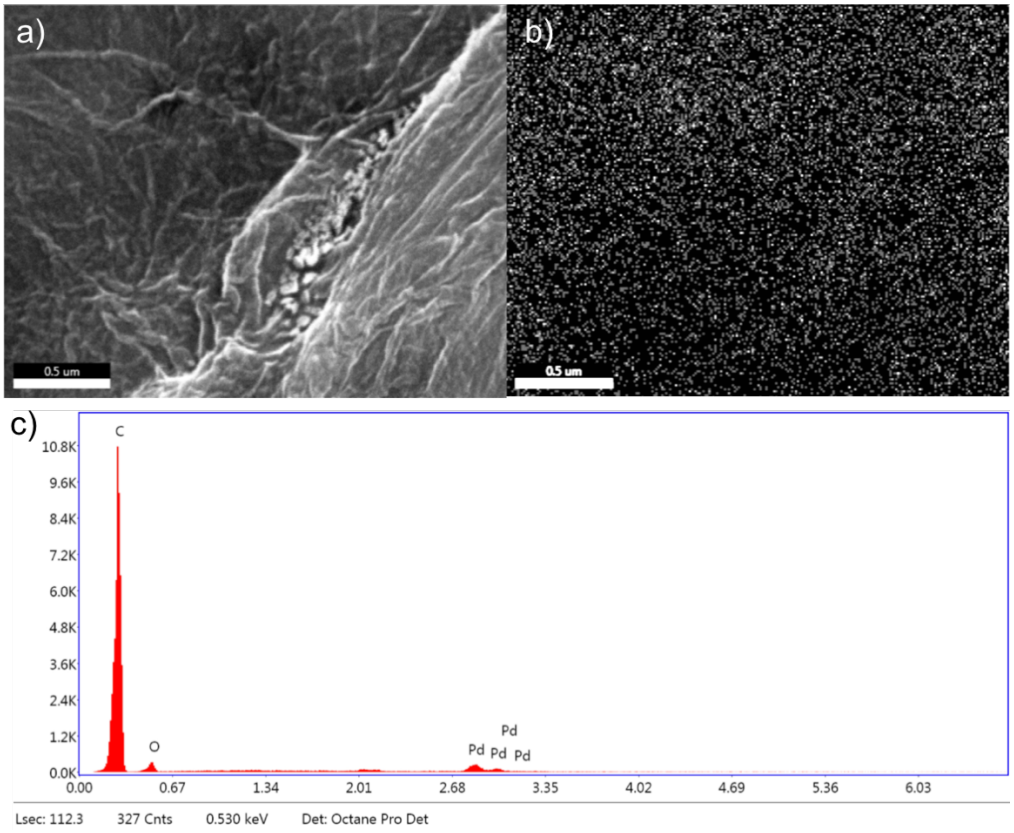

Figure S2.5. EDX analysis mapping for PdNP@cellulose prepared as for Figure S5 prior to coating with Pt. (a) Image of region analysed. (b) Pd counts detected. (c) Spectrum of elements detected.

X-ray Photoelectron Spectroscopy (XPS)

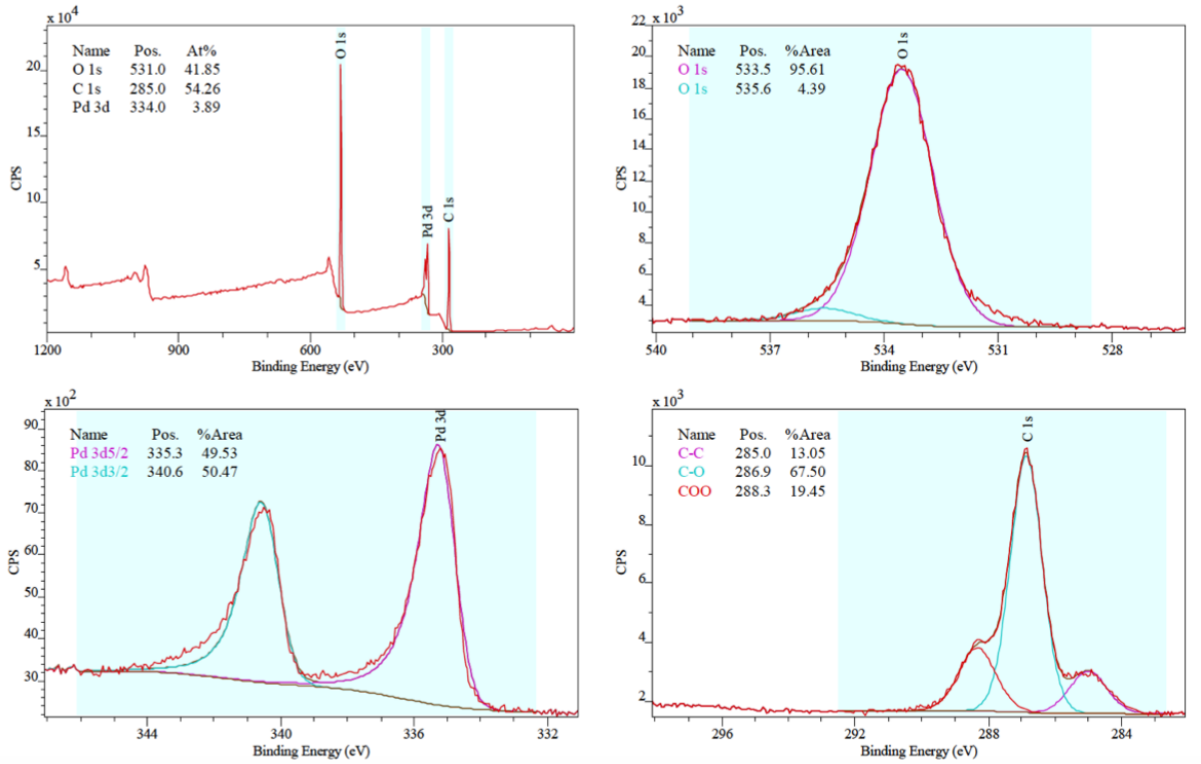

Figure S2.6. XPS Spectra of PdNP@cellulose prepared by soaking cellulose with $Pd(OAc)_2$ in methylene chloride and dried, then soaked with water and treated with H_2 gas at ambient pressure and room temperature.

X-ray Diffraction (XRD)

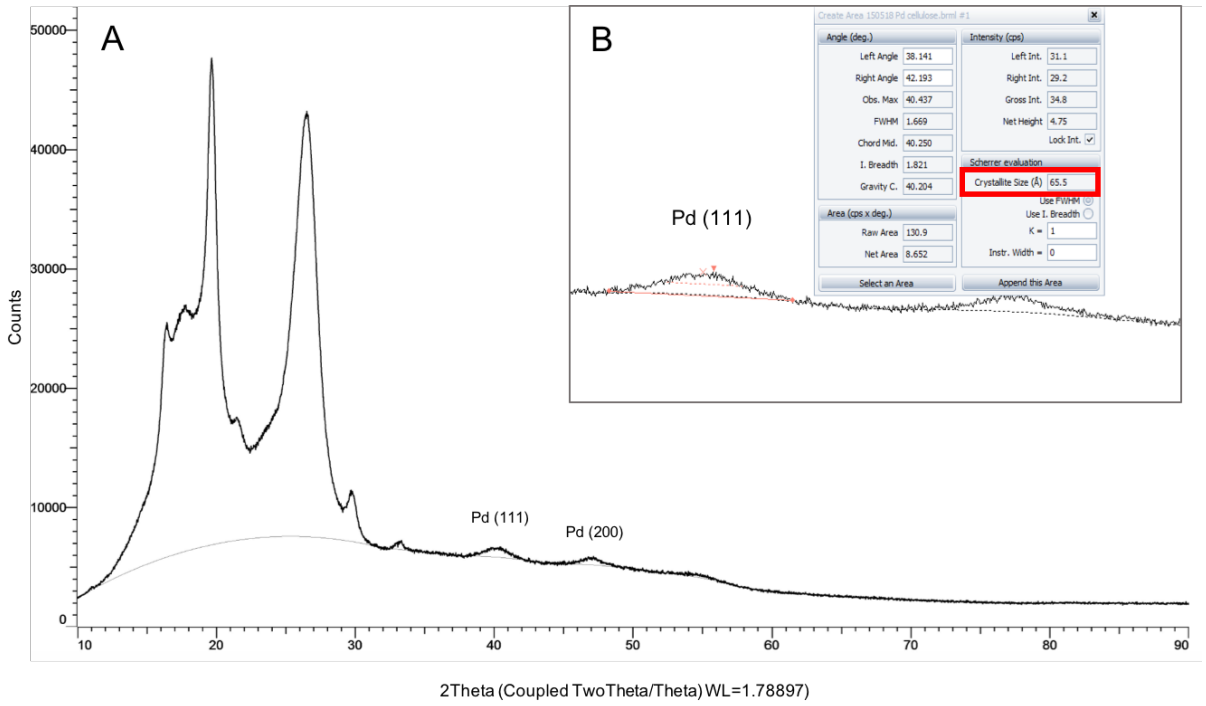

Figure S2.7. (A) XRD pattern of PdNP@cellulose prepared by soaking cellulose with $Pd(OAc)_2$ in methylene chloride and dried, then soaked with water and treated with H_2 gas at ambient pressure and room temperature. (B) Area of the peak corresponding to Pd (111) and the corresponding Scherrer evaluation showing a crystallite size of 65.5Å (6.6 nm).

High Resolution Transmission Electron Microscopy (HRTEM)

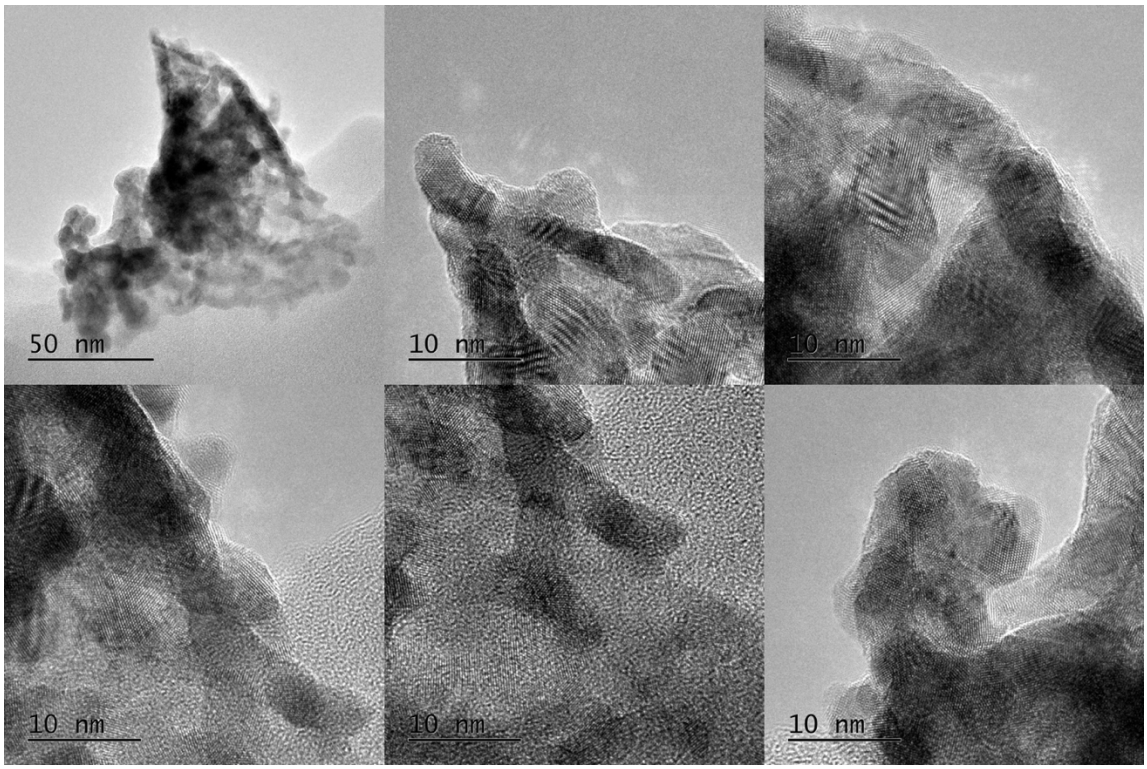

Figure S2.8. HRTEM images of PdNP@cellulose prepared by soaking cellulose with $Pd(OAc)_2$ in methylene chloride and dried, then soaked with water and treated with H_2 gas at ambient pressure and room temperature, prior to use in hydrogenation reactions.

Fourier-Transform Infrared Spectroscopy (FTIR)

The FTIR spectra was obtained for the pure cellulose, the cellulose after $Pd(OAc)_2$ deposition and dichloromethane evaporation, and the PdNP@cellulose after reduction of $Pd(OAc)_2$ (Figure S11). The band, occurring at 1650cm^{-1}, can be observed in the spectra for the cellulose supported $Pd(OAc)_2$ (green line), which corresponds to the carbonyl bond in the acetate ligands. This band disappears in the spectra for the PdNP@cellulose (blue line), which indicates the acetate ligands are no longer present. This result suggests during the reduction of $Pd(OAc)_2$ to Pd(0) the acetate evaporates off as acetic acid.

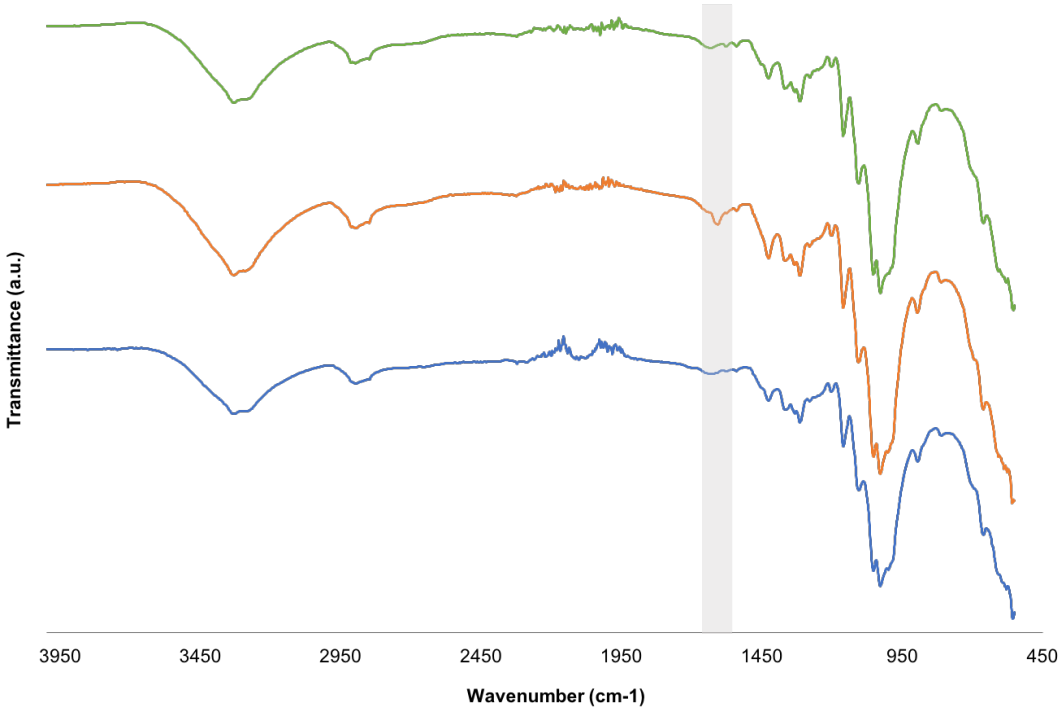

Figure S2.9. FTIR spectrum of pure cellulose paper (green line), cellulose supported $Pd(OAc)_2$ (orange line), and PdNP@cellulose (blue line).

Hydrogenation of Cinnamic Acid

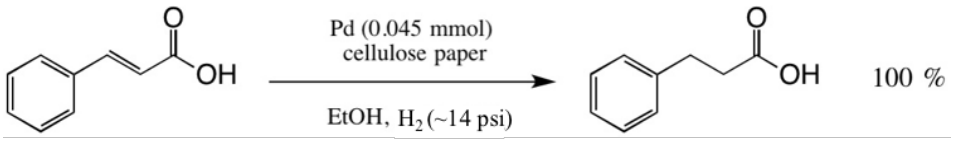

Scheme S2.1. Hydrogenation of cinnamic acid.

The hydrogenation of cinnamic acid was achieved in 100% yield to 3-phenylpropanoic acid. m.p. 47-49°C [Lit m.p. 44-46°C].[33] ^{1}H NMR (600 MHz, DMSO-d_6) δ 7.30 (t, J = 7.6 Hz, 2H), 7.21 (m, J = 7.5 Hz, 3H), 2.97 (t, J = 7.8 Hz, 2H), 2.69 (t, J = 7.8 Hz, 2H). ^{13}C NMR (150 MHz, DMSO-d_6) δ 173.8 ($\underline{C}O_2H$), 140.9 (4° Ar), 128.3 (2 x Ar), 128.2 (2 x Ar), 125.9 (Ar),

35.3 (CH_2), 30.4 (CH_2). IR (υ_{max}, crystals ATR): 3029, 1693, 1602, 1584, 1496, 1453, 1427, 1408, 1301, 1218, 1001, 930, 700 cm^{-1}. MS $[M]^{\bullet+}$ *m/z*: 150. Spectroscopic data was consistent with that previously reported in the literature [1].

Hydrogenation of 4-Nitrophenol

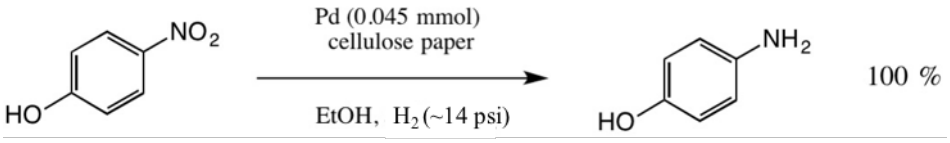

Scheme S2.2. Hydrogenation of 4-nitrophenol.

The hydrogenation of 4-nitrophenol was achieved in 100% yield to 4-aminophenol. m.p. 177-181°C [Lit m.p. 187°C].[34] ^{1}H NMR (600 MHz, DMSO-d_6) δ 8.31 (s, 1H), 6.46 (d, J = 8.3 Hz, 2H), 6.41 (d, J = 8.3 Hz, 2H), 4.46 (s, 1H). ^{13}C NMR (150 MHz, DMSO-d_6) δ 148.2 (Ar-OH), 140.6 (Ar-NH_2), 115.5 (2 x Ar), 115.2 (2 x Ar). IR (υ_{max}, crystals ATR): 3339, 3280, 1614, 1593, 1508, 1470, 1256, 1235, 1167, 1092, 822, 749. MS $[M]^{\bullet+}$ *m/z*: 139. This compound had spectra previously reported in the literature [2].

Hydrogenation of Benzophenone

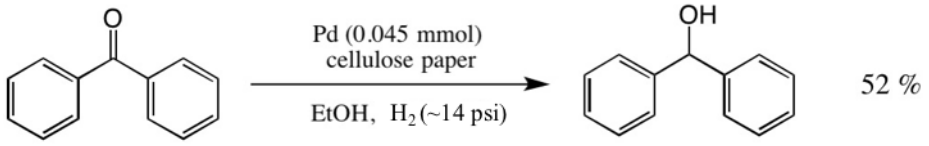

Scheme S2.3. Hydrogenation of benzophenone.

The hydrogenation of benzophenone was achieved in 52% yield (67% conversion) to diphenylmethanol, with the crude product recrystallized from hexane. m.p. 66-68 °C [Lit m.p. 65-66 °C].[35] ^{1}H NMR (600 MHz, DMSO-d_6) δ 7.39 – 7.34 (m, 2H), 7.29 (t, J = 7.6 Hz, 2H),

7.19 (t, J = 7.3 Hz, 1H), 5.86 (d, J = 3.9 Hz, 1H), 5.69 (d, J = 3.9 Hz, 1H). ^{13}C NMR (151 MHz, DMSO-d_6) δ 146.2 (2 x 4°Ar), 128.5 (4 x Ar), 127.1 (2 x Ar), 126.7 (4 x Ar), 74.7 (CHOH). IR (υ_{max}, crystals ATR): 3380, 1494, 1446, 1017, 734, 695. MS $[M]^{\bullet+}$ *m/z*: 184. Spectroscopic data was consistent with that previously reported in the literature [3].

Hydrogenation of N-(1-Phenylvinyl)acetamide

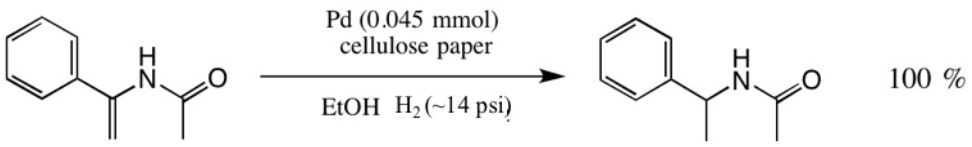

Scheme S2.4. Hydrogenation of N-(1-phenylvinyl)acetamide.

The reduction of N-(1-Phenylvinyl)acetamide was achieved in 100% yield to N-(1-Phenylethyl)acetamide. m.p. 71-73 °C [Lit. m.p. 72-73 °C] [4]. ^{1}H NMR (600 MHz, DMSO-d_6) δ 8.27 (d, J = 8.1 Hz, 1H), 7.34 – 7.27 (m, 4H), 7.21 (td, J = 6.1, 2.8 Hz, 1H), 4.90 (p, J = 7.2 Hz, 1H), 1.84 (s, 3H), 1.33 (d, J = 7.0 Hz, 3H). ^{13}C NMR (151 MHz, DMSO) δ 168.2 (C=O), 144.8 (4° Ar), 128.2 (2x Ar), 126.5 (Ar), 125.9 (2x Ar), 47.7 (C-N), 22.7 (CH_3), 22.5 (CH_3). IR (υ_{max}, crystals ATR): 3280, 1645, 1547, 1449, 750, 698. MS $[M]^{\bullet+}$ *m/z*: 163. Spectroscopic data was consistent with that previously reported in the literature [5].

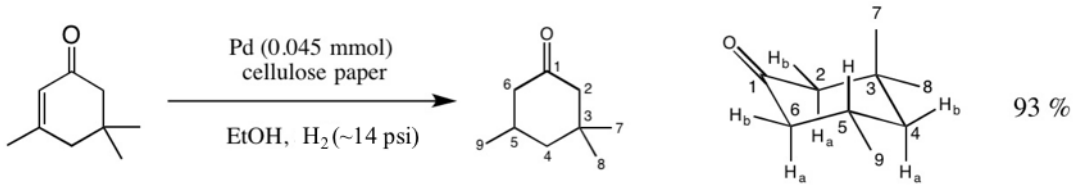

Scheme S2.5. Hydrogenation of isophorone.

The reduction of isophorone was achieved in 93% conversion to 3,3,5-trimethylcyclohexanone. ^{1}H NMR (600 MHz, $CDCl_3$) δ 2.31 (ddt, *J* = 13.5, 4.1, 2.0 Hz, 1H), 2.15 (d, *J* = 13.4 Hz, 1H), 2.05 (dt, *J* = 13.6, 2.4 Hz, 1H), 1.92 – 1.84 (m, 1H), 1.58 (ddt, *J* = 13.4, 4.0, 2.2 Hz, 1H), 1.29 (t, *J* = 12.8 Hz, 1H), 1.05 (s, 3H), 1.01 (d, *J* = 6.4 Hz, 3H), 0.88 (s, 3H). ^{13}C NMR (151 MHz, $CDCl_3$) δ 212.2 (C=O), 54.4 (CH_2), 49.4 (CH_2), 47.5 (CH_2), 35.5 (-C-), 32.3 (CH_3), 29.9 (CH), 26.0 (CH_3), 22.6(CH_3). IR (υ_{max}, liquid ATR): 2935, 1693, 1408, 1301, 1219, 930, 700. MS $[M]^{\bullet+}$ *m/z*: 140. Spectroscopic data was consistent with that previously reported in the literature [6].

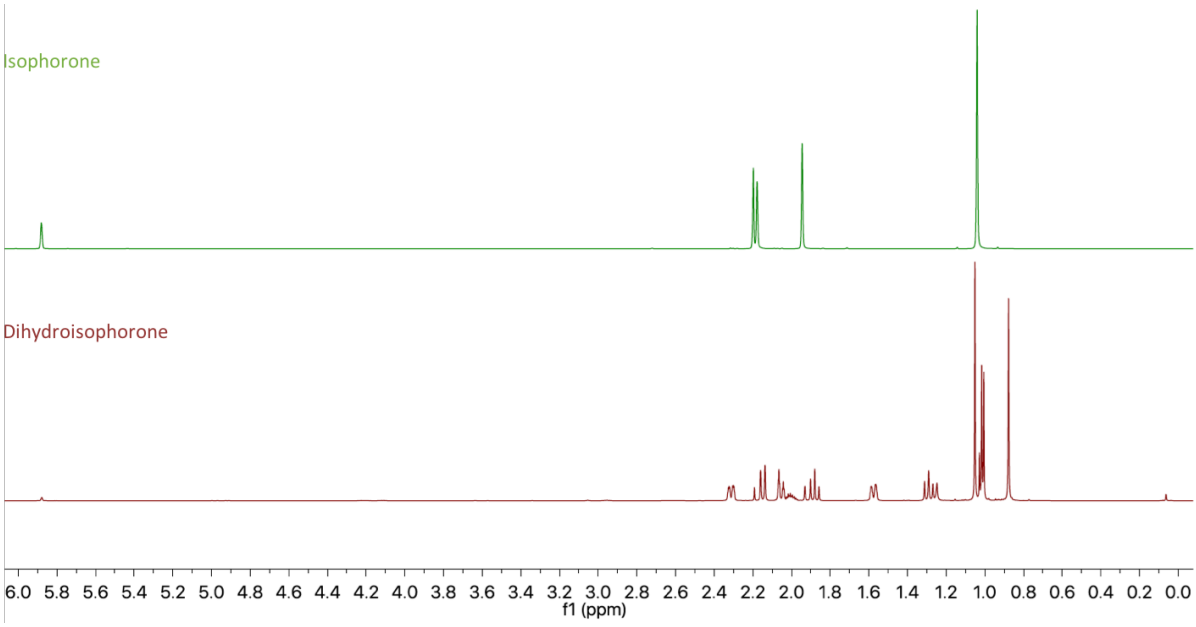

Figure S2.10. ^{1}H NMR spectra of isophorone (top) and dihydroisophorone (93 %) containing residual starting material (bottom).

Selective Hydrogenation of (-)-Levoglucosenone

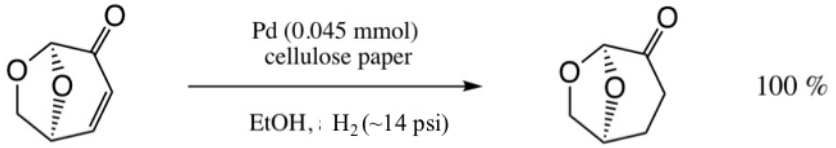

Scheme S2.6. Hydrogenation of (-)-levoglucosenone.

The reduction of (-)-levoglucosenone (provided by Circa Pty Ltd) was achieved in 100% conversion to Cyrene. ^{1}H NMR (600 MHz, $CDCl_3$) δ 5.11 (s, 1H), 4.70 (t, J = 4.6 Hz, 1H), 4.04 (dd, J = 7.4, 1.0 Hz, 1H), 3.96 (ddd, J = 7.1, 5.1, 1.6 Hz, 1H), 2.65 (dddd, J = 16.5, 11.7, 8.6, 0.7 Hz, 1H), 2.39 (ddq, J = 16.5, 7.0, 1.2 Hz, 1H), 2.31 (tddd, J = 12.3, 7.0, 3.8, 1.6 Hz, 1H), 2.02 (dddt, J = 13.9, 8.6, 1.8, 0.9 Hz, 1H). ^{13}C NMR (151 MHz, $CDCl_3$) δ 200.46, 101.56,

73.27, 73.21, 67.62, 31.17, 30.02, 29.95. IR (υ_{max}, liquid ATR): 2962, 2903, 1742, 1724,1699, 1110, 986, 883. MS $[M]^{\bullet+}$ *m/z*: 128. Spectroscopic data was consistent with that previously reported in the literature [7].

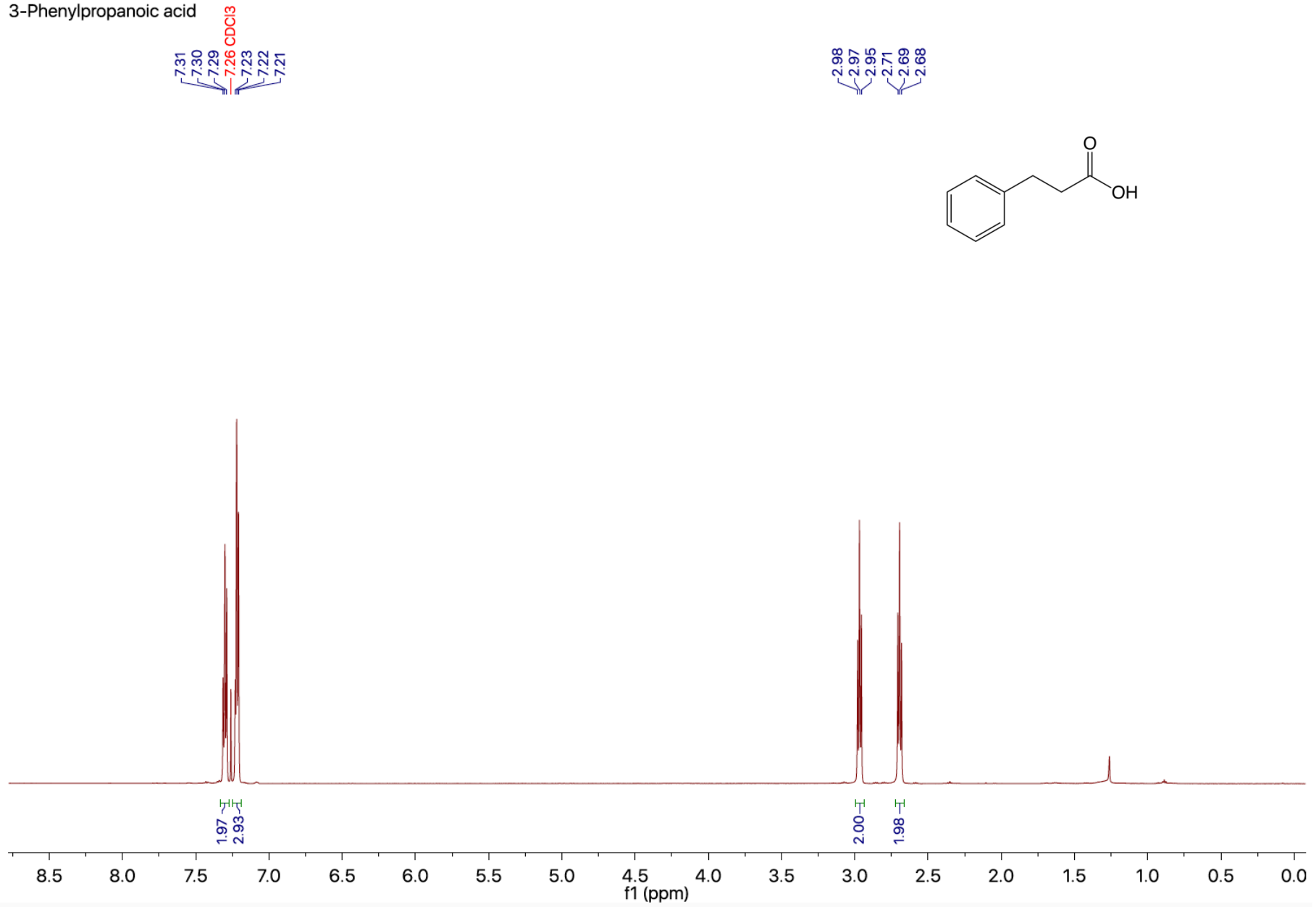

Figure S2.11. ^{1}H NMR spectrum of **2** from the hydrogenation of **1**.

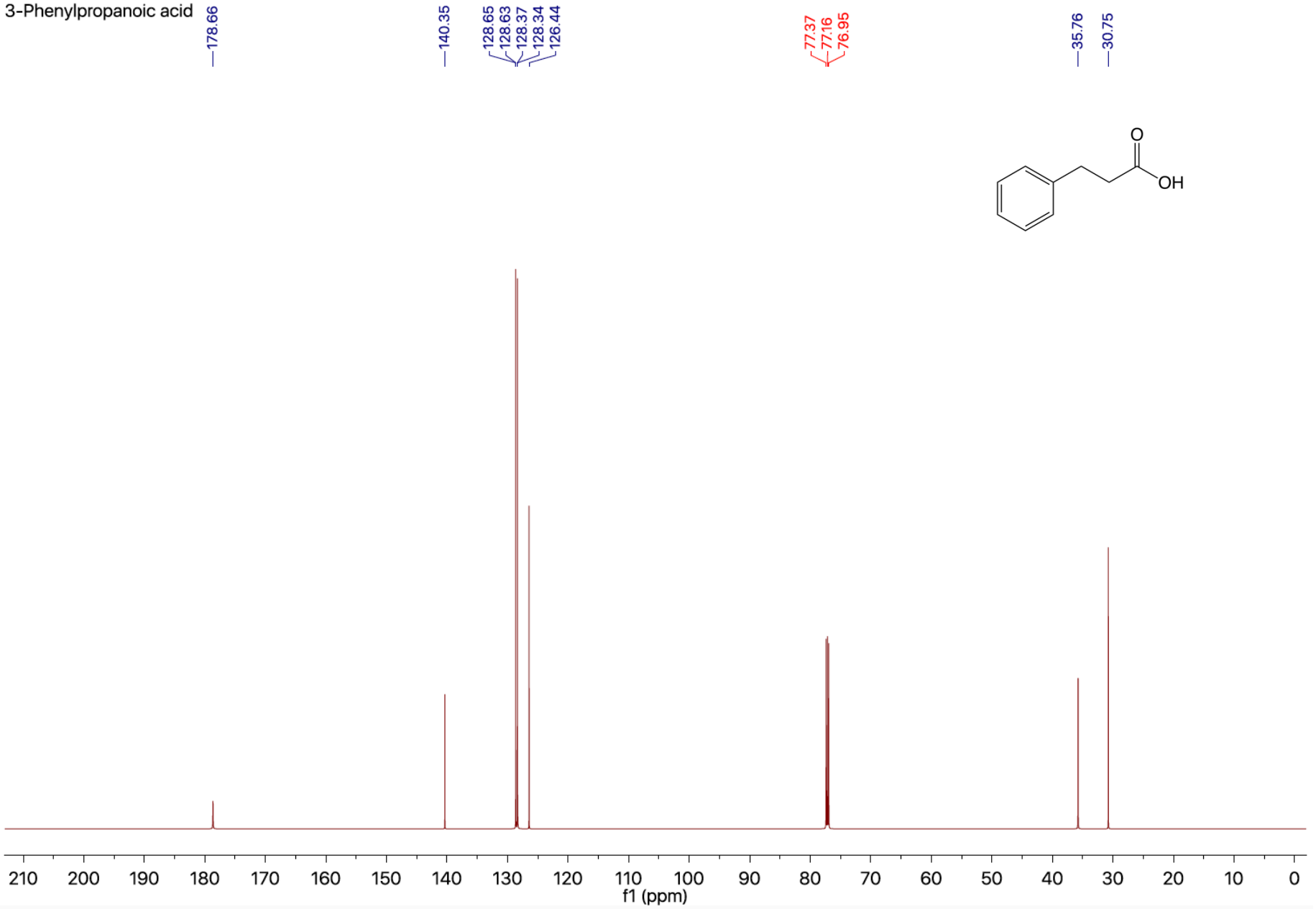

Figure S2.12. ^{13}C NMR spectrum of **2** from the hydrogenation of **1**.

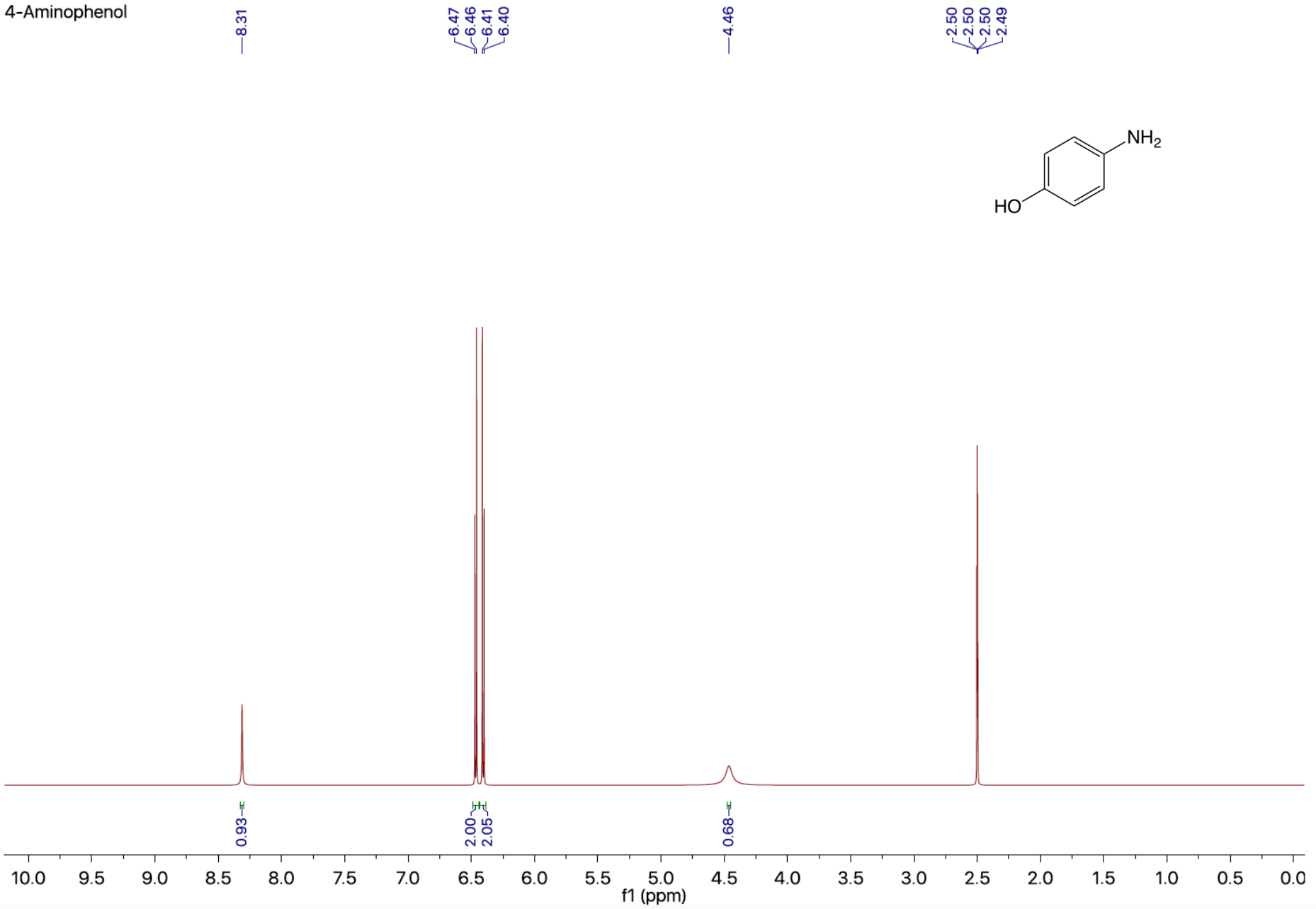

Figure S2.13. ^{1}H NMR spectrum of **4** from the hydrogenation of **3**.

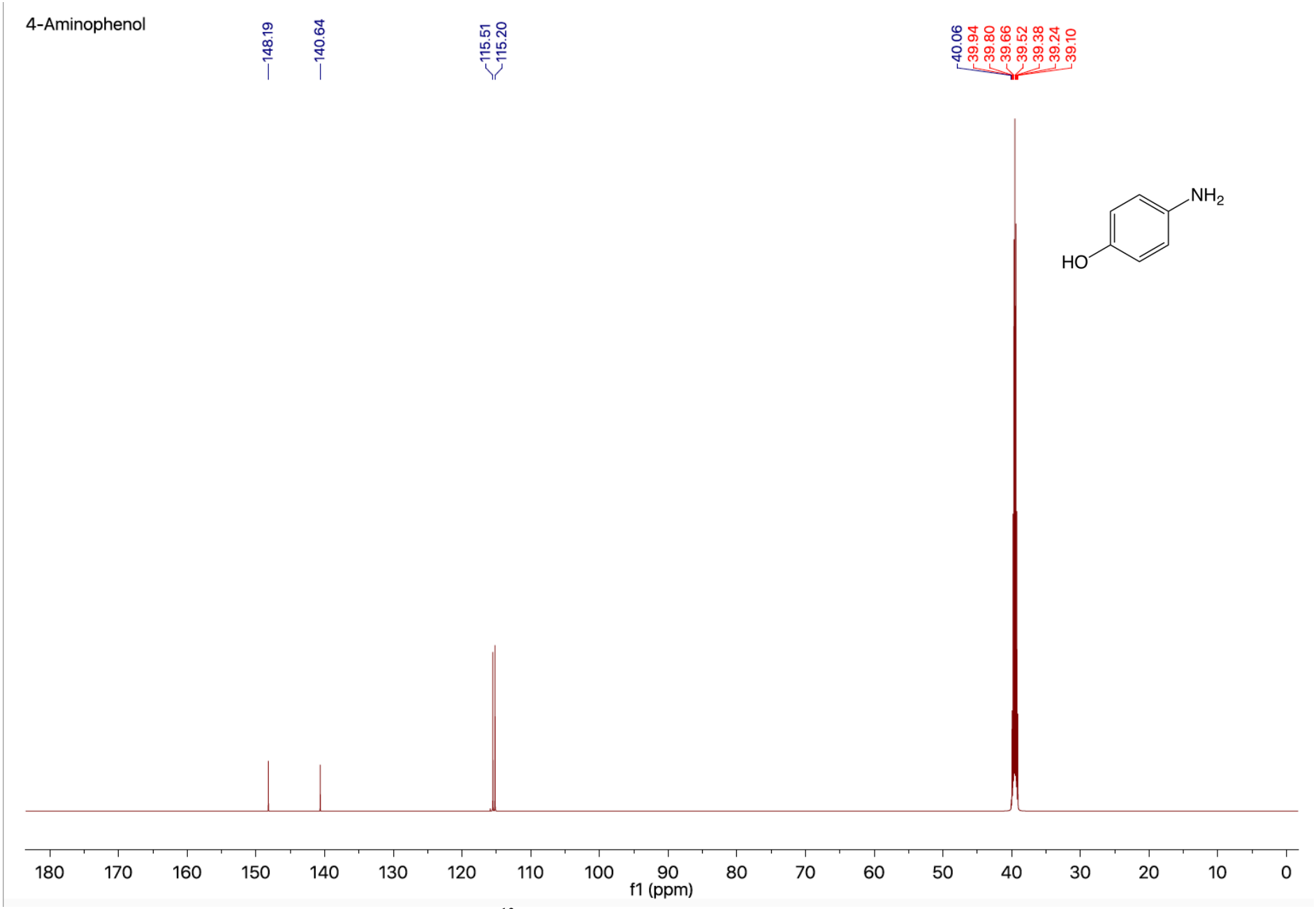

Figure S2.14. ^{13}C NMR spectrum of **4** from the hydrogenation of **3**.

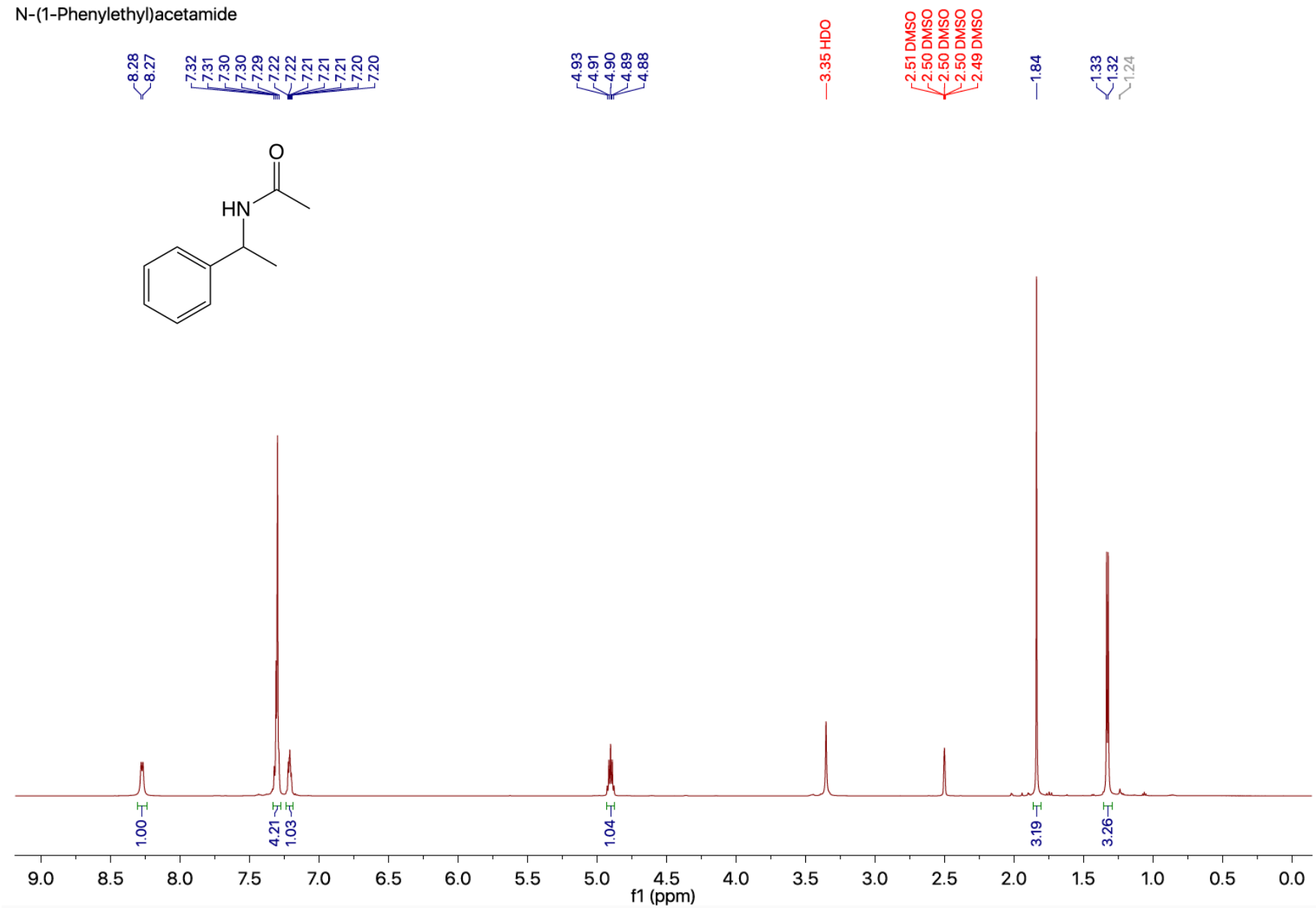

Figure S2.15. ^{1}H NMR spectrum of **6** from the hydrogenation of **5**.

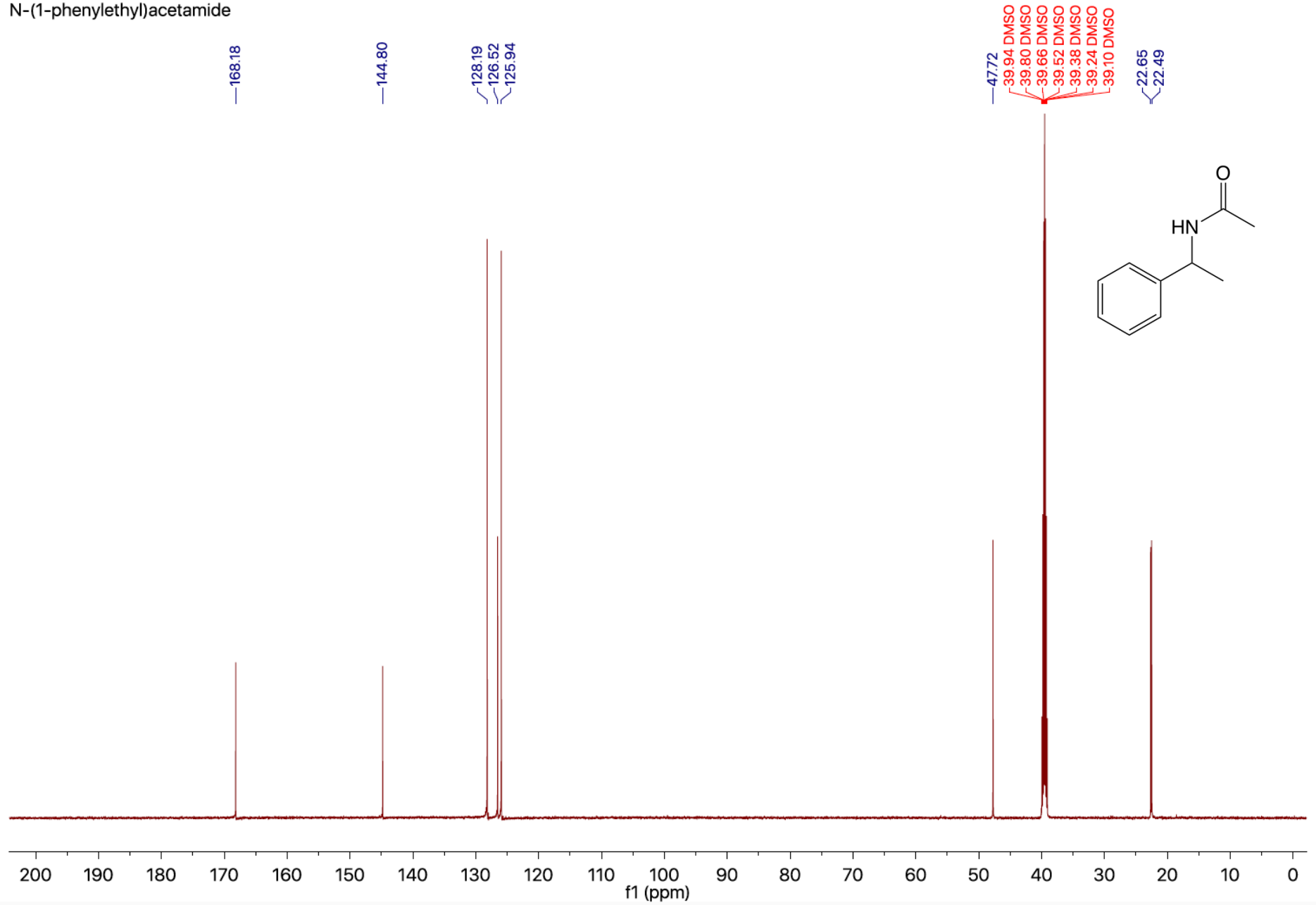

Figure S2.16. ^{13}C NMR spectrum of **6** from the hydrogenation of **5**.

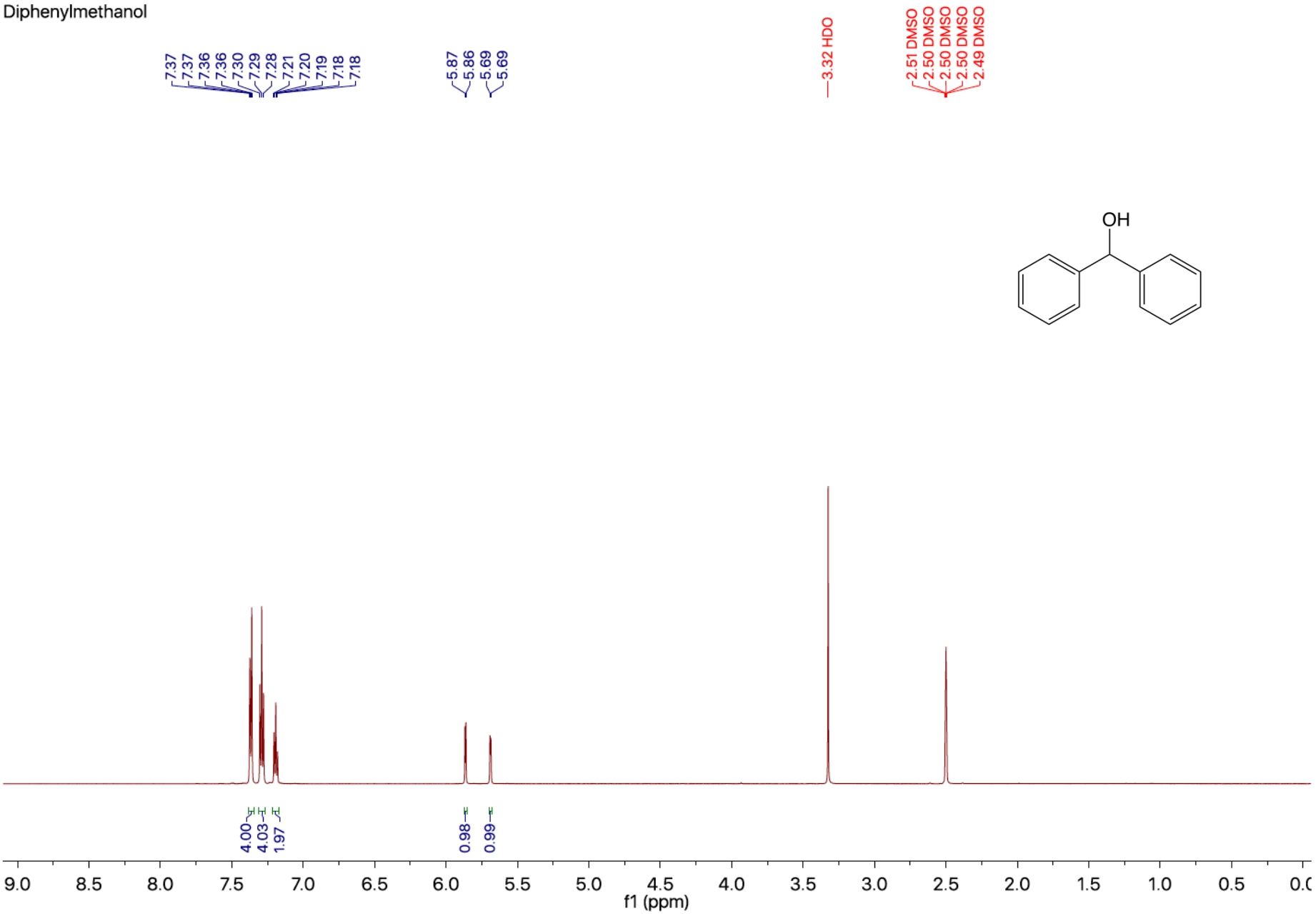

Figure S2.17. ^{1}H NMR spectrum of **8** from the hydrogenation of **7**.

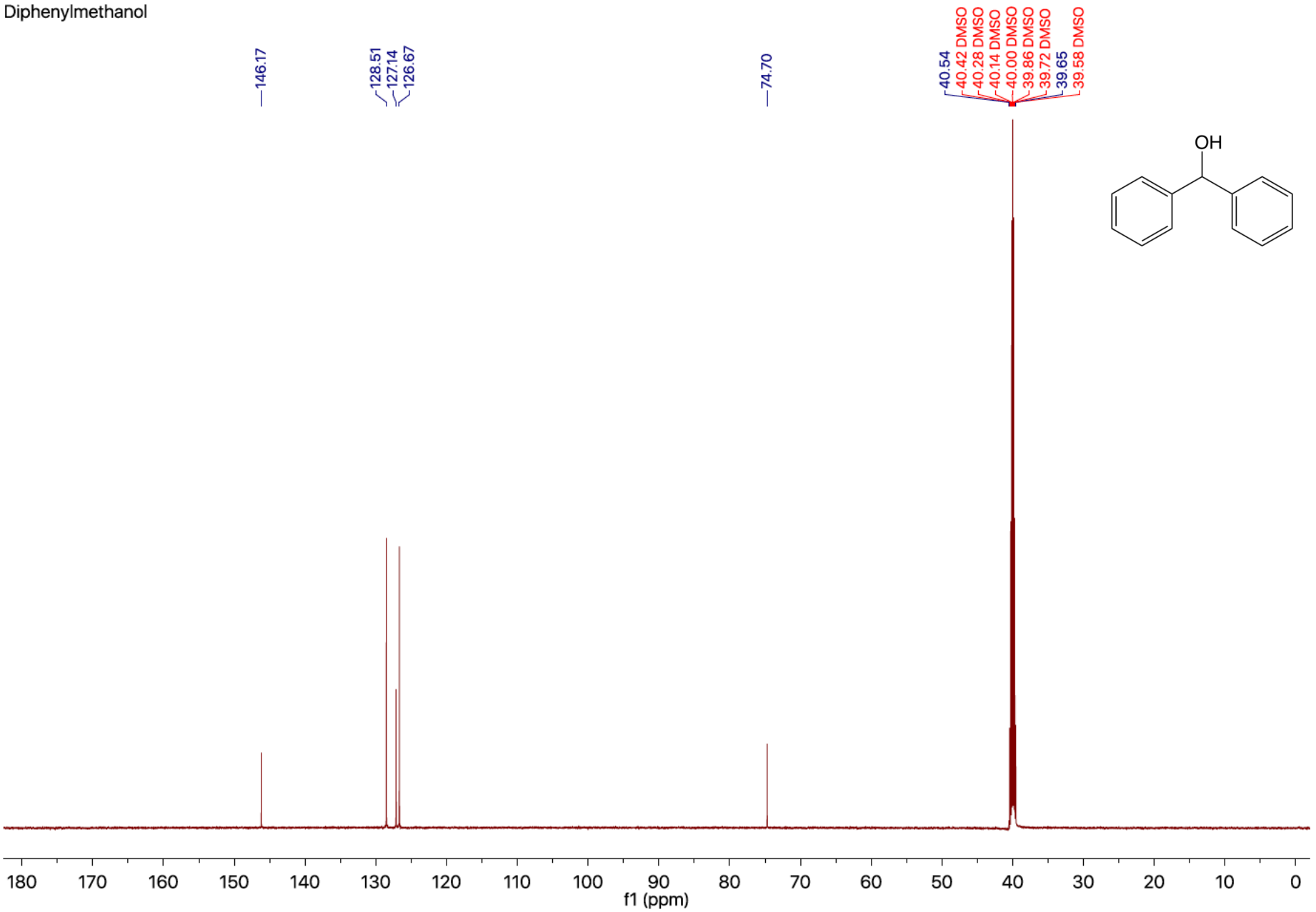

Figure S2.18. ^{13}C NMR spectrum of **8** from the hydrogenation of **7**.

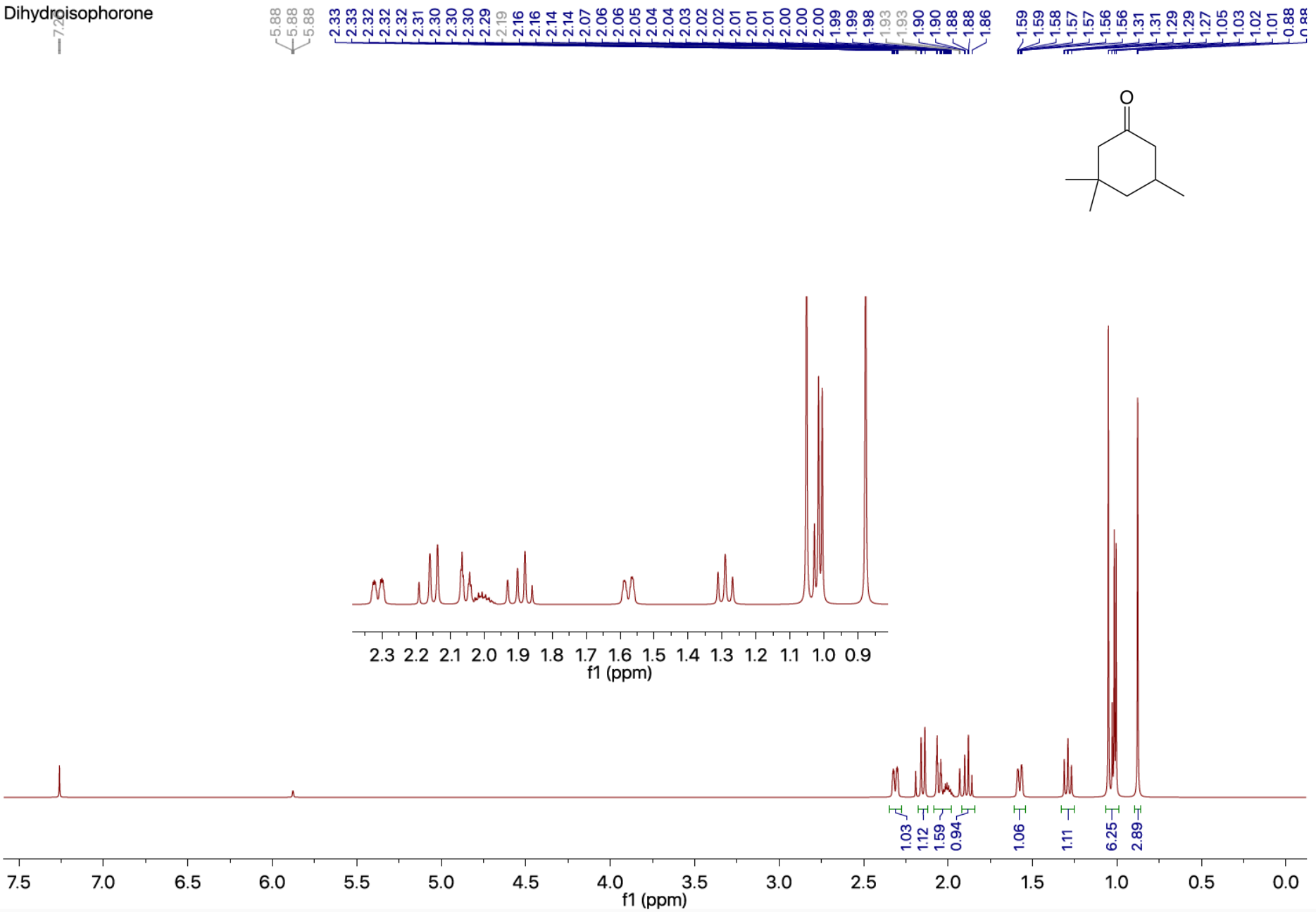

Figure S2.19. ^{1}H NMR spectrum of **10** from the hydrogenation of **9**.

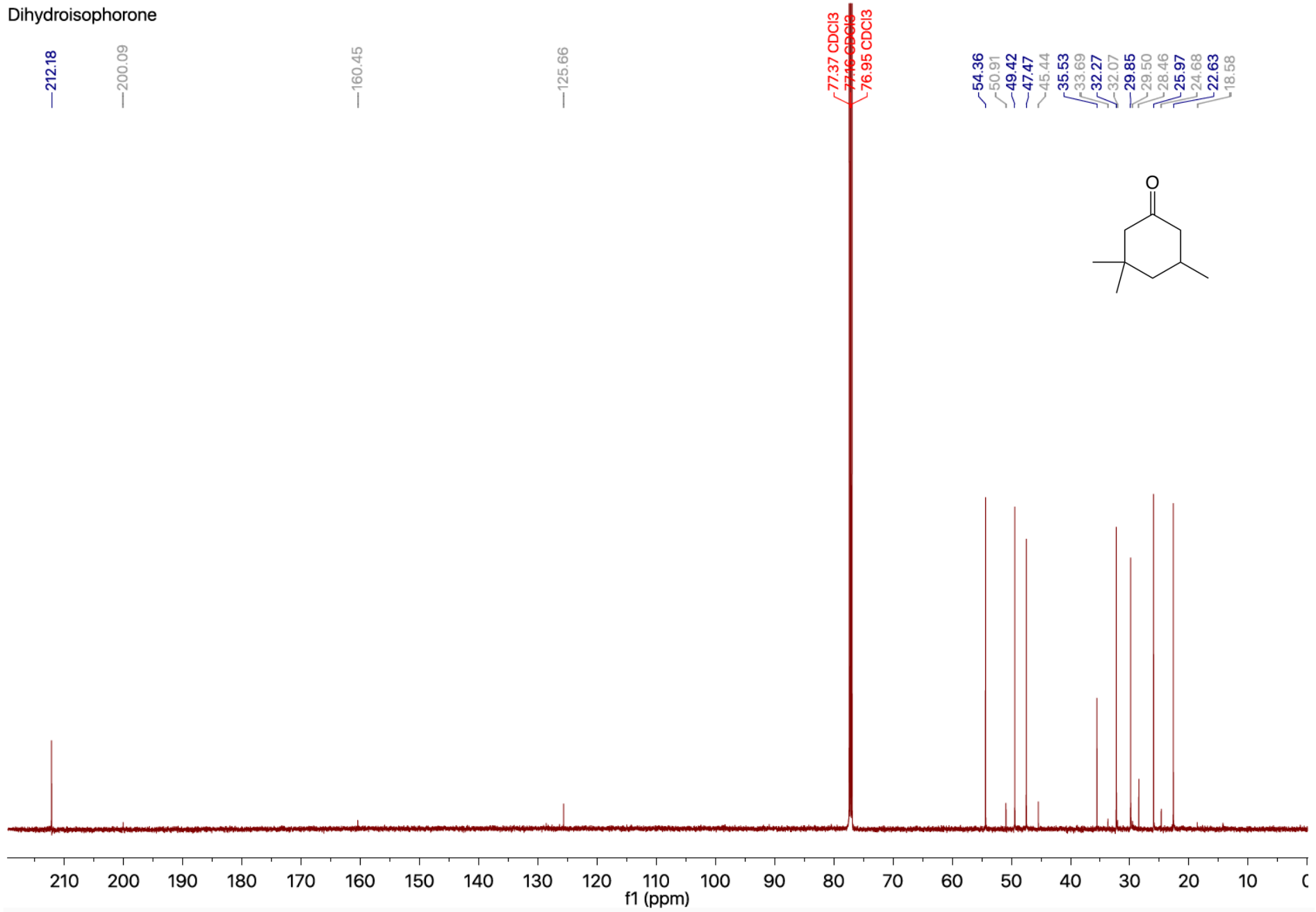

Figure S2.20. ^{13}C NMR spectrum of **10** from the hydrogenation of **9**.

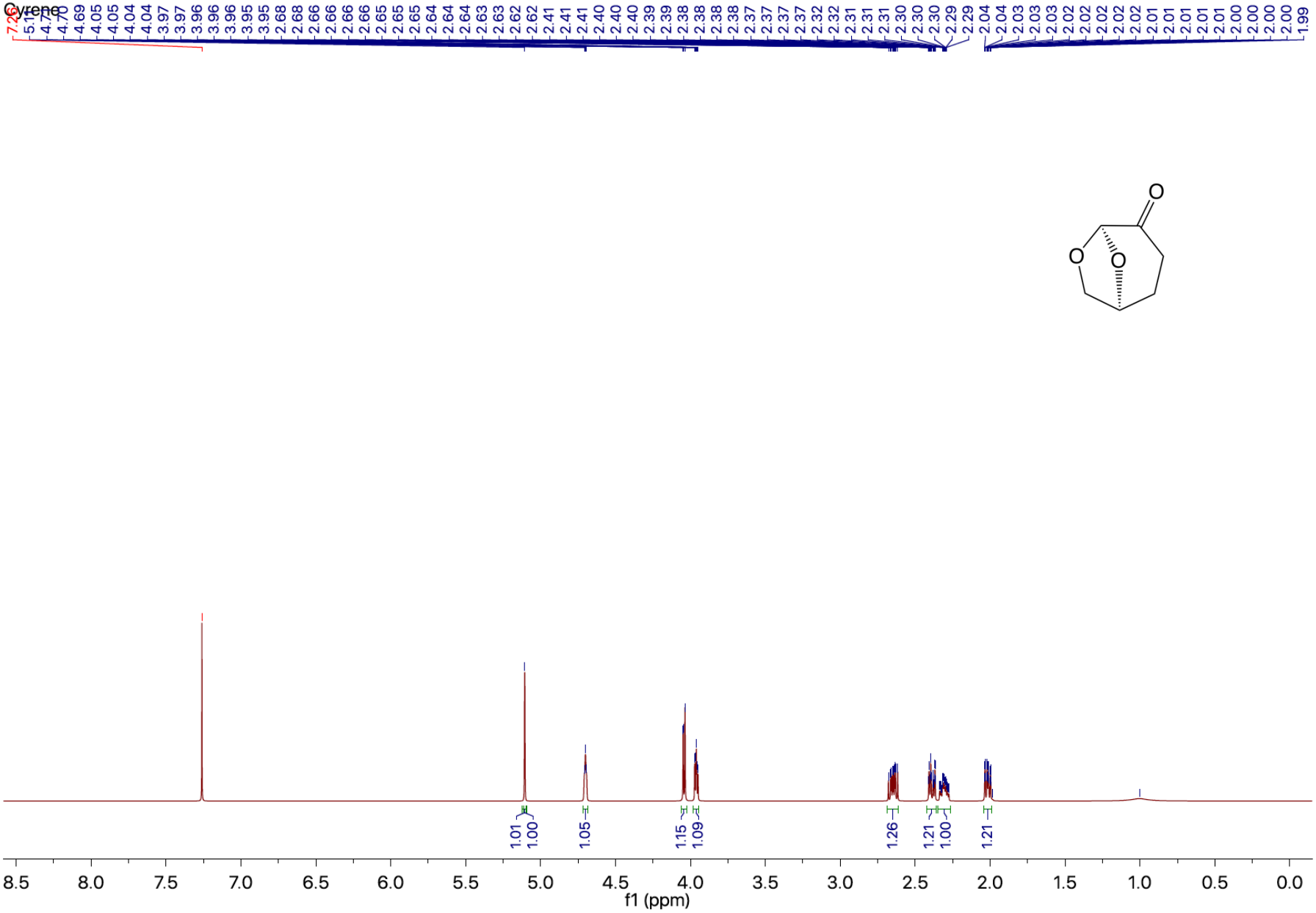

Figure S2.21. ^{1}H NMR spectrum of **12** from the hydrogenation of **11**

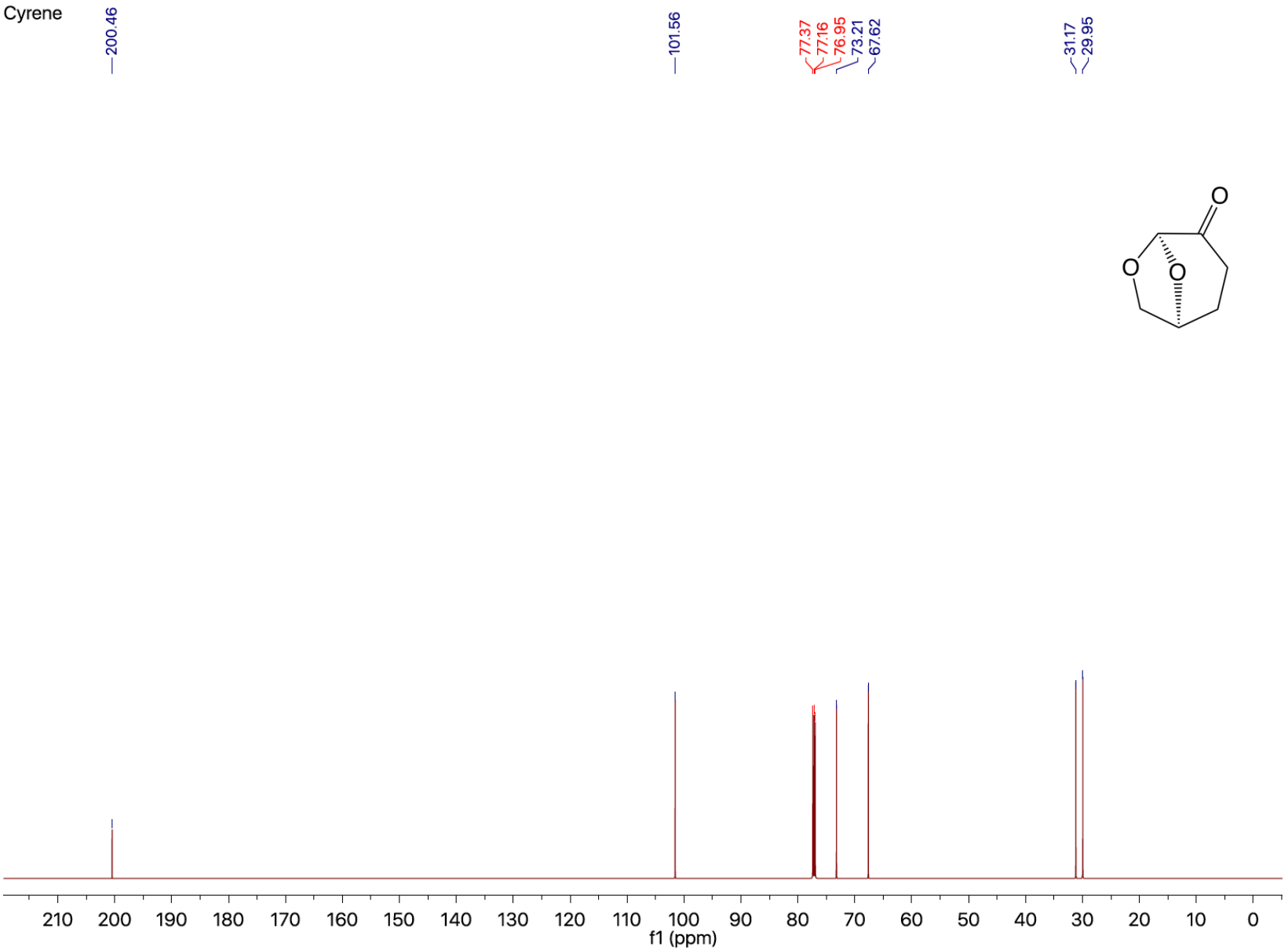

Figure S2.22. ^{13}C NMR spectrum of **12** from the hydrogenation of **11**.

Continuous Flow Hydrogenation of Isophorone

Table S2.1. Continuous flow hydrogenation of isophorone using PdNP@cellulose.

Entry	Flow rate (ml/min)	Solvent	Conversion (%)
1	0.5	EtOH	40
2	0.3	EtOH	53
3	0.1	EtOH	Solvent Evap.
4	0.1	n-PrOH	Solvent Evap.
5	0.2	n-PrOH	63
6	0.1	n-BuOH	65

The obtimised flow rate was found to be 0.3ml/min, with lower flow rates resulting in solvent evaporation, due to the high shear experienced with VFD, leaving the substrate immobilised in the tube with no product being collected. A mixture of isophorone (1.53g, 11.1mmol) in ethanol (80ml, 0.13M) was injected via syringe pump, at 0.3mL/min, using conditions described above. In another jet feed of the VFD, a stream of H_2 gas was introduced so that the flow rate was no more than 0.5L/min. The product was collected and concentrated under vacuum to afford a crude mixture of isophorone and dihydroisophorone (1.39g, 53% conversion). The crude product was diluted with EtOH (73mL, 0.13M) and fed back into the VFD using the procedure described above. This afforded a crude product (1.28g) of 80% conversion to dihydroisophorone. This procedure was repeated a third time to afford crude product of 93% conversion (1.14g). These results are summarised in Table S2 and Figure S13.

Table S2.2. Continuous flow hydrogenation of isophorone in EtOH (0.13M), with H_2 atmosphere, over PdNP@cellulose, 7k rpm, 0.3mL/min flow rate, tilt angle 45°, with the product re-cycled through the device.

Cycle	Conversion (%)
1	53
2	80
3	93

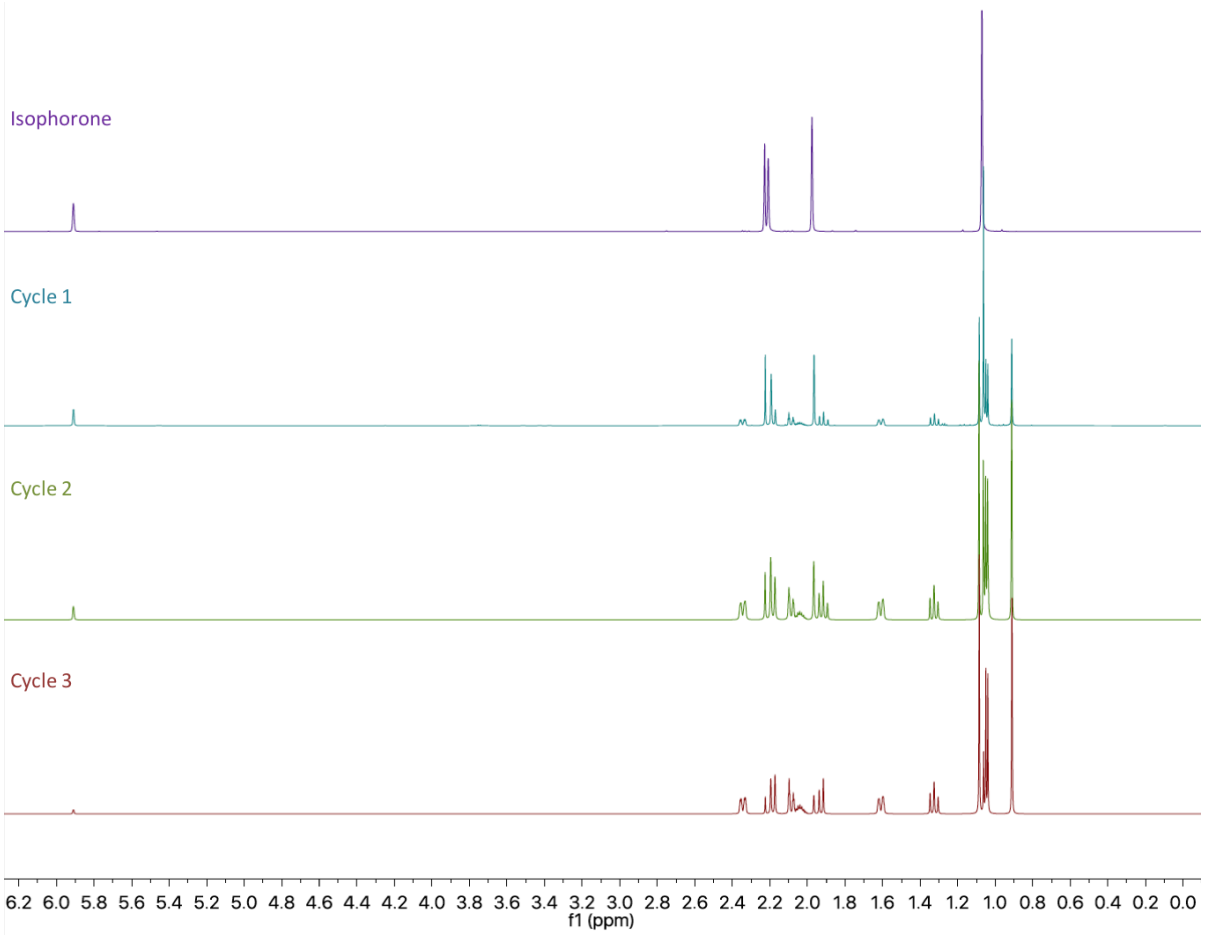

Figure S2.23. ^{1}H NMR spectra for the hydrogenation of isophorone cycle 1-3.

Transfer Hydrogenation Confined Mode VFD Processing

A number of hydrogen sources were explored in confined mode. Cinnamic acid (0.3mmol), and hydrogen source (see Table S3) were dissolved in a solvent (1.5mL) and transferred to a 20mm O.D. VFD tube containing PdNP@cellulose paper. The tube was sealed with a rubber stopper. The VFD was operated at 7k rpm for 20mins with the tube inlcied at 45^{o} tilt angle. The reaction mixture was removed from the tube and the PdNP@cellulose paper washed with solvent. All organic liquid was combined and concentrated under vacuum. The reaction conversion was determined using ^{1}H NMR spectroscopy (Table S3).

Table S2.3. Confined mode operation of the VFD for transfer hydrogenation of cinnamic acid.

Hydrogen Source	**Molar Equivalents**	**Solvent**	**Conversion (%)**
H_2O, $B_2(OH)_5$	5	EtOH	0
Formic acid	10	MeOH	2
Ammonium formate	8	MeOH	97

The substrate scope was explored using ammonium formate, where similar conversions were achieved compared to using hydrogen gas, provided the reaction mixture was heated to 60°C (Table 3, manuscript). Each product was characterised with NMR and were consistant with the spectra shown above. The product for the transfer hydrogenation of benzophenone, isophorone and levoglucosenone were confirmed using GCMS (Figure S14-S17).

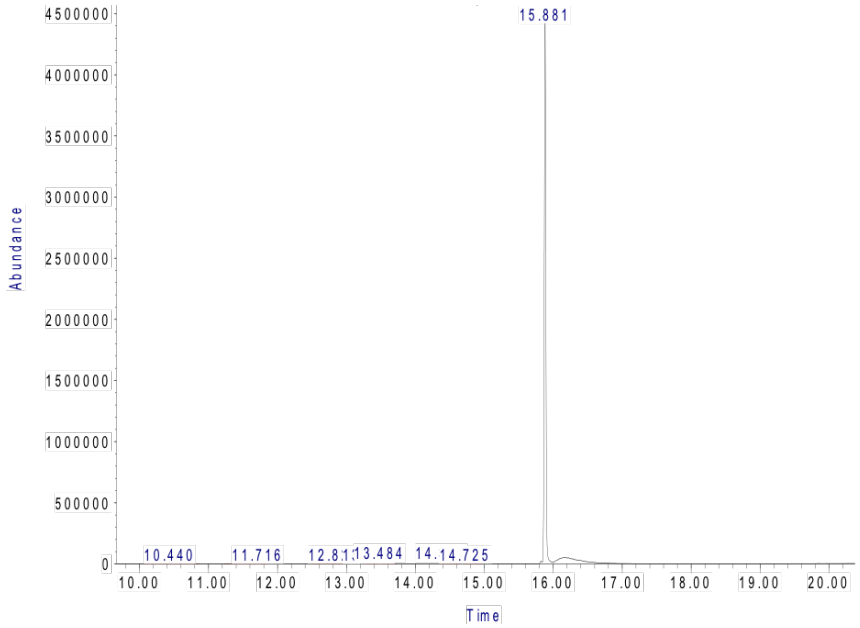

Figure S2.24. Chromatogram of the product from the transfer hydrogenation of benzophenone, showing benzophenone (15.9 min) and diphenylmethanol (16.2 min), with corresponding mass spectra shown in Figure S15.

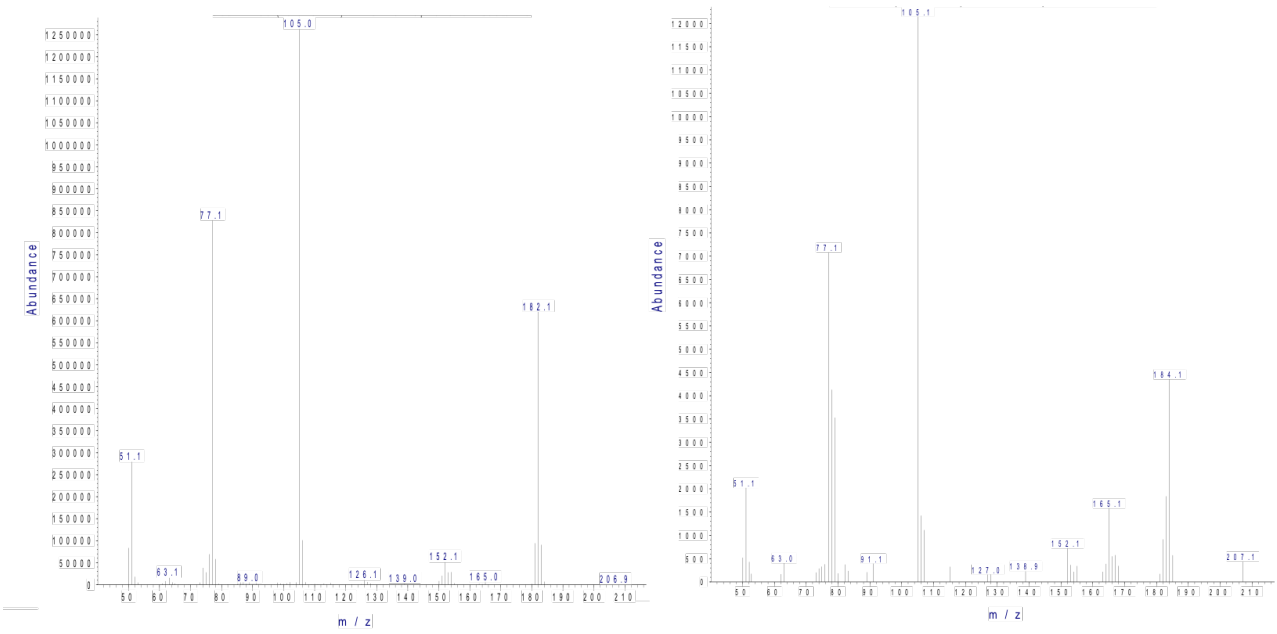

Figure S2.25. Mass spectrum of benzophenone (15.9 min, left) and Diphenylmethanol (16.2 min, right).

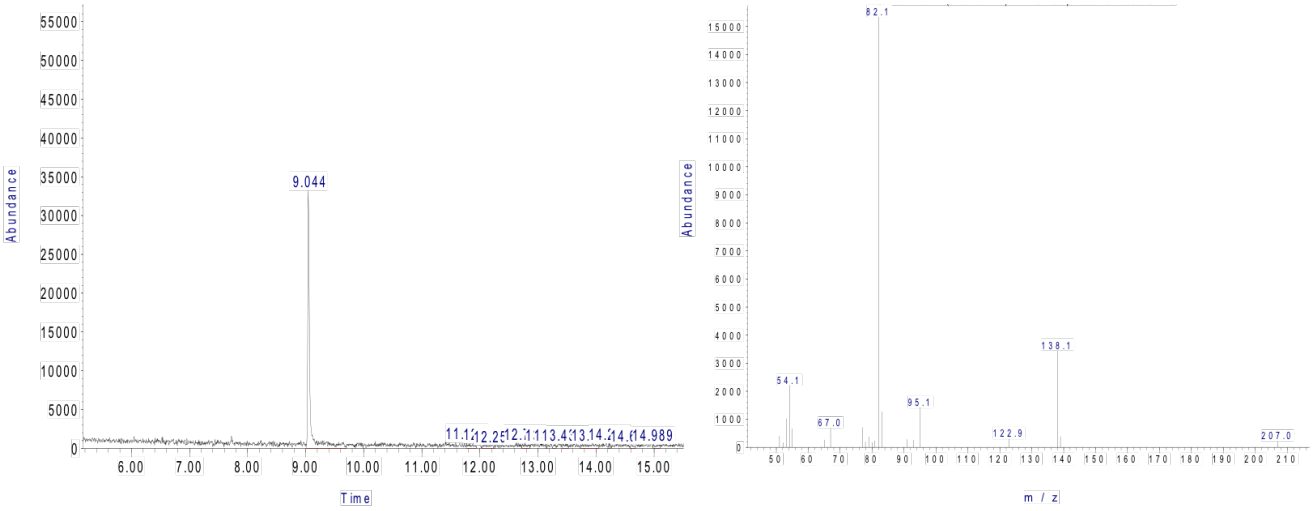

Figure S2.26. Chromatogram of the product from the attempted transfer hydrogenation of isophorone, showing isophorone (9.0 min, left) and corresponding mass spectrum (right).

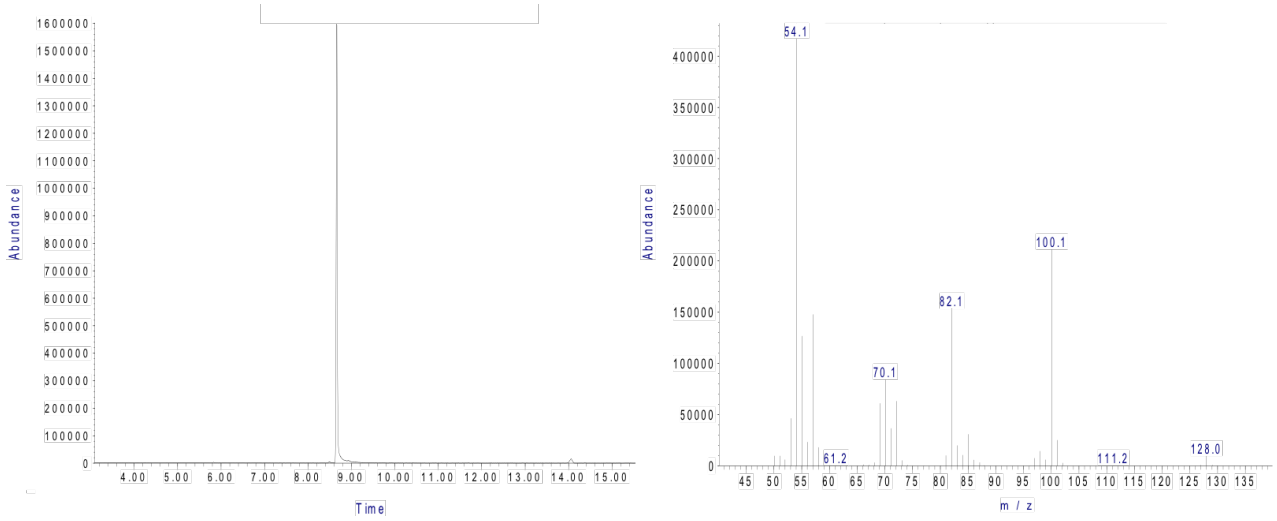

Figure S2.27. Chromatogram of the product from the transfer hydrogenation of (-)-levoglucosenone, showing cyrene at 8.7 mins (left), and corresponding mass spectrum (right).

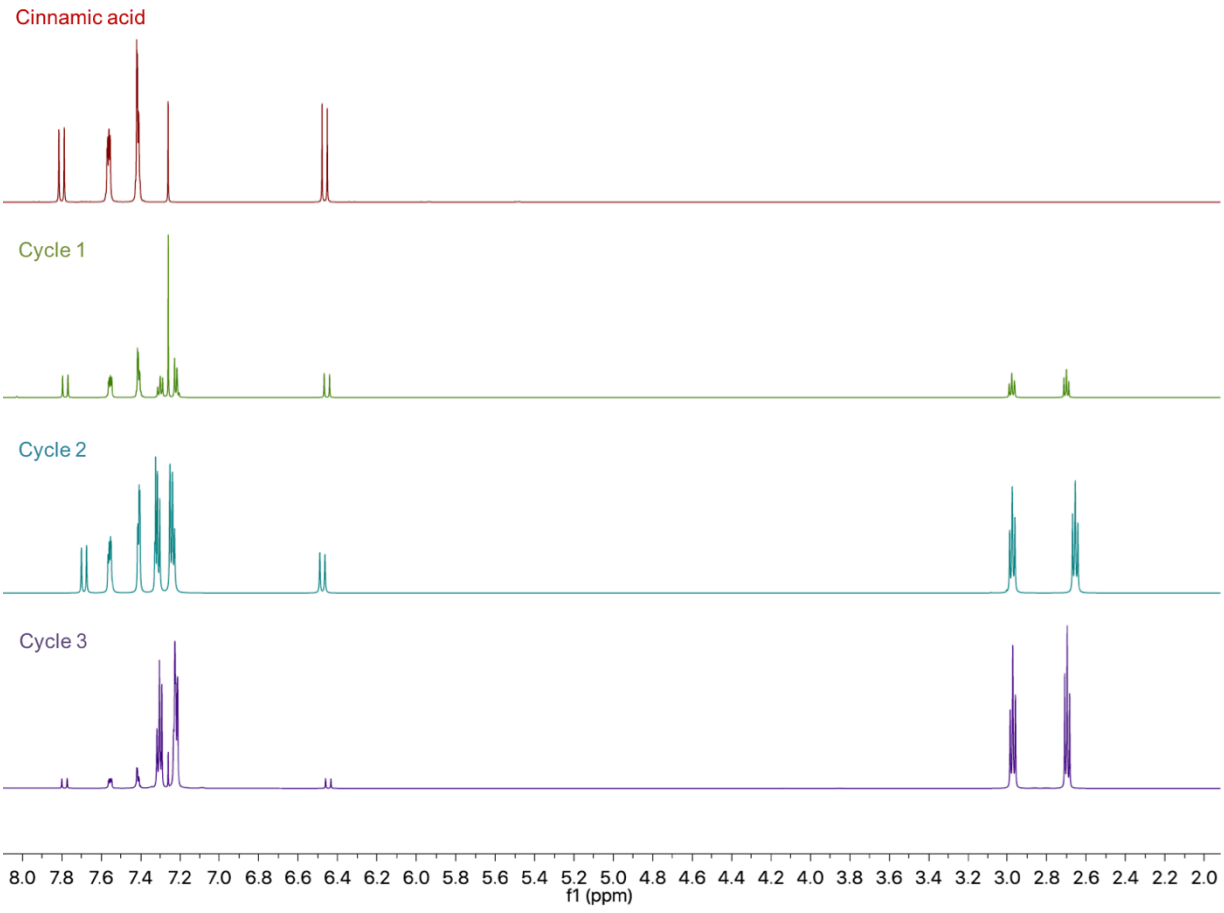

Figure S2.28. ^{1}H NMR spectra for transfer hydrogenation of cinnamic acid under continuous flow for cycles 1-3.

The transfer hydrogenation of (-)-levoglucosenone was attempted in continuous flow using the same method as described above. However, hydrogenation at the ketone as well as the ring double bond prevailed as shown by the presence of a peak at 11.7 min in the gas chromatogram, corresponding to **14** (Figure S19 and S20).

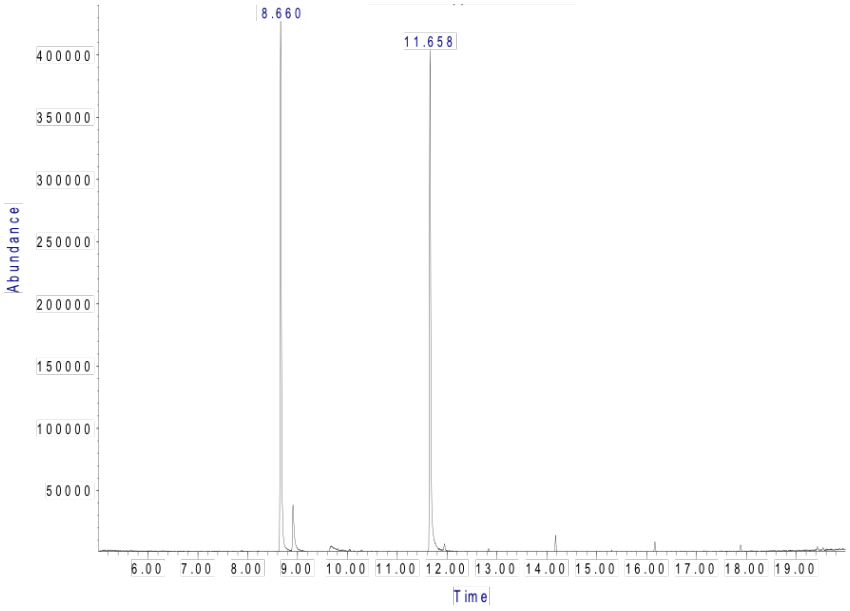

Figure S2.29. Chromatograph of the product from the continuous flow transfer hydrogenation of (-)-levoglucosenone, showing cyrene (8.7 min), (-)-levoglucosenone (8.9 min) and 14 (11.7 min. The corresponding mass spectrum for cyrene is as shown in Figure S16 (right) and for (-)-levoglucosenone and **14** is shown in Figure S20.

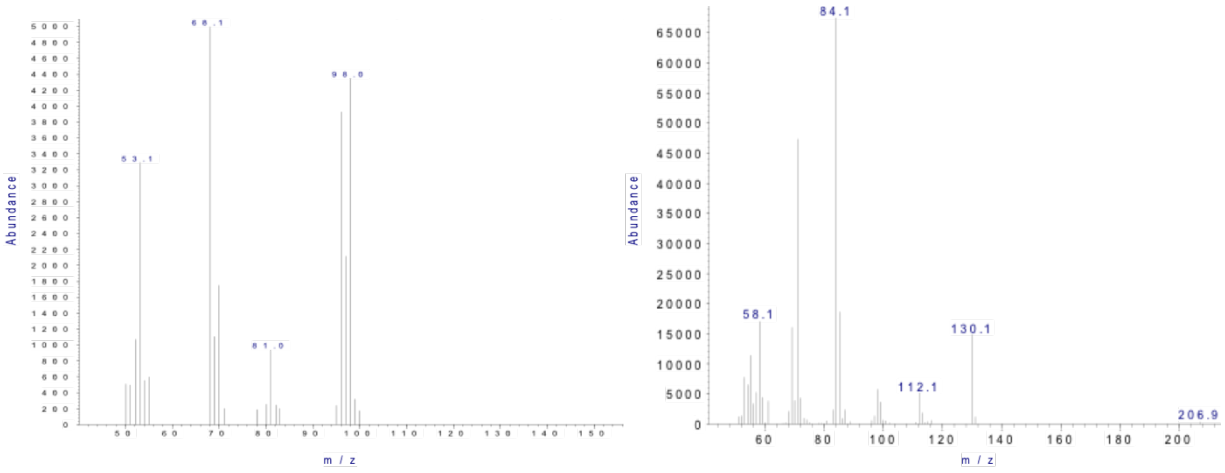

Figure S2.30. Mass spectra of levoglucosenone (8.9 min, left) and byproduct **14** (11.7 min, right).

Re-usability studies

The reduction of cinnamic acid, detailed above, was used to evaluate the re-usability of the PdNP@cellulose. This reaction was repeated ten times, with the PdNP@cellulose washed with EtOH between each run, and the percentage conversion to 3-phenylpropanoic acid determined using ^{1}H NMR analysis. The results are detailed in Table S4 and Figure S21.

Table S2.4. Hydrogenation of cinnamic acid (0.3mmol) in EtOH (1.5ml), under a H_2 atmosphere, over PdNP@cellulose , 7k rpm, 20 mins, tilt angle 45^{o}.

Run	**% Conversion**
1	100
2	97
3	97
4	99
5	99
6	99
7	99
8	99
9	99
10	99

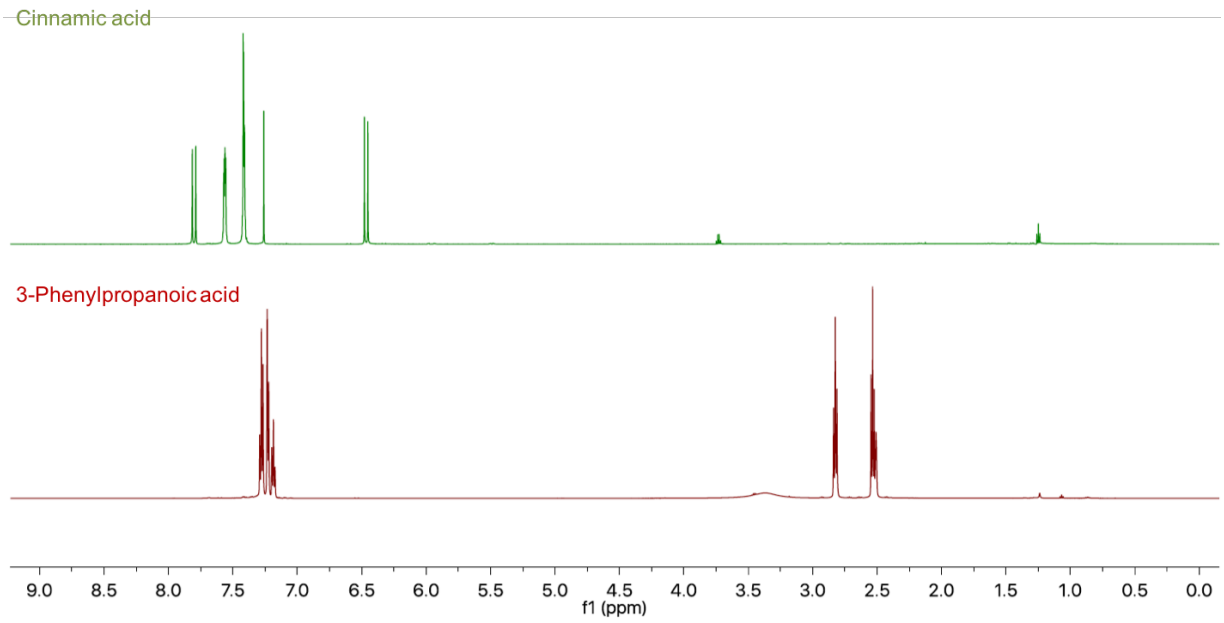

Figure S2.31. ^{1}H NMR spectra for cinnamic acid (top) and the product after the 10th reaction (bottom).

Characterisation of Pd on Cellulose Post-Reaction

Parameters and conditions used for SEM and high resolution TEM imaging, EDX mapping and XPS analysis are as stated above.

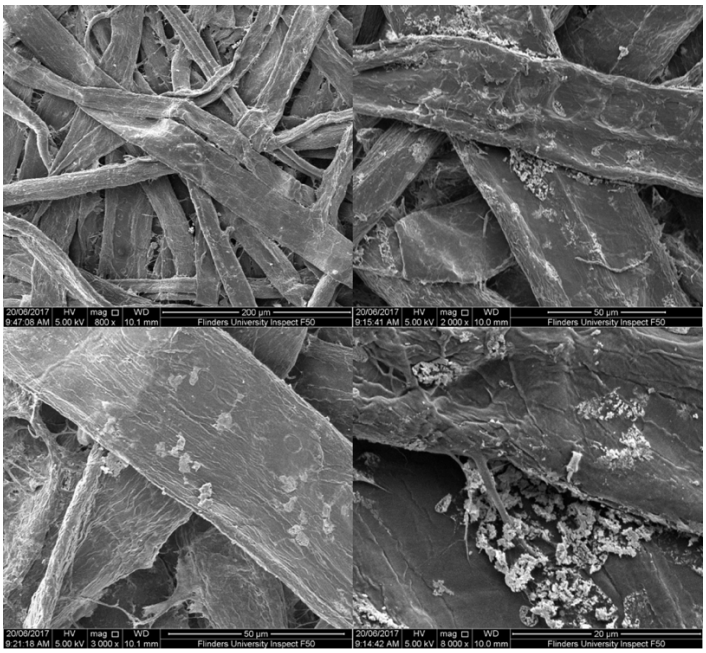

Figure S2.32. SEM images of PdNP@cellulose paper post ten reaction cycles, coated with a 10 nm layer of Pt, showing some agglomeration of particles.

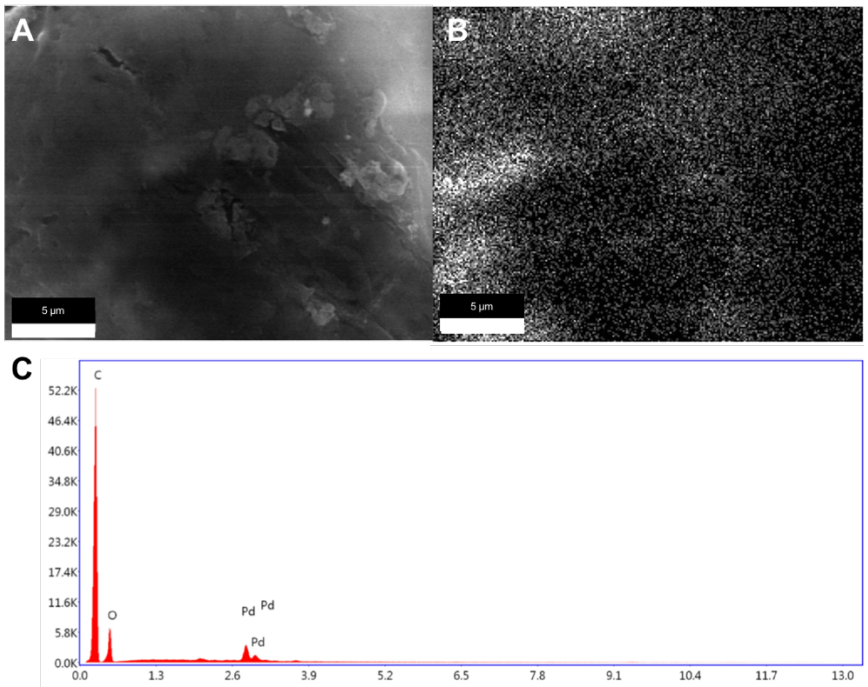

Figure S2.33. EDX mapping of PdNP@cellulose paper after ten reaction cycles showing, a) image of region analysed, b) Pd counts detected, c) spectrum of elements detected.

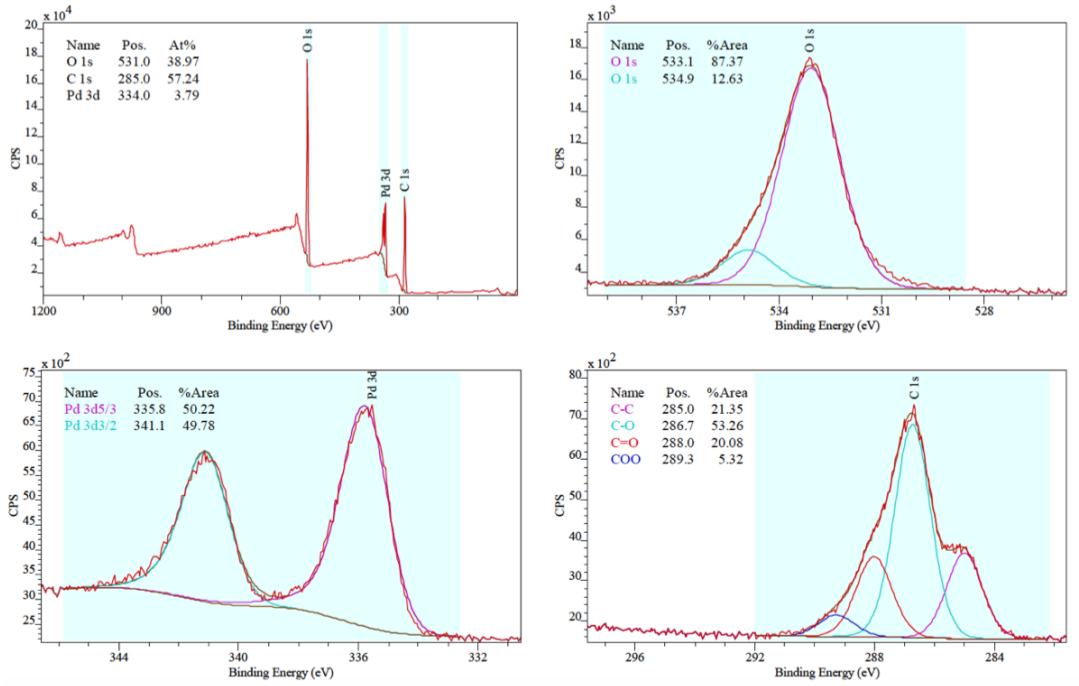

Figure S2.34. XPS spectra of PdNP@cellulose paper after ten reaction cycles.

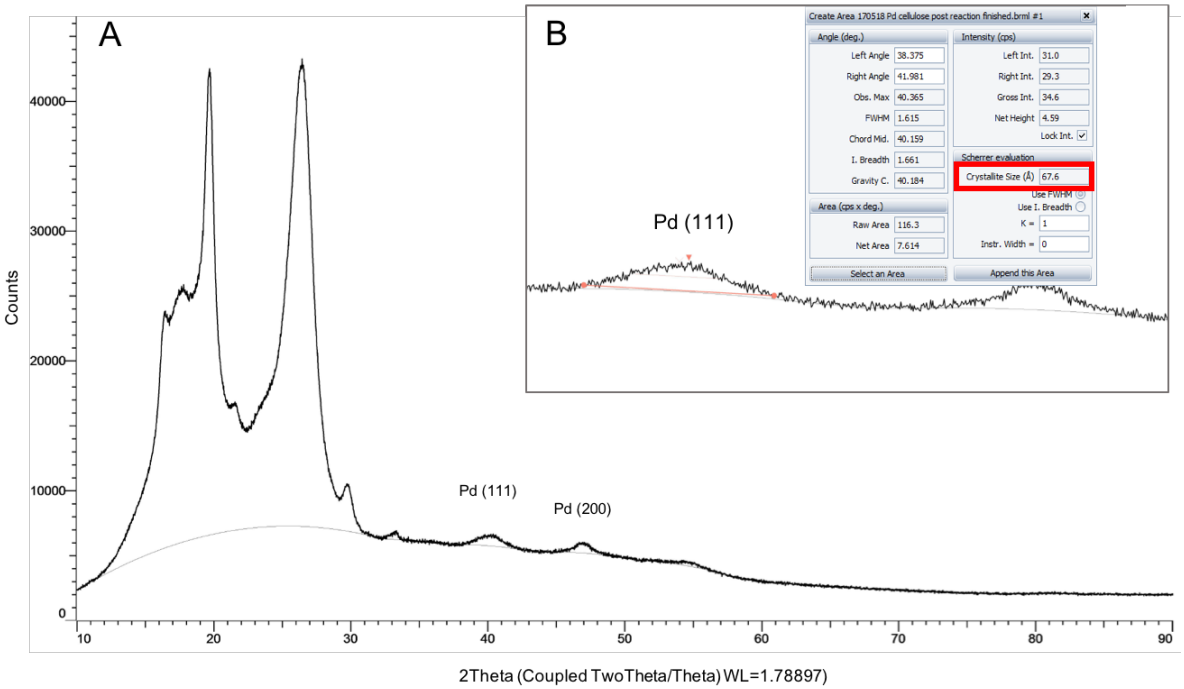

Figure S2.35. (A) XRD pattern of PdNP@cellulose after three continuous flow hydrogenation reaction (total 3 hours), where the paper was washed with ethanol and dried under N_2 (B) Area

of the peak corresponding to Pd (111) and the corresponding Scherrer equation evaluation showing a crystallite size of 67.6Å (6.8 nm).

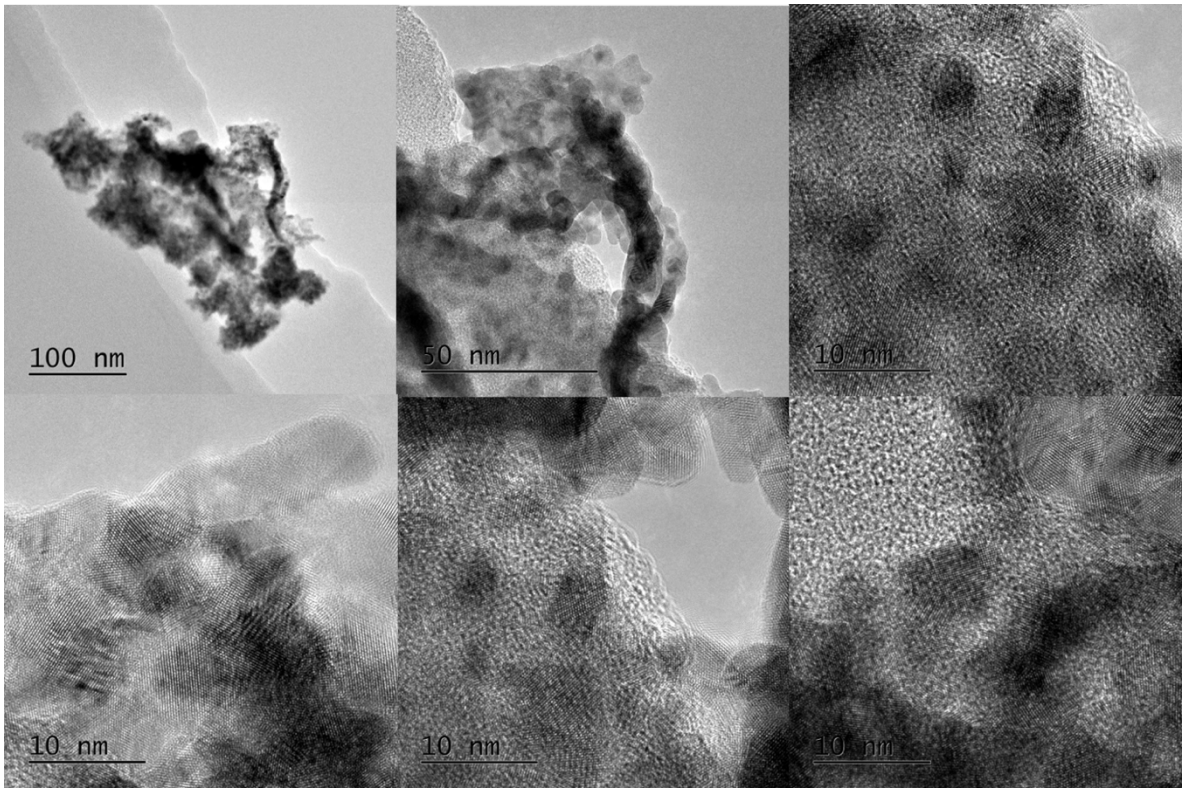

Figure S2.36. HRTEM images of PdNP@cellulose paper post ten reaction cycles.

Palladium Leaching Experiment with ICP-MS

A solution of cinnamic acid (1.33 mmol) in ethanol (10 ml, 0.13 M) was injected via syringe pump, at varying flow rates, into the base of the VFD tube, operating at 7k rpm with a 45° tilt angle. In another jet feed of the VFD, a stream of H_2 gas was introduced so that the flow rate was no more than 0.5 L/min. The reaction solution was collected in four fractions (3mL each). Each fraction was diluted with 2% HNO_3 and the palladium content analysed using a Perkin-Elmer NexION ICP-MS. No significant leaching of palladium was detected, with less

than 100 ppb palladium found in each of the undiluted reaction solutions (Table S2.5). Fraction 1 shows a higher level of Pd relative to fractions 2-4, which the amount of Pd being leached under steady-state conditions. This result could be due to residual 'free' palladium being released into solution in the first fraction.

Table S2.5. Palladium concentration in undiluted reaction solution detected using ICP-MS.

Fraction	Concentration (ppb)
1	89
2	55
3	48
4	52

Fluid Flow Experiments

Fluid flow experiments were conducted to observe how the solution flows through the VFD with the cellulose paper present. Methylene blue (2mg) was dissolved in ethanol (10mL) and injected into a VFD containing cellulose paper, soaked in water, at 0.5mL/min (Figure S27). The paper was soaked in water to enable the paper to stick to the surface of the tube. The experiment showed visually that the methylene blue/ethanol solution flows through the cellulose as opposed to flowing below (unlikely under high centrifugal forces) or above the cellulose paper.

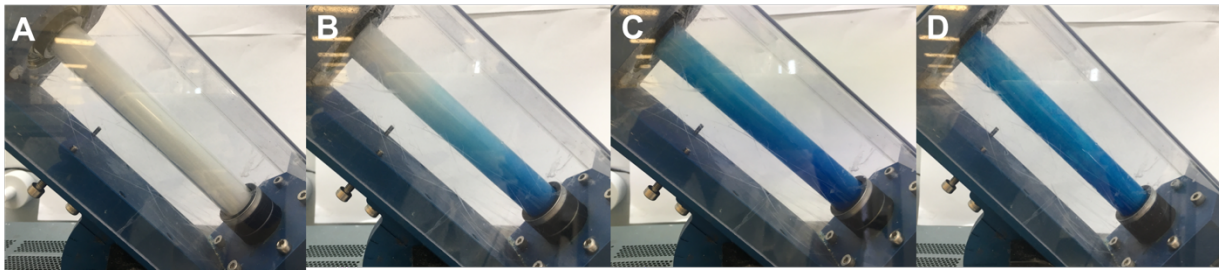

Figure S2.37. Fluid flow experiments where A) cellulose paper soaked in water, lining the surface of the tube, rotating at 7k rpm 45° tilt angle, B and C) blue dye in EtOH continuously added to the tube at 0.5mL/min, and D) showing the cellulose soaked with the blue dye when the VFD tube was stopped.

Batch Synthesis of (E)-Acetophenone oxime

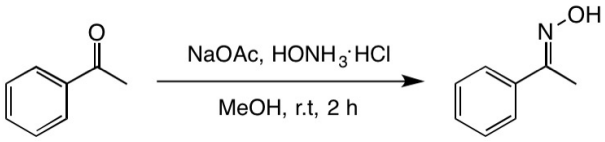

Scheme S2.7. Synthesis of (E)-Acetophenone oxime from acetophenone.

Acetophenone (2.01g, 16.7mmol, 1.0 eq), sodium acetate (2.51g, 30.6mmol, 1.8 eq) and hydroxylamine hydrochloride (1.35g, 19.4mmol, 1.2 eq) were dissolved in MeOH (40mL). The reaction mixture was stirred at RT overnight, then MeOH was evaporated and the crude product was diluted with DCM (25mL) and washed with H_2O (2 × 10 mL). The combined organic extracts were dried ($MgSO_4$) and evaporated to give *the oxime* as a pale yellow solid (1.98g, 87%). R_F 0.32 (9:1 Hexane:EtOAc). m.p. 58-59°C [Lit m.p. 56-58°C].[40] ^{1}H NMR (600 MHz, DMSO -d_6) δ 7.75 (s, 1H), 7.66 – 7.60 (m, 2H), 7.38 (dd, J = 5.1, 2.0 Hz, 3H), 7.26 (s, 1H), ^{13}C NMR (151 MHz, $CDCl_3$) δ 156.1 (C=N), 136.6 (4° Ar), 129.4 (Ar), 128.6 (2x Ar), 126.2 (2x

Ar), 12.6 (<u>C</u>H_3). IR (υ_{max}, crystals ATR): 3207, 2918, 1496,1446, 1364, 1303, 1080, 1001, 925, 761, 693, 653. MS $(MH)^+$ *m/z*: 135. This compound had spectra previously reported in the literature [8].

Batch Synthesis of N-(1-Phenylvinyl)acetamide

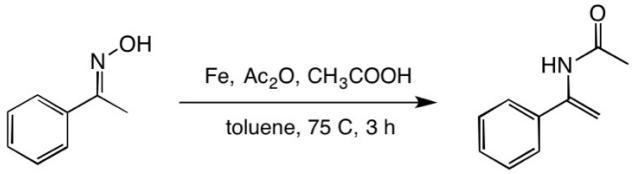

Scheme 2.8. Synthesis of N-(1-Phenylvinyl)acetamide from (E)-acetophenone oxime.

(*E*)-Acetophenone oxime (570mg, 4.2mmol, 1.0 eq) was dissolved in toluene (9mL), acetic anhydride (1.29g, 12.6mmol, 3.0 eq) and acetic acid (760mg, 12.7mmol, 3.0 eq) were added. Fe powder (512mg, 9.2mmol, 2.2 eq) was added portionwise under constant stirring and then the reaction mixture was heated to 75^{o}C for 3 h. (Note: The reaction mass turned a blood red colour after one hour heating). Fe (powder) was filtered followed by toluene evaporation gave crude product, which was purified by flash column chromatography (7:1 Hexane:EtOAc) to give *the amide* as a yellow solid (386 mg, 57%). R_F 0.30 (7:3 Hexane:EtOAc). m.p. 89-91°C [Lit m.p. 82-84°C].[41] ^{1}H NMR (600 MHz, DMSO-d_6) δ 9.32 (s, 1H), 7.44 (d, J = 6.8 Hz, 2H), 7.37 (dt, J = 12.7, 6.8 Hz, 3H), 5.62 (s, 1H), 4.98 (s, 1H), 2.02 (s, 3H). ^{13}C NMR (151 MHz, DMSO-d_6) δ 169.1 (C=O), 141.5 (<u>C</u>-N), 138.0 (4° Ar), 128.3 (3x Ar), 126.2 (2x Ar), 101.9 (C=<u>C</u>H_2), 23.7 (<u>C</u>H_3). IR (υ_{max}, crystals ATR): 3254, 1659, 1629, 1524, 882, 773, 693. MS $(MH)^+$ *m/z*: 161. This compound had spectra previously reported in the literature [9].

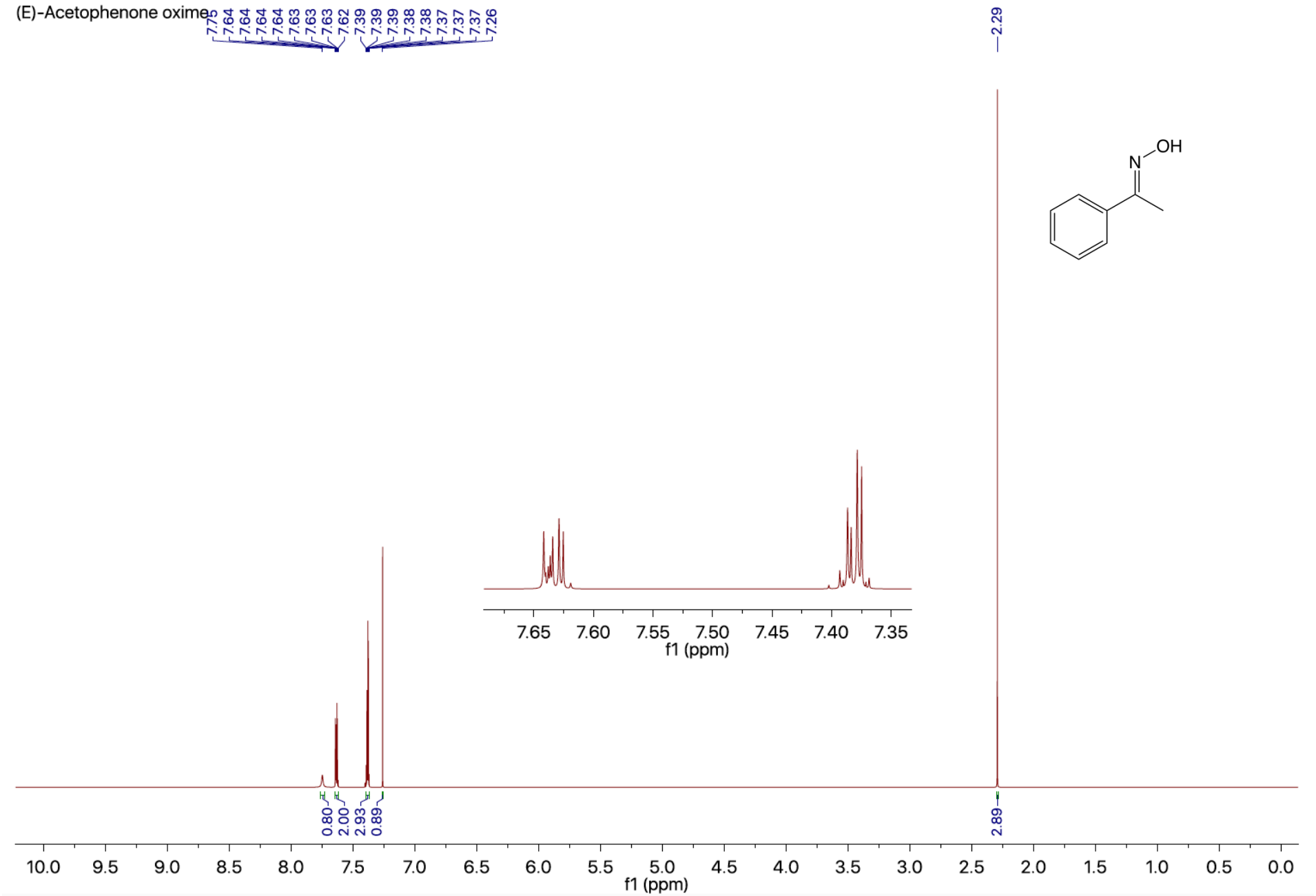

Figure S2.38. ^{1}H NMR spectrum of (E)-Acetophenone oxime

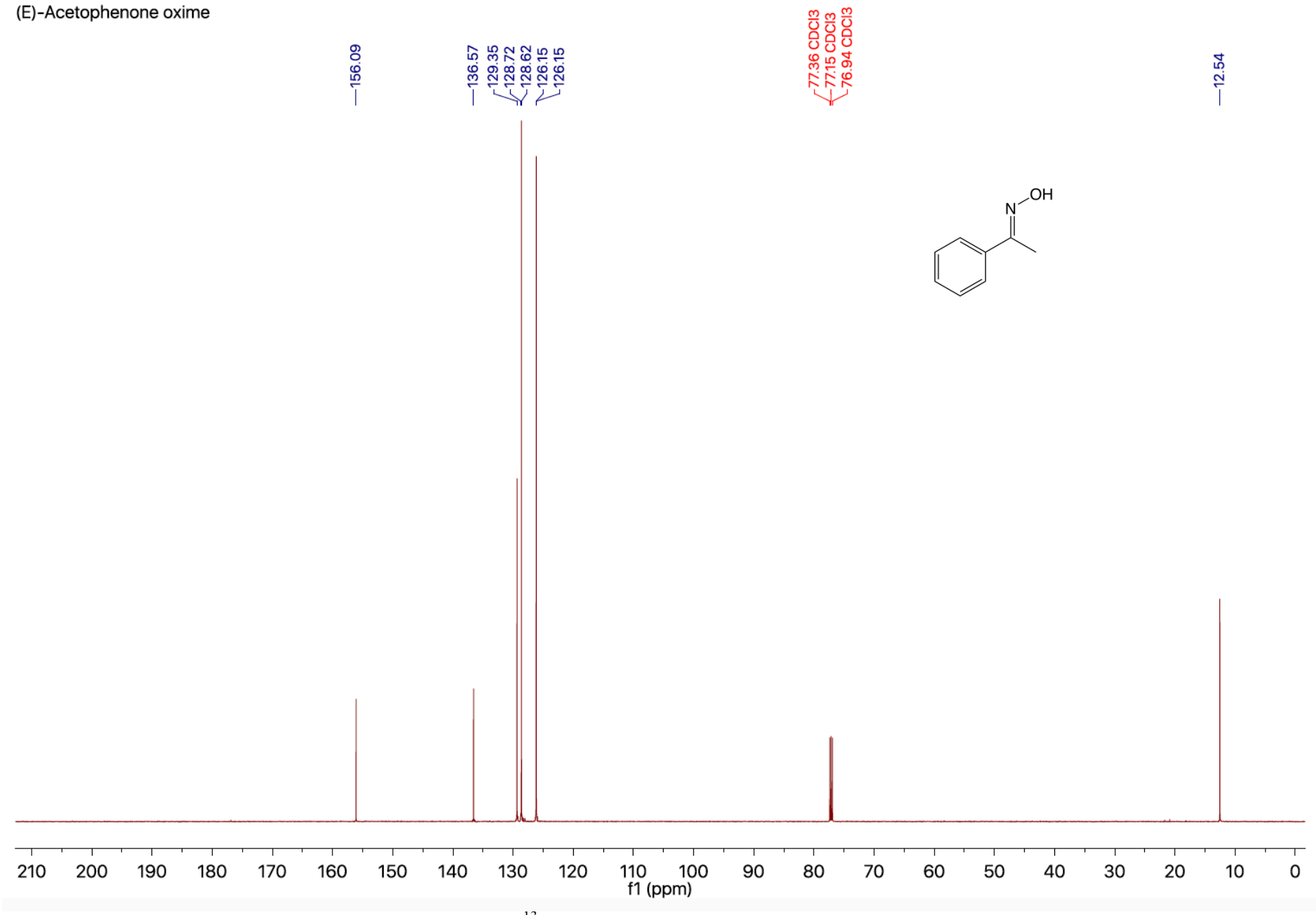

Figure S2.39. ^{13}C NMR spectrum of (E)-Acetophenone oxime

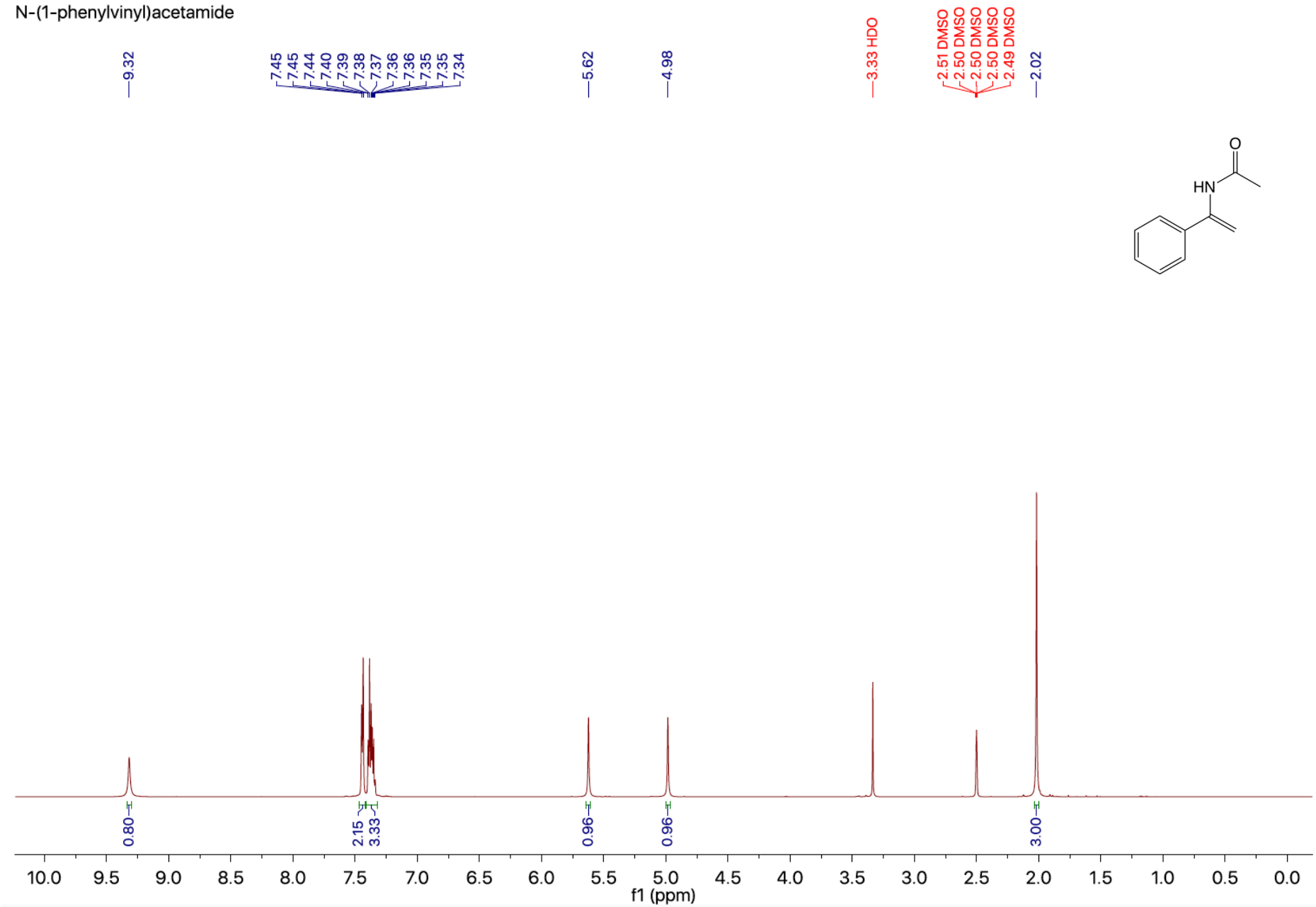

Figure S2.40. ^{1}H NMR spectrum of N-(phenylvinyl)acetamide.

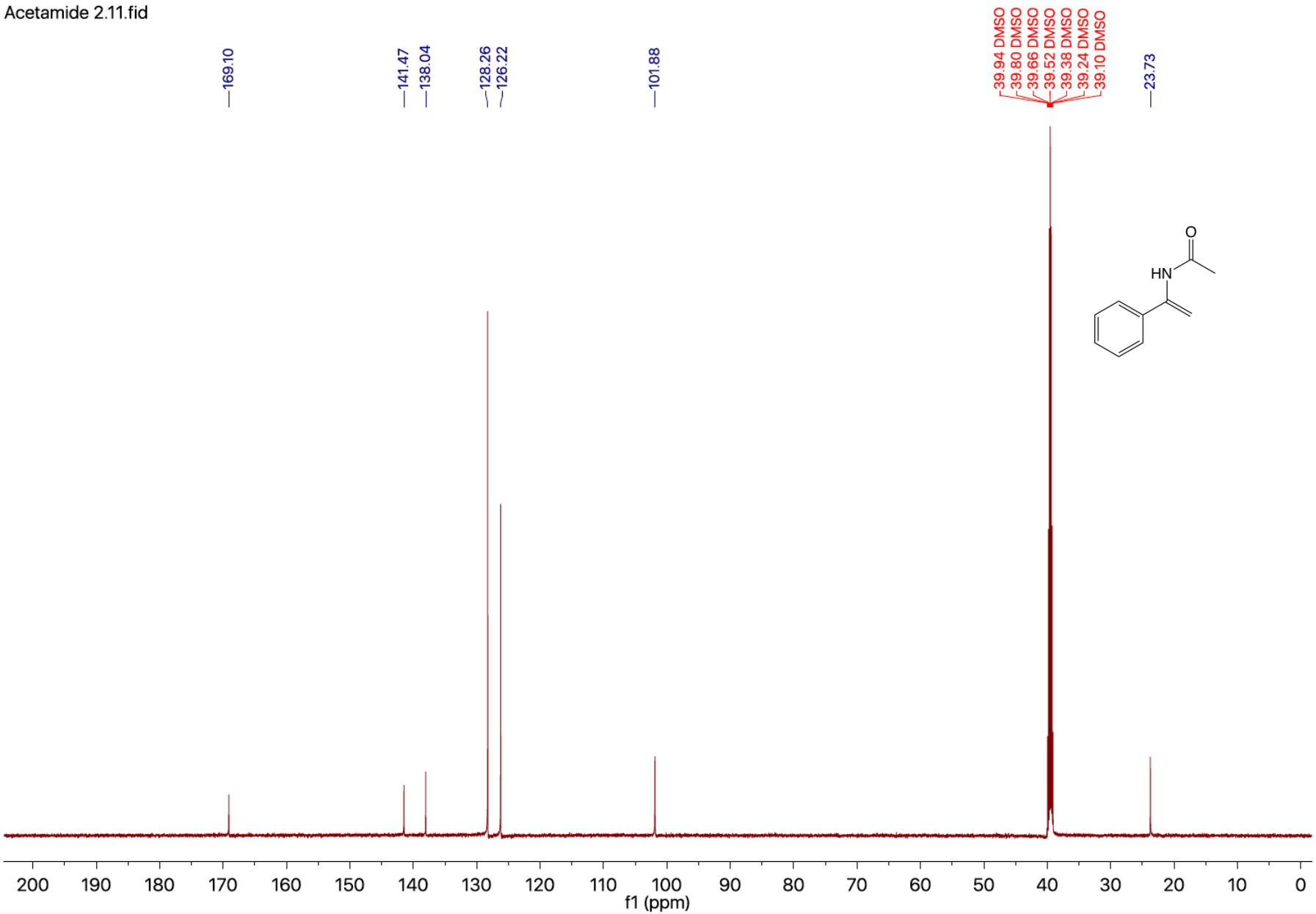

Figure S2.41. ^{13}C NMR spectrum of (E)-Acetophenone

Supplementary References

[1] Schmidt, A. K. C.; Stark, C. B. W. TPAP-Catalyzed Direct Oxidation of Primary Alcohols to Carboxylic Acids through Stabilized Aldehyde Hydrates. *Org. Lett*., **2011**, *13*, 4164-4167.

[2] Motoyama, Y.; Kamo, K.; Nagashima, H. Catalysis in Polysiloxane Gels: Platinum-Catalyzed Hydrosilylation of Polymethylhydrosiloxane Leading to Reusable Catalysts for Reduction of Nitroarenes. *Org. Lett*., **2009**, *11*, 1345-1348

[3] Kuriyama, M.; Shimazawa, R.; Shirai, R. Efficient 1,2-Addition of Aryl- and Alkenylboronic Acids to Aldehydes Catalyzed by the Palladium/Thioether–Imidazolinium Chloride System. *J. Org. Chem*., **2008**, *73*, 1597-1600.

[4] Ritter, J. J.; Minieri, P. P. A New Reaction of Nitriles. II. Synthesis of t-Carbinamines. *J. Am. Chem. Soc*., **1948**, *70*, 4045-4048.

[5] Burk, M. J.; Casy, G.; Johnson, N. B. A Three-Step Procedure for Asymmetric Catalytic Reductive Amidation of Ketones. *J. Org. Chem*. **1998**, *63*, 6084-6085.

[6] Mirza-Aghayan, M.; Boukherroub, R.; Bolourtchian, M.; Rahimifard, M. Palladium Catalyzed Mild Reduction of α,β-Unsaturated Compounds by Triethylsilane. *J. Orgomet. Chem*., **2007**, *692*, 5113-5116.

[7] Clark, J. H.; De bruyn, M.; Constantinou, A.; Moity, L.; McElroy, C. R.; Farmer, T. J.; Duncan, T.; Raverty, W.; Hunt, A. J.; Clark, J. H. Dihydrolevoglucosenone (Cyrene) as a Bio-Based Alternative for Dipolar Aprotic Solvents. *Chem*. *Comm*., **2014**, *50*, 9650-9652

[8] Ngwerume, S.; Camp, J. E. Synthesis of Highly Substituted Pyrroles via Nucleophilic Catalysis. *J. Org. Chem*., **2010**, *75*, 6271-6274.

[9] Guan, Z. H.; Zhang, Z. Y.; Ren, Z. H.; Wang, Y. Y.; Zhang, X. Synthesis of Enamides via CuI-Catalyzed Reductive Acylation of Ketoximes with $NaHSO_3$. *J. Org. Chem.*, **2011**, *76*, 339-341.

Chapter 3: Covalent Immobilisation of Enzymes on Cellulose Paper for Continuous-Flow Biocatalysis

3.1. Abstract

Immobilisation of enzymes have been the focus of applied biocatalysis as it enables isolation and reuse of the catalyst and allows opportunities for use in continuous-flow manufacturing. Here, enzymes were rapidly immobilised through covalent attachment onto a cellulose support through APTES-glutaraldehyde functionalisation in the vortex fluidic device (VFD). The stable and re-usable enzyme-cellulose catalyst can be easily and efficiently used in the VFD for continuous-flow biocatalysis with comparable rates to batch. The method was further applied to the continuous-flow synthesis of a valuable chiral terpene, aristolochene, through the immobilisation of aristolochene synthase from *Aspergillus terreus*. This immobilisation method and application in creating complex natural products further expands the versatility of the VFD for thin-film continuous flow biocatalysis, without clogging issues occurring with conventional channel based microfluidics.

3.2. Introduction

The use of enzymes for biocatalysis has gained interest in recent decades due the ability to create complex molecules that would otherwise require multiple synthetic steps [1]. Enzymatic processes are conducted under mild temperatures, can have high rates, and high selectivity, making them more economic and energy efficient [1, 2]. Overall, enzymatic processing is more environmentally friendly, more cost-effective, and ultimately, more

sustainable, than conventional organic synthesis [2]. Long term stability, recovery and re-use of enzymes has hampered their ability to be applied in industry [2-4]. Therefore, immobilisation of enzymes is fundamentally important for their recovery and reuse for more sustainable use of biocatalysis. In addition, their immobilisation onto solid supports allows for their use in continuous-flow devices, which potentially reduced the cost of processing, using small reactors in contrast to those used in conventional batch processing.

As discussed in previous chapters, the use of continuous flow has been widely utilised for the synthesis of active pharmaceutical ingredients and other value-added compounds as it allows for efficient scale up, mixing and enhanced heat and mass transfer [5]. The specificity and high turn over rates of enzymes allows them to be effectively applied to continuous flow devices [4]. The ability to immobilise large quantities of an enzyme for continuous use can be be beneficial for low expressing enzymes and enzymes with low turn over rates that require larger quantities for higher throughput. Enzymes can be highly valuable and take days to weeks to produce, therefore, the ability to easily scale-up and reuse enzymes is a priority for industrial applications, as well as developing sustainable technologies for the future.

Proteins can be immobilised through adsorption, covalent attachment, cross-linking, affinity and entrapment [4, 6, Chapter 1]. Several supports have been applied for enzyme immobilisation, including silica and inorganic oxides, mineral materials, carbon materials including synthetic polymers and biopolymers [4, 6a]. Cellulose is one of the most abundant biopolymers, is biodegradable, and chemically stable, making it an attractive support [7]. Furthermore, cellulose is robust, having dual hydrophobic and hydrophilic property, and is non-toxic, and relatively chemically inert, which is beneficial for the survival of enzymes. Importantly cellulose contains several hydroxyl groups capable of chemical modification, making it suitable for enzyme immobilisation [7, 8].

In this work, the efficacy of using a cellulose support to immobilise enzymes in the vortex fluidic device (VFD) for continuous-flow biocatalysis has been investigated. The VFD processes liquids as thin-films by rapid rotation in a glass tube, where the liquid experiences high shear and micro-mixing [9]. Examples of applications of the VFD include single and multi-step chemical transformation [9-12], biocatalysis [13-15], rapid purification of proteins [15], protein folding [16], and fabrication of micro and nanomaterials [17-21]. Immobilisation of enzymes in the VFD has been previous explored through functionalisation of the borosilicate glass surface for non-covalent and covalent attachment [14]. However, this method resulted in low immobilisation efficiency, and the inability to wash off catalyst to re-use the glass tube. Control over the immobilisation process is also difficult and does not allow for easy use of multiple enzymes attached within a single tube. Immobilisation of enzymes on nickel-affinity resin, painted on the surface of the VFD tube, has also been reported [15]. Here high amounts of enzyme can be immobilised, however, painting resin on the tube can be difficult to manage. Moreover, the Ni-ITA ligands can be unsuitable for many bio-catalytic reactions due to its Lewis acidity reactive with substrates. The use of a covalent attachment to a cellulose support could overcome these drawbacks by increasing the amount of enzyme immobilised compared to glass functionalisation and by increasing the stability and ease of usability, compared to resin attachment.

Herein, cellulose paper, previously applied to the synthesis and immobilisation of Pd nanoparticles for continuous-flow hydrogenations [11], has been developed for enzyme immobilisation. Cellulose paper is low cost, easy usability and can be rolled up and inserted into the VFD, where it lines the surface of the tube when wet. In principle, this ultra-thin ‘cartridge’ technology allows for a simple and efficient scale-up of continuous-flow biocatalysis, further increasing the versatility of the VFD.

3.3. Results and Discussion

3.3.1. Enzyme Immobilisation on Cellulose Paper

Hydroxyl groups on the cellulose fibres can be functionalised by nucleophilic amines using APTES. Enzymes can be immobilised onto the APTES layer through hydrogen bonding and salt bridges. Alternatively, covalent immobilisation can be achieved by modifying the APTES amine groups with glutaraldehyde. The glutaraldehyde-modified linker can form imine bonds with surface lysine chains on the protein (Figure 3.1) [22]. By creating longer spacers off the solid support, by glutaraldehyde modification, the stability of the enzymes is increased [23]. The resulting imine bonds can be reduced to amines using a $NaBH_3CN$ solution [24], resulting in a more stable attachment [14]. Each step of functionalisation and immobilisation was performed in the VFD at 7.5k rpm at 45 tilt angle over 30 min to 1 hour (Figure 3.1). The rotational speed and tilt angle were chosen as they have been shown to be optimal for a myriad of applications, including enzyme acceleration [9, 13]. Notably, performing each step in the VFD greatly reduces the volume of reagents and buffers required.

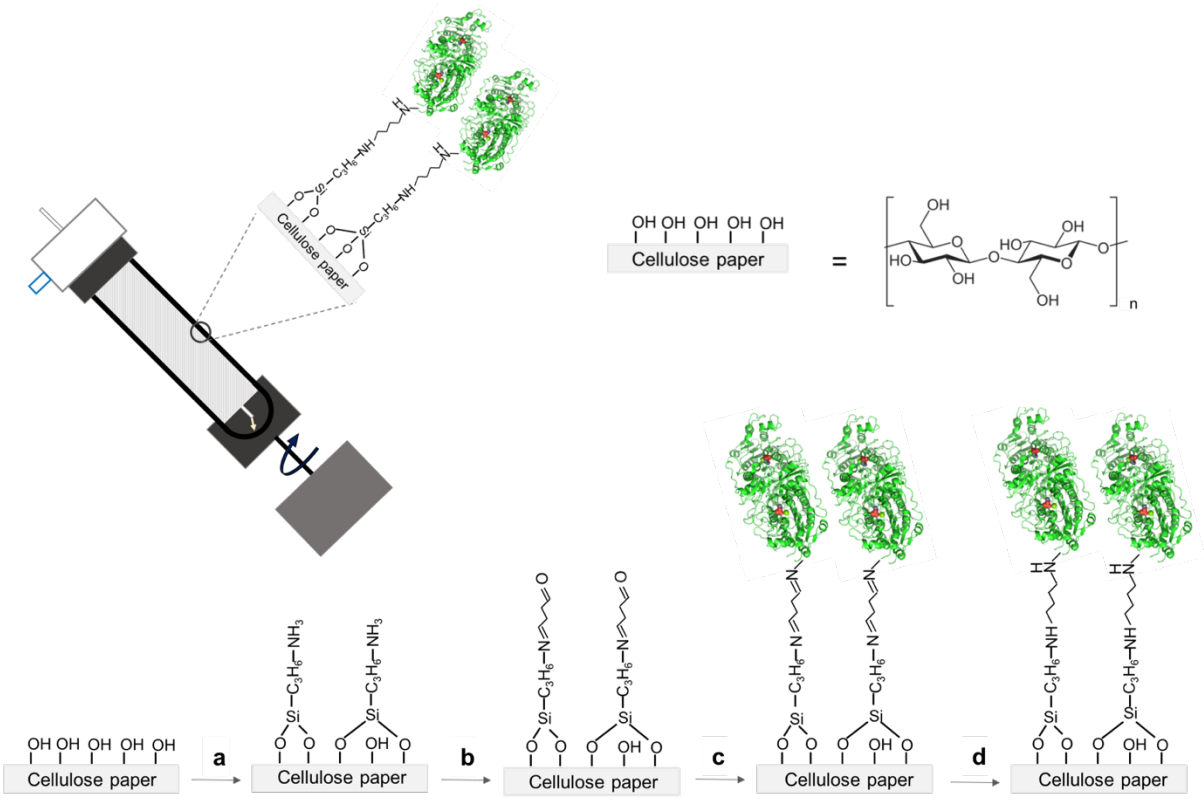

Figure 3.1. Immobilisation of enzymes on cellulose paper through covalent attachment. All steps were processed in the VFD in confined mode at 7.5k rpm, at 45° tilt angle, with 3 mL volume solutions. a) APTES (30% v/v) in MeOH, 1h, washed with MeOH (3x5mL), followed by 1h in an oven at 120°C. b) Glutaraldehyde (2.5% final concentration) in PBS buffer (pH 8.0), 1h; washed with PBS (5 x 5mL). c) AP solution (2mg/mL) in PBS Buffer (pH 7.0-8.0) 45 mins. d) $NaBH_3CN$ (0.11M) in sodium acetate buffer (pH 5.0), 30 mins.

3.3.2. Alkaline Phosphatase (AP) on Cellulose

Alkaline phosphatase (AP) was used to test the efficacy of these immobilisation methods. AP, as a proof of concept enzyme, is convenient as it is expressed in high yield in *E. coli* cells. Additionally, it catalyses the hydrolysis of 4-nitrophenyl phosphate (**1**), a commercially available and relatively inexpensive substrate, to 4-nitrophenol (**2**), which is a

colorimetric product that can be detected at 405 nm, allowing a straightforward measure of the activity of AP (Figure 3.2) [25]. The amount of AP immobilised on the cellulose through APTES-glutaraldehyde crosslinking was determined to be 0.16nmol/cm^2, by measuring the concentration of AP in solution before and after immobilisation, including wash solutions, with a Bradford protein assay (Table 3.1). This is a significant improvement compared to immobilisation on the borosilicate glass tube for use in the VFD. However, the amount of immobilisation is moderate compared to commercially using available resins for then coating the inside of the VFD tube.

As discussed above, the biocatalytic efficiency of the AP-cellulose catalyst was determined, first, using a confined mode assay, where a solution of 4-nitrophenyl phosphate (**1**), in diethanolamine buffer was processed in a sealed tube containing the catalyst, rotating at 7.5k rpm, at a 45° tilt angle, for 5 mins (Figure 2A). The solution was then immediately removed and quenched with 4.0M NaOH, followed by detection of the product, 4-nitrophenol (**2**), at 405nm.

The difference between two different types of cellulose paper was initially evaluated. Whatman Grade 1 cellulose paper is the most widely used filter paper for various applications, with a particle retention and nominal thickness of 11μm and 180μm, respectively. Alternatively, Whatman's Grade 4 filter paper has a particle retention and nominal thickness of 25μm and 210μm, respectively. A slightly higher conversion results from the use of Grade 1 filter paper due to increased levels of immobilisation. However, when translating to continuous flow, cellulose fibres shear off of the surface of the filter paper, resulting in catalyst leaching (Figure 3.2B, Figure S3.1). Therefore, Grade 4 was chosen for further experimentation. Notably, no conversion was observed with functionalised cellulose with no protein immobilised. The shearing of the cellulose for Grade 1 filter paper is likely to arise from the induced mechanical energy associated with the complex fluid flow in the device.

Understanding the fluid flow in the VFD has been a major undertaking for several years, and a pattern of behaviour is beginning to emerge to account for all the processing in the device.

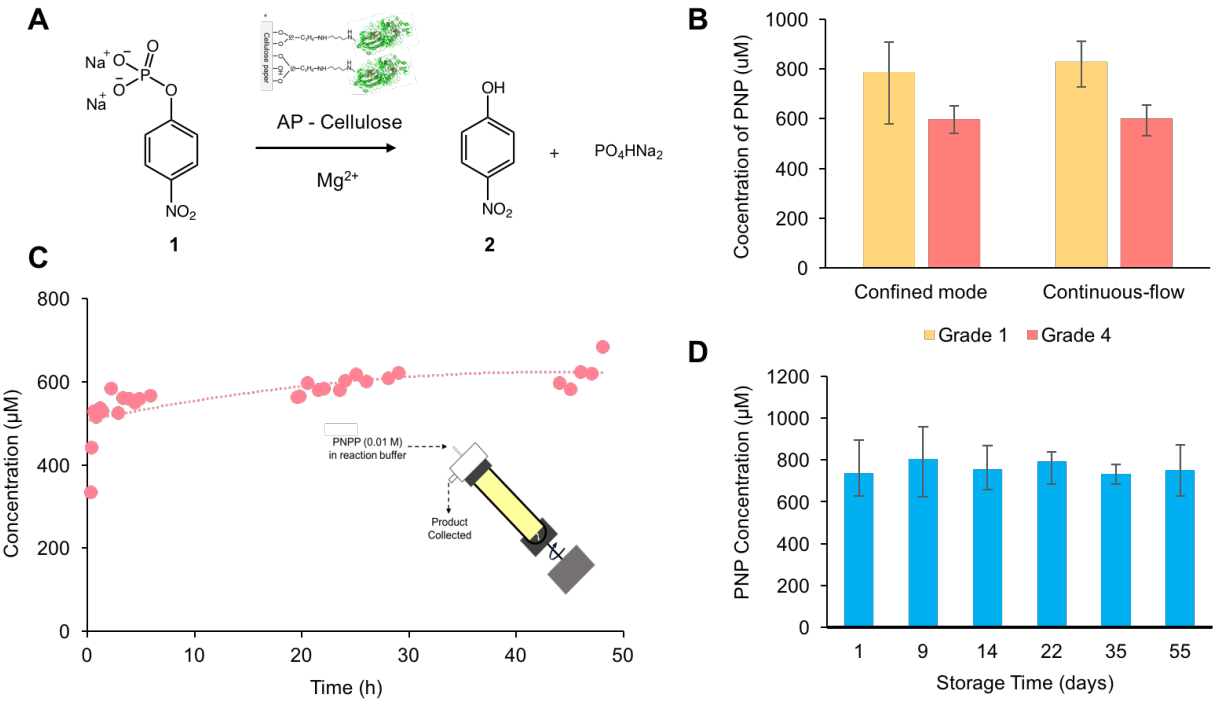

Figure 3.2. Biocatalysis in the VFD using AP immobilised on cellulose paper. All reactions are performed at 7.5k rpm, at a 45° tilt angle. (A) AP-cellulose catalysed hydrolysis of 4-nitrophenyl phosphate (**1**, 10 mM) to 4-nitrophenol (**2**), in 1 M diethanolamine buffer (pH 9.6, 2mM $MgCl_2$). (B) Whatman cellulose paper grade comparison in confined mode, after 5 mins, and continuous-flow mode, with a 1.0mL/min flow rate (n = 6). (C) Continuous-flow reaction running 48h. (D) Storage stability at 4°C measured using confined mode reactions, after 5 minutes (n=3). Reaction solutions are quenched with 4.0M NaOH, and substrate turn-over measured at 405nm.

When translated in continuous-flow, no significant difference in conversion was observed (Figure 3.2B and C). A continuous-flow reaction was performed over 48 hours, with

a flow rate of 1.0mL/min, at 7.5k rpm and a 45° tilt angle. No decrease in conversion was observed over this time, indicating no catalyst deactivation or significant leaking of the catalyst (Figure 3.2C). To further confirm no leaching was occurring, aliquots were collected and half the solution was quenched immediately and the other half quenched after 1 hour. No further turn-over was detected after this time. This indicates the catalyst is stable during extended reaction times and demonstrates the ability of the system to be scaled up. The stability of the catalyst after long term storage was also evaluated with no noticeable decrease in activity of AP-cellulose after 55 days stored at 4°C (Figure 3.2D). Finally, the rate of reaction, Kcat apparent, was derived for the AP-cellulose VFD processing and non-VFD processed solutions (Table 3.1, Figure S3.3). The AP-cellulose catalyst in the VFD shows similar rates to non-VFD processed solutions. Even so, the ability to use the enzyme tethered to the cellulose matrix in the VFD has a distinct advantage in avoiding the need for separating the enzyme from product under batch processing, and the ability to directly scale up the processing under continuous flow conditions.

3.3.3. Aristolochene Synthase (AS) on Cellulose

Terpenes are one of the most common classes of natural products, with varied structures ranging from linear hydrocarbons to complex cyclic molecules [26]. Terpenes are abundant in nature and have diverse applications, including in the agrochemical and pharmaceutical industries [27, 28]. Enzymes that catalyse the synthesis of these molecules are termed terpene synthases. Specific class of terpene synthases called sesquiterpene cyclases, catalyse the cyclisation of the isoprenoid, farnesyl pyrophosphate (**6**), to chiral cyclic C15 terpenes [29]. The regio- and stereoselectivity of these sesquiterpene synthesis make them an attractive catalyst for the synthesis of this class of complex natural products.

The sesquiterpene cyclases, aristolochene synthase (AS, **8**) from *Aspergillus terreus* [29] and amorpha-4,11-diene synthase (ADS, **7**) from *Artemisia annua* [30], was explored. ADS catalyses the first and rate-limiting step in the biosynthesis of artemisinin [31, 32], which is an important antimalarial natural compound. AS is an intermediate in several fungal toxins, including gigantenone, sporogen-AO1, bipolaroxin, and PR-toxin [33]. The substrate for these enzymes, Farnesyl pyrophosphate (**6**), can be synthesised from the sequential condensation of isopentenyl pyrophosphate (**4**) with dimethylallyl pyrophosphate (**3**), followed by the resulting geranyl pyrophosphate (**5**), catalysed by farnesyl pyrophosphate synthase (FDPS) (Figure 3.3) [34].

The efficiency and utility of sesquiterpene cyclases is limited by the slow release of reaction products. Due to the low solubility of the hydrophobic sesquiterpenes in water, the aqueous reaction buffer reaches saturation quickly, leading to their retention within the active site [35]. Therefore, the overall rate of reaction is low. Combining Immobilisation and continuous-flow of sesquiterpene cyclases for application in continuous-flow could have the potential to overcome this drawback and improve efficacy of the reaction. Immobilisation of high amounts of enzymes to increase yield while also flowing new buffer through the VFD could be beneficial, with saturated buffer replaced with fresh buffer [36].

The genes encoding for ADS and AS were cloned into pET28 expression vectors and expressed in BL21 *E.coli* cells. Soluble AS is expressed in high yields (Figure S3.6), however ADS expression was inconsistent and when optimised still resulted in low yields of soluble protein (Figure S3.8). Therefore, further studies were performed on AS.

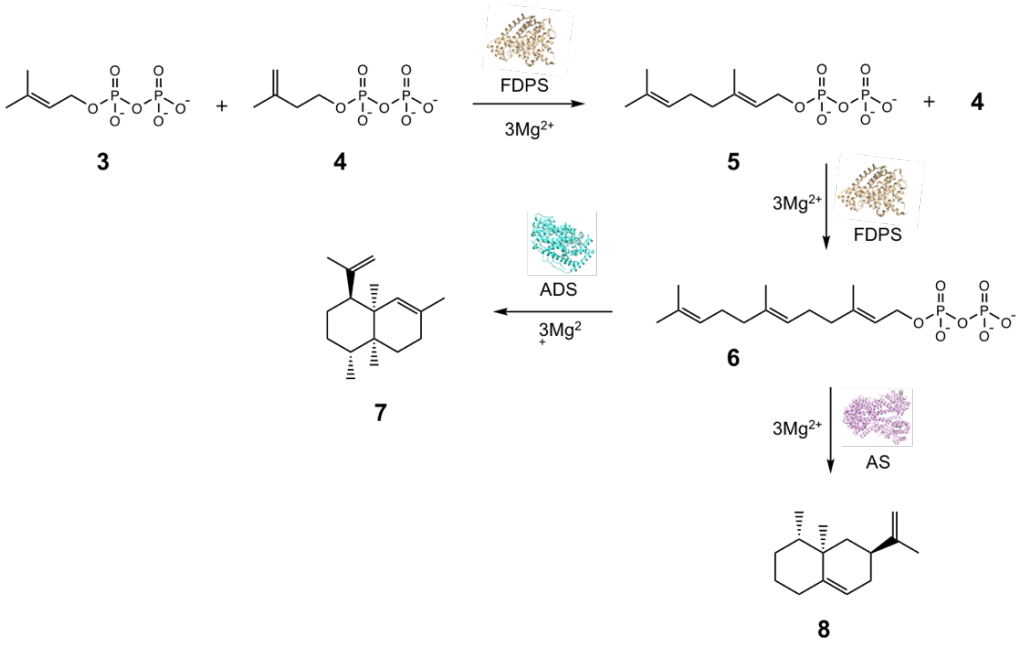

Figure 3.3. Multi-enzyme synthesis of sesquiterpene synthases, amorpha-4,1-diene (**7**) and aristolochene (**8**). Farnesyl pyrophosphate synthase (FDPS) mediates the condensation of isopentenyl pyrophosphate (**4**) with dimethylallyl pyrophosphate (**3**) to produce geranyl pyrophosphate (**5**). FDPS further catalyses the condensation of **4** and **5** to produce farnesyl pyrophosphate (**6**) which can be converted to **7** and **8**, catalysed by amorpha-4,11-diene synthase (ADS) and aristolochene synthase (AS), respectively. FDPS, ADS and AS require a cofactor, 3 Mg^{2+} ions per monomer.

The cellulose immobilisation method was followed for AS, as detailed above, however, the phosphate buffer was switched to a HEPES buffer. As will be discussed below, the malachite green assay, used to monitor the activity of aristolochene synthase, functions by detecting phosphate. Therefore, the use of phosphate in the expression, immobilisation and use of AS should be avoided. Similar levels of immobilisation were observed for AS, at 0.09 nmol/$cm^{2,}$ as measured by Bradford protein concentration assay (Table 3.1).

Table 3.1. Enzyme immobilisation quantity, reaction rate in the VFD and batch.

Enzyme	Amount of Enzyme Immobilised (nmol/cm^2)	Kcat apparent VFD (min^{-1})	Kcat apparent Batch (min^{-1})
AP	0.16	45 ± 5	40 ± 4
AS	0.09	1.0 ± 0.4	1.3 ± 0.1

A continuous-flow reaction was performed using the AS-cellulose catalyst in the VFD at 7.5k rpm, 45° tilt angle, at a flow rate of 1.0mL/min. The continuous-flow reaction successfully catalysed the conversion of farnesyl pyrophosphate to aristolochene synthase (Figure 3.4). The amount of aristolochene produced and released from AS can be determined using a Malachite green phosphate assay [37]. The Malachite Green functions by detecting free monophosphate in solution by formation of a complex that absorbs at 620nm. Using a phosphate standard curve, the concentration of monophosphate can be quantitatively determined. Pyrophosphate, the by-product of AS, can be hydrolysed to give monophosphate by inorganic pyrophosphatase (PPiase) (Figure 3.4A). Due to the high turn-over rate of PPiase (200-400s^{-1}), it can be assumed that all pyrophosphate is converted into monophosphate [38]. Thus, by detecting the concentration of monophosphate in solution, the concentration of aristolochene released from AS can also be determined. The rate of reaction, Kcat apparent, was derived for AS-cellulose in the VFD, 1.0 ± 0.4 min^{-1}, and for non-VFD processed AS, 1.3 ± 0.1 min^{-1} (Table 3.1, Figure S3.4). The AS-cellulose catalyst in the VFD shows similar rates to non-VFD processed solutions.

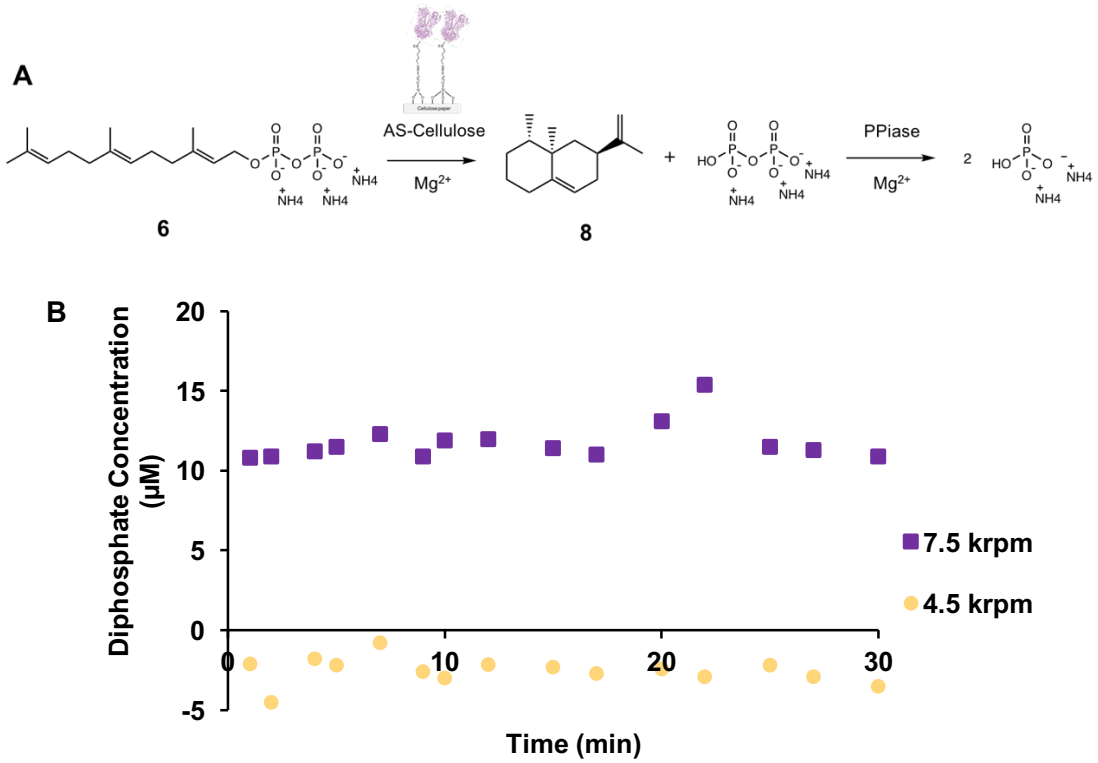

Figure 3.4. Biocatalysis in the VFD using AS immobilised on cellulose paper. (A) AS-cellulose mediated cyclisation of farnesyl pyrophosphate (**6**) into aristolochene (**8**). The pyrophosphate by-product can be hydrolysed using inorganic pyrophosphate synthase (PPiase), affording two monophosphate ions. The monophosphate ions are detected using a Malachite Green phosphate assay. (B) Continuous-flow VFD reaction, where **6** (500μM) in a Tris-HCl buffer (pH 7.5) is fed through the borosilicate glass tube containing immobilised AS-Cellulose, at a flow rate of 1.0mL/min.

When the continuous-flow reaction was performed at 4.5k rpm no conversion was detected (Figure 3.4B). We hypothesis that the difference in catalytic efficiency possibly arises from the different fluid dynamics at different rotational speeds. High localized mixing at rotational speeds between 3.8k and 4.5k rpm arises from the interplay of Faraday-wave double helical flow and circular flow [39]. Alternatively, for rotation speeds ≥ 6k rpm, eddies associated with Faraday waves striking the surface of the tube result in higher shear stress [39].

The effect of this complex fluid flow on enzyme structure and catalytic activity is not well understood. Previous experiments have shown VFD-mediated enzyme acceleration with free enzymes in solution processed between 6k and 8k rpm [13]. Hypotheses attributes this acceleration to the Faraday wave induced shear-stress and high mass transfer, resulting in increase substrate accessibility and removal from the enzyme active site. Although enhancement has not yet been demonstrated using immobilised enzymes, it is hypothesised here that while the fluid flow at high rotational speeds can accelerate free-enzyme activity, the fluid flow at lower rotational speeds could de-activate or lower the activity of certain immobilised enzymes.

3.4. Conclusion

An enzyme immobilisation method involving covalent attachment onto functionalised cellulose paper for use in thin-film continuous-flow biocatalysis has been developed. The catalyst was found to be active and stable over a 48h continuous-flow reaction, processing 2.9L with a 0.01 M substrate concentration,, and after days stored at 4°C. The method was further applied to the continuous-flow synthesis of an anti-malarial drug intermediate, aristolochene, following the immobilisation of aristolochene synthase derived from *Aspergillus terreus*. Immobilisation and application of a valuable terpene cyclase for the synthesis of complex chiral terpene is a significant finding, having potential application for the synthesis of complex molecules in general in the VFD.

The VFD presents advantages relative to conventional methods, including the use of a single continuous reaction vessel, high surface to volume ratio of the enzyme support and substrate solution, and the ability to reuse and recycle the enzyme. Furthermore, this ultra-thin cellulose ‘cartridges’ technology could be applied for multi-step and multi-enzyme assembly

line synthesis, where the substrate undergoes one reaction for the first band of tethered enzyme encountered in the VFD tube, then another reaction for the second band with a different enzyme attached, and so on. The ability to perform assembly line synthesis enzymatic catalysis expands the versatility of the VFD.

Future research in this area should focus on developing the technology for performing cascade reactions for the synthesis of complex natural products. In addition, enhancing the activity of enzymatic catalysis while enzymes are immobilised should be explored for further increasing through-put and utility of valuable enzymes in the pharmaceutical and fine-chemical industry. This would build on the enhanced enzymatic activity for non-tethered enzymes in the VFD [13].

3.5. Experimental

3.5.1. Overexpression and Purification of recombinant AP

AP-pET46 construct [15] was transformed *via* heat shock into *E.coli* BL21 (DE3) cells. The transformed cells were transferred to a LB agar plate containing 50μg/mL of carbenicillin antibiotic, and incubated at 37°C for 14h. A seed culture was prepared by inoculating a single colony into 50mL of LB media with 50μg/mL of carbenicillin antibiotic and shaking the culture at 220rpm for 14h at 37°C in a 125mL baffled flask. The expression culture was prepared by inoculating 10mL of seed culture into 1L of LB media with 50μg/mL of carbenicillin antibiotic and shaking at 220 rpm at 37°C in a 4L baffled flask. When the culture reached an OD_{600} of 0.8, the cells were induced with 0.5mM IPTG. The induced expression culture was incubated by shaking at 220 rpm for 20-24h at 18°C. The cells were then centrifuged at 6,360g for 20 mins at 4°C and resuspended in 25mL lysis buffer (20mM Tris-HCl, 500mM NaCl, pH 8.00,

10mM BME, 1mM PMSF). The cell lysate was prepared by sonication (Digital Sonifier 450; std. horn, 7 min sonication, 30 sec on, 40 sec off, 40% amplitude), centrifuged at 28,900g for 1h at 4°C and the supernatant purified using a nickel affinity chromatography involving a gravity column containing charged (with 1M $NiSO_4$) and equilibrated iminodiacetic acid (IDA) resin (3g, Purolite). The following buffers were used to purify AP and each collected separately: lysis buffer (50mL), wash buffer (50mL, 20mM Tris-HCl, 500mM NaCl, pH 8.00, 40mM imidazole, 10mM BME), and elution buffer (50mL, 20mM Tris-HCl, 500mM NaCl, pH 8.00, 250mM imidazole, 10mM BME). Fractions containing purified protein, identified by SDS-PAGE, were combined and dialysed for 14-16h in dialysis buffer (20mM Tris-HCl, 500mM NaCl, pH 8.00, 10mM BME, 10% glycerol). The dialysed protein solution was concentrated in a 30kDa micro-concentrator. The purity of the protein was confirmed using 12% SDS-PAGE (Figure S3.5).

3.5.2. Cloning of AS in pET28 Vector

The codon optimised gene coding for aristolochene synthase from *Aspergillus terreus* was synthesised and purchased from Genewiz in a pUC57 vector. The following PCR parameters and oligonucleotides (integrated DNA Technologies) were used to amplify the AS gene for ligation independent cloning (LIC) into pet28 vector. The PCR reaction mixture consisted of Herculase ii DNA polymerase (New England Biolabs) and buffer (5 x diluted final concentration, New England Biolabs), dNTPs (0.5mM each final concentration, New England Biolabs), primers (33ng each final concentration, Integrated DNA Technologies). PCR was performed with 1 cycle of 95°C for 5 min followed by 25 cycles of 95°C for 1 min, 65°C for 1 min, and 72°C for 2 min, followed by 1 cycle of 72°C for 5 min. Forward: 5'- CAG GGC GCC

AAT GGC GCT GAC CGA AGA AAA ACC GAT CCG -3'. Reverse: 5'- GAC CCG ACG CGG TTA TTA GAT AGA CAT CGG GTA AAC CAG -3'.

The DNA (~1045bp) was extracted from a 1% agarose gel using a Zymoclean Gel DNA Recovery Kit and sequenced by Genewiz. This DNA was cloned into a pet 28 vector using LIC to generate the AS protein expression vector. The DNA was treated with T4 DNA polymerase (New England Biolabs) to create overhangs with complementary between the vector and the DNA insert. The following reaction solution was incubated at 22°C for 30 mins, then heat activated for 20 mins at 75°C: 500ng of DNA was treated with 2μL T4 DNA polymerase, 2μL 10x NEB 2 buffer, 0.5μL of 100mM dATP, 1.0μL of 100mM DTT, 0.2μL of 100x BSA and autoclaved water to give a reaction volume of 20μL. The T4 treated DNA was annealed to the pet28LIC_Tev vector. The vector was prepared for annealing with the insert outlined below. The T4 treated DNA (10uL) was incubated with 40ng of vector (2uL) at 22°C for 5 mins. EDTA (25mM, 1uL) and T4 DNA Ligase (1μL, New England BioLabs) were added to the annealing solution prior to incubation at 22 °C for 45 mins. *E. coli* Nova blue cells were used to isolate the plasmid prior to transformation into other heterologous hosts. The isolated plasmid was sequenced using Sanger sequencing (Genewiz).

Pet28 LIC vector was digested and treated with T4 DNA polymerase for use in LIC cloning. The pet28 vector was digested by incubating the following reaction solution at 37°C for 3h and at 50°C for 1h: 15μL of plasmid DNA (50ng), 1μL of BSAI-HF (New England Biolabs), 0.2μL 100 x BSA, 2.0μL 10 x Cutsmart Buffer (New England Biolabs). The DNA was extracted from a 1% agarose gel using a Zymoclean Gel DNA Recovery Kit and immediately treated with T4 DNA polymerase, to avoid vector reannealing. The following reaction solution was incubated at 22°C for 30 min and heat activated at 75°C for 20 min: 11.0μL digested plasmid DNA, 1.5μL 10 x T4 DNA polymerase buffer, 1.5μL 25mM dTTP

(NEB), 0.75μL 100mM DTT, and 0.25μL T4 DNA polymerase. The DNA was isolated from the reaction solution using a Zymoclean Clean and Concentrator Kit and stored at -20°C until use in LIC cloning.

3.5.3. Overexpression and Purification of Recombinant AS

AS-pET28a plasmid was transformed *via* heat shock into *E.coli* BL21 (DE3) cells. The transformed cells were transferred to a LB agar plate containing 40μg/mL of kanamycin antibiotic, and incubated at 37°C for 14h. A seed culture was prepared by inoculating a single colony into 50mL of LB media with 40μg/mL of kanamycin antibiotic and shaking the culture at 220 rpm for 14h at 37°C in a 125mL baffled flask. The expression culture was prepared by inoculating 10mL of seed culture into 1L of LB media with 40μg/mL of kanamycin antibiotic and shaking at 220 rpm at 37°C in 4L baffled flask. When the culture reached an OD_{600} of 0.7 the cells were induced with 0.5mM IPTG. The induced expression culture was incubated by shaking at 220 rpm for 5h at 25°C. The cells were centrifuged at 6,360 g for 20 mins at 4°C and resuspended in 25mL lysis buffer (25mM HEPES, 200mM NaCl, 10mM $MgCl_2$, 10mM imidazole, pH 7.50, 1mM BME, 1mM PMSF). The cell lysate was prepared by sonication (Digital Sonifier 450; std. horn, 7 min sonication, 30 sec on, 40 sec off, 40% amplitude), centrifuged at 28,900g for 1h at 4°C and the supernatant purified using nickel affinity chromatography using a gravity column containing charged (with 1mM $NiSO_4$) and equilibrated IDA resin (3g, Purolite). The following buffers were used to purify AP with each collected separately: lysis buffer (50mL), wash buffer (50mL, lysis buffer with 40mM imidazole), and elution buffer (50mL, lysis buffer, 250mM imidazole, 10% glycerol). Fractions containing purified protein, identified by SDS-PAGE, were combined and dialysed for 14-16h

in dialysis buffer (lysis buffer, 10% glycerol). The dialysed protein solution was concentrated in a 30kDa microconcentrator. The purity of the protein was confirmed using 12% SDS-PAGE (Figure S3.6 and S3.7). The protein is stored at -20°C.

3.5.4. Enzyme Immobilisation on Cellulose Paper in the VFD

Cellulose paper (Grade 4, 50mm x 150mm) was placed into a 20mm borosilicate glass tube and placed in an oven (~160°C) for 1h, then immediately capped. The cellulose paper is wet with MeOH, followed by processing a solution of APTES (1mL) in MeOH (2mL) in the VFD at 7.5k rpm for 1h. The tube (with cellulose paper) is washed with MeOH (5 x 5mL) and inverted, then placed in the oven for 1h. After cooling the tube with cellulose paper is wet with PBS buffer (pH 8.0), followed by processing a solution of glutaraldehyde (25%, 700uL, 5% of total volume) in PBS buffer (2.3mL) in the VFD at 7.5k rpm for 1h. The cellulose paper is washed with PBS buffer pH 8.0 (3 x 5mL) and PBS buffer pH 7.0 and inverted. Enzyme solution (2.0mg/ml, in PBS buffer, pH 7.0) was used for immobilisation in the VFD at 7.5k rpm for 45 mins. The immobilisation solution was taken and used to dissolve 100mg of $NaBH_3CN$. Without washing the tube, the solution is placed back in the tube and processed in the VFD at 7.5k rpm for 30 mins. The tube is then washed with PBS buffer pH 7.0 (5 x 5mL), followed by diethanolamine buffer (pH 9.8, 3 x 5mL) prior to use.

3.5.5. Confined Mode VFD Activity Assay for AP

PNPP (0.01M) in diethanolamine buffer (3.0mL, pH 9.8) was added to a borosilicate glass tube (20mm OD, 17.5 ID, 18.5cm long) containing cellulose paper immobilised AP. The tube was capped with a rubber septum and processed in the VFD for 5 mins at 7.5k rpm, at a

45° tilt angle. The solution is then immediately transferred to a 5.0mL Eppendorf tube containing 400μL of 4.0 M NaOH. 100μL of this solution is transferred to a 96-well plate (Corning) and analysed at 405nm using a Biotek UV-Vis microplate reader.

3.5.6. Continuous-Flow VFD Activity Assay for AP

PNPP solution (0.01M) in diethenolamine buffer (1.0M, $MgCl_2$, pH 9.8) is continuously fed through the VFD tube, containing cellulose paper immobilised AP, at 1.0ml/min, rotating at 8k rpm, at a 45° tilt angle. Aliquots were collected and 1.0mL of each immediately added to a 1.5mL Eppendorf tube containing 133.3μL of 4.0M NaOH. 100μL of this solution is transferred to a 96-well plate (Corning) and analysed at 405nm using a Biotek UV-Vis microplate reader. Aliquots were collected periodically over 48h.

3.5.7. Activity Assay for AP in 96-well plate

Standard solutions of AP (0-18μM), were prepared in diethanolamine buffer (1.0M diethanolamine, 2mM $MgCl_2$, pH 9.8). A sample of each solution (100μL) was then added to a 96-well plate (Corning), in triplicate, followed by 100μL of PNPP (0.02M) in diethanolamine buffer was added and allowed to incubate for 5 minutes. The standard solutions were quenched with 26.6μL of 4.0M NaOH. The quenched standard solutions were diluted, by adding 20μL of each solution to a separate well containing 80μL ddH_2O, prior to analysis at 405nm on a Biotek microplate reader.

3.5.8. Confined Mode VFD Activity Assay for AS

Farnesyl pyrophosphate (500μM) in 3mL Tris Buffer (20mM Tris-HCl, 2mM $MgCl_2$, pH 7.5, 2mM DTT, 1.25μM inorganic pyrophosphate synthase) was added to a borosilicate glass tube containing cellulose paper immobilised AS. The tube was then capped with a rubber septum and processed in the VFD for 5 mins at 7.5k rpm, at a 45° tilt angle. The solution was then immediately removed from the tube and transferred to a 5.0mL Eppendorf tube. A sample (40μL) is transferred to a 96-well plate (Corning) containing 40μL of ddH_2O, in triplicate. Malachite Green reagent (20μL, Sigma Aldrich, MAK307) is added to each well and incubated for 30 minutes. The plate is read at 620nm using a Biotek UV-Vis microplate reader. The concentration of free phosphate is calculated using a phosphate standard curve (0-40μM).

3.5.9. Continuous-Flow VFD Activity Assay for AS

Farnesyl pyrophosphate (500μM) in Tris Buffer (20mM Tris-HCl, 2mM $MgCl_2$, pH 7.5, 2mM DTT, 1.25μM inorganic pyrophosphate synthase) is continuously fed through the VFD tube, containing cellulose paper immobilised AS, at 1.0ml/min, rotating at 7.5k rpm, at a 45° tilt angle. Aliquots are collected and 1.0mL of each immediately added to a 1.5mL Eppendorf tube. A sample (40μL) is transferred to a 96-well plate (Corning) containing 40μL of ddH_2O, in triplicate. Malachite Green reagent (20μL, Sigma Aldrich, MAK307) is added to each well and incubated for 30 minutes. The plate was read at 620nm using a Biotek UV-Vis microplate reader. The concentration of free phosphate was calculated using a phosphate standard curve (0-40μM).

3.5.10. Activity Assay for AS in 96-Well Plate with Varied Concentrations of FPP

Standard solutions of FPP (0-375μM), in triplicate, were prepared in Tris Buffer (20mM Tris-HCl, 2mM $MgCl_2$, pH 7.5, 2mM DTT, 1.25μM inorganic pyrophosphate synthase) in a 96-well plate (Corning). A sample (67μL) of each standard solution was transferred to separate wells each containing 33μL of AS (21.4μM in 25mM HEPES buffer, 200mM NaCl, pH 7.5), and incubated for 5 minutes. A sample (20μL) of each is transferred separate wells containing 60μL of ddH_2O. Malachite Green reagent (20μL, Sigma Aldrich, MAK307) is added to each well and incubated for 30 minutes. The plate is read at 620nm using a Biotek UV-Vis microplate reader. The concentration of free phosphate is calculated using a phosphate standard curve (0-40μM).

3.5.11. Activity Assay for AS in 96-Well Plate with Varied Concentrations of AS

Standard solutions of AS (0-10μM), in triplicate, were prepared in Tris Buffer (20mM Tris-HCl, 2mM $MgCl_2$, pH 7.5, 2mM DTT, 1.25μM inorganic pyrophosphate synthase) in a 96-well plate (Corning). A sample (95.7μL) of each standard solution was transferred to separate wells, each containing 4.3μL of FPP (5.77mM in ddH_2O), and incubated for 5 minutes. A sample (20μL) of each was transferred to separate wells containing 60μL of ddH_2O. Malachite Green reagent (20μL, Sigma Aldrich, MAK307) is added to each well and incubated for 30 minutes. The plate was read at 620nm using a Biotek UV-Vis microplate reader. The concentration of free phosphate was calculated using a phosphate standard curve (0-40μM).

3.6. Acknowledgements

This work is supported by the Australian Research Council and the South Australian Government. Special thank you for the support of Prof. Gregory Weiss, and for giving me the opportunity to visit his laboratory at the University of California, Irvine, where this research was conducted. Also, thank you to Rodger de Miranda and Dr Sudipta Majumdar for their assistance.

3.7. References

[1] Sheldon, R. A. and Woodley, J. M. Role of Biocatalysis in Sustainable Chemistry. *Chem. Rev*. **2018**, *118*, 801-838.

[2] Sheldon, R. A. and Pelt, S. V. Enzyme immobilisation in biocatalysis: why, what and how. *Chem. Soc. Rev.* **2013**. *42*, 6223-6235.

[3] DiCosimo, R., McAuliffe, J., Pouloseb, A. J., Bohlmann, G. Industrial use of immobilized enzymes. *Chem. Soc. Rev*. **2013**, *42*, 6437-6474.

[4] Britton, J., Majumdar, S., Weiss, G. A. Continuous flow biocatalysis. *Chem. Soc. Rev*. **2018**, *47*, 5891-5918.

[5] Gutmann, B.; Cantillo, D.; Kappe, C. O. Continuous-Flow Technology—A Tool for the Safe Manufacturing of Active Pharmaceutical Ingredients. *Angew. Chem. Int. Ed*. **2015**, *54*, 6688-6728.

[6] Romero-Fernández, M., Paradisi, F. Protein immobilization technology for flow biocatalysis. *Curr. Opin. Chem. Biol.* **2020**, *55*, 1-8.

[6a] Zdarta, J., Meyer, A. S., Jesionowski, T., Pinelo, M. A General Overview of Support Materials for Enzyme Immobilization: Characteristics, Properties, Practical Utility. *Catalysts* **2018**, *8*, 92, 1-27.

[7] Klemm, C., Heublein, B., Fink, H. P., Bohn, A. Cellulose: Fascinating Biopolymer and Sustainable Raw Material. *Angew. Chem. Int. Ed.* **2005**, *44*, 3358 – 3393.

[8] Liu, Y., Chen, J. Y. Enzyme immobilization on cellulose matrixes. *J. Bioact. Compat. Pol.* **2016**, *31*, 553-567.

[9] Britton, J, Stubbs, KA, Weiss, GA, Raston, CL: Vortex Fluidic Chemical Transformations, *Chem. Euro. J.,* **2017**, *23*, 13270-13278.

[10] Pye, S. J., Dalgarno, S. J., Chalker, J. M., Raston, C. L. Organic oxidations promoted in vortex driven thin films under continuous flow, *Green Chemistry*, **2018**, *20*, 118 – 124.

[11] Phillips, J. M., Ahamed, M., Duan, X. F., Lamb, R. N., Qu, X., Zheng, K., Zou, J., Chalker, J. M., Raston, C. L. Chemoselective and continuous flow hydrogenation in thin films using a palladium nanoparticle catalyst embedded in cellulose paper. *ACS App. Bio Mat*. **2019**, 2, 488-494.

[12] Wills, S. S., Raston, C. L., Stubbs, K. A.. Integrating thin film microfluidics in developing a concise synthesis of DGJNAc: A potent inhibitor of α-N-acetylgalctosaminidases, Bioorganic Med. Chem. Lett. **2018**, *28*, 3748-3751.

[13] Britton, J., Meneghini, L. M., Raston, C. L, Weiss, G. A. Accelerating Enzymatic Catalysis Using Vortex Fluidics, *Angew. Chem. Int. Ed*. **2016**, *55*, 11387 – 11391.

[14] Britton, J., Raston, C. L., Weiss, G. A. Rapid protein immobilization for thin film continuous flow biocatalysis. *Chem. Commun*., **2016**, *52*, 10159-10162.

[15] Britton, J., Dyer, R. P., Majumdar, S., Raston, C. L., Weiss, G. A. Ten-Minute Protein Purification and Surface Tethering for Continuous-Flow Biocatalysis. *Angew. Chem. Int. Ed*. **2017**, *56*, 2296-2301.

[16] Yuan, T. Z., Ormonde, C. F. G., Kudlacek, S. T., Kunche, S., Smith, J. N., Brown, W. A., Pugliese, K. M., Olsen, T. J., Iftikhar, M., Raston, C. L., Weiss, G. A. Shear stress-mediated refolding of proteins from aggregates and inclusion bodies. *ChemBioChem*. **2015**, *16,* 393-396.

[17] Britton, J., Smith, J. N., Raston, C. L., Weiss, G. A. Protein folding using a vortex fuidic device. *Methods Mol. Biol.* **2017,** *1586*, 211-220.

[18] Luo, X. Al-Antaki, A. H. M., Harvey D. P., Ruan, Y., He, S., Zhang, W., Raston, C. L. Vortex Fluidic Mediated Synthesis of Macroporous Bovine Serum Albumin-Based Microspheres. *ACS Appl Mater Interfaces*. **2018**, *10*, 27224-27232.

[19] Luo, X. Al-Antaki, A. H .M., Pye, S., Meech, R., Zhang, W., Raston, C.L. High-Shear-Imparted Tunable Fluorescence in Polyethylenimines, *ChemPhotoChem*, **2018**, *2*, 343 –348.

[20] Luo, X. Al-Antaki, A.H.M., Vimalanathan, K., Moffatt, J., Zheng, K., Zou, Y., Zou, J., Duan, X., Lamb, R. N., Wang, S., Li, Q., Zhang, W., Raston, C.L. Laser irradiated vortex fluidic mediated synthesis of luminescent carbon nanodots under continuous flow, *React. Chem. Eng.*, **2018**, ***3***, 164-170.

[21] Tong, C. L., Stroeher, U. H., Brown, M. H., Raston, C. L. Continuous flow vortex fluidic synthesis of silica xerogel as a delivery vehicle for curcumin, *RSC Adv.*, **2015**, ***5***, 7953-7958.

[22] Migneault, I., Dartiguenave, C., Bertrand, M. J., Waldron, K. C. Glutaraldehyde: behavior in aqueous solution, reaction with proteins, and application to enzyme crosslinking. *BioTechniques*, **2004**, *37*, 790–802.

[23] Mateo, C., Palomo, J. M., Fernandez-Lorente, G., Guisan, J. M., Fernandez-Lafuente, R. Improvement of enzyme activity, stability and selectivity via immobilization techniques. *Enzyme Microb. Technol*., **2007**, *40*, 1451–1463.

[24] Miller, A. W., Robyt, J. F. Sodium cyanoborohydride in the immobilization of proteins to glutaraldehyde-activated aminoalkyl silica. *Biotechnol. Bioeng.*, **1983**, *25*, 2795 —2800.

[25] Dean, R. L. Kinetic studies with alkaline phosphatase in the presence and absence of inhibitors and divalent cations. *Biochem. Mol. Biol. Edu*. **2002**, *30*, 401-407.

[26] Christianson, D. W. Structural and Chemical Biology of Terpenoid Cyclases. *Chem. Rev*. **2017**, *117*, 11570-11648.

[27] Greenhagen, B., Chappell, J. Molecular scaffolds for chemical wizardry: Learning nature's rules for terpene cyclases. *PNAS*. **2001**, *98*, 3479–13481.

[28] Brill, Z. G., Condakes, M. L., Ting, C. P., Maimone, T. J. Navigating the Chiral Pool in the Total Synthesis of Complex Terpene Natural Product. *Chem. Rev.* **2017**, *117*, 11753-11795.

[29] Diaz, J. E., Lin, C. S., Kunishiro, K., Feld, B. K., Avrantinis, S. K., Bronson, J., Greaves, J., Saven, J. G., Weiss, G. A. Computational design and selections for an engineered, thermostable terpene synthase. *Protein Sci*. **2011**, *20*, 1597-606.

[30] Abdallah, I. I., van Merkerk, R., Klumpenaar, E., Quax, W. J. Catalysis of amorpha-4,11-dienesynthase unraveled and improved by mutability landscape guided engineering. *Nature Sci. Rep.* **2018**, *8*, 9961, 1-11.

[31] Schmid, G., Hofheinz, W. Total Synthesis of Qinghaosu. *J. Am. Chem. Soc*. **1983**, *105*, 624-625.

[32] C. J. Paddon, P. J. Westfall, D. J. Pitera, K. Benjamin, K. Fisher, D. McPhee, M. D. Leavell, A. Tai, A. Main, D. Eng, D. R. Polichuk, K. H. Teoh, D. W. Reed, T. Treynor, J. Lenihan, M. Fleck, S. Bajad, G. Dang, D. Dengrove, D. Diola, G. Dorin, K. W. Ellens, S.

Fickes, J. Galazzo, S. P. Gaucher, T. Geistlinger, R. Henry, M. Hepp, T. Horning, T. Iqbal, H. Jiang, L. Kizer, B. Lieu, D. Melis, N. Moss, R. Regentin, S. Secrest, H. Tsuruta, R. Vazquez, L. F. Westblade, L. Xu, M. Yu, Y. Zhang, L. Zhao, J. Lievense, P. S. Covello, J. D. Keasling, K. K. Reiling, N. S. Renninger & J. D. Newman. High-level semi-synthetic production of the potent antimalarial artemisinin. *Nature*. **2013**, *963*, 528-532.

[33] Proctor, R. H., Hohn, T. M. Aristolochene Synthase. Isolation, Characterization, and Bacterial Expression of a Sesquiterpenoid Biosynthetic Gene (aril) from Penicillium Roqueforti. *J. Biol. Chem.* **1993**, *268*, 4543-4546.

[34] Kavanagh KL, Guo K, Dunford JE, Wu X, Knapp S, Ebetino FH, Rogers MJ, Russell RG, Oppermann U. The molecular mechanism of nitrogen-containing bisphosphonates as antiosteoporosis drugs. *PNAS*, **2006**, *103*, 7829-7834.

[35] Weidenhamer, J. D., Macias, F. A., Fisher, N. H., Williamson, B. Just how insoluble are monoterpenes? *J. Chem. Ecol*. **1993**, *19*, 1799–1807.

[36] Tang, X., Allemann, R. K., Wirth, T. Optimising Terpene Synthesis with Flow Biocatalysis. *European J. Org. Chem*. **2017**, *2017*, 414-418.

[37] Vardakou, M.; Salmon, M.; Faraldos, J. A.; O'Maille, P. E. Comparative analysis and validation of the malachite green assay for the high throughput biochemical characterization of terpene synthases. *MethodsX*, **2014**, *1*, 187–196.

[38] Kajander, T., Kellosalo, J., Goldman, A. Inorganic pyrophosphatases: One substrate, three mechanisms. *FEBS Letters*, **2013**, *587*, 1863-1869.

[39] Alsulami, I. K., Alharbi, T. M. D., Harvey, D. P., Gibson, C. T. & Raston, C. L. Controlling the growth of fullerene C_{60} cones under continuous flow, *Chem. Commun*. **2018**, *54*, 7896-7899.

3.8. Supporting Information

Cellulose Paper Grade Comparison

Two different cellulose paper grade/types were explored for the immobilisation of AP, Whatman's Cellulose paper Grade 1 and Grade 4. Grade 1 cellulose paper is the most widely used in laboratories for filtering in routine applications requiring medium retention and flow rate with particle retention of ~ 11μm, nominal thickness of 180μm and nominal basis weight of 87g/m^2. Grade 4 cellulose paper is a fast filter material with particle retention of ~ 25μm, nominal thickness of 210μm and nominal basis weight of 92g/m^2.

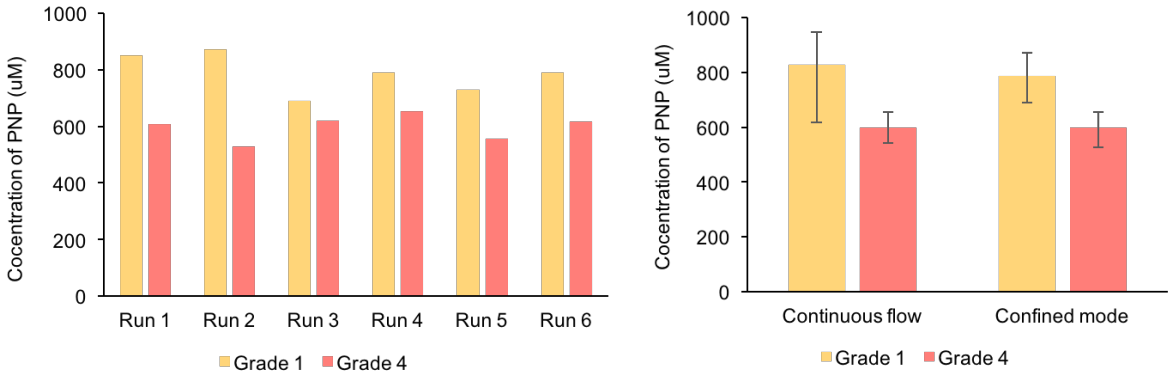

Figure S3.1. Effect of cellulose paper on substrate conversion. Conversion of PNPP (0.01M) in confined mode (7.5k rpm, 45°) over 6 cycles in the same AP-cellulose VFD tube (top graph). The average conversion of PNPP (0.01M) in continuous flow (1.0ml/min) and confined mode (7.5k rpm, 45°, n = 6, bottom graph).

Optimising Substrate Solution Volume

The effect of volume of substrate solution was explored in the confined mode operation of the VFD. The volume in the tube can determine the thickness of the film, which can effect how much solution comes into contact with the AP on the cellulose paper. Low volumes can lead to the solution not covering the entire AP-cellulose and higher volumes can lead to over dilution of the solution with no additional substrate turnover. The highest concentration of PNP results from 2mL of substrate solution and decreases when using 3mL, however, 3mL gives a larger amount of PNP produced in total.

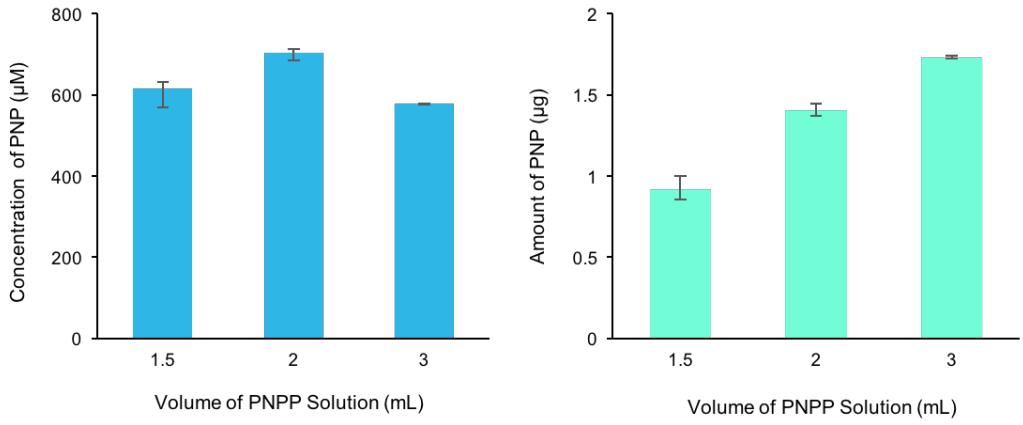

Figure S3.2. Effect of the volume of substrate solution on product conversion. PNPP (0.01M) in diethanolamine buffer processing under confined mode at 7.5k rpm, at 45°, in a VFD tube containing cellulose paper immobilised AP. The product solution is quenched in 200µL of 4.0M NaOH. Concentration of PNP (µM) shown on the left and amount of PNP (µg) shown on the right.

Activity Assay for AP in 96-well plate

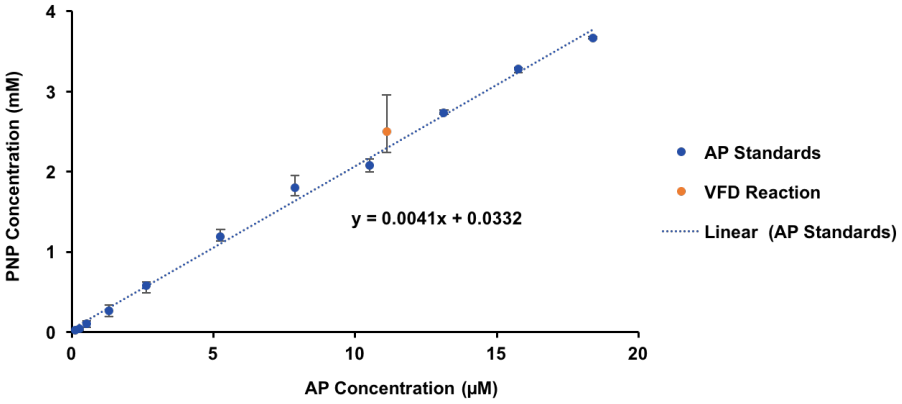

Figure S3.3. Activity Assay for AP with Varying Enzyme Concentration. The activity of AP was determined by measuring the conversion of 4-nitrophenyl phosphate (10mM) to 4-nitrophenol (PNP) using different concentrations of AP (0-18µM final concentration) in 1M diethanolamine buffer (pH 9.6, 2mM $MgCl_2$) after 5 mins incubation at RT. After quenching with 4.0M NaOH, PNP concentration was measured at 405nm, using a Biotek microplate reader. Molar extinction coefficient of PNP = 15644$M^{-1}cm^{-1}$.

Activity Assay for AS in 96-well plate

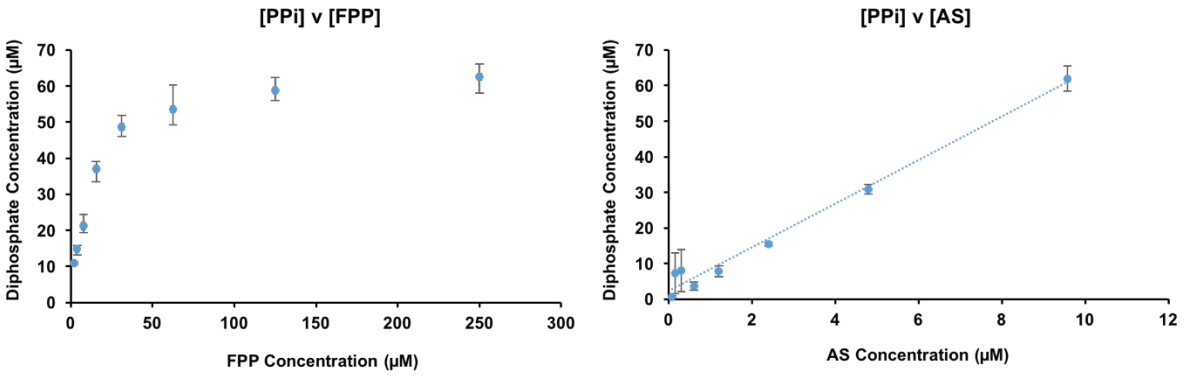

Figure S3.4. Activity Assay for AP with Varying Enzyme Concentration. The activity of AS was determined by measuring the conversion of farnesyl pyrophosphate (FPP) to aristolochene in Tris Buffer (pH 7.5, 2mM $MgCl_2$) after 5 mins incubation at RT, by varying FPP (using 9.6μM, left) and AS (using 500μM FPP, right) concentration. The reaction solution is diluted 1:4 in ddH_2O, followed by addition of Malachite Green reagent (1:4) and incubation for 30 minutes. The plate is read at 620nm using a Biotek UV-Vis microplate reader. The concentration of free phosphate is calculated using a phosphate standard curve (0-40μM).

Purification of AP

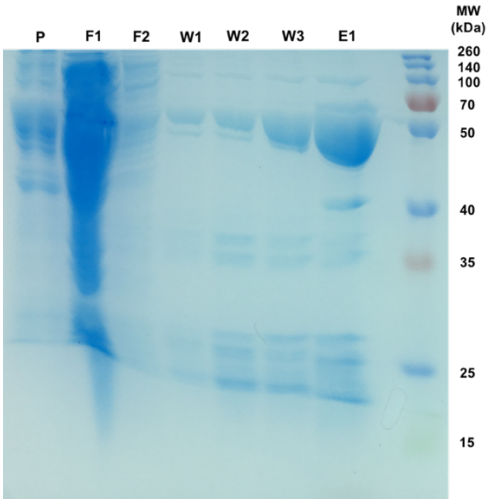

Figure S3.5. Purification of AP. In this 12% tris-glycene SDS-PAGE gel, each lane was loaded with 19μL of sample unless otherwise indicated. PageRuler pre-stained protein ladder (10μL, Thermo Fisher Scientific) was used. Lane P: 1μL of insoluble pellet in 18μL of ddH_2O. Lane F1: flow through after batch binding the cell lysate to the resin. Lane F2: flow through after batch binding the cell lysate to the resin and 30mL 10mM imidazole wash. Lane W1-3: column wash with 25mL each of buffers with 30, 75, 100mM imidazole, respectively. Lane E1: AP eluted with 30mL buffer containing 250mM imidazole. Buffer: 20mM Tris-HCl, 500mM NaCl, pH 8.00, 10mM BME.

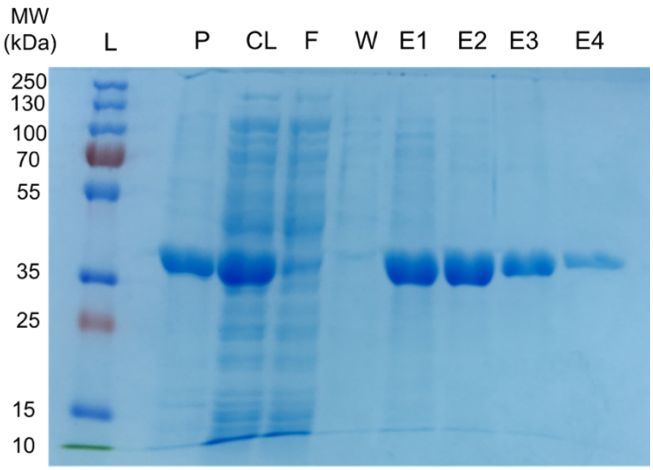

Figure S3.6. Purification of AS. In this study 12% tris-glycene SDS-PAGE gel, each lane was loaded with 19μL of sample unless otherwise indicated. Lane L: PageRuler pre-stained protein ladder (10μL, Thermo Fisher Scientific) was used. Lane P: 1μL of insoluble pellet in 18μL of ddH_2O. Lane F1: flow through after batch binding the cell lysate to the resin. Lane F2: flow through after batch binding the cell lysate to the resin and 30mL 10mM imidazole wash. Lane W: column wash with 50mL each of buffers with 40mM imidazole, respectively. Lane E1-4: As eluted with 50mL buffer containing 250mM imidazole, collected as four fractions. Buffer: 25mM HEPES, 200mM NaCl, 10mM $MgCl_2$, 10mM imidazole, pH 7.50, 1mM BME.

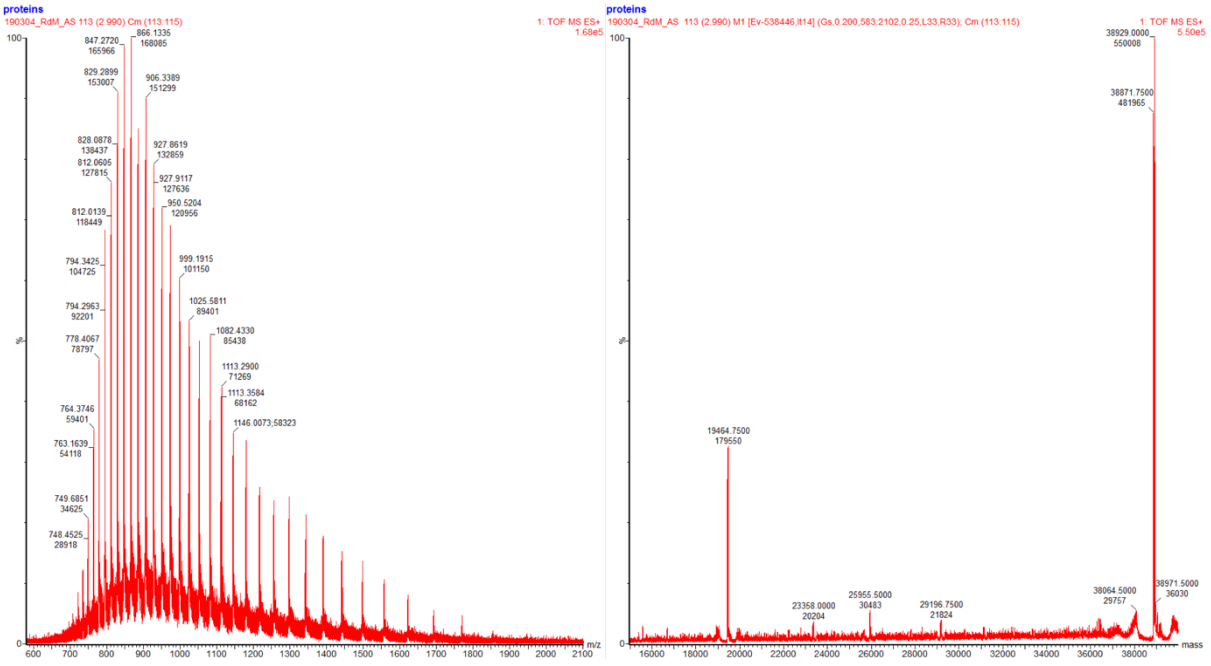

Figure S3.7. High resolution mass spectrometry analysis of AS. Charge series (left) and mass spectra showing the dominant proteoform at 38929m/z corresponding to AS with Mg^{2+} bound (right). Analysed on a Xevo QTOF instrument. Protein samples were diluted to 0.02mg/mL in water before analyzing with the Xevo quadrupole time-of-flight-mass spectrometer with a 2µL injection onto a phenyl desalting column. Chromatograms generated were analyzed with MassLynx software (Waters).

Cloning of ADS into pET28 vector

The codon optimised gene coding for amorpha-4,11-diene synthase (ADS) from *Artemisia annua* was synthesised and purchased from Genewiz in a pUC57 vector. The PCR and LIC cloning protocol, outlined above for AS, was followed for cloning the ADS gene into pET28 vector. The following primers were used for PCR amplification; Forward: CAG GGC GCC AAT GAA AAA ACC GAA CGG TAC CAA CGG GCT C -3'. Reverse: 5'- GAC CCG ACG CGG TTA CTA GTC AAC AAC AAC AGA GTA ACG -3'.

The ADS-pET28a plasmid was transformed *via* heat shock into *E.coli* BL21 (DE3) cells. The transformed cells were transferred to a LB agar plate containing 40μg/mL of kanamycin antibiotic, and incubated at 37°C for 14h. A seed culture was prepared by inoculating a single colony into 50mL of LB media with 40μg/mL of kanamycin antibiotic and shaking the culture at 220rpm for 14h at 37°C in a 125mL baffled flask. The expression culture was prepared by inoculating 10mL of seed culture into 1L of LB media with 40μg/mL of kanamycin antibiotic and shaking at 220 rpm at 37°C in 4L baffled flask. When the culture reached an OD_{600} of 0.7 the cells were induced with 0.5mM IPTG. The induced expression culture was incubated by shaking at 220 rpm for 20-24h at 18°C.

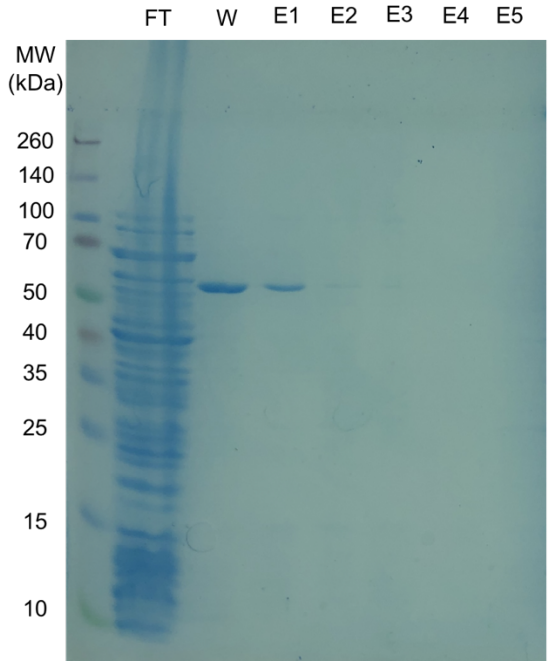

Figure S3.8. Purification of ADS. 12% tris-glycene SDS-PAGE gel was used with each lane loaded with 19μL of sample unless otherwise indicated. PageRuler pre-stained protein ladder

(10µL, Thermo Fisher Scientific) was used. Lane FT: flow through after batch binding the cell lysate to the resin. Lane W: column wash used 50mL of buffers with 40mM imidazole, respectively. Lane E1-4: As eluted with 50mL buffer containing 250mM imidazole, collected as four fractions. Buffer: 25mM HEPES, 200mM NaCl, 10mM $MgCl_2$, 10mM imidazole, pH 7.50, 1mM BME.

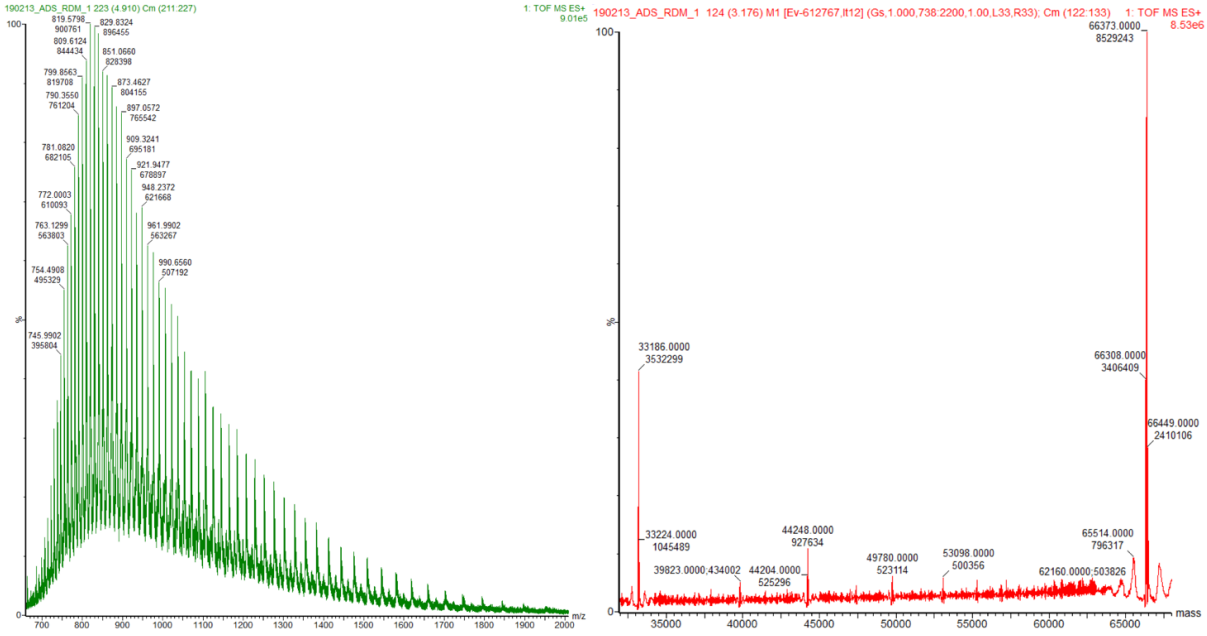

Figure S3.9. High resolution mass spectrometry analysis of ADS. Charge series (left) and mass spectra showing the dominant proteoform at 66373m/z corresponding to ADS with Mg^{2+} bound (right). Analysed on a Xevo QTOF instrument. Protein samples were diluted to 0.02mg/mL in water before analyzing with the Xevo quadrupole time-of-flight-mass spectrometer with a 2µL injection onto a phenyl desalting column. Chromatograms generated were analyzed with MassLynx software (Waters).

Chapter 4: Continuous-Flow Antibody and Peptide Phage-Displayed Selections for DJ-1, a Bladder Cancer Biomarker

4.1. Abstract

Isolation of antibody fragments and peptide molecules that bind to specific molecular targets are an essential tool for diagnostics and targeted therapeutics. Phage display methodologies offer a versatile platform for the isolation of these valuable affinity reagents. Here, a vortex fluidic-based approach was applied for efficient continuous-flow antibody and peptide selections through immobilisation of a target antigen using His_n epitope immobilisation. With this system Fab and peptide binders were isolated for binding with high affinity and specificity to a bladder cancer biomarker, DJ-1. This continuous-flow system can be used with different libraries and target molecules and demonstrates an effective approach towards discovery of recognition elements for biosensor development and research applications.

4.2. Introduction

Phage display offers a powerful tool for protein engineering and ligand discovery. First invented by Noble laureate George Smith in 1985 [1], the technique was further refined by Jim Wells [2] and then applied by co-Noble laureate Gregory Winter [3]. Since these seminal contributions, phage display has been applied to drug discovery [4-6], enzyme optimization [7], and phage-based biosensor diagnostics [8-11].

In this technique a protein is fused or “displayed” on the surface of the harmless bacteria-infecting virus or “phage”. Mutagenesis of DNA encapsulated inside the phage generates a collection or “library” of different protein variants for selection and propagation [12, 13]. Selections typically apply binding to a target molecule attached to a solid support. For example, tailor-made antibody fragments can be displayed and selected for specific and high affinity recognition of a target molecule.

Phage-display is a valuable tool for vaccine and antiviral development. This high-throughput method for the production of monoclonal antibody (mAbs) fragments that recognise and target viruses such as the coronavirus are highly valuable given the current threat to public health [14, 15]. Furthermore, when a vaccine or antiviral medication has yet to be developed, selected mAbs can also be used to develop reliable diagnostic tests, which can be important to stop the global spread [16, 17].

Selections for phage-displayed antibody fragments and peptides typically enrich high affinity binding partners. This is achieved by multiple rounds of binding to a target, washing to remove non-specific phage and elution for collection of specific binders. Several methods for phage selections [18] and library construction [19-21] have been established, however, the need for several rounds of laborious *in vitro* selections and screening steps to sufficiently enrich desired binders and remove non-specific phage remains.

A potential opportunity for process optimization is the use of microfluidics, especially when operating under continuous flow. Research groups have previously utilized dynamic, pressure-driven laminar flow systems [21-26]. A microfluidic approach was utilized for enrichment of binder-specific phage particles using antigen-coated beads under particle-focusing acoustic forces [20]. A microfluidic magnetic separator (MMS), involving ferromagnetic structures within channels to enable trapping and release of phage particles on

magnetic beads, was employed to allow stringent control over the washing conditions [23]. This system also allows for controlling the isolation process by tailoring wash duration and flow rate. Another system was developed which exploits alternating current electro-hydrodynamics (AC-EHD) to enhance micro-mixing, which increased phage-antigen collisions, resulting in improved capture [24].

The vortex fluidic device (VFD) inputs mechanical energy into solution by rapid rotation until the solution forms a thin film. The VFD processing has demonstrated to have advantages over batch processing, including increased micro-mixing for enhanced kinetics, and shear stress for high mass transfer [27, 28]. Examples of application of the VFD include single and multi-step transformations [27-30], biocatalysis [31-33], protein folding [34, 35], rapid purification of proteins [32] and the fabrication of nano- and micro-materials for biomedical application [36-39].

Protein and antigen targets containing a His_n epitope can be immobilised by attachment onto Ni-affinity resin coating the surface of the reactor tube in the VFD [32]. It was hypothesised that target specific antibody or peptide binders could be selected for by continuous-flow of phage-displayed libraries through the microfluidic platform. This system allows for stable immobilisation of the target molecule with the use of continuous flow allowing for increased stringency with the ability to inject higher volumes for the block and wash steps.

This chapter reports on the continuous flow selections for synthetic phage-displayed Fab antibody and peptide binders selective for protein deglycase 1 (DJ-1), a bladder cancer biomarker [40]. The selection of antibodies and peptides ligands to DJ-1 presents an example of how this system can be used for finding valuable recognition elements, which can incorporated into biosensors designed for early cancer detection.

4.3. Results and Discussion

4.3.1. Phage-Displayed Antibody Selections for DJ-1

DJ-1 is a protein, encoded by the gene Parkinson disease 7 (PARK7), identified as a potential diagnostic biomarker due to its elevated serum levels in pancreatic cancer patients and its correlation with bladder cancer [40-42]. Finding recognition elements for cancer biomarkers, such as DJ-1, can be used to develop biosensors for early bladder cancer detection. Phage-display has become a useful tool for the identification of bio-recognition elements, in part due to the ability to screen and select on this basis, with assemblies of 10 billion phage clones displaying different peptide or protein variants [10, 43].

For continuous-flow phage-display binding selections in the VFD, DJ-1 was first immobilised. Recombinant DJ-1 (2.0mg), with a C-terminal fused His_n epitope, was immobilised onto nickel-affinity chromatography resin (4.0g) by batch binding overnight. Following the procedure established by Britton *et al*., the DJ-1 bound resin was then coated onto the inner surface of the VFD tube by pipetting the homologous solution (suspended in 15mL PBS buffer) into the rapidly rotating tube ($\geq$ 6k rpm). After 3 minutes, a clay-like coating is created that remains painted on the tube. As previously reported, proteins can also be immobilised by first coating the VFD with protein free resin and feeding unbound protein through the reactor [32]. However, coating with pre-batch bound protein was used here to obtain more consistent results.

For phage-displayed antibody libraries, monoclonal antibody fragments are displayed on the PIII coat protein of a M13 bacteriophage (Figure 4.1). The antibody fragments are typically short-chain variable fragments (scFv) or antigen-binding fragments (Fab) [12]. Here,

a synthetic phage-displayed Fab library was used, constructed and provided by S. Sidhu [45]. The diversity, $10^9 – 10^{10}$, of this library was derived from the site-directed mutagenesis of four complementarity-determining regions (CDRs) of the Fab fragment, one in the light chain (CDR-L3) and three in the heavy chain (CDR-H1, CDR-H2, and CDR-H3).

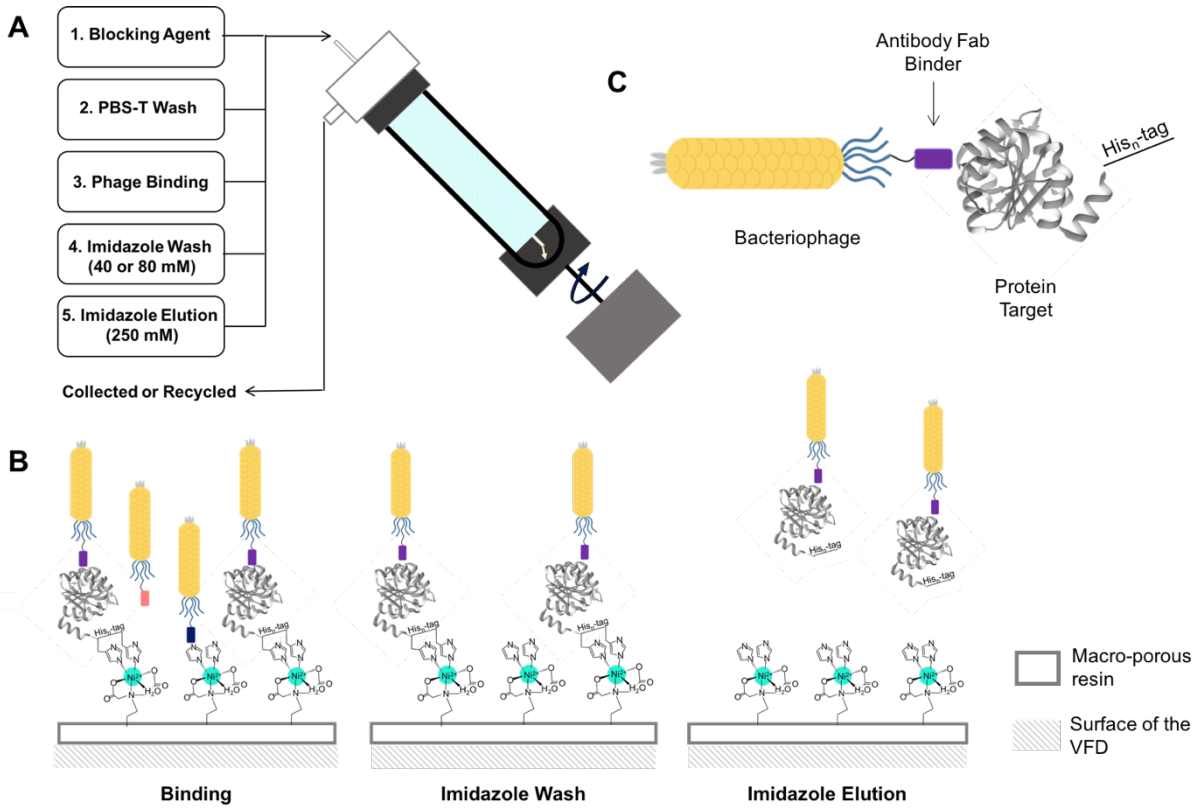

Figure 4.1. VFD continuous-flow DJ-1 immobilisation and antibody-phage selections. For thin-film continuous flow selections, all protein, phage and buffer solutions are fed into the reactor via a peristaltic pump at a flow rate of 1.0mL/min (A). Recombinant DJ-1 with 6 x His epitope is bound to the Ni-MIDA resin coating the surface of the VFD (B). The phage-displayed libraries used consist of either Fab fragments fused to the P3 protein (C). The phage bound to the target protein is eluted from the VFD and then screened and amplified in SS320 cells for analysis and use for the next selection round, respectively.

Prior to binding the phage, a blocking solution, consisting of a non-relevant protein in PBS-T, is fed through the VFD tube. The resin is then washed with PBS-T to remove excess blocking agent. Each step of the selection process is performed at a flow rate of 1.0 mL/min, and a 45° tilt angle (Figure 4.1). This flow rate allows for efficient scale up without compromising on the complex fluid flow which diminishes for higher flow rates [27]. As mentioned, the 45° tilt angle has shown to be optimal for various applications [27].

Next, the phage binding step is achieved by feeding through a synthetic phage-displayed Fab library (60nM in blocking solution). Phage binding is followed by stringent washing with a low concentration of imidazole in PBS-T to remove unbound or non-specifically bound phage. For each round, the stringency is increased by increasing the volume pass through the tube (25-115mL) and the concentration of the imidazole (40-100mM). Lastly, the DJ-1, with phage-displayed antibodies bound, is eluted by feeding a solution of 250mM imidazole in PBS-T through the VFD tube. The eluted phage is used to infect SS320 *E. coli* cells, allowing for amplification of the phage for use in the next selection round.

Four rounds of selections were performed at 4k and 8k rpm. Each round and rotational speed was accessed based on phage enrichment, measured by phage titers, and binding hit rate (%) from ELISA spot assays (Table 4.1, Fig. S4.2 and S4.3). A phage-based ELISA spot assay is performed to identify potential binding hits for DJ-1. This assay involves growing 96 randomly selected phage colonies from the titer agar plates and comparing their binding to DJ-1, compared to the negative control, BSA. Phage that demonstrate binding to DJ-1 x3 above the background are classified as a hit.

The high phage titers combined with low ELISA hit rates for the selection rounds at 4k rpm indicate non-specific binding of phage is occurring, despite stringent washing (Table 4.1).

High phage titer values can indicate enrichment of binding partners, but they can also be due to a high amount of non-specifically bound phage carried through the reactor [44]. In contrast, selections at 8k rpm show a decrease in phage enrichment and a significantly higher hit rate of 75 and 96.7% after round 1 and 2, respectively. An increase in phage enrichment and a significant decrease in spot assay hit rate is observed for selections round 3 and 4. It is suspected that after multiple rounds of bacterial amplification, phagemids that have an intrinsic growth advantage are propagated rather than antibody binding characteristics [46].

It was hypothesized that the difference in selection efficiency at 4 and 8k rpm are the result of different fluid dynamics at these speeds. A model has been developed which is consistent with this finding [47]. In water in a 20mm OD tube, this model has high localized mixing at rotational speeds between 3.8k and 4.5k rpm, arising from the interplay of Faraday-wave double helical flow and circular flow [47]. While such mixing can potentially increase phage to antigen interactions, the associated binding to the the resin or VFD surface is non-specific. For rotational speeds ≥ 6k rpm, the model has eddies associated with Faraday waves striking the surface of the tube resulting in higher shear stress on the surface of the tube [47].

Table 4.1. Phage library enrichment and ELISA hit rates (>3x above background).

	4k rpm		8k rpm	
Round	**Titer (CFU)**	**ELISA Hit Rate (%)**	**Titer (CFU)**	**ELISA Hit Rate (%)**
1	1.9×10^{9}	6.3	2.0×10^{9}	75
2	1.8×10^{10}	1	2.2×10^{8}	96.9
3	1.3×10^{10}	1	2.7×10^{9}	1
4	4.6×10^{9}	0	2.3×10^{9}	4.2

a >3x above background

Randomly selected hits from each round and rotational speed were subjected to sequence analysis and revealed no repeating of sequences across all selected phage hits. DJ-1 binding of random selected hits were further accessed by dose-dependent phage-based ELISA (Figure S4.5 and S4.6). Hits from R1 showed low to no binding to DJ-1 (Figure S4.4). Stop 4, an M13 phage with both the PIII and PVIII coat proteins with no protein fragment displayed, was used as a negative control (Fig. 4.2A).

Phage-displayed Fab, R2C68, identified from selection round 2, shows significant binding to DJ-1 (Figure 4.2A and B). Stop 4 shows low background binding, however, the binding is less than 1/5x the affinity compared to R2C68 (Figure. 4.2A). The specificity of R2C68 for DJ-1 was determined by testing against a panel of proteins using a phage-based ELISA (Figure 4.2B). DJ-1 shows very low binding to human serum albumin (HSA), *E.coli*, two proteins present in urine, and bovine serum albumin (BSA). R2C68 show medium level binding to hemoglobin (HG). Notably, R2C68 exhibits low binding to truncated nuclear matrix protein (tNMP22), another identified bladder cancer biomarker [44-46]. R2C68 was tested against hen egg-white lysozyme (HEWL) to rule out non-specific binding to proteins with high isoelectric point (pI).

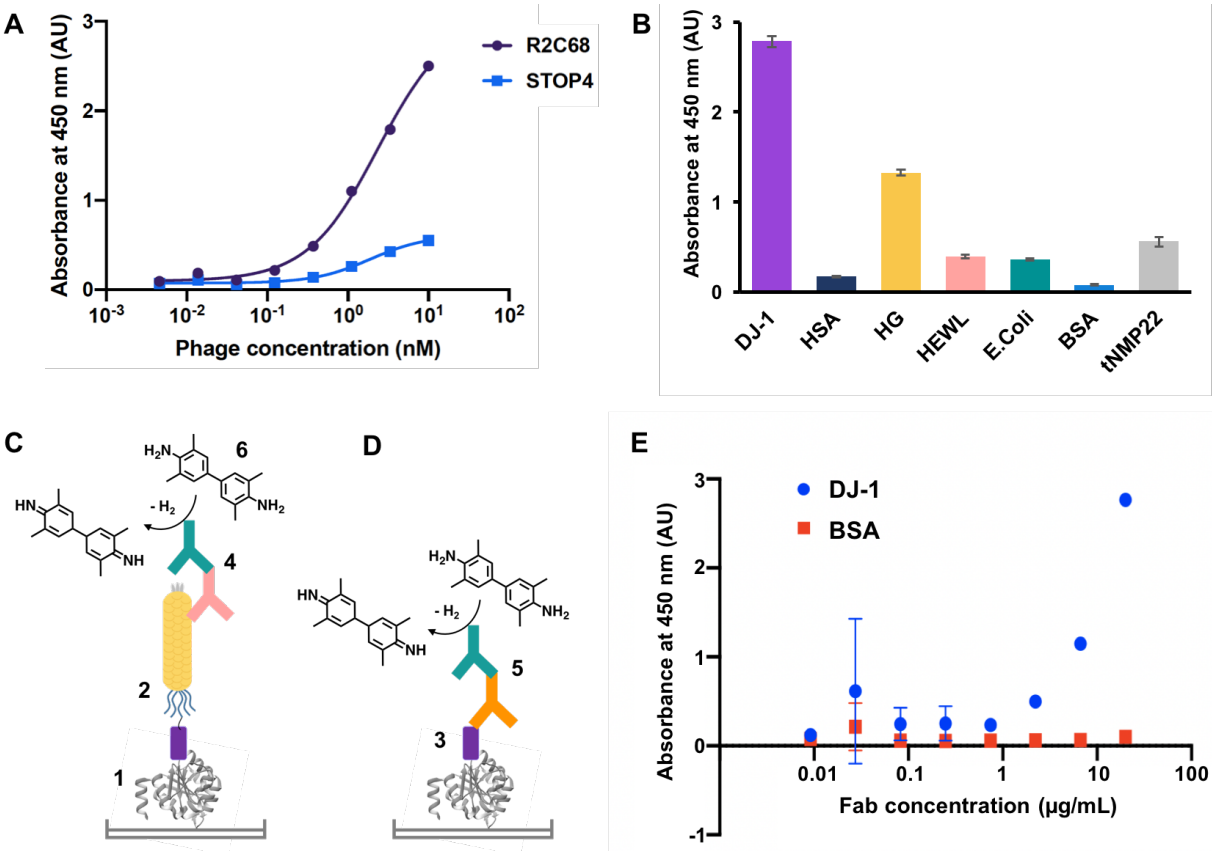

F

Mutated Region	CDR-L3	CDR-H1	CDR-H2	CDR-H3
Amino Acid Sequence	GGYYL	DFAGYSM	AYISSSGGYTD	YFGSSWGGYYFYSYSYDGL

Figure 4.2. Characterisation of Fab R2C68 Binder Selected for DJ-1. (A) Dose-dependent phage-based ELISA demonstrating binding affinity of R2C68 to DJ-1. Stop 4 phage, an M13 phage with no protein fragment displayed, was used as a negative control. Data was fit with a non-linear regression curve with variable slope (four parameters). (B) Phage-based specificity ELISA for DJ-1 against a panel of proteins with a 10nM [phage]. Schematic representation of phage-based (C) and free Fab ELISA, showing DJ-1 (1) coated on an ELISA plate. After blocking with BSA, phage-displayed (2) or free (3) Fab R2C68, is bound. For identification of the bound phage or Fab, HRP/anti-M13 (4) or HRP/anti-FLAG monoclonal conjugate (5)

is bound, respectively, followed by reaction with TMB (6), quenching with H_2SO_4 and measurement of absorbance at 450nm. (E) Dose-dependent ELISA demonstrating binding of free Fab R2C68 to DJ-1. BSA was used as a negative control. Error bars represent standard deviation about the mean, n = 3. (F) The amino acid sequence for the four mutated binding regions of the Fab antibody fragment.

Once antibody Fab binders have been identified, the genes encoding for the Fab can be cloned from the phagemid into an expression vector and optimized for expression in bacterial cells [51-54]. This is performed for further characterization of binding to the binding partner and for its potential application in non-phage based biosensors or use in therapeutics. Several methods for expression of the Fab binder were explored (Supplementary Information). Finally, the phagemid was converted to an expression vector by inserting an amber stop codon into the DNA at the fusion point between the heavy chain and the phage coat protein 3, a method previously reported my Sidhu and co-workers [51]. A 6x His epitope was also added immediately up stream of the stop codon, for purification of the expressed Fab. The Fab R2C68 expression construct was successfully transformed and expressed in BL21 (DE3) *E. coli* cells and purified using nickel-affinity chromatography (Figure S4.6). The purified Fab R2C68 was used in a dose-dependent ELISA, independent of phage, to confirm binding to DJ-1, using BSA as a negative control (Figure 4.2 D and E).

tNMP22, a bladder cancer biomarker mentioned above, was successfully expressed in BL21 *E. coli* cells and three rounds of phage-displayed antibody selections were performed in the VFD (Supporting Information). Each round of selections resulted in high phage enrichments and no ELISA hits, with the exception of a single 'hit' from round 2 (Table S4.4). The phage hit was propagated in SS320 cells and its binding to tNMP22 accessed using a phage-based ELISA. The ELISA results show no binding of the phage-displayed Fab to

tNMP22 (Fig. S4.18). Subsequently, generalizability of this continuous-flow method could not be demonstrated using another relevant protein biomarker, therefore another phage-display library, utilizing displayed peptides, was used in continuous-flow selections for DJ-1.

4.3.2. Phage-Displayed Peptide Selections for DJ-1

Phage-display peptide libraries have been widely used for various applications such as biosensing [10], epitope mapping [55], anti-viral research [56], immunotherapy [57], vaccine development [58] and protein to protein interaction research [59]. The library of peptides is fused to the N-terminus of the P8 proteins of the phage (Figure 4.3A). Fusion with P8 proteins will typically lead to multivalent display, whereas displaying protein fragments on P3 proteins result in lower display levels, between 1-5 copies per phage [10].

Four rounds of peptide selections for DJ-1 were performed as described above, using a mega random peptide library (MRPL) library. The library contains a theoretical diversity of 10^{23}, and an estimated actual diversity of 10^{11}, of different peptides between 5 to 18 naturally occurring amino acids in length [8]. Based on the non-specific phage binding observed in previous selection experiments, a round of subtracted selections was performed prior to the first selection round with DJ-1. The subtracted selection round consists of flowing the peptide library through the VFD tube containing protein-free Ni-MIDA resin. Peptide phage variants that non-specifically bind to the resin are removed from the library with unbound phage collected from the VFD for immediate use in the first selection round.

Table 4.2. Phage library enrichment and ELISA hit rates

Round	Titer (CFU)	ELISA Hit Rate[a] (%)
1	6.6×10^9	0
2	6.6×10^9	0
3	9.7×10^8	37.5
4	2.8×10^9	8

a >3x above background

Potential peptide binding hits were detected after the third round of selections, with phage enrichment also decreasing after this round (Table 2). Unlike selections performed on the phage-displayed antibody library, the first and second round of selections resulted in a decrease in enrichment and no binding hits were observed. It was postulated that potential peptide binders were removed during the subtraction selection round. Alternatively, the high diversity of the peptide library can require more rounds of selections to identify binding partners. Hits were randomly selected and subjected to sequence analysis and DJ-1 binding of random selected hits were further characterized using a dose-dependent phage-based binding ELISA. Phage-displayed peptide, R3C2, showed high binding to DJ-1 (Figure 4.3B).

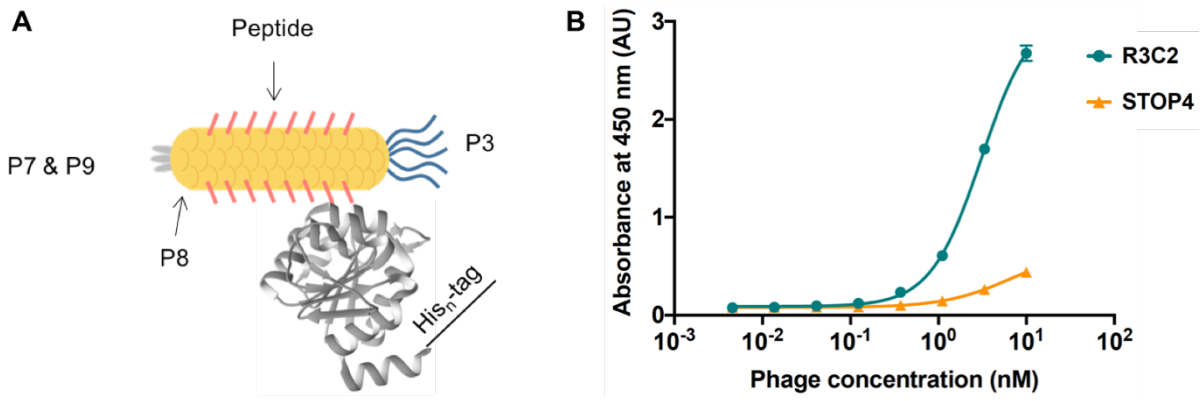

C

	Peptide Amino Acid Sequence
R3C2	LRCGYCTCC

Figure 4.3. (A) Diagram of phage-displayed peptides binding DJ-1. (B) Dose-dependent phage-based ELISAs demonstrating binding affinity of R3C2 to DJ-1 (A). (C) The amino acid sequence of the peptide binders. Stop 4 phage, an M13 phage with with no peptide or Fab displayed, was used as a negative control. Data was fit with a non-linear regression curve with variable slope (four parameters). Error bars represent standard deviation about the mean, n = 3.

4.4. Conclusions

This VFD-based approach allows for efficient continuous-flow antibody and peptide selections under continuous-flow through immobilisation of a target antigen through his-tag immobilisation. With this system a Fab binder and peptide binder for DJ-1were isolated, from two diverse libraries, after two and three rounds of selections, respectively. These binders have

the potential to be used as recognition elements for DJ-1, a bladder cancer biomarker, through their incorporation into biosensors that can be utilized for early bladder cancer detection.

This system allows for several parameters to be easily tailored to further improve the selection efficiency, including washing stringency, through modifying the volume and flow rate of the wash solution. A key example is the change in selection efficiency that resulted, due to the different fluid dynamics in the VFD. Additionally, the amount of target molecule with a fused his-tag, in the system can be tightly controlled using this immobilisation technique. Reducing the amount of protein attached after the first or second round could result in the selection of higher affinity binders. Furthermore, combining continuous-flow selections with the ability to rapidly purify cell lysate containing the target protein *in-situ* could allow for a high-throughput multiply process system.

Further analysis of the binding characteristics of the selected binders could shed light on the potential differences in binding mechanism that could arise in binders selected for under shear in the VFD verses the use of batch processing (Chapter 6.2.3). Identification of different binding mechanisms could provide the ability to select recognition elements based on binding characteristics by varying the level of shear stress imparted in the reactor.

4.5. Experimental

4.5.1. Overexpression and Purification of Recombinant DJ-1

DJ-1 pET 3a (purchased from Addgene) plasmid was transformed into BL21(DE3) cells were used to inoculate a 25mL seed culture of LB and 50μg/mL of carbenicillin, and incubated at 37°C for 14h. The expression cultures were prepared by inoculating 5mL of seed

culture per 500mL of LB media with 50μg/mL of carbenicillin. The cultures are shaken at 220 rpm at 37°C until OD600 reached 0.6, followed by induction with 1.0mM IPTG. The induced expression cultures was incubated by shaking at 220 rpm at 27°C for 5h. The cells were harvested by centrifugation, resuspended and sonication in 25 mL lysis buffer (50mM Na_2HPO_4, 300mM NaCl, 10mM imidazole, pH 8.0, 10mM BME, 100μL HALT protease inhibitor). The supernatant purified using nickel affinity chromatography using a gravity column containing charged (with 100mM $NiSO_4$) and equilibrated nitriloacetic acid (NTA) resin (2g, Biorad). The following buffers were used to purify DJ-1: lysis buffer (50mL), wash buffer (50mM Na_2HPO_4, 300mM NaCl, pH 8.0, 50mM imidazole, 10mM BME), and elution buffer (60mL collected as three fractions, 50mM Na_2HPO_4, 300mM NaCl, 250mM imidazole, pH 8.0, 10mM BME). Fractions containing purified protein, identified by SDS-PAGE (Figure S4.1). The purity of the protein was confirmed using 12% SDS-PAGE and the concentration determined using the Bradford assay.

4.5.2. Protein Immobilisation in the VFD

Ni-IDA affinity resin was prepared by washing 4.0g of macroporous polymethacrylate resin (purchase from Purolite) with ddH_2O (3 x 5mL), followed by PBS buffer (5mL, pH 8.0). The resin was charged with 1M aqueous $NiSO_4$ (8mL), stirring for 5 minutes at room temperature. The Ni-charged resin is washed with ddH_2O (2 x 5mL), followed by PBS buffer (2 x 5mL, pH 8.0). A solution of DJ-1 (2mg total) in PBS buffer was added to the charged resin suspended in 10mL PBS buffer and stirred at 4°C for 2-18h. The protein supernatant was removed and the amount of protein immobilised on the resin was determine using Bradford Assay (Fisher Scientific).

A 17.5mm internal diameter VFD tube (20mm OD) was filled with fresh piranha solution and left for one hour. Following this, the tube was rinsed with Milli-Q water (5 x 40mL) and autoclaved, followed by storage at at 180°C for > 12h. The DJ-1 on Ni affinity resin is pipetted into the VFD tube, rotating at 6k rpm rotational speed and 45 ° tilt angle. The tube is spun for 3 minutes, then immediately used for selections.

4.5.3.VFD Selections for DJ-1 Antibody Binders

All VFD selection steps are performed at 4 or 8k rpm, at a 45° tilt angle, with all solutions injected into the reactor at 1.0mL/min. After each round of selections, described below, the second elution fraction is collected and concentrated to 500μL using a 3,000MW Vivaspin protein concentrator. The solution is used to infect a 22mL culture of *E. coli* SS320 cells in 2YT supplemented with 15μg/mL tetracycline (OD_{600} of 0.5-0.7), with shaking at 225 rpm for 1 hour at 37°C . A small aliquot (40μL) was removed, serially diluted and tittered on agar plates before the culture was infected with M13K07 to give a MOI of 4.6 and shaken for 1h. The culture is transferred to 500mL of 2YT containing 50μg/mL carbenicillin and 20μg/mL kanamycin, and grown for 18h at 37°C. The phage is separated and precipitate with 20% w/v PEG8000 in 2.5M NaCl and resuspended in PBS buffer.

Round 1: Blocking: 10mL of SuperBlock PBS Buffer (Fisher Scientific) solution, *Wash:* 25mL of PBS-T, *Phage Binding:* 5mL of synthetic phage-displayed Fab library [33] (60nM in SuperBlock PBS buffer from Thermo Fisher Scientific) recycled through the VFD three times, *Imidazole Wash:* 25mL of 40mM imidazole in PBS-T, *Elution:* 15mL of 250mM imidazole in PBS-T, collected at 3 x 5ml fractions.

Round 2: Blocking: 5mL of 1.0% HSA and 1.0% BSA in PBS-T, *Wash:* 25mL of PBS-T, *Phage Binding:* 5mL Round 1 antibody phage binders (60nM in PBS-T, 1.0% HSA (Sigma Aldrich), 1.0% BSA (Thermo Fisher Scientific)), *Imidazole Wash:* 25mL of 40mM and 25mL of 100mM imidazole in PBS-T, *Elution:* 20mL of 250mM imidazole in PBS-T, collected at 3 x 5ml fractions.

Round 3: Blocking: 5mL of 0.5% hemoglobin (Sigma Aldrich) and 1.0% non-fat milk in PBS-T, *Wash:* 25mL of PBS-T, *Phage Binding:* 5mL round 2 antibody phage binders (60nM in PBS-T, 0.5% hemoglobin, 1.0% non-fat milk), *Imidazole Wash:* 25mL of 40mM and 50mL of 100mM imidazole in PBS-T, *Elution:* 20mL of 250mM imidazole in PBS-T, collected at 3 x 5ml fractions.

Round 4: *Blocking:* 5mL of SuperBlock PBS buffer, *Wash:* 25mL of PBS-T, *Phage Binding:* 5mL third round antibody phage binders (60nM in PBS-T, 0.2% BSA), *Imidazole Wash:* 100mL of 100mM imidazole in PBS-T, *Elution:* 20mL of 250mM imidazole in PBS-T, collected at 3 x 5ml fractions.

4.5.4. Subtracted Selections

Ni-IDA affinity resin was prepared and immobilised in a VFD tube as described above, without protein immobilised. To this tube 10mL of SuperBlock PBS Buffer (Fisher Scientific) solution was fed through the tube, followed by 25mL of PBS-T to wash. The phage-display library (synthetic phage-displayed Fab library or MRPL library) (5mL, 60nM in SuperBlock PBS buffer) was fed through the tube. The unbound phage was collected and immediate used for the first round of selections for the target protein.

4.5.5. Spot Assay

After each round an aliquot of SS320 cells, infected with the eluted phage, were plated on LB plates supplemented with carbenicillin (50μg/ml). Ninety-six colonies were picked and grown at 37 °C, in a shaking incubator (225 rpm) in 800 uL 2YT supplemented with carbenicillin (50μg/ml), kanamycin (20μg/ml) and helper phage, M13K07 (16ρM). The cultures were grown in a deep 96-well plate for 18 h, followed by centrifugation at 4°C at 3,000 rpm for 30 mins. The top 270μL of supernatant was transferred to 96-well dilution plate containing 30μL of 10 x PBT (10 x PBS, 0.5% Tween20, 2.0% BSA).

A phage based ELISA was used to examine binding to target protein by specific spot assay isolates. The top 48 wells of two maxisorp 96-well plate was coated with 100μL of target protein (10μg/mL) in sodium carbonate buffer (50mM, pH = 9.6) and the bottom 48 wells with buffer alone. The plates were shaken (150 rpm) at 4°C overnight. The ELISA protocol was followed as detailed below, with the culture supernatant used for the phage binding step. Phage bound to DJ-1 but not to BSA were randomly selected and subjected to DNA sequence analysis. The highest assay hits were propagated and subjected to further analysis.

4.5.6. General Method for Propagating and Precipitating Phage-Displayed Ligands

Phagemid vector for phage-dispayed antibody binders is transformed into CaCl2 competent SS320 cells. A seed culture containing 22mL of 2YT and 15μg/mL tetracycline is inoculated with a single colony and grown at 37°C until the culture reaches OD600 of 0.5. The culture is infected with M13K07 to give a MOI of 4.6 and shaken for 1h. The culture is transferred to 500mL of 2YT containing 50μg/mL carbenicillin and 20μg/mL kanamycin, and

grown for 18h at 30°C. The phage is separated from the cells by centrifugation (7890g, 4°C) and the phage precipitated from the supernatant by incubation with 20% w/v PEG8000 in 2.5M NaCl for 45 min. The phage is separated by centrifugation (7890 , 4°C) and resuspended in PBS buffer.

4.5.7. Phage-Based Enzyme-Linked Immunosorbent Assay (ELISA)

Phage-based ELISAs were used to asses binding affinity of selected phage-displayed antibody binders. Nunc Maxisorp 96-well plates (Thermo Fisher Scientific, #442404) were coated with 10 μL of 10μg/mL of DJ-1 in 50mM sodium carbonate buffer (pH 9.6) overnight at 4°C. After blocking with 0.2% BSA for 30 minutes at RT, wells were washed with 3 x 200μL PBS-T and incubated with 100μL of phage solution for 1h. Wells were washed with 3 x 200μL PBS-T, followed by addition of 100μL of 1:500 HRP/anti-M13 monoclonal conjugate (GE Healthcare) and incubated for 30 mins. After washing wells with 5 x 200μL PBS-T and 1 x 200μL, 100μL of TMB (Thermo Fisher Scientific) is added to each well and allowed to incubate for 5 minutes. The reaction is quenched with 100uL of 6M H_2SO_4 and the absorbance read at 450nm on a BioTek 96-well plate reader. To further assess binding specificity, phage ELISAs were used to measure binding to a panel of proteins in triplicate.

4.5.8. Production of Fab Binder R2C68 Expression Vector

The Fab R2C68 phagemid vector was converted to an expression vector by inserting an amber (TAG) stop codon into the DNA at the fusion point between the heavy chain and the phage coat protein 3. A 6x histidine tag was also added immediately up stream of the stop

codon, for purification of the expressed Fab. The following PCR parameters and oligonucleotides (integrated DNA Technologies) were used to amplify the Fab R2C68 phagemid with overhangs encoding for the 6 x histidine tag and amber stop codon. PCR reaction mixture (25μL) contains Herculase ii DNA polymerase (New England Biolabs), following the manufacturers instructions, and buffer (5× diluted final concentration, New England Biolabs), DMSO (5% v/v final concentration), dNTPs (0.5mM each final concentration, New England Biolabs), primers (33ng each final concentration, Integrated DNA Technologies), and R2C68 phagemid (50ng). PCR reaction was as follows: one cycle at 95°C for five min, 25 cycles at 95°C for 1.5min, 70°C for 1.5 min, 72°C for 3.5 min, and one cycle at 72°C for five min. Fwd primer: 5'- CCACCACTGATGCGGCCGGCCCTCTGGT -3', Rev primer: 5'-TGGTGGTGGTGTGTGTGAGTTTTGTCACAAGATTTGGGCTCAACTTTCT

TGTC -3'

The PCR product were extracted from a 1% agarose gel using a Zymoclean Gel DNA Recovery Kit. The following Gibson Assembly reaction mixture was used: 150ng of Fab R2C68 Phagemid PCR product, 2μL of NEBuilder ® HiFi DNA Assembly Master Mix (NEB), and autoclaved ddH_2O to a total volume of 4μL. The reaction mixture was incubated at 50°C for 1h, and stored at 4°C. The reaction product was transformed into *E. coli* Nova blue cells and plated on an agar plate supplemented with kanamycin (40μg/mL), followed by incubation at 37°C for 18h. A single colony is used to inoculate 5mL of 2YT supplemented with kanamycin (40μg/mL), and grown at 37°C for 18h. The DNA plasmid is isolated, purified and sequenced by Genewiz.

4.5.9. Periplasmic Expression and Purification of Recombinant Fab Binder R2C68

The below protocol was used for periplasm expression of Fab R2C68 binder in *E. coli*. The Fab R2C68 expression construct was transformed *via* heat shock into *E.coli* BL21 (DE3) cells and transferred to a LB agar plate containing 50μg/mL of carbenicillin, and incubated at 37°C for 14h. A seed culture was prepared by inoculating a single colony into 25mL of LB media with 50μg/mL of carbenicillin and shaken (220 rpm) in a 125mL baffled flask at 37°C for 14h. The expression culture was prepared by inoculating 125mL of LB media with 40μg/mL of kanamycin with 1.5mL of seed culture into and shaking at 220 rpm at 37°C in 500mL baffled flask. When the culture reached an OD_{600} of 0.6-0.7 the cells were induced with 0.5mM IPTG. The induced expression culture was incubated by shaking at 220 rpm for 20-30°C. The cells were centrifuged at 3k rpm for 20mins at 4°C and resuspended in 8mL Tris-sucrose-EDTA extraction buffer: 200mM Tris-HCl, pH 8.0, 500mM sucrose, 1mM EDTA, Halt™ protease inhibitor cocktail (Thermofisher Scientific). Lysozyme (1mg/mL) was added to the suspended cell lysate and the mixture was gently stirred at 4°C for 1h. The cell suspension was centrifuged at 13,000k rpm at 4°C for 1h, and the supernatant separated from the cellular debris. The supernatant purified using nickel affinity chromatography using a gravity column containing charged (with 100mM $NiSO_4$) and equilibrated IMAC resin (2g, Purolite). The following buffers were used to purify the Fab: lysis buffer (50mM Tris-HCl, 300mM NaCl, pH 8.0, 50mL), wash buffer (50mL lysis buffer with 50mM imidazole), and elution buffer (25mL, lysis buffer with 250mM imidazole). Fractions containing purified protein, identified by SDS-PAGE (Figure S4.6). The purity of the protein was confirmed using 12% SDS-PAGE and the concentration determined using the Bradford assay.

4.5.10. Free Fab Enzyme-Linked Immunosorbent Assay (ELISA)

A dose-dependent ELISA was used to asses binding affinity of the expressed Fab R2C68 binder. Nunc Maxisorp 96-well plates (Thermo Fisher Scientific, #442404) were coated with 100μL of 10μg/mL of DJ-1 in 50mM sodium carbonate buffer (pH 9.6) overnight at 4°C. After blocking with 0.2% BSA for 30 minutes at RT, wells were washed with 3 x 200μL PBS-T and incubated with 100μL of a solution of Fab R2C68 in PBS-T for 1h. Wells were washed with 3 x 200μL PBS-T, followed by addition of 100μL of 1:500 HRP/anti-FLAG monoclonal conjugate (GE Healthcare) and incubated for 30 mins. After washing wells with 5 x 200μL PBS-T and 1 x 200μL, 100μL of TMB (Thermo Fisher Scientific) is added to each well and allowed to incubate for 5 minutes. The reaction is quenched with 100uL of 6M H_2SO_4 and the absorbance read at 450nm on a BioTek 96-well plate reader. To further assess binding specificity, phage ELISAs were used to measure binding to a panel of proteins in triplicate.

4.5.11. Over Expression and Purification of Recombinant tNMP22

tNMP22 pET28 plasmid transformed into BL21(DE3) cells were used to inoculate a 25mL seed culture of LB and 40μg/mL of kanamycin, and incubated at 37°C for 14h. The expression cultures were prepared by inoculating 5mL of seed culture per 500mL of LB media with 40μg/mL of kanamycin. The cultures are shaken at 220rpm at 37°C until OD600 reached 0.6, followed by induction with 0.5mM IPTG. The induced expression cultures was incubated by shaking at 220 rpm at 18°C for 20-24h. The cells were harvested by centrifugation, resuspended and sonication in 25mL lysis buffer (50mM Na_2HPO_4, 300mM NaCl, 10mM imidazole, pH 8.0, 10mM BME, 100μL HALT protease inhibitor). the supernatant purified

using nickel affinity chromatography using a gravity column containing charged (with 100mM $NiSO_4$) and equilibrated IMAC resin (3.0g, BioRad). The following buffers were used to purify tNMP22: lysis buffer (50mL), 50mM and 100nM imidazole wash buffers (50mM Na_2HPO_4, 300mM NaCl, pH 8.0, 10mM BME), and elution buffer (60mL collected as three fractions, 50mM Na_2HPO_4, 300mM NaCl, 10mM imidazole, pH 8.0, 10mM BME). Fractions containing purified protein, identified by SDS-PAGE (Figure S4.12). The purity of the protein was confirmed using 12% SDS-PAGE and the concentration determined using the Bradford assay.

4.6. Acknowledgements

Thank you for the support of Prof. Gregory Weiss, and for giving me the opportunity to visit his laboratory at the University of California, Irvine, where this research was conducted. Special thank you to Jason Garrido, Emily Sanders, Alicia Santos and Dr. Sudipta Majumdar for their assistance.

4.7. References

[1] Smith, G. P. Filamentous fusion phage: novel expression vectors that display cloned antigens on the virion surface. *Science,* **1985**, *228*, 1315-1317.

[2] Sidhu, S. S., Lowman, H. B., Cunningham, B. C., Wells, J. A. Phage display for selection of novel binding peptides. *Methods Enzymol*. **2000**, *328*, 333–363.

[3] Winter G., Griffiths A.D., Hawkins R.E., Hoogenboom H.R. Making antibodies by phage display technology, *Ann. Rev. Immunol.* **1994**, *12*, 433–455.

[4] Sioud, M. Phage display libraries: From binders to targeted drug delivery and human therapeutics. Mol. *Biotechnol*. **2019**, 61, 286-303.

[5] Frenzel, A., Schirrmann, T., Hust, M. Phage display-derived human antibodies in clinical development and therapy. *mAbs*, **2016**, *8*, 1177-1194.

[6] Sidhu, S. S., Geyer, C. R., Eds.; Phage Display in Biotechnology and Drug Discovery, 2nd ed.; CRC Press: Boca Raton, **2015**.

[7] Fernandez-Gacio, A., Uguen, M., Fastrez J. Phage display as a tool for the directed evolution of enzymes. *Trends Biotechnol*. **2003**, *21*, 408-414.

[8] Mohan, K., Donavan, K. C. Arter, J.A., Penner, R.M., Weiss, G.A. Sub-nanomolar Detection of Prostate-Specific Membrane Antigen in Synthetic Urine by Synergistic, Dual-Ligand Phage. *Am. Chem. Soc*. **2013**, *135*, 7761−7767.

[9] Attar, A. M., Richardson, M.B., Speciale, G., Majumdar, S., Dyer, R. P., Sanders, E. C., Penner, R. M., Weiss, G. A. Electrochemical quantification of glycated and non-glycated human serum albumin in synthetic urine. *ACS Appl. Mater. Inter.* **2019**, *11*, 4757–4765.

[10] Peltomaa, R., Benito-Peña, E. Barderas, R. Moreno-Bondi, M. C., Phage Display in the Quest for New Selective Recognition Elements for Biosensors, *ACS Omega*, **2019**, 4, 11569−11580.

[11] Deutscher, S. L. Phage display in molecular imaging and diagnosis of cancer. *Chem Rev*. **2010**, *110*, 3196-211.

[12] Smith, G. P., Petrenko, V. A. Phage Display. *Chem Rev* **1997**, *97,* 391-410.

[13] Sidhu, S. S., Weiss, G. A. *Phage Display: A Practical Approach*, Oxford University Press, New York, **2004**.

[14] Jin, Y., Lei, C., Hu, D., Dimitrov, D. S., Ying, T. Human monoclonal antibodies as

candidate therapeutics against emerging viruses, *Front. Med*. **2017**, *11*, 462–470.

[15] Huang, S. H., Lee, T. Y., Lin, Y. J., Wan, L., Lai, C. H., Lin, C. W. Phage display technique identifies the interaction of severe acute respiratory syndrome coronavirus open reading frame 6 protein with nuclear pore complex interacting protein NPIPB3 in modulating Type I interferon antagonism, *J. Microbiol. Immunol. Infect.* **2017**, *50*, 277-285.

[16] Kim, Y., Lee, H., Park, K., Park, S., Lim, J. H., So, M. K., Woo, H. M., Ko, H., Lee, J. M., Lim, S. H., Ko, B. J., Park, Y. S., Choi, S. Y., Song, D. H., Lee, J. Y., Kim, S. S., Kim, D. Y. Selection and Characterization of Monoclonal Antibodies Targeting Middle East Respiratory Syndrome Coronavirus through a Human Synthetic Fab Phage Display Library Panning, *Antibodies*, **2019**, *8*, 42.

[17] Wang, C., Sun, X., Suo, S., Ren, Y., Li, X., Herrler, G., Thiel, V., Ren, X. Phages bearing affinity peptides to severe acute respiratory syndromes-associated coronavirus differentiate this virus from other viruses, *J. Clin. Virol*. **2013**, *57*, 305-310.

[18] Galan, A., Comor, L., Horvatić, A., Kuleš, J., Guillemin, N., Mrljak, V., Bhide, M. Library-based display technologies: where do we stand? *Mol. Bio. Syst.*, **2016**,*12*, 2342-2358.

[19] Reader, R.H., Workman, R. G., Maddison, B. C. Gough, K.C. Advances in the Production and Batch Reformatting of Phage Antibody Libraries. *Mol. Biotechnol*, **2019**, *61*, 801-815.

[20] Caucheteur D., Robin G., Parez V., Martineau P. (2018) Construction of Synthetic Antibody Libraries. In: Nevoltris D., Chames P. (eds) Antibody Engineering. Methods in Molecular Biology, vol 1827. Humana Press, New York, NY

[21] Persson, J., Augustsson, P., Laurell, T., Ohlin, M. Acoustic microfluidic chip technology to facilitate automation of phage display selection, *FEBS J.*, **2008**, *275*, 5657–5666.

[22] Liu, Y., Adam, J. D., Turner, K., Cochran, F. V., Gambhir, S. S., Soh, H. T. Controlling the selection stringency of phage display using a microfluidic device, *Lab Chip*, **2009**, *9*, 1033–1036.

[23] Wang, J., Liu, Y., Teesalu, T., Sugahara, K. N., Kotamrajua, V. R., Adams, J. D., Ferguson, B. S., Gong, Q., Oh, S. S., Csordas, A. T., Cho, M., Ruoslahti, E., Xiao, Y., Soh, H. T., Selection of phage-displayed peptides on live adherent cells in microfluidic channels, *Proc. Natl. Acad. Sci. U. S. A.*, **2011**, *108*, 6909–6914.

[24] Raftery, L. J., Howard, C. B., Grewal, Y. S., Vaidyanathan, R., Jones, M. J., Anderson, W., Korbie, D., Duarte, T., Cao, M. D., Nguyen, S. H., Coin, L. J. M., Mahler, S. M., Trau, M. Retooling phage display with electrohydrodynamic nanomixing and nanopore sequencing, *Lab Chip*, **2019**, *19*, 4083-4092.

[25] Che, Y. J., Wu, H. W., Hung, L. Y., Liu, C. A., Chang, H. Y., Wang, K., Lee, G. B. An integrated microfluidic system for screening of phage-displayed peptides specific to colon cancer cells and colon cancer stem cells, *Biomicrofluidics*, **2015**, *9*, 054121.

[26] Raftery, L. J., Howard, C. B., Grewal, Y. S., Vaidyanathan, R., Jones, M. J., Anderson, W., Korbie, D., Duarte, T., Cao, M. D., Nguyen, S. H., Coin, L. J. M., Mahler, S. M., Trau, M. Retooling phage display with electrohydrodynamic nanomixing and nanopore sequencing, *Lab Chip*, **2019**, *19*, 4083-4092.

[27] Britton, J, Stubbs, KA, Weiss, GA, Raston, CL: Vortex Fluidic Chemical Transformations, *Chem. Euro. J.,* **2017**, *23*, 13270-13278.

[28] Pye, S. J., Dalgarno, S. J., Chalker, J. M., Raston, C. L. Organic oxidations promoted in vortex driven thin films under continuous flow, *Green Chemistry*, **2018**, *20*, 118 – 124.

[29] Phillips, J. M., Ahamed, M., Duan, X. F., Lamb, R. N., Qu, X., Zheng, K., Zou, J., Chalker, J. M., Raston, C. L. Chemoselective and continuous flow hydrogenation in thin films using a

palladium nanoparticle catalyst embedded in cellulose paper. *ACS App. Bio Mat*. **2019**, *2*, 488-494

[30] Wills, S. S., Raston, C. L., Stubbs, K. A.. Integrating thin film microfluidics in developing a concise synthesis of DGJNAc: A potent inhibitor of α-N-acetylgalctosaminidases, *Bioorganic Med. Chem. Lett*. **2018**, *28*, 3748-3751.

[31] Britton, J., Meneghini, L.M., Raston, C.L, Weiss, G.A. Accelerating Enzymatic Catalysis Using Vortex Fluidics, *Angew. Chem. Int. Ed*. **2016**, *55*, 11387 – 11391.

[32] Britton, J., Dyer, R. P., Majumdar, S., Raston, C. L., Weiss, G. A. Ten-Minute Protein Purification and Surface Tethering for Continuous-Flow Biocatalysis. *Angew. Chem. Int. Ed*. **2017**, *56*, 2296-2301.

[33] Britton, J., Raston, C. L., Weiss, G. A. Rapid protein immobilization for thin film continuous flow biocatalysis. *Chem. Commun*., **2016**, *52*, 10159-10162.

[34] Yuan, T. Z., Ormonde, C. F. G., Kudlacek, S. T., Kunche, S., Smith, J. N., Brown, W. A., Pugliese, K. M., Olsen, T. J., Iftikhar, M., Raston, C. L., Weiss, G. A.. Shear stress-mediated refolding of proteins from aggregates and inclusion bodies. *ChemBioChem*. **2015**, *16,* 393-396.

[35] Britton, J., Smith, J.N., Raston, C.L., Weiss, G.A. Protein folding using a vortex fuidic device. *Methods Mol. Biol.* **2017,** 1586, 211-220.

[36] Luo, X. Al-Antaki, A. H. M., Harvey D. P., Ruan, Y., He, S., Zhang, W., Raston, C.L. Vortex Fluidic Mediated Synthesis of Macroporous Bovine Serum Albumin-Based Microspheres. *ACS Appl Mater Interfaces*. **2018**, *10*, 27224-27232.

[37] Luo, X. Al-Antaki, A. H. M., Pye, S., Meech, R., Zhang, W., Raston, C. L. High-Shear-Imparted Tunable Fluorescence in Polyethylenimines, *ChemPhotoChem*, **2018**, *2*, 343 –348.

[38] Luo, X. Al-Antaki, A.H.M., Vimalanathan, K., Moffatt, J., Zheng, K., Zou, Y., Zou, J., Duan, X., Lamb, R. N., Wang, S., Li, Q., Zhang, W., Raston, C.L. Laser irradiated vortex fluidic mediated synthesis of luminescent carbon nanodots under continuous flow, *React. Chem. Eng.*, **2018**, *3*, 164-170

[39] Tong, C. L., Stroeher, U. H., Brown, M. H., Raston, C. L. Continuous flow vortex fluidic synthesis of silica xerogel as a delivery vehicle for curcumin, *RSC Adv.*, **2015**, *5*, 7953-7958.

[40] Kumar, P. Nandi, S., Tan, T. Z. Siok, Ler, G., Chia, K. S., Lim, W. Y., Bütow, Z., Vordos, D., De laTaille, A., Al-Haddawi, M., Raida, M., Beyer, M., Ricci, E., Colombel, M., Chong, T. W., Chiong, E., Soo, R., Park,M. K., Ha, H.K., Gunaratne, J., Thiery. J. P. Highly sensitive and specific novel biomarkers for the diagnosis of transitional bladder carcinoma, *Oncotarget.* **2015**, *6*, 13539–13549.

[41] He, X. Y., Liu, B. Y., Yao, W. Y., Zhao, X. J., Zheng, Z., Li, J. F., Yu, B. Q., Yuan, Y. Z. Serum DJ-1 as a diagnostic marker and prognostic factor for pancreatic cancer. *J Dig Dis*, **2011**, *12*, 131-137.

[42] Lee, H., Choi, S.K., Ro, J.Y. Overexpression of DJ-1 and HSP90alpha, and loss of PTEN associated with invasive urothelial carcinoma of urinary bladder: Possible prognostic markers. *Oncol Lett*, **2012**, *3*, 507-512.

[43] Zourob, M., Ed.; Recognition Receptors in Biosensors; Springer: New York, 2010.

[44] Frei, J. C., Lai, J. R. Protein and Antibody Engineering by Phage Display. *Methods Enzymol.* **2016**, *580*, 45-87.

[45] Huang, G., Zhong, Z., Miersch, S., Sidhu, S.S., Hou, S.c., Wu, D. Construction of Synthetic Phage Displayed Fab Library with Tailored Diversity. *J. Vis. Exp*. **2018**, *135*, e57357.

[46] t Hoen, P. A., Jirka S. M. G, ten Broeke, B. R., Erik A. Schultes, E. A., Aguilera, B., Pang, K. M., Heemskerk, H., Aartsma-Rus, A., van Ommena, G.J., den Dunnen, J. T. Phage display

screening without repetitious selection rounds, *Anal. Biochem*., **2012**, *421*, 622–631.

[47] Alsulami, I. K., Alharbi, T. M. D., Harvey, D. P., Gibson, C. T. & Raston, C. L. Controlling the growth of fullerene C_{60} cones under continuous flow, *Chem. Commun*. **2018**, *54*, 7896-7899.

[48] Szymańska, B., Sawicka, E., Guzik, A., Zdrojowy, R., Glugosz, A. The Diagnostic Value of Nuclear Matrix Proteins in Bladder Cancer in the Aspect of Environmental Risk from Carcinogens, *BioMed Res. Int.* **2017**, *2017*, Article ID 9643139.

[49] Jamshidian, H., Kor, K., Djalali, M. Urine concentration of nuclear matrix protein 22 for diagnosis of transitional cell carcinoma of bladder, *Urology*, **2008**, *5*, 243–247.

[50] Huber, S., Schwentner, C., Taeger, D., Pesch, B., Nasterlack, M., Leng, G., Mayer, T., Gawrych, K., Bonberg, N., Pelster, M., Johnen, G., Bontruo, H., Wellhäusser, H., bierfreund, H. G., Wiens, C., Bayer, C., Eberle, F., Scheuermann, B., Kluckert, M. Feil, G., Brüning, T., Stenzi, A. Nuclear matrix protein-22: a prospective evaluation in a population at risk for bladder cancer. Results from the UroScreen study, *BJU Int*., **2012**, *110*, 699–708.

[51] Fellouse, F. A., Sidhu, S. S. *Making antibodies in bacteria*. In: Howard, GC.; Kaser, MS., editors. Making and Using Antibodies. CRC Press; Boca Raton, FL: 2007. p. 157-180.

[52] Nam, D. H., Rodriquez, C., Remacle, A. G., Strongin, A. Y., Ge, X. Active-site MMP-selective antibody inhibitors discovered from convex paratope synthetic libraries, *PNAS*, **2016**, *113*, 14970-14975.

[53] Kwong, K. Y., Rader, C. *E. coli* Expression and Purification of Fab Antibody Fragments, Curr. *Prot. Prot. Sci*. **2009**, *6*, 10.1-10.14.

[54] Oliver D.B., Beckwith J. Regulation of a membrane component required for protein secretion in Escherichia coli, *Cell*, **1982**, *30*, 311–319.

[55] Luzar, J., Štrukelj, B., Lunder, M. Phage display peptide libraries in molecular allergology: from epitope mapping to mimotope-based immunotherapy. *Allergy*, **2016**, *71*,

1526−1532.

[56] Castel, G., Chtéoui, M., Heyd, B., Tordo, N. Phage display of combinatorial peptide libraries: Application to antiviral research. *Molecules*, **2011**, *16*, 3499−3518.

[57] Wai, C. Y. Y., Leung, N. Y. H., Leung, P. S. C., Chu, K. H. Immunotherapy of food allergy: A comprehensive review. *Clin. Rev. Allergy Immunol.* 2017.

[58] Aghebati-Maleki, L., Bakhshinejad, B., Baradaran, B., Motallebnezhad, M., Aghebati-Maleki, A., Nickho, H., Yousefi, M., Majidi, J. Phage display as a promising approach for vaccine development. J. Biomed. Sci. **2016**, *23*, No. 66.

[59] Sundell, G. N., Ivarsson, Y. Interaction analysis through proteomic phage display. Biomed. Res. Int. **2014**, No. 176172.

4.8. Supporting Information

Purification of DJ-1

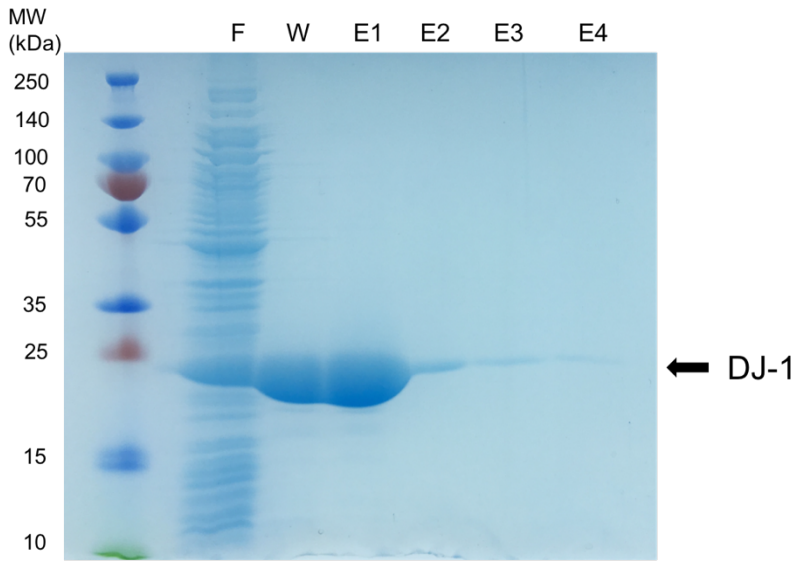

Figure S4.1. Purification of DJ-1. In this 12% tris-glycene SDS-PAGE gel, each lane was loaded with 19µL of sample unless otherwise indicated. PageRuler pre-stained protein ladder (10µL, Thermo Fisher Scientific) was used. Lane F: flow through after batch binding the cell lysate to the resin. Lane W: column wash with 50mL of buffer with 50mM imidazole. Lane E1-4: DJ-1 eluted with buffer containing 250mM imidazole and collected as 4 x 15mL fractions. Buffer: 50mM Na_2HPO_4, 300mM NaCl, pH 8.0, 250mM imidazole, 10mM BME.

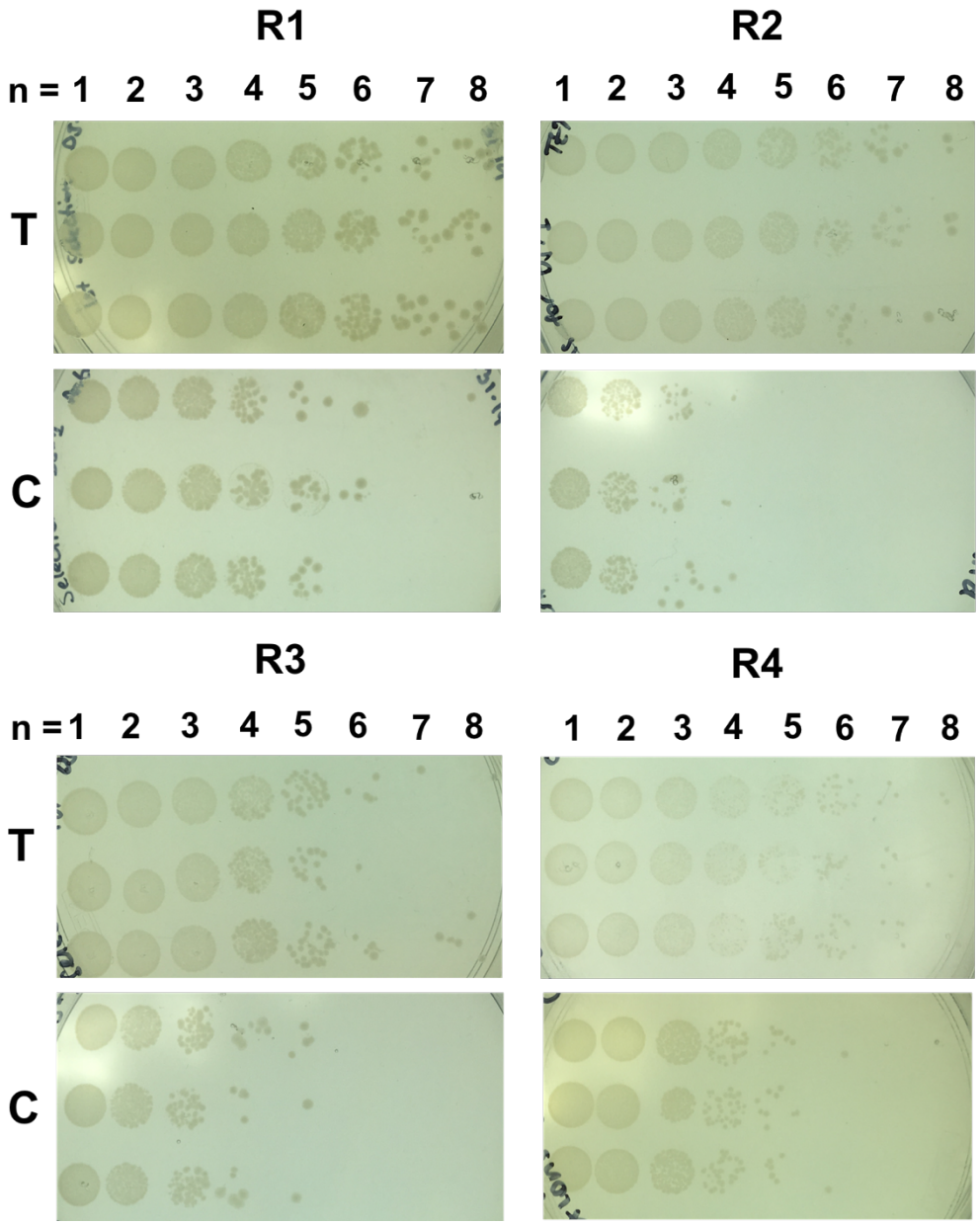

Figure S4.2. Phage titer plates from phage-displayed antibody selections for DJ-1 at 8k rpm. n = dilution fold 10^{n}, T = tetracycline, C = carbenicillin. Formula to calculate phage titer: M x 10^{n} x (Vculture/Vplated) cfu, where M is the average colony number counted from the most diluted fold 10^{n} in triplicate. 10μL of each dilution was plated.

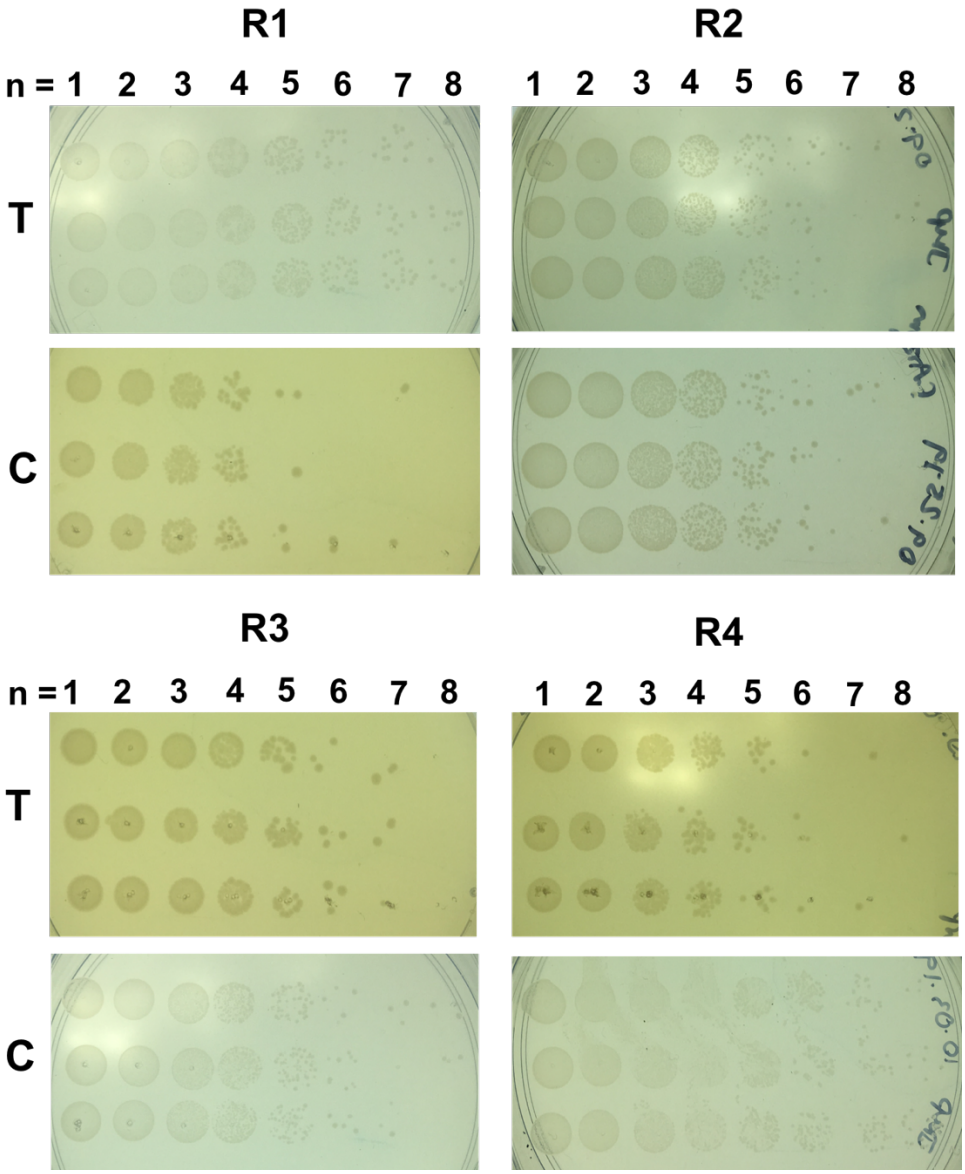

Figure S4.3. Phage titer plates from phage-displayed antibody selections for DJ-1 at 4k rpm. n = dilution fold $10^{n.}$, T = tetracycline, C = carbenicillin. Formula to calculate phage titer: M x 10^n x (Vculture/Vplated) cfu, where M is the average colony number counted from the most diluted fold 10^n in triplicate. 5μL of each dilution was plated.

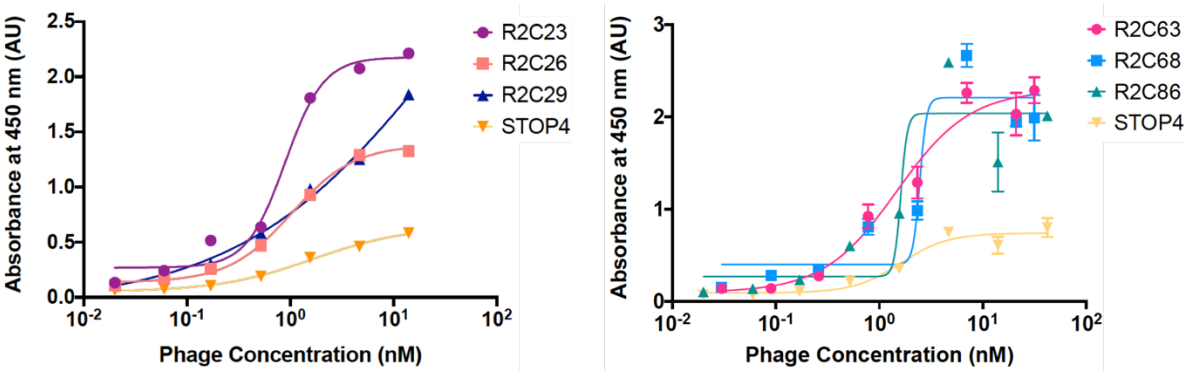

Figure S4.4. Dose-dependent phage-based ELISA for randomly selected binding hits from round 2 phage-displayed Fab selections in the VFD at 8k rpm. Stop 4 phage, an M13 phage with no protein fragment displayed, was used as a negative control.

Table S4.1. Amino acid sequences of the mutated binding regions of the selected and screened Fab fragments in Figure S5.

Fab ID	CDR-L3	CDR-H1	CDR-H2	CDR-H3
R2C23	RHYHAL	FGAAWM	GIYASGGDTD	GSRAHGYSHPSGSYGM
R2C26	SSYYYSHPI	FGSDDI	YIYPSGGYTD	YSYDSSYHYYFYGL
R2C29	HYYHYPYPI	FGGAWI	RISASGGDTA	YYYYYGSSRYYYSGRSAM
R2C63	DYYGDGYL	FSSSSI	SGFDFSSSYGYTY	TVRGSKKPYFSGWAM
R2C68	GGYYL	DFAGYSM	AYISSSGGYTD	YFGSSWGGYYFYSYSYDGL
R2C86	SGSYALI	FGSSAM	GISASGGYTD	YSYYGYPFSGI

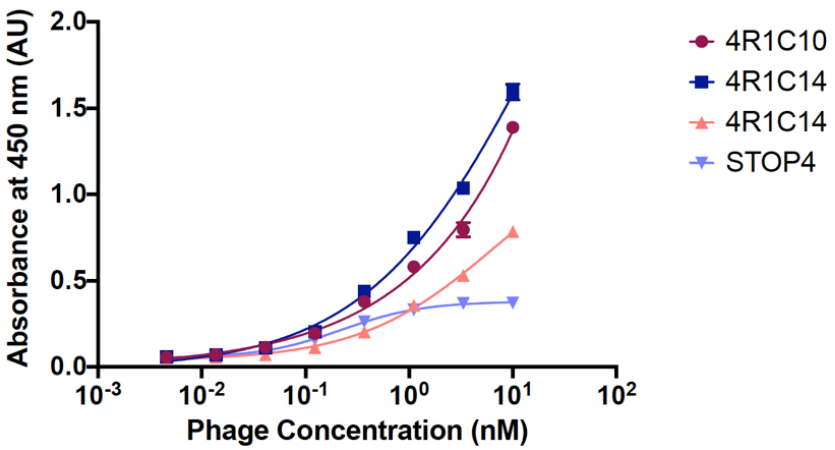

Figure S4.5. Dose-dependent phage-based ELISA for randomly selected binding hits from round 1 and round 2 phage-displayed Fab selections in the VFD at 4k rpm. Stop 4 phage, an M13 phage with no protein fragment displayed, was used as a negative control. Low to insignificant binding to DJ-1 is observed for all phage-displayed Fabs.

Purification of Fab Binder R2C68

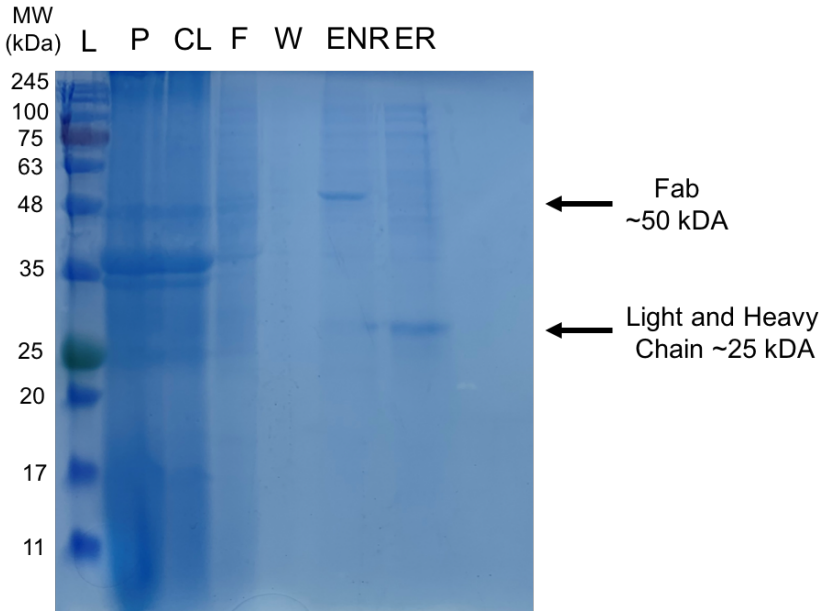

Figure S4.6. Purification of Fab R2C68. In this 12% tris-glycene SDS-PAGE gel, each lane was loaded with 19μL of sample unless otherwise indicated. Lane L: BLUEstain protein ladder (10μL, GoldBio) was used. Lane P: 1 μL of cell pellet in 18μL of ddD_2O. Lane CL: cell lysate. Lane F: flow through after batch binding the cell lysate to the resin. Lane W: column wash with 50mL of buffer with 50mM imidazole. Lane ENR: 15mL elution fraction with buffer containing 250mM imidazole under non-reducing conditions. Lane ER: elution fraction under reducing conditions. Buffer: 50mM Tris-HCl, 300mM NaCl, pH 8.0.

Previous Attempts for Expression of Fab R2C68 in E. coli

Achieving periplasmic expression of Fab proteins in *e.coli* expression cells was explored. Expression of the Fab to the oxidative periplasm is required for the formation of the disulphide bonds that bind the light and heavy chains. First, the gene encoding for Fab R2C86 was cloned out of the phagemid and into a pET28 expression vector using Gibson Assembly.

The expression construct contains a T7 promotor, a ribosomal binding site (rbs) and STII signal peptide upstream of both the light (VL_VC) and heavy (VL_CH1) chain for co-expression, and a C_{H1} C-terminal his-tag for purification (Figure S4.7, Table S4.2). The periplasmic expression was attempted in BL21 (DE3) cells using different expression temperatures and IPTG concentrations (Table S4.3, Entry 1-7). Periplasmic extraction was achieved using Tris-Sucrose-EDTA extraction [6]. The extraction supernatant and cell pellet were analysed using SDS-PAGE (Figure S4.8 and S4.9). Results suggest the presence of the light (~23kDa) and heavy (~27kDa) chains in the cell pellet, however are not detected in the periplasmic extract.

Next, an expression vector, pGEX-4t1, containing a Ptac promoter was explored. The Ptac promoter induces expression at a slower rate relative to the T7 promotor, therefore, it is postulated that using a slower expression vector may lead to periplasmic expression [8]. The gene encoding for the Fab R2C86, with the C-terminal his-tag, was cloned out of the pET28 vector and into a vector containing a Ptac promoter, pGEX-4t1 (Addgene). The periplasmic expression was attempted in BL21 (DE3) cells using different expression temperatures and IPTG concentrations (Table S4.3, Entry 8-11). Expression of the light and heavy chain appears to have increased, however, no Fab is detected in the periplasmic extract. Another Fab construct, C2R68 (identified as a real binder) was expressed, but also failed to secrete to the periplasm (Table S4.3, Entry 12-15, Figure S4.10).

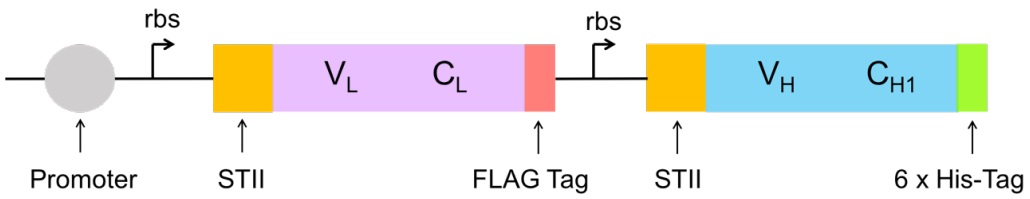

Figure S4.7. Diagram of Fabs bicistronic expression construct (~1.7kb). A T7 or Ptac promoter was used, with a ribosomal binding site (rbs) before the light (VL_VC) and heavy (VL_CH1) chain for co-expression. There is signal peptide sequence, STII, before both VL_VC and VL_CH1 sequences for expression to the periplasm. FLAG tag and 6 x His-tag for potential ELISA analysis, immobilisation, and purification. pET28 and pGEX-4T1 vectors used in this study.

Table S4.2. The amino acid sequence for the four mutated binding regions of the Fab antibody fragments used in this study [7].

Fab ID	CDRL3	CDRH1	CDRH2	CDRH3
R2C68	GGYYL	DFAGYSM	AYISSSGGYTD	YFGSSWGGYYFYSYSYDGL
R2C86	SGSYALI	FGSSAM	GISASGGYTD	YSYYGYPFSGI

Table S4.3. Optimizing expression conditions for periplasmic expression of Fabs in BL21 *E. coli* cells.

Entry	Fab ID	Promoter	Expression Volume (mL)	IPTG Induction Concentration (mM)	Expression Temp. (ºC)	Figure
1	R2C86	T7	250	0.5	18	S4.8A
2	R2C86	T7	250	0.5	25	S4.8B
3	R2C86	T7	250	0.5	30	S4.8C, S4.9A
4	R2C86	T7	250	0.25	18	S4.9C
5	R2C86	T7	250	0.25	25	S4.9D
6	R2C86	T7	250	0.25	37	S4.9E
7	R2C86	T7	250	1	37	S4.9B
8	R2C86	Ptac	125	0.25	25	S4.10A
9	R2C86	Ptac	125	0.25	37	S4.10C
10	R2C86	Ptac	125	0.5	25	S4.10B
11	R2C86	Ptac	125	0.5	37	S4.10D
12	R2C68	Ptac	125	0	37	S4.10E
13	R2C68	Ptac	125	0.1	37	S4.10F
14	R2C68	Ptac	125	0.25	37	S4.10G
15	R2C68	Ptac	125	0.5	37	S4.10H

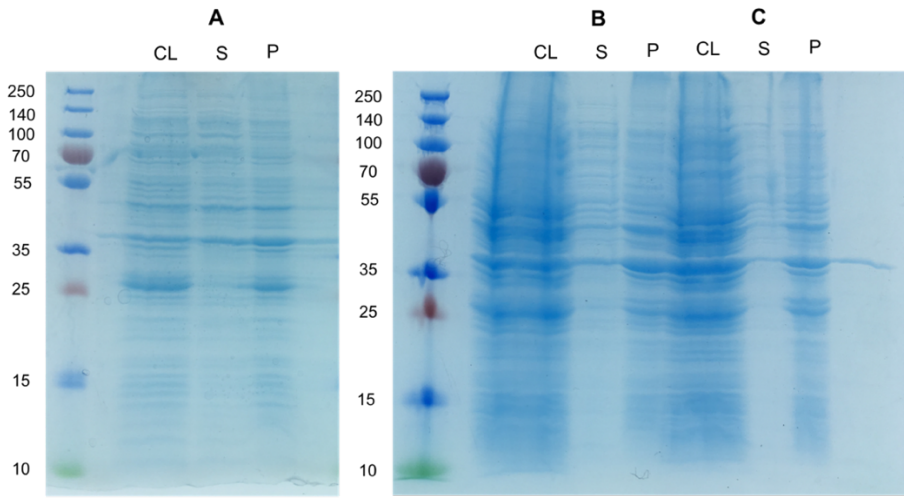

Figure S4.8. SDS-PAGE gel of Fab pET28 expression after TSE extraction (see Table 2, Entry 1-3). A) 18°C expression, 0.5mM IPTG. B) 25°C expression, 0.5mM IPTG. C) 30°C expression, 0.5mM IPTG. CL= cell lysate, S= extraction supernatant, P = cell pellet.

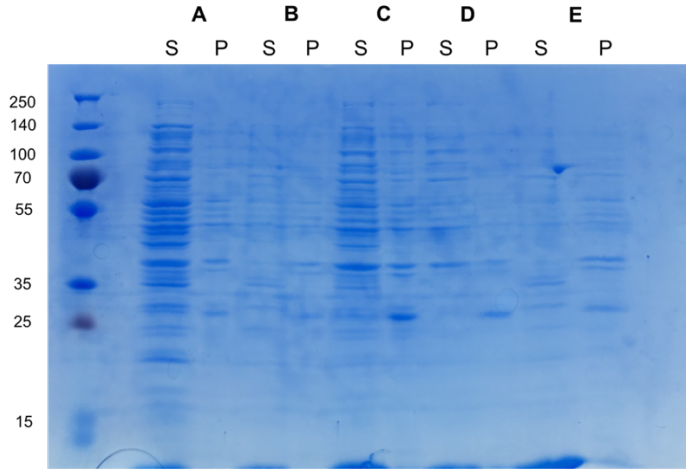

Figure S4.9. SDS-PAGE gel of Fab pET28 expression (see Table 2, Entry 3-7). A) 30°C expression, 0.5mM IPTG. B) 37°C expression, 1 mM IPTG. C) 18°C expression, 0.25mM IPTG. D) 25°C expression, 0.25mM IPTG. E) 37°C expression, 0.25mM IPTG. S= extraction supernatant, P = cell pellet.

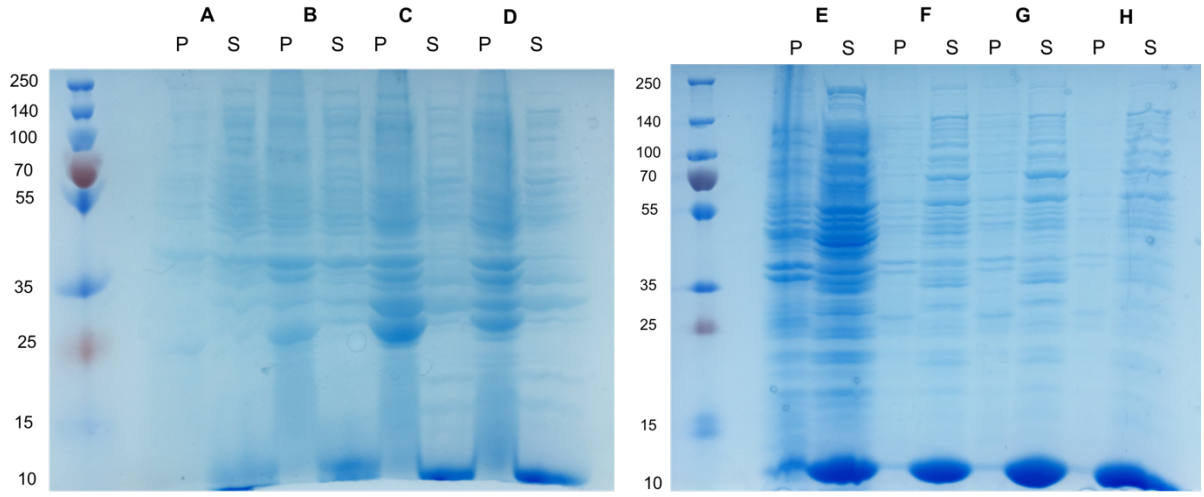

Figure S4.10. SDS-PAGE gel of R2C86 (left) and R2C68 (right) pGEX Fab expression constructs (see Table S1, Entries 8-15). R2C86 expression, A) 25°C expression, 0.25mM IPTG. B) 25°C expression, 1mM IPTG. C) 37 °C expression, 0.25mM IPTG. D) 37°C expression, 0.5mM IPTG. R2C68 expression at 25°C expression, E) 0.5mM IPTG. F) 0.1mM IPTG. G) 0.25mM IPTG. H) 0.5mM IPTG. S= extraction supernatant, P = cell pellet.

Cloning Fab Binder into pET 28 Vector:

The gene coding for Fab binder R2C86 was cloned from the phagemid into a pET28 vector using Gibson Assembly. The following PCR parameters and oligonucleotides (integrated DNA Technologies) were used to amplify the R2C86 Fab gene with overhangs complimentary to the pET28 vector. PCR reaction mixture (25µL) contains Herculase ii DNA polymerase (New England Biolabs), following the manufacturers instructions, and buffer (5× diluted final concentration, New England Biolabs), dNTPs (0.5mM each final concentration, New England Biolabs), primers (33ng each final concentration, Integrated DNA Technologies), and R2C86

phagemid (50ng). PCR reaction was as follows: one cycle at 95°C for five min, 25 cycles at 95°C for one min, 50°C for one min, 72°C for three min, and one cycle at 72°C for five min.

Fwd: 5'- GAAGGAGATATACCATGAAAAAGAATATCGCATTTCTTC -3'

Rev : 5'- CGTGGTGACCCGACGCGGTGTGTGAGTTTTGTCACAAG -3'

The following PCR parameters and oligonucleotides (integrated DNA Technologies) were used to amplify the pET28 vector with 6 x histidine tag (for C-terminus) overhangs complimentary to the Fab gene. PCR reaction mixture was as described above with DMSO (5 % v/v final concentration). PCR reaction was as follows: one cycle at 95°C for five min, 25 cycles at 95°C for 1.5 min, 60°C for 1.5 min, 72°C for 3.5 min, and one cycle at 72°C for five min. Fwd primer: 5'-CAAAACTCACACACCGCGTCGGGTCAC -3', Rev primer: 5'-GCGATATTCTTTTTCATGGTATATCTCCTTCTTAAAGTTAAAC -3'

The PCR products were extracted from a 1% agarose gel using a Zymoclean Gel DNA Recovery Kit. The following Gibson Assembly reaction mixture was used: 50ng of Fab PCR product, 100ng of pET28 PCR product, 2μL of NEBuilder ® HiFi DNA Assembly Master Mix (NEB), and autoclaved ddH2O to a total volume of 4μL. The reaction mixture was incubated at 50°C for 1h, and stored at 4°C. The reaction product was transformed into *E. coli* Nova blue cells and plated on an agar plate supplemented with kanamycin (40μg/mL), followed by incubation at 37°C for 18 h. A single colony is used to inoculate 5mL of 2YT supplemented with kanamycin (40μg/mL), and grown at 37°C for 18h. The DNA plasmid is isolated, purified and sequenced by Genewiz.

Cloning Fab Binder into pGEX-4T1 Vector from pET28 Vector:

The gene coding for Fab binder R2C86 with C-terminal histidine tag was cloned from the pET28 vector into a pGEX -4T1 vector using the protocol above, with the following modifications. For cloning the R2C68 Fab gene, R2C68 pET28, cloned above, was used as a template, with an annealing temperature of 50°C. The following primers were used,

Fwd: 5'- GGAAACAGTATTCATGAAAAAGAATATCGCATTTCTTC -3',

Rev: 5'- GCGAGGCAGATCGTCAGTCAGTGGTGGTGGTGGTG -3'. The pGEX-4T1 vector backbone was cloned from original vector (purchase from Addgene) using an annealing temperature of 50°C. The following primers were used,

Fwd: 5'- CCACCACCACCACTGACTGACGATCTGCCTCGC -3',

Rev : 5'- GCGATATTCTTTTTCATGAATACTGTTTCCTGTGTG -3'

Cloning Fab Binder into pGEX-4T1 Vector from Phagemid:

The R2C68 Fab gene was cloned from the phagemid into the pGEX vector using the protocol above, with the following modifications. For cloning the R2C68 Fab gene, the R2C68 phagemid was used as a template, using an annealing temperature of 50°C. The following primers were used, Fwd: 5' GGAAACAGTATTCATGAAAAAGAATATCGCATTTCTTC 3', Rev: 5' CGTGGTGACCCGACGCGGTGTGTGAGTTTTGTCACAAG 3'. The pGEX vector, containing a 6x histidine tag (C-terminal after once cloned), was cloned from the R2C86 pGEX construct, using an annealing temperature of 60°C, and the following primers were used, Fwd: 5' CAAAACTCACACACCGCGTCGGGTCACC 3', Rev: 5' GCGATATTCTTTTTCATGAATACTGTTTCCTGTGTG 3'

Expression of Fab Binders in E. coli BL21(DE2) Cells:

The below protocol was used for attempting periplasm expression of Fab binders for DJ-1 in *E. coli* with conditions varied according to Table 1. The Fab pET28 or pGEX construct was transformed *via* heat shock into *E.coli* BL21 (DE3) cells and transferred to a LB agar plate containing 40μg/mL of kanamycin, and incubated at 37°C for 14h. A seed culture was prepared by inoculating a single colony into 25mL of LB media with 40 μg/mL of kanamycin and shaken (220 rpm) in a 125mL baffled flask at 37°C for 14h. The expression culture was prepared by inoculating 125mL of LB media with 40μg/mL of kanamycin with 1.5mL of seed culture into and shaking at 220 rpm at 37°C in 500mL baffled flask. When the culture reached an OD_{600} of 0.6-0.7 the cells were induced with 0.1-1.0mM IPTG. The induced expression culture was incubated by shaking at 220 rpm for 20-24h at 18, 25, 30, or 37°C. The cells were centrifuged at 3k rpm for 20 mins at 4°C and resuspended in 8 mL Tris-sucrose-EDTA extraction buffer: 200mM Tris-HCl, pH 8.0, 500mM sucrose, 1mM EDTA, Halt™ protease inhibitor cocktail (Thermofisher Scientific). Lysozyme (1mg/mL) was added to the suspended cell lysate and the mixture was gently stirred at 4°C for 1h. The cell suspension was centrifuged at 13,000k rpm at 4°C for 1h, and the supernatant separated from the cellular debre. All fractions (19μL) were analysed by SDS-PAGE analysis.

Expression of NMP22 and tNMP22 for Phage-Displayed Antibody Selections

Recombinant Nuclear Matric Protein 22 (NMP22) was expressed for the purpose of performing phage-displayed antibody selections in the VFD. NMP22 has been identified as a bladder cancer biomarker. NMP22 is involved in cell mitosis, and is released from the cells

during apoptosis [35-37]. The level of NMP22 is higher in bladder cancer cells compared to normal cells, resulting in an increase in its concentration in the urine of bladder cancer patients [35-37]. Therefore, identifying antibody binders can be valuable for application in early detection bio-diagnostics. Attempts to achieved soluble expression of NMP22 in *E. coli* BL21 cells was unsuccessful. Optimization of several parameters including IPTG concentration, expression scale and expression temperature were explored. High levels of expression was observed in the insoluble inclusion bodies, with small levels detected in the soluble fraction after sonication, centrifugation and Ni-NTA purification (Figure S4.11). After concentration of the protein solution, the NMP22 is no longer present, indicating the NMP22 is improperly folded leading to aggregation and precipitation out of solution. A truncated construct of NMP22 (tNMP22) was successfully expressed in *e.coli* BL21 cells (Figure S4.12). Phage-displayed fab selections were performed on this tNMP22 construct and the results are shown in Table S4.4.

Over Expression and Purification of Recombinant NMP22

NMP22 pET28 plasmid transformed into BL21(DE3) cells were used to inoculate a 25mL seed culture of LB and 40μg/mL of kanamycin, and incubated at 37°C for 14h. The expression cultures were prepared by inoculating 5mL of seed culture per 500mL of LB media with 40μg/mL of kanamycin. The cultures are shaken at 220rpm at 37°C until OD600 reached 0.6, followed by induction with 0.5mM IPTG. The induced expression cultures was incubated by shaking at 220 rpm at 16°C for 20-24h. The cells were harvested by centrifugation, resuspention and sonication in 25mL lysis buffer (50mM Na_2HPO_4, 300mM NaCl, 10mM imidazole, pH 8.0, 10mM BME, 100μL HALT protease inhibitor). The supernatant was purified using nickel affinity chromatography using a gravity column containing charged (with

100mM $NiSO_4$) and equilibrated IDA resin (3g, Purolite). The following buffers were used to purify tNMP22: lysis buffer (50mL), wash buffer (50mM Na_2HPO_4, 300mM NaCl, pH 8.0, 50mM imidazole, 10mM BME), and elution buffer (60mL collected as three fractions, 50mM Na_2HPO_4, 300mM NaCl, pH 8.0, 500mM imidazole, 10mM BME). Fractions containing purified protein, were identified using SDS-PAGE. The purity of the protein was confirmed using 12% SDS-PAGE and the concentration determined using the Bradford assay.

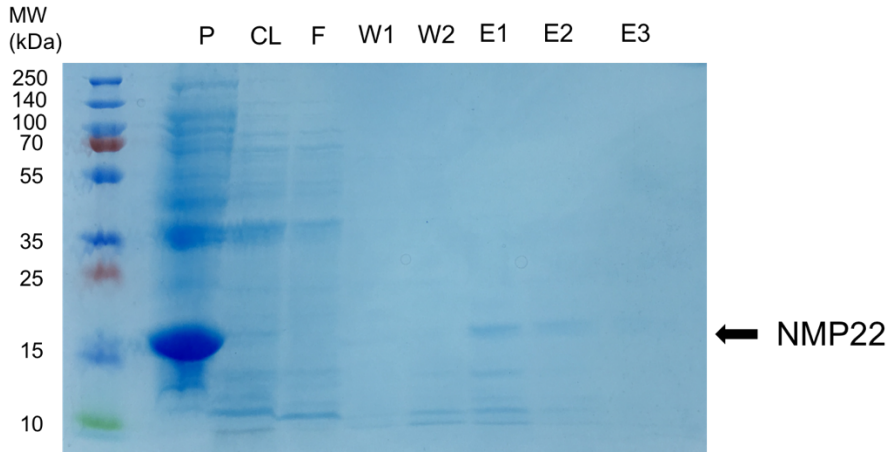

Figure S4.11. Purification of NMP22. In this 12% tris-glycene SDS-PAGE gel, each lane was loaded with 19μL of sample unless otherwise indicated. Lane L: PageRuler pre-stained protein ladder (10μL, Thermo Fisher Scientific) was used. Lane P: 1μL of insoluble pellet in 18μL of ddH_2O. Lane CL: soluble cell lysate. Lane F: flow through after batch binding the cell lysate to the resin. Lane W1: column wash with 50mL of buffer with 50mM imidazole. Lane W2: column wash with 25mL of buffer with 100mM imidazole. Lane E1-4: DJ-1 eluted with buffer containing 500mM imidazole and collected as 4 x 15mL fractions. Buffer: 50mM Na_2HPO_4, 300mM NaCl, pH 8.0, 250mM imidazole, 10mM BME.

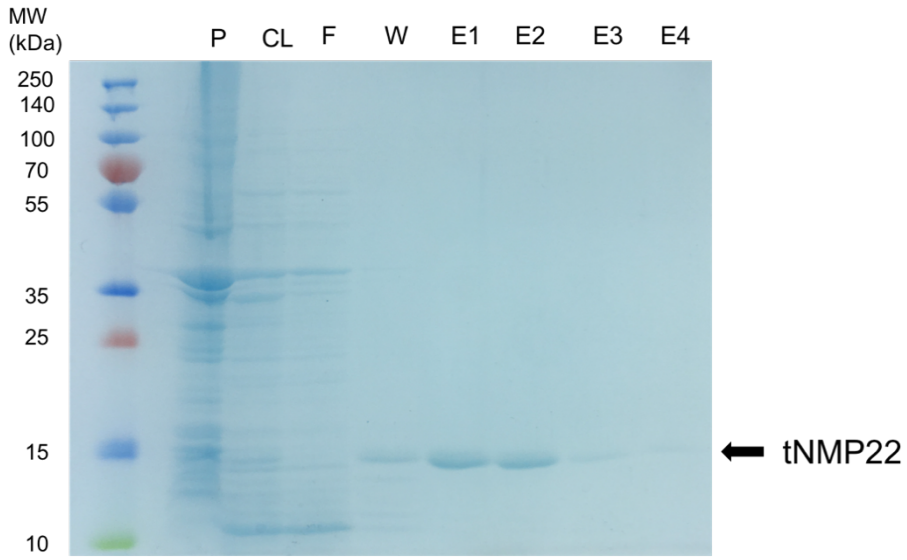

Figure S4.12. Purification of tNMP22. In this 12% tris-glycene SDS-PAGE gel, each lane was loaded with 19μL of sample unless otherwise indicated. Lane L: PageRuler pre-stained protein ladder (10μL, Thermo Fisher Scientific) was used. Lane P: 1μL of insoluble pellet in 18μL of ddH_2O. Lane CL: soluble cell lysate. Lane F: flow through after batch binding the cell lysate to the resin. Lane W1: column wash with 50mL of buffer with 50mM imidazole. Lane W1: column wash with 25mL of buffer with 100mM imidazole. Lane E1-4: DJ-1 eluted with buffer containing 250mM imidazole and collected as 4 x 15mL fractions. Buffer: 50mM Na_2HPO_4, 300mM NaCl, pH 8.0, 250mM imidazole, 10mM BME.

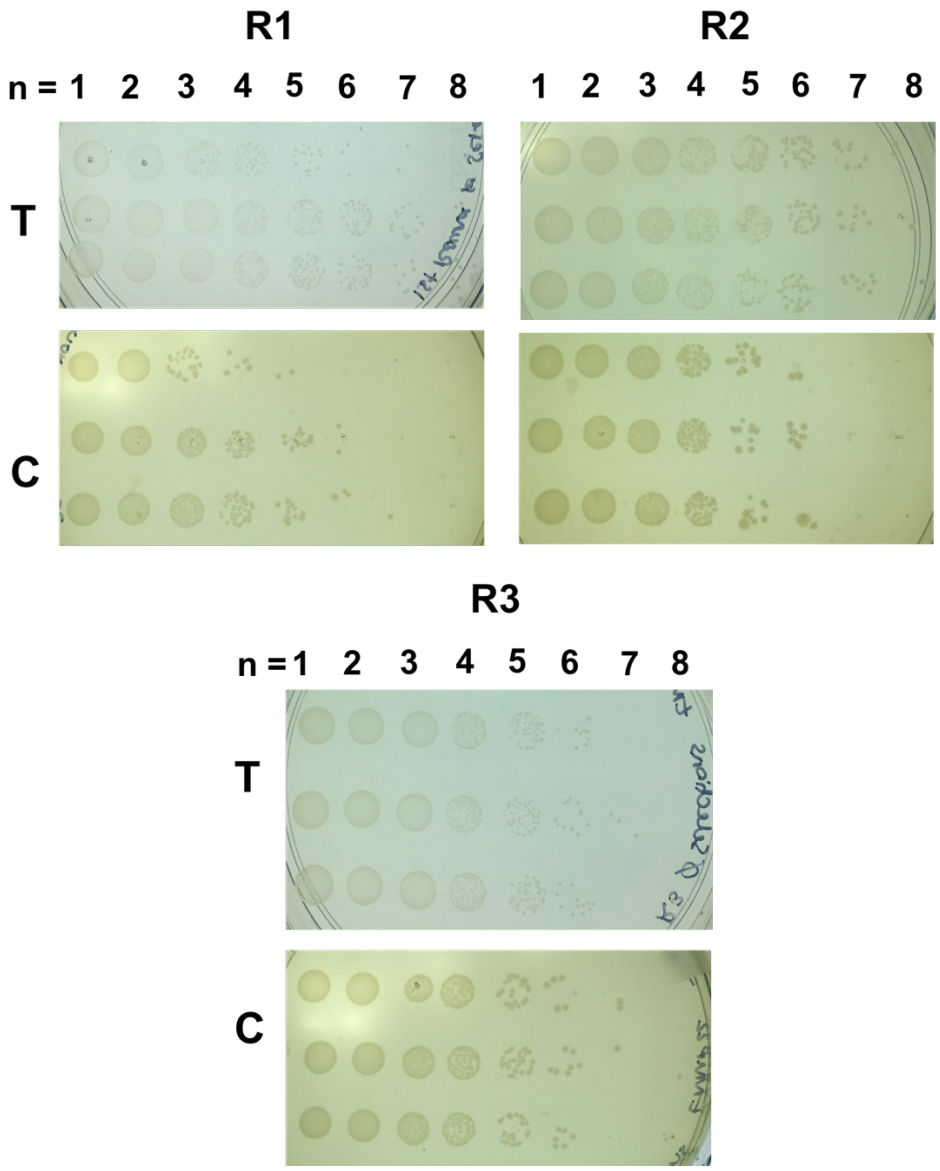

Figure S4.13. Phage titer plates from phage-displayed antibody selections for tNMP22 at 8k rpm. n = dilution fold 10^{n}, T = tetracycline, C = carbenicillin. Formula to calculate phage titer: M x 10^{n} x (Vculture/Vplated) cfu, where M is the average colony number counted from the most diluted fold 10^{n} in triplicate. 5μL of each dilution was plated.

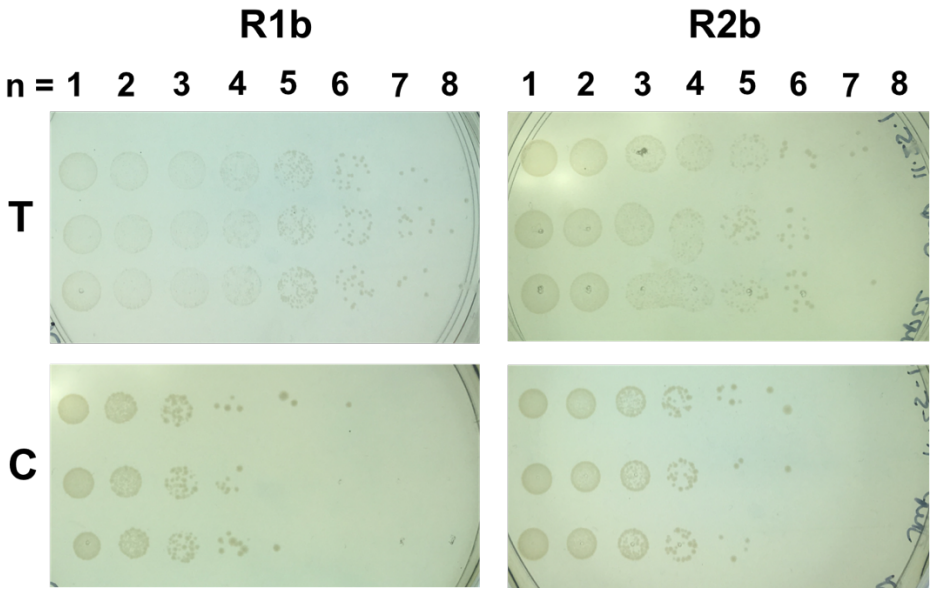

Figure S4.14. Phage titer plates from phage-displayed antibody selections for tNMP22 repeated after subtracted selection round. n = dilution fold 10^n, T = tetracycline, C = carbenicillin. Formula to calculate phage titer: M x 10^n x (Vculture/Vplated) cfu, where M is the average colony number counted from the most diluted fold 10^n in triplicate. 5μL of each dilution was plated.

Table S4.4. Phage library enrichment and ELISA hit rates (%)(hits a >x3 above background).

Round	Titer (CFU)	ELISA Hit Rate (%)
1	5.3×10^9	0
2	4.8×10^9	0
3	1.2×10^{10}	0
1b	3.4×10^8	0
2b	2.3×10^9	1

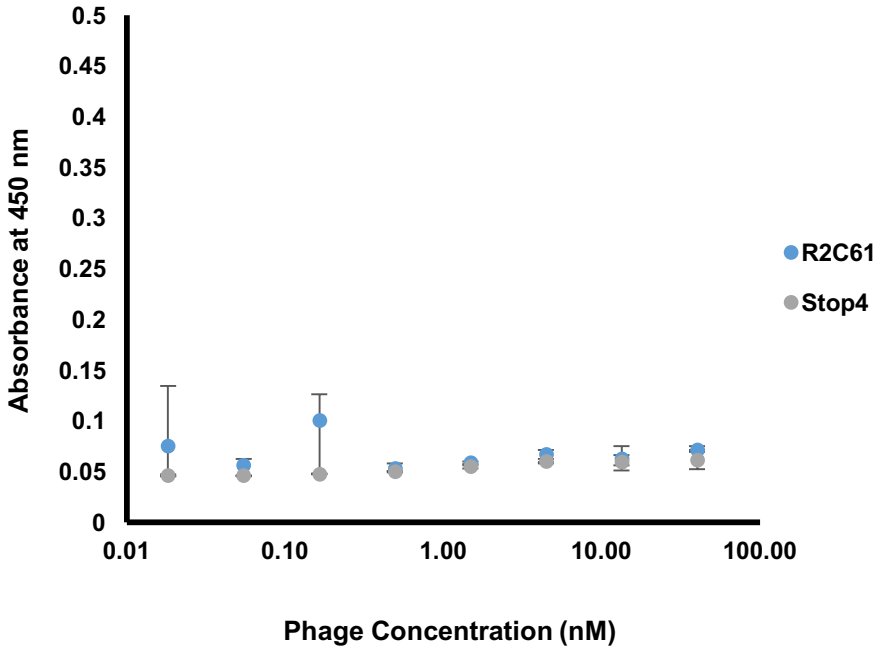

Figure S4.15. Dose-dependent phage-based ELISA on tNMP22 for binder, R2C61, selected during round 2 of phage-displayed Fab selections in the VFD at 8k rpm. Stop 4 phage, an M13 phage with no protein fragment displayed, was used as a negative control. No binding to tNMP22 is observed.

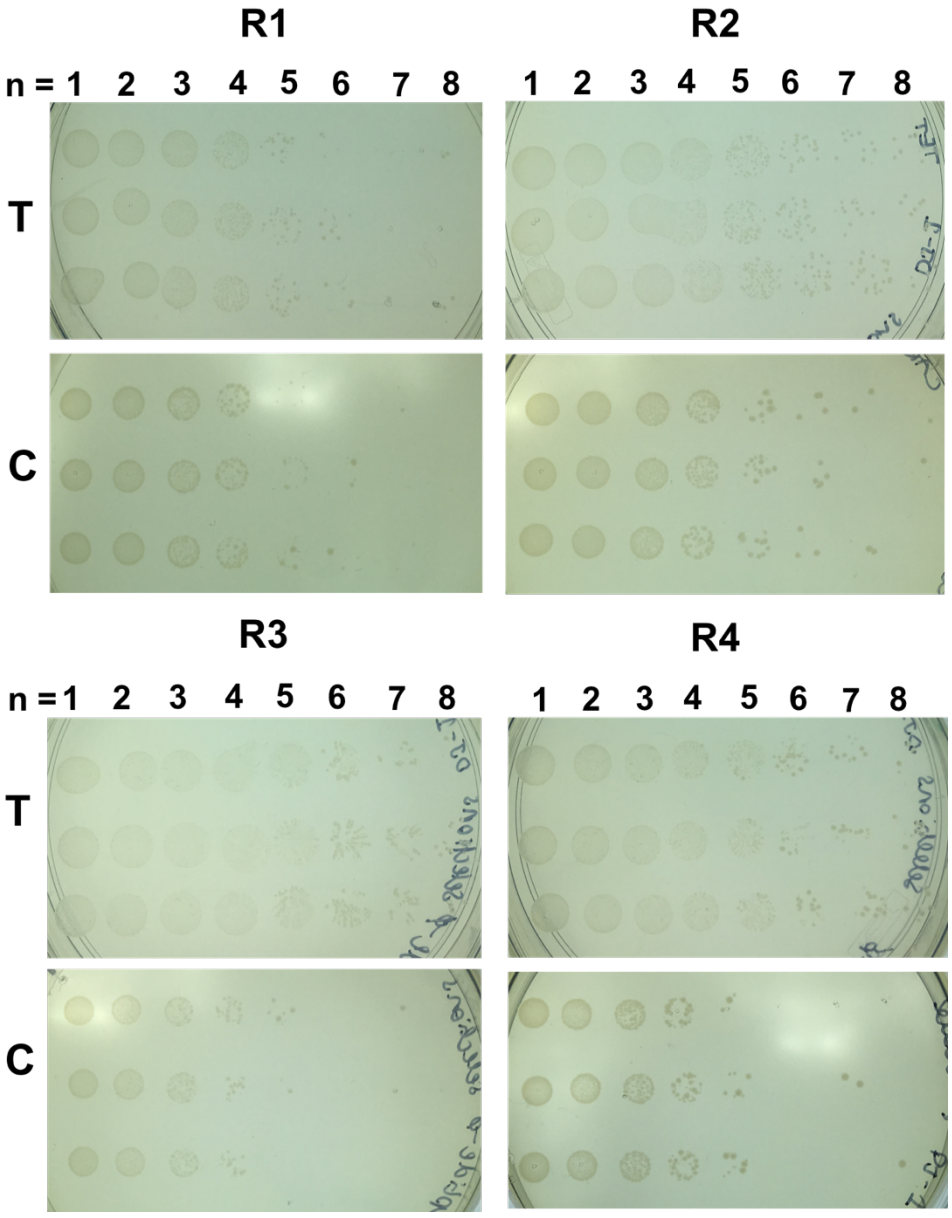

Figure S4.16. Phage titer plates from phage-displayed peptide selections for DJ-1 after subtracted selection round. n = dilution fold 10^{n}, T = tetracycline, C = carbenicillin. Formula to calculate phage titer: M x 10^{n} x (Vculture/Vplated) cfu, where M is the average colony number counted from the most diluted fold 10^{n} in triplicate. 5μL of each dilution was plated.

Chapter 5: DNA Extraction from Formalin-Fixed Marine Specimen using Vortex Fluidics-Mediated Processing

---

This chapter is based on a publication: Totoiu, C. A., Phillips, J. M., Reese, A. T., Majumdar, S., Girguis, P. R., Raston, C. L., Weiss, G. A. Vortex fluidics-mediated DNA rescue from formalin-fixed museum specimens. *PLoS ONE*, **2020**, *15*(1).

5.1. Abstract

Important genetic information can be revealed from DNA in formalin-preserved tissue stored in museums around the world. However, preserving specimens in formaldehyde creates protein and DNA crosslinks that prevent DNA amplification and sequencing. Proteinase K proteolysis of DNA-protein crosslinks is used to recover DNA, however, current methods are slow, harsh and low-yielding. Here the mechanical energy in the vortex fluidic device (VFD) is applied to enhance the catalytic activity of proteinase K and extract DNA from American lobster tissue (*Homarus americanus*) fixed in 3.7% formalin for >1 year. Through optimization, the optimal VFD rotational speed was identified for recovery of PCR-amplified DNA. Although 500+ base pairs were sequenced from the organism, shorter amplicon lengths were obtained more consistently. This method allows for the exploration of DNA from millions of historical and extinct species.

5.2. Introduction

Archived biological samples offer an important source of genetic information for

diverse fields including ecology, evolutionary biology, phylogenetic, biodiversity, and epidemiology [1-2]. For >150 years, tissues samples to complete organisms have been effectively preserved in aqueous formaldehyde (termed formalin), retaining their morphological features and hindering parasitic microbial growth [3]. A great array of formalin-fixed samples exists, including at least 400 million samples across 13 large institutions [1]. In several cases, these samples are the only remaining specimens that can provide genetic information about the organisms, such as their environments, microbiomes, diets, and other characteristics [4-6]. However, formalin preservation of these samples can inhibit the amplification and sequencing of DNA [7]. New methods to recover DNA from formalin-fixed samples could improve our ability to access genetic information about organisms to advance our understanding of how species populations and ecosystems have responded to natural and anthropogenic changes over time [1-2, 8, 9-10].

Inhibition of DNA amplification and sequencing from formalin-fixed samples can occur due to damages in the DNA [11-12]. During the preservation process, electrophilic formaldehyde leads to base deglycosylation, by covalent modification of DNA bases, followed by strand breakage [13]. DNA fragmentation can also occur after long periods of storage, independent of formalin [14]. Therefore, greater amounts of DNA template are required for PCR amplification of larger sequences [15-16]. PCR and DNA sequencing can also be hindered by the introduction of formaldehyde induced intrastrand and protein-DNA crosslinking [17-18]. This is a result from the nucleophilic attack on formaldehyde by the primary amines on the surface proteins, yielding imines and iminium ions. These further react with less nucleophilic primary amines of DNA bases to generate a protein-DNA crosslink (Figure 5.1A) [19, 20]. Multiple crosslinks can slowly form over time, as a result of the high density of surface amines of the protein. Additionally, point mutations can result during PCR amplification due to the incorporation of adenine as the incorrect complement to degraded cytosine [11].

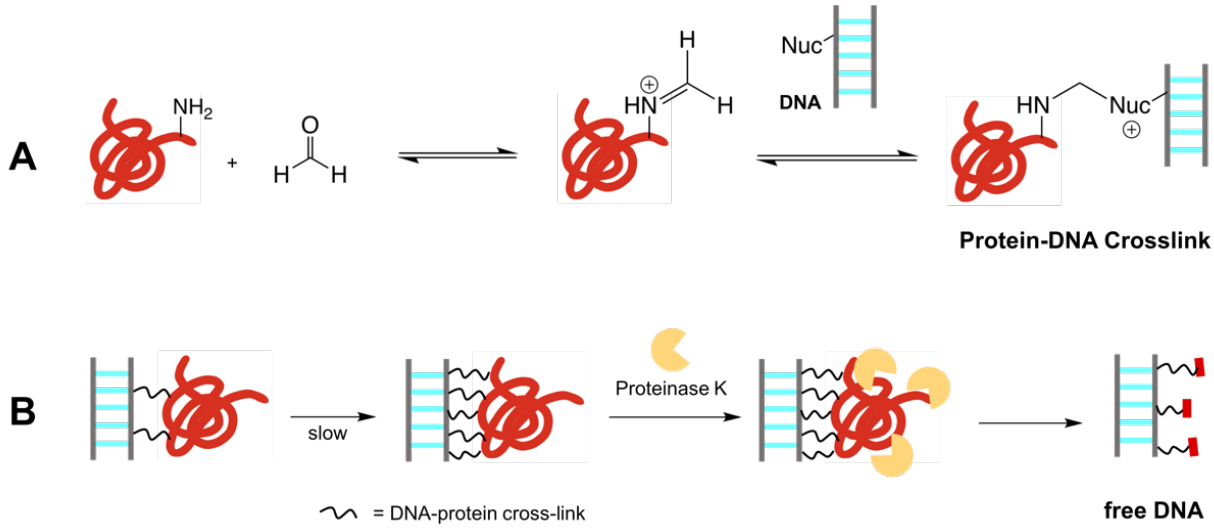

Figure 5.1. Schematic representation of formalin-induced crosslinking and the breakdown of cross-linked proteins by proteinase K treatment. (A) During preservation with formaldehyde, amines on the surface of proteins undergoes nucleophilic attack on the carbonyl of formaldehyde to produce an iminium ion, which can further react with a primary amine from DNA, RNA, or proteins to form crosslinks. (B) Treatment with a protease, proteinase K, allows for the recovery of free DNA.

DNA recovery techniques have previously been developed to overcome these challenges, most of which involve the use of proteinase K, a thermostable serine protease with broad substrate specificity [21] which digests crosslinked proteins (Figure 5.1B) [21-23]. However, the free DNA recovery rate of proteinase K, at its optimal temperature (49 ± 2°C), is low, yielding approximately 4.4% per hour, with the enzyme's half-life of 11.3h also limiting the reaction [21, 22]. When the enzymatic reaction is conducted at room temperature, the rate decreases to 1.1% per hour [24]. Free DNA can be extracted with a 0.1M NaOH buffer solution (pH 12), processing at 120°C for 25 min [8, 25]. However, these harsh conditions can damage DNA by Brønsted-based strand cleavage. Although this method can be valuable for samples

that require the digestion of excess tissue, they should be avoided when processing delicate samples. Overall, current methods for extracted free DNA require harsh conditions, are low yielding, low throughput and time consuming. The development of more high throughput processing techniques that are efficient and use mild reaction conditions are of great interest in being able to tap into the wealth of preserved specimens around the world.

Table 5.1. Current methods for crosslink breakdown and DNA recovery from formalin-fixed specimens.

Method	Temperature (°C)	Time (h)
Proteinase K treatment[25]	56	~17
Proteinase K treatment in Tris-NaCl-EDTA-SDS buffer[26]	55	68
Hot alkali buffer treatment[8][24]	100 - 120	0.4 - 0.7
Cetyltrimethylammonium bromide (CTAB) & proteinase K[27]	65 and 56	0.5 and 1-72
QIAamp DNA Mini Kit[27]	56	not reported
QIAamp DNA FFPE Kit[27]	56 and 90	not reported

It was hypothesized that the application of mechanical energy within the vortex fluidic device (VFD) could enhance the extraction of free DNA from formalin-fixed samples. This thin-film microfluidic platform has been shown to disrupt membranes, fold proteins [28] and accelerate enzymatic catalysis [29]. The VFD has the potential to assist in the deaggregation and solubilisation of formalin-fixed samples, as well as accelerate the activity of proteinase K. Here, the VFD was applied and optimized to the recovery of free DNA from formalin-fixed specimens, in combination with purification post VFD processing The results suggest a 40 to

85% increase in yield of free DNA using this VFD method compared to conventional methods without the use of harsh conditions, reducing the processing time from days to hours.

5.3. Results and Discussion

The recovery of free DNA using mechanical stimulation and enzyme acceleration in the VFD in less than 2h has been established for tissue from a lobster claw (*H. americanus*) that has been preserved in formalin (3.7% formaldehyde in phosphate-buffered saline, iso-osmotic with seawater). The key variables that required optimization where mechanical breakage of the tissue sample, the length of the free DNA to be amplified, and the rotational speed of the VFD. As previously observed for other enzymes [29], proteinase K activity an be accelerated using the VFD. The rotational speed in the VFD determines the fluid dynamics, level of shear, and micro-mixing experienced by the thin film of liquid [30]. The tilt angle of the VFD is an important parameter, with 45° being the optimal angle for a variety of applications, including accelerating enzymatic catalysis and refolding of proteins [28-30].

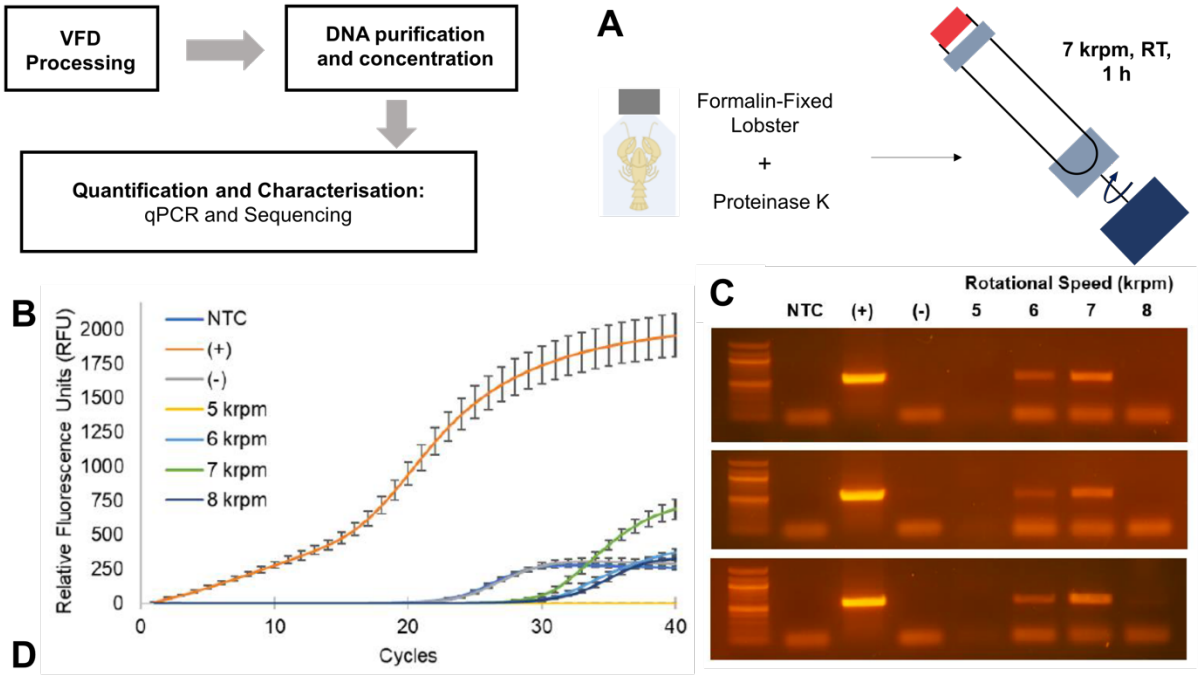


```
Previous Sequence:  ATTCCCTACCTTTATTGAGCAGCACCCTCACGTTGAGCATTAGTTTGATCCAAAATTATGC
*Forward:           ------------------------------GTTGAGCATTAGTTTGATCCAAAATTATAC
*Reverse:           ATTCCCTACCTTTATTGAGCAGCACCCTCACGTTGAGCATTAGTTTGATCCAAAATTATAC

AACTTCTTCACAATGAATTTCAAGCAATTTTAGGACAAGCCACTAAAGGTTCAACTATTTTATTCATTTCTTTTTCAATAA
AACTTCTTCACAATGAATTTCAAGCAATTTTAGGACAAGCCACTAAAGGTTCAACTATTTTATTCATTTCTTTTTCAATAA
AACTTCTTCACAATGAATTTCAAGCAATTTTAGGACAAGCCACTAAAGGTTCAACTATTTTATTCATTTCTTTTTCAATAA

CACTCTCGGGCTGCTCCCATATGTGTTTACTAGATCAAGACACCTTGCGATAACTCTTAGCGTTGCTTTACCTTTATGGCT
CACTCTCGGGCTGCTCCCATATGTGTTTACTAGATCAAGACACCTTGCGATAACTCTTAGCGTTGCTTTACCTTTATGGCT
CACTCTCGGGCTGCTCCCATATGTGTTTACTAGATCAAGACACCTTGCGATAACTCTTAGCGTTGCTTTACCTTTATGGCT

AACTTTTATTTTATTTGGTTGAATTAACCATACCCAACACATGCTTGCTCATATGGTTCCCCAAGGAACACCAGGGCTTCT
AACTTTTATTTTATTTGGTTGAATTAACCATACCCAACACATGCTTGCTCATATGGTTCCCCAAGGAACACCAGGGCTTCT
AACTTTTATTTTATTTGGTTGAATTAACCATACCCAACACATGCTTGCTCATATGGTTCCCCAAGGAACACCAGGGCTTCT

GATACCATTTATAGTGTTAGTAGAAACTTTAAGAAATATTATTCGACCAGGAACTTTAGCCGTTCGACTAGCAGCTAACAT
GATACCATTTATAGTGTTAGTAGAAACTTTAAGAAATATTATTCGACCAGGAACTTTAGCCGTTCGACTAGCAGCTAACAT
GATACCATTTATAGTGTTAGTAGAAACTTTAAGAAATATTATTCGACCAGGAACTTTAGCCGTTCGACTAGCAGCTAACAT

AATTGCAGGACATCTTTTGTTGACACTTTTAGGCAATATAGGCCCTTCTTTGTCTTTTGTCGTTTTTAATACTAGCTCAAA
AATTGCAGGACATCTTTTGTTGACACTTTTAGGCAATATAGGCCCTTCTTTGTCTTTTCTCGTTTTTAATACTAGCTCAAA
AATTGCAGGACATCTTTTGTTGACACTTTTAGGCAATATAGGCCCTTCTTTGTCTTTTCTCGTTTTTAATACTAGCTCAAA

TCCTTCTTTTAATACTAGAATCTGCTGTTGCAATAATTCAATCGTATGTATTTGTGTTCTAAGGACTTTATATGCCA
TCCTTCTTTTAATACTAGAATCTGCTGTTGCAATAATTCAATCGTATGTATTTGTGTTCTAAGGACTTTATATGCCA
TCCTTCTTTTAATACTAGAATCTGCTGT-GCAAT----------------------------------------
```

Figure 5.2. Schematic representation of the VFD-mediated recovery of free DNA. (A) The protocol consists of VFD processing of a mixture of frozen, macerated tissue and proteinase K, at 7k rpm, at RT, for 1h. The solid material and DNA polymerase inhibitors are removed

through further processing. The free DNA is purified and concentrated. The resulting DNA was amplified, quantified, and characterized by qPCR (B, C) and Sanger Sequencing (D). (B) qPCR was used to quantify DNA encoding ATP synthase (579 bp) extracted by VFD processing at the indicated rotational speeds, and non-VFD processing (-) (1h, 37°C. DNA extracted from fresh lobster was used as the positive control (+). (C) Following qPCR, the DNA was visualized by 1% agarose gel electrophoresis. Both negative controls, including the no template control (NTC), show the formation of primer dimers. Error bars indicate standard deviation (technical replicate, n = 3). (D) Sanger DNA sequencing of the target mitochondrial ATP synthase sequence from formalin preserved lobster tissue after VFD processing (9k rpm, 1h, RT). Two mutations (G2728A and G3136C, GenBank No. HQ402925) were observed, within the range of accuracy for Sanger sequencing, as indicated. The reference sequence has been reported previously [31].

An important variable for efficient recovery of free DNA was the mechanical breakage performed prior to VFD processing. Smaller fragments of tissue increase surface area to volume ratio, allowing greater access and efficiency of proteinase K. Additionally, the centrifugation experienced in the VFD leads to the separation of solids from, therefore, smaller fragments allow for greater efficiency in VFD-mediated extraction. The formalin-fixed tissue was frozen in liquid nitrogen and ground into small particles. Traditional extraction methods resulted in modest and inconsistent quantities of free DNA from the ground sample (Figure 5.2). The lack of reproducibility suggested a need for further mechanical breakdown of the tissue. Bead bearing and sonication lead to an increase in tissue breakdown, however, both failed to improve PCR product yields. It was postulated the increase in heat generated from both methods leads to further fragmentation of the DNA required to be amplified. Lastly, an

additional mincing step, using a sterile razor blade, consistently improved free DNA recovery and amplification (Figure 5.5).

Next, the length of the DNA to be amplified was found to be important for consistent analysis of free DNA. Initially, we amplified a 579 bp sequence of free DNA, corresponding to the ATP synthase gene found in this species of lobster. The resulting amplified DNA was the correct sequence (Figure 5.2 and 5.5), however failed to repeatedly amplify. Therefore, a shorter portion of the ATP synthase gene, 183 bp, was targeted. Targeting a smaller amplicon increased the chance that fragmented DNA would be amplified and sequenced.

Finally, the rotational speed of the VFD was optimized for free DNA extraction. Previous studies have established that acceleration of enzymatic catalysis occurs at rotational speeds between 5k and 9k rpm in the VFD with a 45° tilt angle [29]. Hypothesis attribute the enzymatic acceleration results to first, the high mass transfer and intense micro-mixing experienced in the thin film, caused by periodic changes in film thickness. Secondly, changing zones of high and low pressure, resulting in Faraday waves, within the reaction mixture. The pressure oscillations and high mass transfer in the VFD could increase substrate accessibility and removal from the enzyme active site.

The rotational speeds of 5k to 9k rpm, at 1k rpm intervals were explored. Following VFD processing (1h, RT), the concentration of free DNA extracted was first quantified by UV-Vis spectrophotometry. These results can be inconsistent due to the inherent heterogeneity of pulverized tissue which imparts uncontrollable variables into this optimization and subsequent recovery of DNA. Though absorbance at 260nm, corresponding to DNA concentrations, increased with VFD processed samples relative to non-VFD processed samples, the ratio of 260 to 280nm absorbance, indicative of DNA purity, was <1.8 for all rotational speeds (Figure 5.3, and Figure S5.3). This likely indicates the presence of proteins in the VFD processed

samples [32]. The DNA-associated absorbance at 260nm was highest for samples processed at 8k rpm, however, those processed at 7k rpm showed more consistent PCR yields (further discussed below, Figure 5.2, 5.5, S5.3, and Table S5.2).

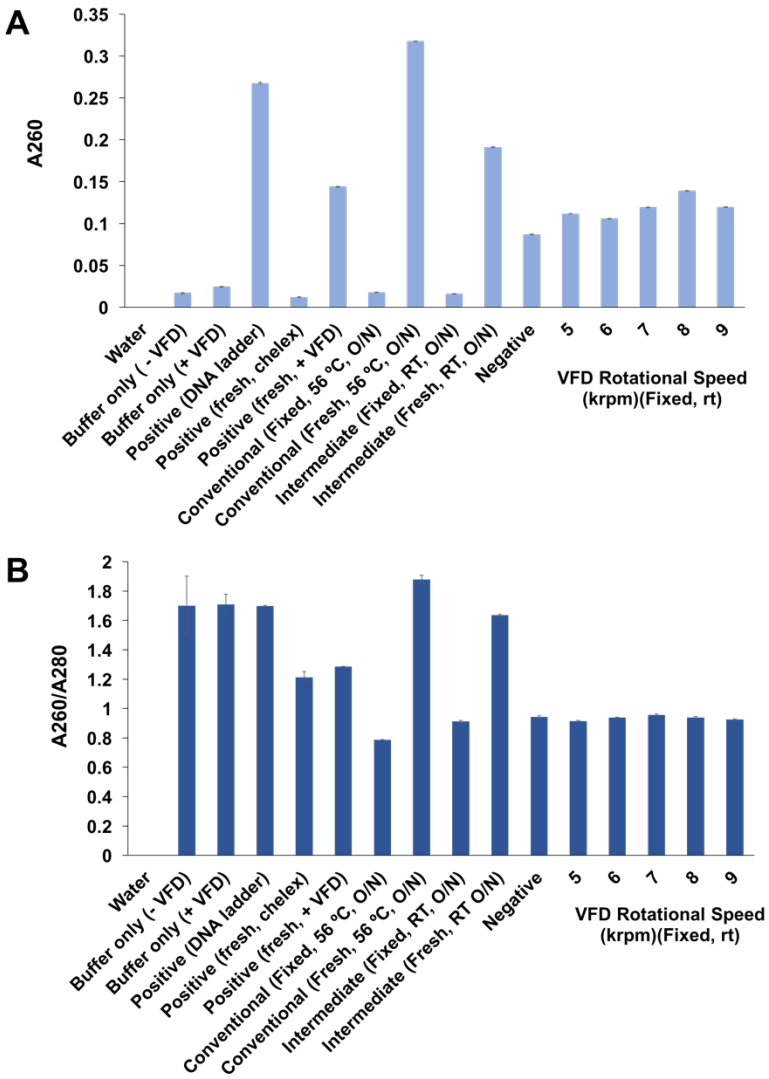

Figure 5.3. Optimizing VFD rotational speed for increasing free DNA yields. Absorbance at 260nm (A) and the ratio of absorbance at 260 and 280nm (B) quantifies DNA and protein yields, respectively. Full UV-Vis absorbance spectra are shown in Figure S3.

To further quantify the concentration of double-stranded DNA (dsDNA) in the free DNA, a fluorescence based intercalating assay was performed using SYBR Green I dye [34]. The fluorescence (λ_{ex} 485nm, λ_{em} 550nm) of diluted samples were measured against a standard curve (Figure S5.4). The assay demonstrated an increase in yield of dsDNA, between 40 to 85% , for the VFD-processed samples relative to the non-VFD processed control sample (Figure 5.4).

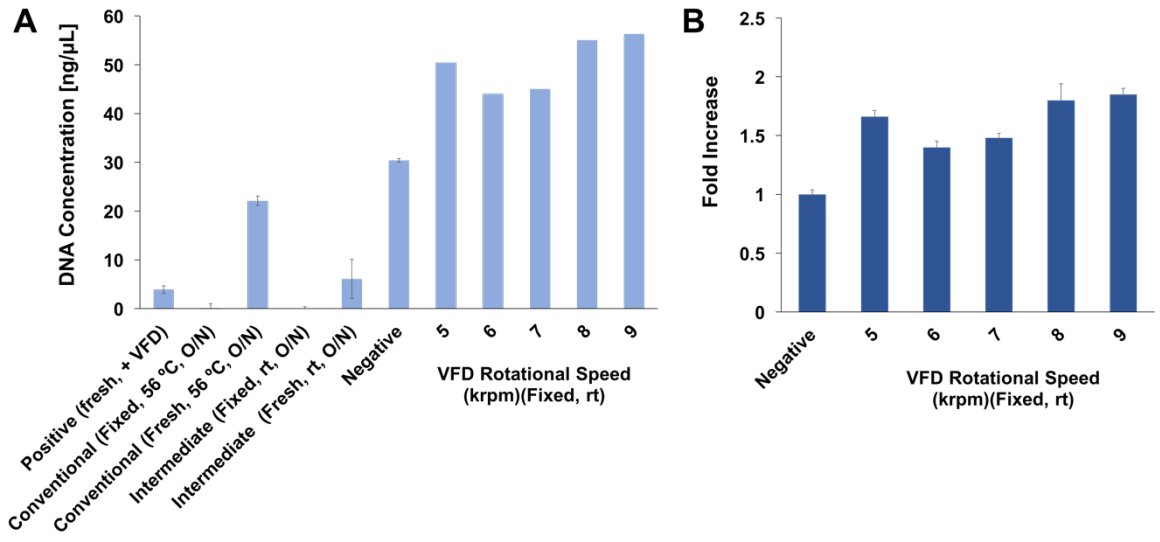

Figure 5.4. Optimizing VFD rotational speed for increasing free DNA yields. SYBR Green I fluorescence-quantified dsDNA concentration (A) and fold increase in dsDNA yield between non VFD processed and VFD processed samples (B).

Finally, DNA recovered using VFD-mediated extraction was amplified via PCR and quantitative PCR (qPCR). Post-VFD processing the samples were purified and concentrated, removing DNA polymerase inhibitors and proteins [16, 34]. Reproducible amplification of the 183 bp ATP synthase gene was observed using qPCR for VFD-processed samples using rotational speeds 6k and 7k rpm (Figure 5.5, Table S5.2). Noticeably, the 8k rpm processed DNA, although yielding higher concentrations of DNA (Figure 5.3), only amplified < 50% of

the time (n = 8, Figure S5.1). It is postulated that the more aggressive processing experienced at 8k rpm results in liberation of other compounds that can inhibit PCR [35], in addition to further fragmenting the DNA, making consistent amplification difficult [16].

The 7k rpm VFD-processed DNA sample generated the highest level of amplification, measured by qPCR (Figure 5.5). An average of 94 ± 4% of the endpoint positive control fluorescence signal was obtained with a low threshold cycle (Ct) value, averaging 35.4 ± 0.7 cycles (Table S5.2). The lower Ct values demonstrated a greater yield of DNA. The 6 krpm VFD-processed DNA resulted in slightly lower yield with an average of 88 ± 17% of the endpoint positive control fluorescence signal and an average Ct value of 35.6 ± 2 cycles. Comparatively, the no template control (NTC) did not surpass the threshold in two of the three trials, with the fluorescence averaged 10 ± 10% of the endpoint positive control fluorescence signal (Table S5.2). Notably, PCR amplification was unsuccessful for the non-VFD processed sample. Additionally, The PCR product obtained from the 7k rpm VFD-process sample was sequenced via Sanger sequencing. The sequence showed 99.5% homogeneity to the expected sequence [36].

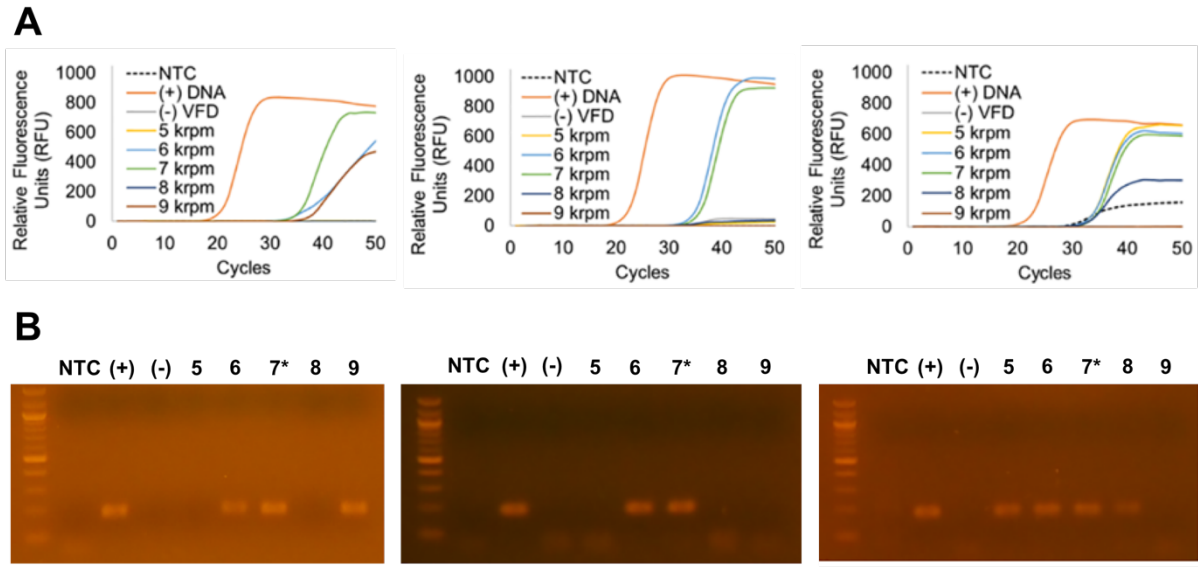

Figure 5.5. Amplification of a 183-bp free DNA target from the ATP synthase gene of the lobster mitochondrial genome. qPCR (A) and agarose DNA gel electrophoresis (B) identified the optimal rotational speed for qPCR amplification as 7k rpm. Threshold cycle and endpoint fluorescence values are shown in Table S2. The VFD processed PCR reactions were compared to a no template control (NTC), a fresh lobster DNA positive control (+), and a non-VFD-processed negative control (-). The 7k rpm VFD-processed qPCR product (*) was subjected to Sanger sequencing (C). A mutation (G2728A, Genbank No. HQ402925) was observed (highlighted).

5.4. Conclusion

This vortex-mediated approach was successful in accelerating the recovery of free DNA from specimens that have been preserved in formaldehyde. The successful amplification, using appropriately designed qPCR assay, of the free DNA was also demonstrated. It is important to note that PCR amplification of samples can be inconsistent due to inherent DNA damage and fragmentation, and can be highly dependent on sample and extraction conditions, primer design, tissue preparation, and other factors. This presents a valuable method for increasing the throughput of free DNA recovery. Increasing the rate of free DNA recovery is important as there are millions of formalin-fixed samples stored in museums around that world. These samples provide important genetic information that could reveal the genomic adaptions of organisms over time, for example arising from climate change over the last 150 years (the formaldehyde preservation era), effectively allowing an understanding of how anthropogenic factors are shaping our biosphere.

5.5. Experimental

5.5.1. Tissue Sample Preparation

One adult male Lobster (*H. americanus*) was purchased in February 2017 from a local lobster fishery in Boston, MA. The lobster was euthanized by quickly severing the ganglia behind the eyes with a sharp knife. The body was then placed whole in a solution of 3.7% formaldehyde in 0.9M phosphate-buffered saline (which approximates the salinity of seawater). The lobster was maintained at room temperature for one month, and then shipped to the University of California Irvine in March 2017. All lobster samples used here are from

muscle recovered from the chelipeds (primary claws), which have remained in formalin for the two-year duration of this study. For experimental treatments, the lobster claw tissue was processed according to the procedure described below.

A small portion (5-10g) of preserved tissue was removed from the preservative, frozen in liquid nitrogen, and ground with a mortar and pestle. The ground tissue was transferred to a 1.5mL Eppendorf tubes and stored at -80°C. Immediately prior to processing, the tissue was minced with a flame-sterilized razorblade. The tissue was washed with proteolysis buffer (3 x 1.5mL) to remove remaining preservative fluid. For each wash step the tube is briefly vortexed, centrifuged (15k rpm, 3 min), and the buffer recanted.

5.5.2. VFD Treatment

The ground, minced tissue was transferred to the bottom of an autoclaved 20mm OD VFD tube (17.5mm ID). A solution of proteolysis buffer (950μL, 20mM Tris-HCl, 50mM EDTA, 1 % w/v SDS, pH 8.0 [37]) and proteinase K solution (50μL, 10mg/mL proteinase K, Promega, V3021, lyophilized, in 20mM Tris-HCl, 1mM $CaCl_2$, 50% glycerol, pH 8.0) was added to the tube. The VFD tube was sealed with a rubber septum and the tube processed in the VFD for 1h at 7k rpm and 45°, at room temperature (RT).

5.5.3. Sample Post Processing and Purification

The VFD treated sample was immediately transferred to an Eppendorf tube and centrifuged (13k rpm, 5 min, RT) to remove the tissue. The supernatant is collected and incubated on ice for 30 min. The sample is centrifuged (13k rpm, 10 min, 4°C) to remove the

precipitated SDS. The supernatant (400μL) was processed with a Zymo DNA Clean & Concentrator Kit (cat. No. D4006) according to the manufacturer's instructions.

5.5.4. PCR and qPCR for Quantification and Characterisation

DNA extraction yields were determined by quantitative PCR (qPCR) (Bio-Rad iCycler). For PCR, reaction mixtures consisted of Phusion DNA polymerase (0.2U final concentration, New England BioLabs) and buffer (5 x diluted final concentration, New England Biolabs), DMSO (10% v/v final concentration), dNTPs (0.5mM each final concentration, New England Biolabs), primers (8-33ng each final concentration, Integrated DNA Technologies) (Table 5.2), and SYBR Green I Dye (10,000 x diluted final concentration, Thermo Fisher Scientific). PCR was performed with 1 cycle of 96°C for 5 min followed by 40 to 50 cycles of 94°C for 1 min, 60°C for 1 min, and 72°C for 2 min, followed by 1 cycle of 72°C for 5 min.

Table 5.2. PCR primer sequences and annealing temperatures for the mitochondrial ATP synthase gene target.

Target Length		Primer	Annealing Temperature (est.)(°C)
579 bp	Forward	GGGTTACTTTTTATTCCCTACCTTTATTGAGC	60
	Reverse	GGCATATAAAGTCCTTAGAACAGCAAATACATACG	
183 bp	Forward	GGGTTACTTTTTATTCCCTACCTTTATTGAGC	60
	Reverse	CAGCCCGAGAGTGTTATTGAATATAATAAATC	

DNA was obtained from fresh, ground lobster claw tissue, for use as the positive controls. Chelex 100 Resin (Bio-Rad, 10% w/v in 500μL in ddH_2O) was used to recover the DNA, following the manufacturer's protocol. The tissue-resin mixture was vortexed briefly before incubation at 90 to 95°C for 35 min. The mixture was briefly vortexed, centrifuged and the supernatant isolated as the positive control for lobster DNA.

5.5.5. UV-Vis for Quantification and Characterisation

The recovered free DNA from the formalin-fixed lobster was quantified using UV-Vis absorbance. The absorbance spectra of each sample, diluted in ddH_2O (1:50) was measured (Jasco V-730 Spectrophotometer). The spectra were recorded from 200 to 400nm, in triplicate (technical replicates), scanning speed of 200nm/min and intervals of 0.5nm, with ddH_2O as a blank. Two controls with buffer only were examined, one with and without processing in the VFD (7.5k rpm, 1h, RT). A positive control of fresh lobster DNA, extracted with Chelex 100 resin as described above, was used. DNA sizes and concentrations were estimated using the 1kb Plus DNA Ladder (10μg/ 1000μL final concentration, Thermo Fisher Scientific, 1.0μg/μl).

5.5.6. SYBR Green I Fluorescence Assay for Quantification and Characterisation

A SYBR Green I fluorescence assay was also used to quantify the concentration of dsDNA. A 1kb Plus DNA Ladder (Thermo Fisher Scientific, 1.0μg/μl), was used to generate a DNA concentration curve between 0ng/μL to 1.25ng/μL. Each dilution (100μL) was added to a black, clear-bottom 96-well plate (Corning, 3615), along with SYBR Green I dye (100μL, Thermo Fisher Scientific, 1250x diluted in ddH_2O). The florescence of each standard, sample

and control, in triplicate, was measured. The dsDNA was estimated using the calibration curve shown in Figure S5.2.

5.6. Acknowledgments

Special acknowledgment to Christian Totoiu who conducted this research along side myself, and who wrote the paper this Chapter is based on. A special thank you for the support of Prof. Gregory Weiss, for giving me the opportunity to visit his laboratory at the University of California, Irvine, where this research was conducted. Also, Dr Sudipta Majumdar, Dr Aspen T. Reese, and Prof. Peter R. Girguis for their support. Acknowledgements to UCI's Department of Molecular Biology and Biochemistry for access to the qPCR thermocycler. This work was supported by the National Human Genome Research Institute (NHGRI) of the National Institutes of Health [1R01HG009188-01 to G.A.W.]; the Star Family Foundation Challenge for Promising Scientific Research [to A.T.R. and P.R.G.]; Funding for open access charge: NHGRI.

5.8. References

[1] Holmes, M. W., Hammond, T. T., Wogan, G. O., Walsh, R. E., LaBarbera ,K., Wommack, E. A., Martins, F. M., Crawford, J. C., Mack, K. L., Bloch, L. M. and Nachman, M. W. Natural history collections as windows on evolutionary processes. *Mol. Ecol*., **2016**, *25*, 864–881.

[2] Suarez, A. V. and Tsutsui, N. D. The value of museum collections for research and society. *BioScience*, **2004**, *54*, 66–74.

[3] Fox, C. H., Johnson, F. B., Whiting, J. and Roller, P. P. Formaldehyde fixation. *J. Histochem. Cytochem*., **1985**, *33*, 845-853.

[4] Pergams, O. R. W. and Nyberg, D. Museum collections of mammals corroborate the exceptional decline of prairie habitat in the Chicago region. *J. Mammal*., **2001**, *82*(4), 984-992.

[5] Lens, L., Van Dongen, S., Norris, K., Githiru, M. and Matthysen, E. (2002) Avian persistence in fragmented rainforest. *Science*, **2001**, *298*, 1236-1238.

[6] Carroll, S. P. and Boyd, C. Host race radiation in the soapberry bug: natural history with the history. *Evolution*, **1992**, *46*, 1052-1069.

[7] Greer, C. E., Lund, J. K. and Manos, M. M. (1991) PCR amplification from paraffin-embedded tissues: recommendations on fixatives for long-term storage and prospective studies. *PCR Methods Appl*., **1991**, *397*, 46-50.

[8] Hykin, S. M., Bi, K. and Mcguire, J. A. Fixing formalin: a method to recover genomic-scale DNA sequence data from formalin-fixed museum specimens using high-throughput sequencing. *PLoS ONE*, **2015**, *10*, e0141579.

[9] Mikheyev, A. S., Tin, M. M. Y., Arora, J. and Seeley, T. D. Museum samples reveal rapid evolution by wild honey bees exposed to a novel parasite. *Nat. Commun*., **2015**, *6*, 7991.

[10] Spurgin, L. G., Wright, D. J., van der Velde, M., Collar, N. J., Komdeur, J., Burke, T. and Richardson, D. S. Museum DNA reveals the demographic history of the endangered Seychelles warbler. *Evol. Appl*., **2014**, *7*, 1134-1143.

[11] Do, H. and Dobrovic, A. Sequence artifacts in DNA from formalin-fixed tissues: causes and strategies for minimization. *Clin. Chem*., **2015**, *61*, 64-71.

[12] Suzuki, T., Ohsumi, S. and Makino, K. Mechanistic studies on depurination and apurinic site chain breakage in oligodeoxyribonucleotides. *Nucleic Acids Res*., **1994**, *22*, 4997-5003.

[13] Lindahl, T. and Andersson, A. Rate of chain breakage at apurinic sites in double-stranded deoxyribonucleic acid. *Biochemistry*, **1972**, *11*, 3618-3623.

[14] Ludyga, N., Grunwald, B., Azimzadeh, O., Englert, S., Hofler, H., Tapio, S. and Aubele, M. Nucleic acids from long-term preserved FFPE tissues are suitable for downstream analyses. *Virchows Arch*., **2012**, *460*, 131-140.

[15] Didelot, A., Kotsopoulos, S. K., Lupo, A., Pekin, D., Li, X., Atochin, I., Srinivasan, P., Zhong, Q., Olson, J., Link, D. R., Laurent-Piug, P., Blons, H., Hutchison, J. B. and Taly, V. Multiplex picoliter-droplet digital PCR for quantitative assessment of DNA integrity in clinical samples. *Clin. Chem*., **2013**, *59*, 815-823.

[16] Dietrich, D., Uhl, B., Sailer, V., Holmes, E. E., Jung, M., Meller, S. and Kristiansen, G. Improved PCR performance using template DNA from formalin-fixed and paraffin-embedded tissues by overcoming PCR inhibition. *PloS ONE*, **2013**, *8*, e77771.

[17] Dutta, S., Chowdhury, G. and Gates, K. S. (2007) Interstrand cross-links generated by abasic sites in duplex DNA. *J. Am. Chem. Soc*., **2007**, *129*, 1852-1853.

[18] Vesnaver, G., Chang, C. N., Eisenberg, M., Grollman, A. P. and Breslauer, K. J. Influence of abasic and anucelosidic sites on the astability, conformation, and melting behavior of a DNA duplex: correlations of thermodynamic and structural data. *Proc. Natl. Acad. Sci. U.S.A*., **1989**, *86*, 3614-3618.

[19] Kennedy-Darling, J. and Smith, L. M. Measuring the formaldehyde protein−DNA cross-link reversal rate. *Anal. Chem*., 2014, *86*, 5678−5681.

[20] Hoffman, E. A., Frey, B. L., Smith, L. M. and Auble, D. T. Formaldehyde crosslinking: A tool for the study of chromatin complexes. *J. Biol. Chem*., **2015**, *290*, 26404-26411.

[21] Yazawa, K., Sugahara, M., Yutani, K., Takehira, M. and Numata, K. Derivatization of proteinase K with heavy atoms enhances its thermal stability. *ACS Catal*., **2016**, *6*, 3036−3046.

[22] Goelz, S. E., Hamilton, S. R. and Vogelstein, B. Purification of DNA from formaldehyde fixed and paraffin embedded human tissue. *Biochem. Biophys. Res. Commun*., **1985**, *130*, 118-

126.

[23] Butler, J. M., Johnson, J. E. and Boone, W. R. The heat is on: room temperature affects laboratory equipment–an observational study. *J. Assist. Reprod. Genet*., **2013**, *30*, 1389-1393.

[24] Campos, P. F. and Gilbert, T. M. P. (2012) DNA extraction from formalin-fixed material. In Shapiro, B. and Hofreiter, M. (eds) *Ancient DNA. Methods in Molecular Biology* (Methods and Protocols). *Humana* Press, Vol. 840.

[25] Munchel, S., Hoang, Y., Zhao, Y., Cottrell, J., Klotzle, B., Godwin, A. K., Koestler, D., Beyerlein, P., Fan, J., Bibikova, M. and Chien, J. Targeted or whole genome sequencing of formalin fixed tissue samples: potential applications in cancer genomics. *Oncotarget*., **2012**, *6*, 25943-25961.

[26] Hassani, A. and Khan, G. A simple procedure for the extraction of DNA from long-term formalin-preserved brain tissues for the detection of EBV by PCR. *Exp. Mol. Pathol.*, **2015**, *99*, 558-563.

[27] Paireder, S., Werner, B., Bailer, J., Werther, W., Schmid, E., Patzek, B. and Cichna-Markl, M. Comparison of protocols for DNA extraction from long-term preserved formalin fixed tissues. *Anal. Biochem*., **2013**, *439*, 152-160.

[28] Yuan, T. Z., Ormonde, C. F. G., Kudlacek, S. T., Kunche, S., Smith, J. N., Brown, W. A., Pugliese, K. M., Olsen, T. J., Iftikhar, M., Raston, C. L. and Weiss, G. A. Shear stress-mediated refolding of proteins from aggregates and inclusion bodies. *ChemBioChem.*, **2015**, *16*, 393-396.

[29] Britton, J., Meneghini, L. M., Raston, C. L. and Weiss, G. A. Accelerating enzymatic catalysis using vortex fluidics. *Angew. Chem. Int. Ed*., **2016**, *55*, 11387-11391.

[30] Britton, J., Stubbs, K. A., Weiss, G. A. and Raston, C. L. Vortex fluidic chemical transformations, *Chem. Eur. J.*, **2017**, *23*, 13270-13278.

[31] Kim, S., Lee, S. H., Park, M.H., Choi, H. G., Park, J.K., Min, G. S. The complete mitochondrial genome of the American lobster, Homarus americanus (Crustacea, Decapoda), *Mitochondrial DNA*. **2011**, *22*, 47-49.

[32] Glasel, J. A. Validity of nucleic acid purities monitored by 260 nm/280nm absorbance ratios. *BioTechniques*., **1995**, *18*, 62-63.

[33] Leggate, J., Allain, R., Isaac, L. and Blais, B. W. Microplate fluorescence assay for the quantification of double stranded DNA using SYBR Green I dye. *Biotechnol. Lett*., **2006**, *28*, 1587-1594.

[34] Hu, Q., Liu, Y., Yi, S. and Huang, D. A comparison of four methods for PCR inhibitor removal. *Forensic Sci. Int. Genet*., **2015**, *16*, 94-97.

[35] Sitepu, E. K., Corbin, K., Luo, X., Pye, S. J., Tang, Y., Leterme, S. C., Heimann, K., Raston, C. L. and Zhang, W. Vortex fluidic mediated direct transesterification of wet microalgae biomass to biodiesel. *Bioresour Technol*., **2018**, *266*, 488-497.

[36] Kim, S., Lee, S.H., Park, M.H., Choi, H.G., Park, J.K. and Min, G.S. The complete mitochondrial genome of the American lobster, Homarus americanus (Crustacea, Decapoda), *Mitochondrial DNA*, **2011**, *22*, 47-49.

[37] Hu, M., Jex, A. R., Campbell, B. E. and Gasser, R. B. Long PCR amplification of the entire mitochondrial genome from individual helminths for direct sequencing. *Nat. Protoc*., **2007**, 2, 2339-2344.

5.9. Supporting Information

VFD Rotation Speed Effects on qPCR and Sequencing (Figure 2):

Table S5.1. Threshold cycle values (Ct) and endpoint fluorescence values of qPCR with the free DNA (Figure 2, S2, and S3).*

Sample	Reaction 1 C_t (fluorescence endpoint)	Reaction 2 C_t (fluorescence endpoint)	Reaction 3 C_t (fluorescence endpoint)
no template control	23.58 (270.38)	23.85 (243.87)	23.84 (255.38)
positive control	2.38 (1993.62)	2.57 (2095.95)	2.97 (1788.01)
negative control (non-VFD-processed)	23.85 (287.53)	23.87 (319.95)	24.26 (261.1)
5 krpm	N/A (-0.79)	N/A (0.35)	N/A (2.23)
6 krpm	31.20 (399.11)	33.68 (351.11)	31.34 (368.75)
7 krpm	29.81 (752.82)	29.87 (609.97)	29.12 (703.95)
8 krpm	N/A (321.42)	31.57 (328.76)	31.72 (332.93)

* N/A = not applicable for samples that failed to amplify.

DNA Quantification by UV-Vis Absorbance:

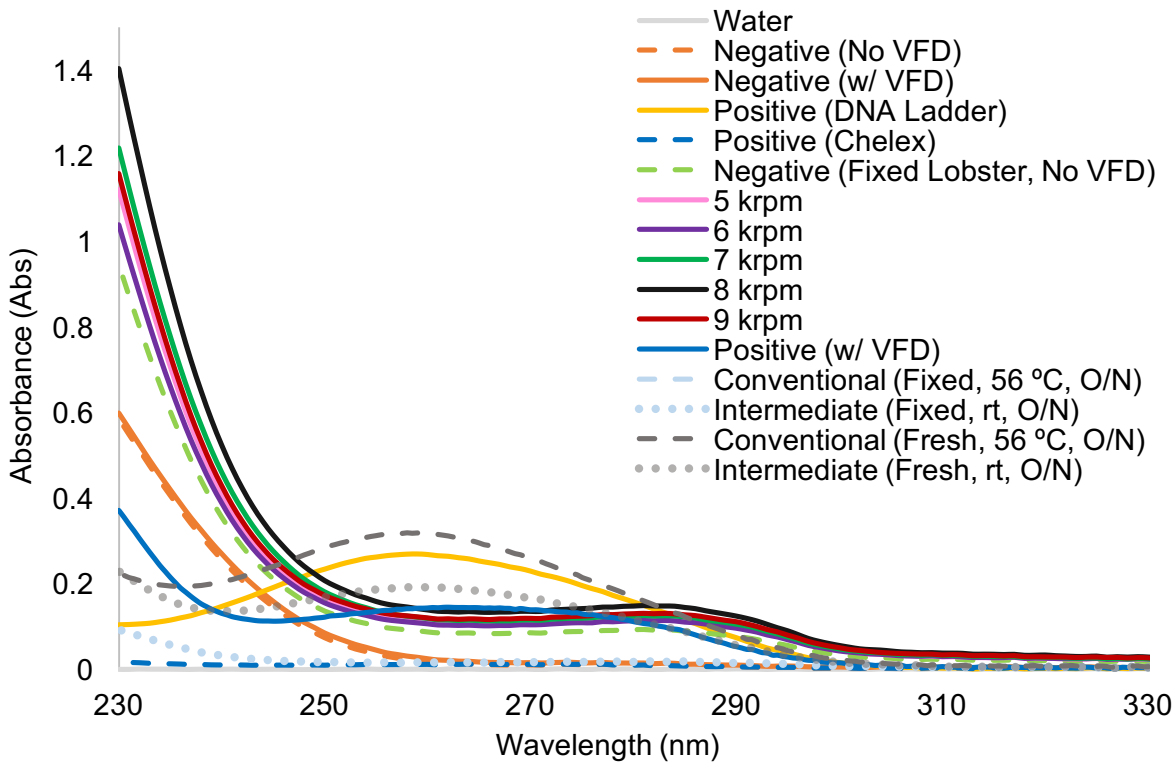

Figure S5.1. The absorbance spectra of reaction supernatants for the fixed lobster samples and positive and negative controls given in Figure 3.

DNA Quantification by SYBR Green I Fluorescence:

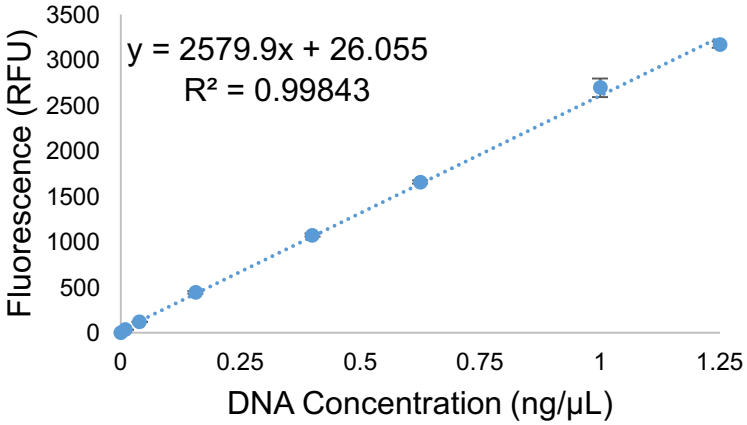

Figure S5.2. The calibration curve for DNA quantification by the SYBR Green I intercalation fluorescence assay.

Table S5.2. Threshold cycle values (C_t) and endpoint fluorescence values of qPCR with the free DNA (Figure 4).*

Sample	Reaction 1 C_t (fluorescence endpoint)	Reaction 2 C_t (fluorescence endpoint)	Reaction 3 C_t (fluorescence endpoint)
no template control	N/A (-0.05)	N/A (0.40)	37.30 (157.00)
positive control	20.80 (778.82)	22.07 (947.89)	22.84 (661.73)
negative control (non-VFD-processed)	N/A (1.38)	N/A (45.51)	N/A (-0.74)
5 krpm	N/A (-0.84)	N/A (23.88)	33.93 (656.01)
6 krpm	37.87 (542.35)	34.80 (987.87)	34.02 (603.64)
7 krpm	35.88 (732.61)	35.75 (925.38)	34.68 (589.66)
8 krpm	N/A (-0.37)	N/A (37.37)	35.15 (301.89)
9 krpm	39.13 (469.08)	N/A (0.06)	N/A (1.07)

* N/A = not applicable for samples that failed to amplify.

Successful PCR's with variable Gene Target Lengths and Primers:

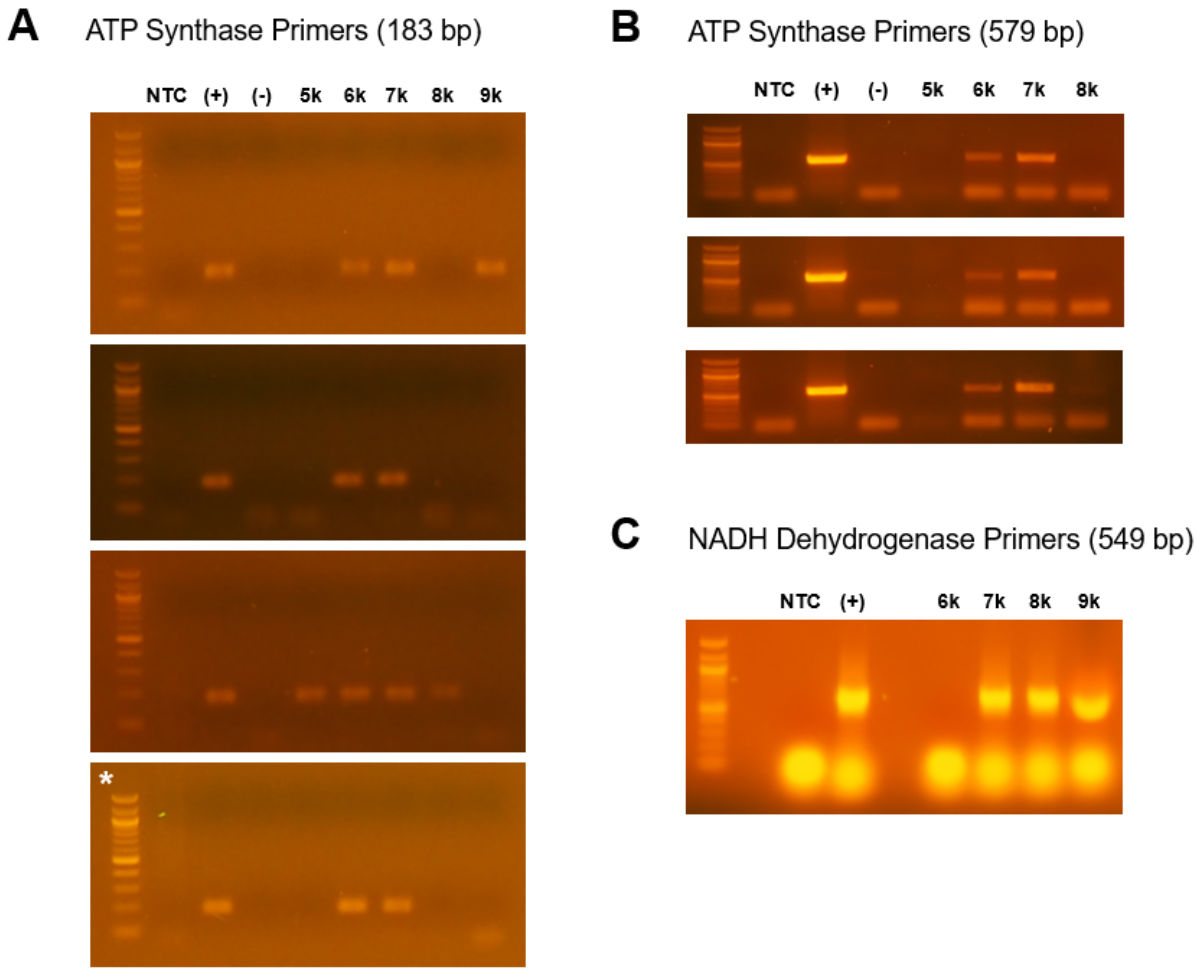

Figure S5.3. qPCR and PCR (*) of free DNA with (A) 183 bp ATP synthase amplicon primers, (B) 579 bp ATP synthase amplicon primers, and (C) 549 bp NADH dehydrogenase amplicon primers (forward: TCATCCATAGTCACCAACCTTC; reverse: TGTTCAAGGCACTCTTATTTATATG; annealing temperature 61°C). The results demonstrate the inconsistency observed for 8k rpm rotation speed of the VFD.

Chapter 6: Conclusion and Recommendations for Future Work

6.1. Conclusion

This dissertation focuses on the use of process intensification methodologies involving the vortex fluidic device (VFD) for improving chemical and biochemical processes. In particular, it presents the use of catalyst and biomolecule immobilisation for the continuous-flow synthesis of organic molecules and the isolation of antibody fragments and peptides.

This dissertation establishes the development of a robust, paper-based palladium catalyst for continuous flow hydrogenations. For any continuous flow reactor, readily available cartridges of transition metal catalysts is critical for a variety of chemical processes. This capability is now realized in the VFD by simply lining the walls of the reaction tube with a sheet of cellulose paper with immobilised palladium (0) nanoparticles (PdNPs). This catalyst system is easily prepared within minutes and displays excellent catalytic activity and chemoselectivity for reductions in the confined and continuous flow modes of the VFD under ambient pressure and temperature. Previously reported continuous flow hydrogenation systems, using conventional devices, exhibit higher throughput but they use high pressure (16-28atm) and higher temperatures (50- 120°C) resulting in a significantly higher energy penalty. This system allows for hydrogenation at ambient pressure and temperature, leading to reduced energy penalty and simpler processing.

Industrially important compounds were prepared on a gram scale using this system, where high atom economy, low toxicity and with safer processing, especially when compared to conventional reactor vessels and other microfluidic devices which often require high pressures and temperatures, and for the former, arduous post production steps. Effective

continuously flow transfer hydrogenation using ammonium formate as the reducing agents was also demonstrated. The PdNP cellulose catalyst can be reused with no loss in catalytic activity after 10 recycles and leaching of palladium is minimal. Overall the findings showcase the versatility, efficiency, and robustness of the cellulose paper impregnated with PdNPs for scalable organic processing. Further exploration of this catalyst and reactor system in the continuous synthesis of valuable fine chemicals and pharmaceuticals is anticipated.

Easy and practical use of cellulose paper as a support in the VFD led to further investigation for immobilisation of other catalysts. Here, enzymes were rapidly immobilised through covalent attachment onto a cellulose support through APTES-glutaraldehyde functionalization in the vortex fluidic device (VFD). Alkaline phosphatase (AP) was used as a proof of concept. The AP-cellulose catalyst was found to be active and stable over a 48 h continuous-flow reaction, and after days of being stored at 4°C, with comparable rates to batch. The method was further applied to the continuous-flow synthesis of a chiral, anti-malarial drug intermediate, aristolochene, following the immobilisation of aristolochene synthase derived from *Aspergillus terreus*. Immobilisation and application of a valuable terpene cyclase for the synthesis of complex chiral terpene is a significant finding, having potential application for the synthesis of complex molecules in general in the VFD.

Immobilisation of biomolecules for additional biological applications was explored. Isolation of antibody fragments and peptide molecules that bind to specific molecular targets are an essential tool for diagnostics and targeted therapeutics. In this dissertation, a vortex fluidic-based approach was applied for efficient continuous-flow antibody and peptide selections under continuous-flow through immobilisation of a target antigen involving his-tag immobilisation. With this system, Fab and peptide binders were isolated for high affinity and specificity to a bladder cancer biomarker, DJ-1. This continuous-flow system can be used with

different libraries and target molecules, and demonstrates an effective approach towards discovery of recognition elements for biosensor development and research applications.

The changing nature of the complex fluid flow in the VFD was also explored in this study. Different selection efficiencies were observed for rotational speeds 4 and 8 krpm, with high non-specific binding occurring at the former. This is consistent with the model that has been developed by Raston and co-workers. In water in a 20mm OD tube, this model has high localized mixing at rotational speeds between 3.8 and 4.5k rpm, arising from the interplay of Faraday-wave double helical flow and circular Coriolis flow. While such mixing can potentially increase phage to antigen interactions, the associated binding to the resin or VFD surface is non-specific. For rotational speeds $\geq$ 6k rpm, the model has eddies associated with Faraday waves striking the surface of the tube resulting in higher shear stress on the surface of the tube.

As presented in this dissertation, mechanical energy in the VFD has been applied to drive the catalytic activity of proteinase K and extract DNA from tissue fixed in formaldehyde. The successful amplification, using appropriately designed qPCR assay, of the free DNA was also demonstrated. The recovery of free DNA using conventional methods applying proteinase K typically require >1 day reaction times. Remarkably, this vortex-mediated approach allowed for recovery of the DNA in less than 2 hours. This study is a further example of the intense micro-mixing and high mass transfer associated with the fluid flow of the Faraday wave induced eddies experienced within the thin-films, which can accelerate enzymatic activity for valuable application. The findings represent a potentially valuable method for increasing the throughput of free DNA recovery form formalin-fixed samples. Increasing the rate of free DNA recovery is important as there are tens of millions of formalin-fixed samples stored in museums around that world. These samples provide important genetic information that could reveal the genomic adaptions of organisms overtime, effectively allowing an understanding of how

anthropogenic factors are shaping our biosphere, as well as studying the DNA of extinct species.

The high yield and inconsistent amplification results obtained from extracting DNA at 8k rpm was attributed to the more aggressive processing experienced at this rotational speed, resulting in the liberation of other compounds that can inhibit PCR, in addition to further fragmenting the DNA. This suggests that exploring rotational speeds > 8k rpm is worthwhile for establishing processes that could potentially benefit from such aggressive environments, presumably under pro-turbulent fluid flow regimes.

6.2. Recommendations for Future Work

6.2.1. Application of Pd@Cellulose Catalyst for Chemical Deuteration

As presented in Chapter 2, the immobilisation of palladium nanoparticles within cellulose paper, centrifugally held against the surface of the tube, was achieved, for use in the VFD. Preparation of the catalyst is remarkably simple and fast, and was effectively applied for hydrogenation reactions. It was hypothesized that this palladium catalyst system could be applied to the deuteration of fatty acid compounds. This new processing offers exciting advantages relative to deuteration using traditional batch processing. This includes reduced energy consumption, due to the ambient pressure and reduced temperatures required in the VFD, higher selectivity, and scalability of the processing under continuous flow.

Feasibility studies were conducted during a visit to the National Deuteration Facility at the Australia's Nuclear Science and Technology Organisation (ANSTO). This initially involved deuteration of octanoic acid in the VFD (Pd@cellulose, 7k rpm, D_2O, NaOD, 90°C),

in confined mode. However, no deuteration was observed after several hours. It is important to note that a temperature of 90°C was chosen due to the boiling point limitation of D_2O (100 °C) at 1atm. Literature states that H_2 can serve as a palladium activator for deuteration at lower temperatures (110 –160°C) for some substrates [1]. Due to the high temperature, pressure and long processing time (days) required to achieve the deuteration of this compound in batch, it was hypothesised that the reduced temperature and ambient pressure, in the VFD, was insufficient for deuteration of octanoic acid. Following this result, another substrate, L-phenylalanine hydrochloride was explored.

In the literature, phenylalanine has been shown to give deuteration at the alpha and beta carbon, at 160°C after 48h, albeit with racemization occurring [2]. Deuteration at a lower temperature (90°C) and a shorter reaction time was investigated with a view high mass transfer in the VFD may be effective for the reaction at lower temperatures. In addition, whether deuteration occurs in the VFD without (or with significantly less) racemization at the alpha position in the VFD was explored.

L-phenylalanine hydrochloride (0.2M) in D_2O was processed in the VFD, containing palladium (0) on cellulose [3], in confined mode under an atmosphere of H_2 for 2 hours at 90°C (Scheme 6.1). Analysis using GC-MS-MS showed two major peaks at 165.7 and 166.7m/z, corresponding to phenylalanine and phenylalanine-d^1, indicating deuterium exchange had occurred with one proton (Figure 6.1B). Analysis using ^{2}H NMR, ^{1}H NMR, and ^{13}C NMR established that deuterium exchange had occurred with a single proton on the beta carbon to the carboxylic acid, with no deuteration observed at the alpha carbon (Figure 6.1A, C, D, respectively). The broad shift at 3.2ppm in the ^{2}H NMR spectrum corresponds to a deuterium present at the beta carbon. This was confirmed using ^{13}C NMR (proton decoupled, deuterium coupled) with a splitting observed next to a singlet at ~35 rpm indicating the presence of a

single deuterium atom adjacent to a proton on the beta carbon. The ^{1}H NMR spectrum showed reduced intensity at the peaks corresponding to the alkyl protons on the beta carbon. The reduced intensity is unsymmetrical which indicates a stereoselective deuterium exchange at the beta carbon. If single deuterium exchange is occurring for both protons randomly an even reduction in intensity of this peak would be expected.

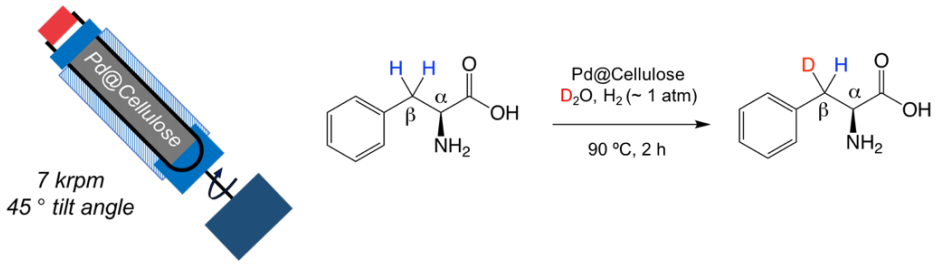

Scheme 6.1. Deuteration of L-Phenylalanine in deuterium oxide (D_2O) at 90°C under an atmosphere of hydrogen in confined mode at 7k rpm.

Partial deuteration of L-phenylalanine at the beta carbon was achieved in the VFD in the confined mode at ambient pressure after 2 hours. It is not known whether the VFD presents a benefit over batch processing for this chemical deuteration as the longer processing time and higher temperatures combined with H_2 gas circumvents the use of continuous flow processing; the maximum residence time in the VFD is about 10 minutes for low flow rates down to 0.1mL/min. However, the potential for stereoselective deuteration in the VFD could be highly beneficial and should be further explored.

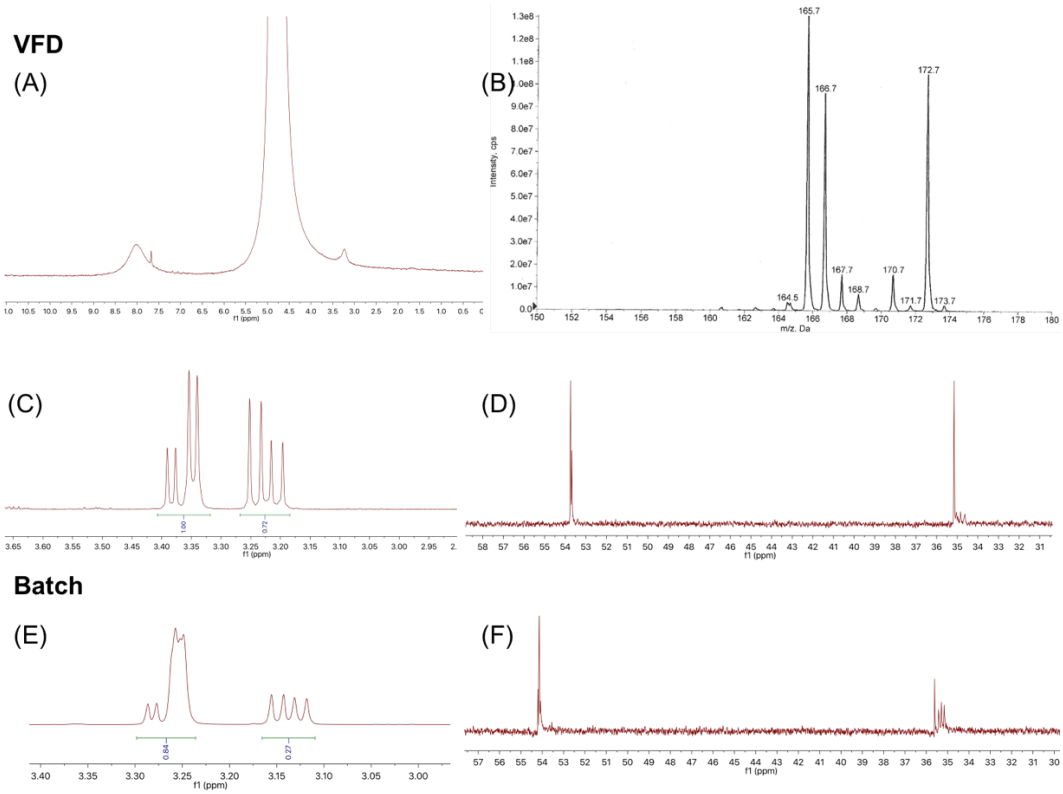

Figure 6.1. Deuteration of L-Phenylalanine in the VFD in the confined mode at 7 krpm, 45° tilt angle, at 90°C for 2h. (A) ^{2}H NMR spectrum, (B) GC-MS-MS spectrum, (C) ^{1}H NMR spectrum of the peaks at 3.2-3.3 rpm corresponding to the protons on the beta carbon, (D) ^{13}C NMR spectrum. (E) ^{1}H NMR spectrum, showing the protons on the beta carbon, and (F) ^{13}C NMR spectrum of deuteration of L-Phenylalanine performed under batch processing, stirring at 90°C for 2h.

The ability to conduct asymmetric synthesis in the VFD is an area of interest in the Raston group, whether induced by the chiral nature of cellulose paper and/or through rotation induced chirality. With advances in understanding the nature of the fluid flow in the device, where there is evidence now for regimes of chiral flow, harnessing this for asymmetric induction would be a major advance in controlling absolute stereochemistry. Changing the chirality of the molecule would then be achieved by reversing the rotational direction of the

tube, for a tilt angle θ of 45^{o}. Furthermore, exploring the use of immobilised transition metal catalyst, including Pd(0), for processing under high mass transfer in the VFD, has potential for reactions that are otherwise not of practical convenience using conventional batch processing. Then there is the prospect of having bands of different catalysts tethered to the surface of the tube, for then sequential reactions in building complex molecules in a single pass using the device, as the liquid whirls up the tube and exiting at the top (assembly line synthesis - see below).

6.2.2. Multi-step Continuous-flow Synthesis using Immobilisation on Cellulose

As demonstrated in Chapter 2 and Chapter 3, cellulose paper can serve as an effect catalyst support for both palladium nanoparticles and enzymes for biocatalysis. This ultra-thin cellulose 'cartridge' technology could be applied for multi-step and multi-enzyme assembly line synthesis, where the substrate undergoes one reaction for the first band of tethered enzyme or metal catalyst encountered in the VFD tube, then another reaction for the second band with a different catalyst attached, and so on (Figure 6.2). The ability to perform assembly line synthesis enzymatic catalysis expands the versatility of the VFD. Future research in this area should focus on developing the technology for performing cascade reactions for the synthesis of complex products.

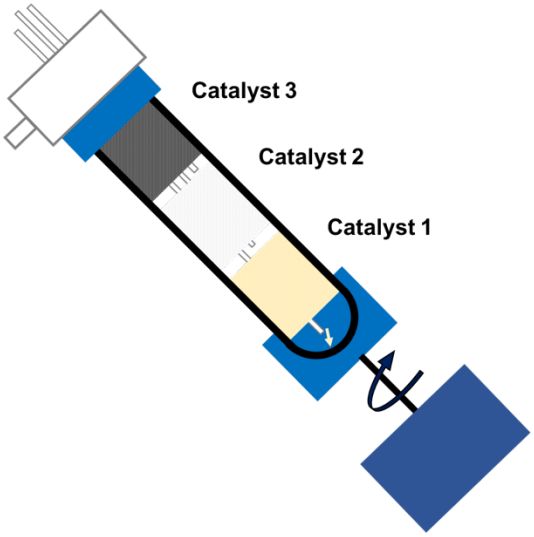

Figure 6.2. Schematic of multi-cellulose bands lining VFD tube representing a multi-catalyst system.

6.2.3. Additional Characterisation of Fab Binding to DJ-1

As demonstrated in Chapter 4, a phage-displayed antibody Fab was selected for binding to a bladder cancer biomarker, DJ-1, in continuous-flow in the VFD. Exploring beyond binding affinity to DJ-1, as presented in this dissertation, further analysis of binding characteristics could reveal potential differences in the binding mechanism of binders selected for under shear stress in the VFD compared to using a traditional micro-well format. Identification of different binding mechanisms could provide the ability to selected recognition elements based on binding characteristics by varying the level of shear stress imparted in the reactor. This is now a reality with an understanding of the different complex fluid flow regimes in the VFD, depending on the operating parameters.

Characterisation techniques that should be explored are isothermal titration calorimetry (ITC) and bio-layer interferometry (BLI). ITC is used to determine the thermodynamic

parameters of a binding interaction which can elucidate the mechanisms underlying molecular interaction [4, 5], whereas BLI is an optical analytical technique that measures the interference pattern of white light reflected from a surface where layer of protein is immobilised [6]. The binding kinetics of a molecule with the immobilised protein can be detected in real time by analysing the shift in interference pattern. However, these techniques are typically not compatible with phage. For this reason, the Fab binder was expressed in *E. coli*, independent of phage (Chapter 4). Based on these recommendations, research, by another graduate student, is continuing in this areas at the University of California, Irvine.

6.2.4. E. coli Cell Immobilisation for Continuous-Flow Phage Propagation

As demonstrated in Chapter 4, phage-displayed antibody and peptide binders can be selected for continuous-flow processing when the antigen is immobilised on resin coating the inner surface of the tube. After elution of the antigen and the antigen-bound phage, the phage is propagated by infection of SS320 *E. coli* cells with then overnight culturing. This remains a major bottleneck of the selection process, therefore, continuous-flow propagation of selected phage could fast track the process, increasing the efficiency, and would be a step towards a fully continuous process.

The first step towards achieving continuous-flow phage propagation in the VFD is cell immobilisation. *E. coli* has been immobilisation onto supports including polyacrylamide, egg white, chitosan, calcium-alginate, polymer beads and sodium cellulose sulphate, for use in a glass packed bed reactor, for use in whole cell biocatalysis [7-11]. High capacity resins are currently being explored for coating of the VFD tube intended for enzyme immobilisation for biocatalysis, as has been reported with Ni-NTA affinity resin [12]. Further application of these resins was considered for cell immobilisation. Immobilisation of SS320 cells, a phage

propagating cell line, was briefly explored on different types of resins, including, styrene quaternary amine, epoxy methacrylate, and two amino C2 methacrylate resins of different pore sizes. All resins showed some level of immobilisation with the epoxy methacrylate resin displaying the highest immobilisation yields (Figure 6.3). These initial experiments await follow up testing viability and stability of the cells, in addition to suitability of the resin for use in the VFD. Other supports should be explored for use in the VFD, including the use of hydrogels. Once this is optimised, exploration into practically propagating cells in continuous-flow will be a reality.

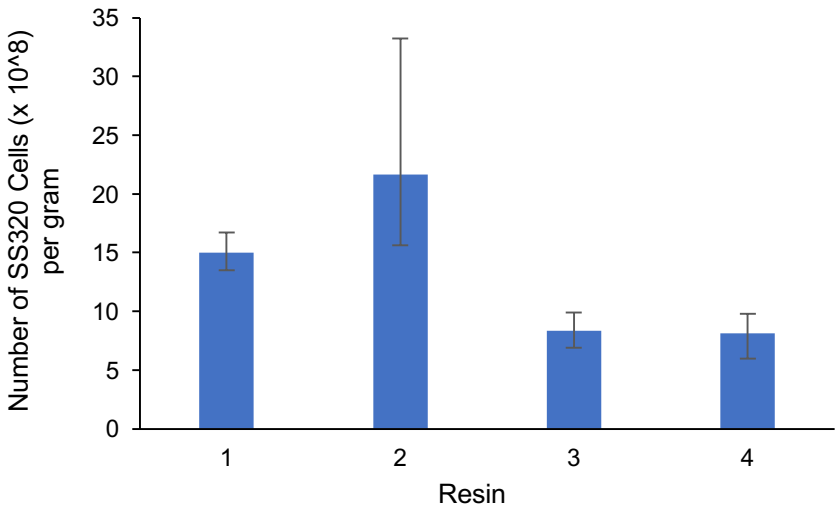

Figure 6.3. Immobilisation of SS320 *E. coli* cells on functionalised resin. Resin 1: styrene quaternary amine (Purolite, ECR1640), Resin 2: epoxy methacrylate (600-1200Å pore diameter, ECR8209F), Resin 3: amino C2 methacrylate (600-1200Å pore diameter, ECR8309), Resin 4: amino C2 methacrylate (1200-1800Å pore diameter, ECR8215). Number of cells was determined by measuring optical density at 600nm using a UV-Vis Spectrometer, where an absorbance of 1.0 = 8.0 x 10^8 cells/mL.

A future goal is to firstly have one VFD performing selections and then a second VFD containing immobilised SS320 for ready for infection with the eluted phage from the first device. This will be a major research initiative with several parameters requiring optimisation and refinement, as a major step towards a rapid, fully-continuous flow processing for finding valuable recognition elements and biotherapeutics.

6.2.5. Extracellular Protein Expression for Continuous-Flow Protein Production

Another potential application of immobilising bacterial cells in the VFD is continuous-flow protein expression. Potential benefits of protein expression in the VFD, beyond continuous production of proteins, is the high gas to liquid mass transfer creating an increased oxygen environment beneficial for cellular growth and expression. The fluid flow in the VFD could also increase diffusion of the protein from the cell membrane. However, one requirement in order to achieve continuous-flow protein expression, using immobilised cells, is that the protein needs to be secreted into the expression media for collection, which will be challenging. While cytoplasmic and periplasmic expression systems are well established, reports regarding protein secretion into the growth medium of *E. coli* remains minimal. Osmotically inducible protein Y (OsmY) is transported into the growth medium without affecting outer cell membrane integrity [13-15].

In this feasibility study, the extracellular expression of eGFP and AS in *E. coli* cells was explored. Firstly, the gene encoding of the OsmY fusion protein and a signal peptide (both amplified from the pCDB180 plasmid purchased from Addgene) was cloned into a pET28 construct, containing the gene encoding aristolochene synthase (AS), or green fluorescent protein (eGFP), using Gibson assembly. The constructs contain a N-terminal 6 x histidine tag of the target protein, after the OsmY fusion protein (Figure 6.4).

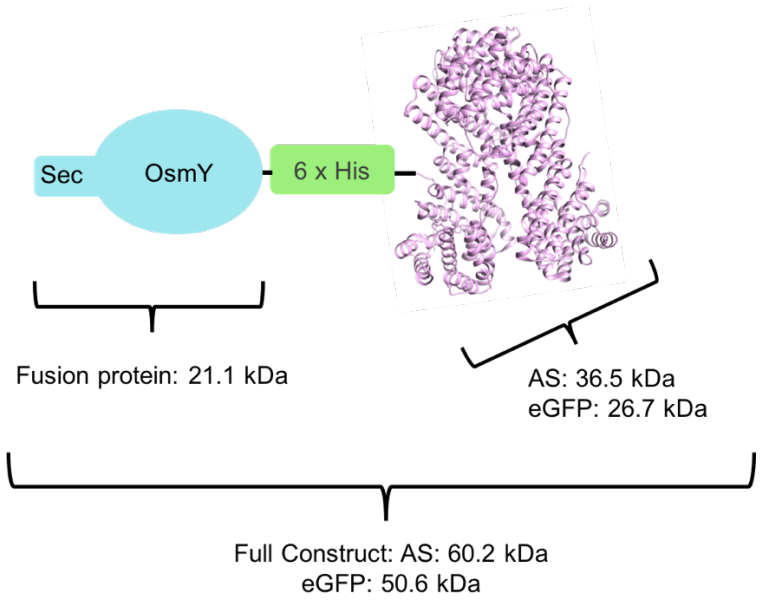

Figure 6.4. Schematic representation of the OsmY construct showing the target protein, AS, fused to a N-terminal 6 x his-tag, OsmY fusion protein, and signal peptide for secretion to the periplasm.

Extracellular expression of OsmY-eGFP and OsmY-AS was attempted in BL21(DE3) cells, at 25 and 30°C, respectively, in LB media. After 24h the cells and supernatant are separated and collected. The cells are lysed and the lysate analysed by SDS-PAGE (Figure 6.5). The supernatant is batch bound to charged Ni-NTA resin overnight and any protein purified by nickel affinity chromatography. All fractions are analysed by SDS-PAGE (Figure 6.5). Figure 7 shows no expression of OsmY-AS or AS in the supernatant or cell fraction. This construct appears to result in no AS expression, which is not seen in expression of AS without the OsmY gene present. Figure 6.7 shows high levels of OsmY-eGFP fusion in the cell pellet and lysate, and small amount present in the supernatant purification fraction 1.

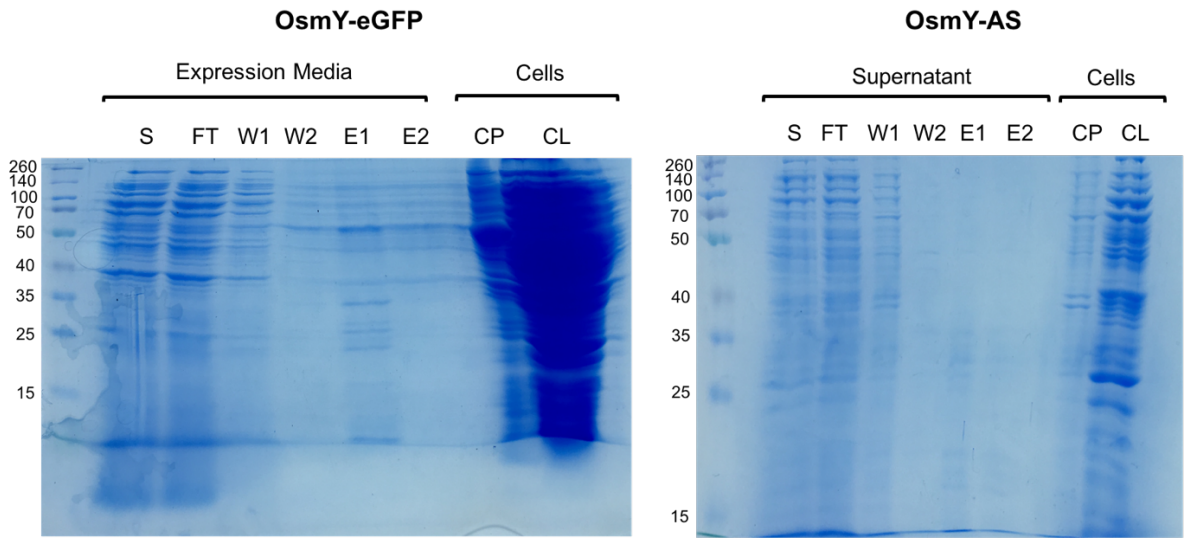

Figure 6.5. SDS-PAGE image of the purification of expression media and cell lysate of OsmY-eGFP construct (left) and OsmY-AS (right). In this 12% tris-glycene SDS-PAGE gel, each lane was loaded with 19µL of sample unless otherwise indicated. PageRuler pre-stained protein ladder (5µL, Thermo Fisher Scientific) was used. Lane S: expression media. Lane FT: flow through after batch binding the expression media to the resin. Lane W1: column wash with 50mL of buffer with 50 mM imidazole. Lane W2: column wash with 25mL of buffer with 100mM imidazole. Lane E1-2: DJ-1 eluted with buffer containing 250mM imidazole and collected as 2 x 15mL fractions. Lane CP: 1µL of insoluble pellet in 18µL of ddH_2O. Lane CL: soluble cell lysate. Buffer: 50mM Na_2HPO_4, 300mM NaCl, pH 8.0, 250mM imidazole, 10mM BME.

Although expression to the media was achieved, the level was small, as is observed for extracellular expression. In order to make it practical for use in continuous-flow (where the residency time is much lower compared to continuous flow) these levels need to be improved. Optimisation of the expression parameters, expression cell line, and methods to aid permeability without compromising cell viability or productivity are required [16-19]. The use

of the VFD for enhancing cell permeability has potential and is attractive for exploration. Initially, expression with the cells in solution should be explored, prior to immobilisation. It is hypothesised that the complex flow at certain rotational speeds in the VFD could increase diffusion of proteins through the cell membrane. This is currently being tested in the Raston research group.

6.2.6. Refolding Proteins Immobilised in the VFD

Overexpression of proteins in bacteria can often result in the formation of aggregates and inclusion bodies [20-22]. Recovery of correctly folded proteins from inclusion bodies can be laborious and expensive [23, 24]. Current methods for refolding proteins involves multi-day dialysis with larger volumes of buffer required (1-10 L for mg quantities of protein) [25]. The application of shear stress and unique fluid dynamics in the VFD has been previously reported for the in-solution refolding of four proteins, including hen egg white lysozyme (HEWL) and cAMP-dependant protein kinase A (PKA) [26, 27]. However, this method still requires a low concentration of protein in solution and the optimal parameters are dependent on the nature of the protein.

Proteins immobilisation has been demonstrated on to Ni-affinity resin immobilised on the VFD for protein purification, biocatalysis [12], and phage selections (as demonstrated in Chapter 4). It was hypothesised that this method could be applied for immobilising denatured proteins in the VFD for continuous refolding. Refolding in packed bed chromatographic columns has previously been developed and has several advantages over conventional dilution and dialysis [24]. Refolding immobilised proteins allows for a higher amount of protein, and allows for spatial segregation which can increase stability and avoid intermolecular interactions. Elution of the refolded protein also results a higher the use of a concentration of

protein then for using conventional methods, which reduces laborious concentrating requirements post-processing. However, any industrial application is limited due to the high processing cost. Combining the benefits of immobilisation of proteins with the unique fluid flow in thin-films in the VFD has potential for improving the quality, scale up, and economics of the refolding process.

In this feasibility study, refolding of nuclear matrix protein 22 (NMP22), conjugated to Ni-MIDA resin through a fused histidine tag, was attempted in the VFD (Figure 6.6). As discussed in Chapter 4, NMP22 is a bladder cancer biomarker which expresses in high amounts as insoluble inclusion bodies. NMP22 was overexpressed in BL21 (DE3) cells (See Chapter 4.8) and extracted from the insoluble cell pellet by denaturing in urea-phosphate buffer (8M Urea, 40mM sodium diphosphate, 250mM NaCl, pH = 8.0). The denatured NMP22 was purified using Ni-affinity chromatography, using urea buffers for decreasing pH. Purified and denatured NMP22 (2mg, urea buffer, pH=8.0) was batch bound to Ni-NIDA (4g) overnight. The resulting resin was used to coat a VFD tube (See Chapter 4.5.2).

Prior to refolding, urea-phosphate buffer (25mL) was fed through the VFD tube (4.0k rpm, 2.0mL/min, 45° tilt angle) to ensure all protein is denatured following immobilisation. Chilled refolding buffer (100mL, 200mM arginine, 150mM Tris-HCl, 0.2mM oxidated glutathione, 2mM reduced glutathione, 10% glycerol, pH = 7.5) was then fed through the VFD tube at 0.2mL/min. A buffer exchange was achieved by feeding PBS buffer (pH 8.0, 50mL) at 1.0mL/min, followed by elution of NMP22 by feeding 500mM imidazole in PBS buffer (40mL, pH = 8.0). The elution fractions (4 x 10mL) were sterile filtered (0.22μm) to remove aggregated, insoluble NMP22, and analysed using SDS-PAGE (Figure 6.7).

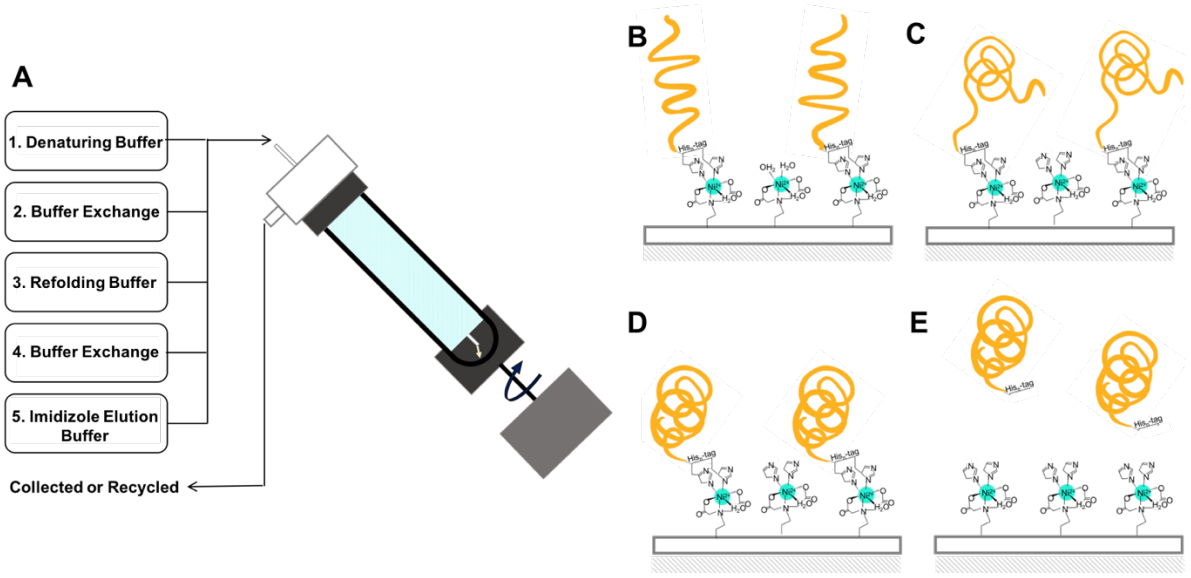

Figure 6.6. Schematic representation of the proposed refolding of proteins immobilised on Ni-MIDA resin in the VFD. For thin-film continuous flow refolding, all buffer solutions are fed into the reactor via a peristaltic pump (A). The protein is denatured when immobilised on Ni-MIDA resin in the VFD (B). A refolding buffer is fed through the VFD (C and D). The buffer is then exchanged with the collection buffer (no imidizole). The protein is then eluted from the VFD using a high concentration of imidizole (E).

The SDS-PAGE gel shows NMP22 in all four fractions, indicating there is soluble protein present in solution. This would suggests that the NMP22 was successfully folded, as denatured or misfolded protein tends to be precipitation and aggregate in PBS buffer. NMP22 remained in solution for several hours on ice, however, when stored at 4°C, precipitation occurred overnight. This could result from the protein being unstable in PBS buffer, and/or that it was only partially folded when eluted from the VFD. Several buffers were explored for buffer exchange and elution, however, the eluted NMP22 was only stable in buffers containing arginine. This indicates the protein was not completely folded. Circular dichroism (CD) was

attempted but was not successful due to the difficulty in finding a CD compatible buffer in which the protein was stable.

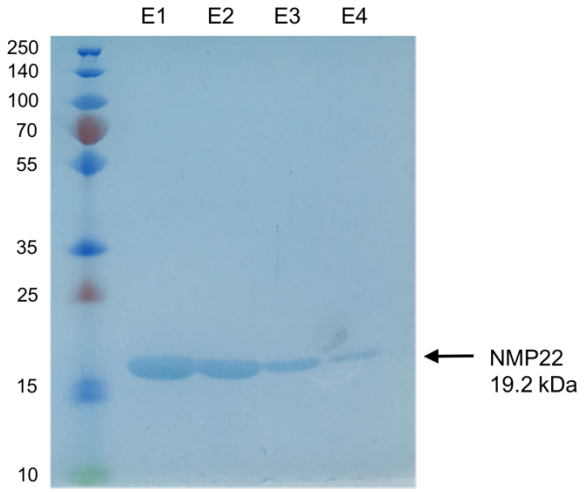

Figure 6.7. SDS-PAGE gel of NMP22 elution fractions from the VFD after attempted refolding. In this 12% tris-glycene SDS-PAGE gel, each lane was loaded with 19µL of sample unless otherwise indicated. PageRuler pre-stained protein ladder (10µL, Thermo Fisher Scientific) was used. Lane E1-4: NMP22 eluted from the VFD with buffer containing 250mM imidazole (50mM Na_2HPO_4, 300 mM NaCl, pH 8.0, 250 mM imidazole, 10mM BME) and collected as 4 x 10mL fractions, using a flow rate of 2.0mL/min.

Future direction should explore varying parameters of the VFD process to achieve complete refolding. This includes varying the refolding buffer, using a gradient, and varying the amount of protein immobilised and the amount of resin. Furthermore, a protein with a simple activity assay should be explored, as a proof of concept, for easier assessment of refolding. Using an activity assay for assessing refolding is potential higher throughput, compared to using CD, which can require difficult optimisation to find a CD compatible buffer and concentration which the protein is also stable in.

In summary, this dissertation has established novel approaches for catalysis and biotechnology in continuous-flow, which have potential for use in different applications. Nevertheless, there are still major research efforts required, in advancing the science further, with new challenging and exciting discoveries awaiting, associated with using the now understood complex fluid dynamics within the VFD.

6.3 Acknowledgments

I would like to acknowledge Dr. Rhys Murphy, Dr. Tamim Darwish and ANSTO for the opportunity to visit the National Deuteration Facility and their support in conducting the research presented here. I would also like to acknowledge Prof. Gregory Weiss for the opportunity to visit his laboratory at the University of California, Irvine and Dr. Sudipta Mujamdar for his guidance.

6.4 References

[1] Atzrodt, J., Derdau, V., Fey, T., Zimmermann, J. The Renaissance of H/D Exchange. *Angew. Chem. Int. Ed*., **2007**, *46*, 7744-7765.

[2] Esaki, H., Aoki, F., Umemura, M., Kato, M., Maegawa, T., Monguchi, Y., Sajiki, H. Efficient H/D Exchange Reactions of Alkyl-Substituted Benzene Derivatives by Means of the Pd/C–H_2–D_2O System. *Chem. Eur. J.*, 2007, *13*, 4052-4063.

[3] Phillips, J. M., Ahamed, M., Duan, X. F., Lamb, R. N., Qu, X., Zheng, K., Zou, J., Chalker, J. M., Raston, C. L. Chemoselective and continuous flow hydrogenation in thin films using a palladium nanoparticle catalyst embedded in cellulose paper. *ACS App. Bio Mat*. **2019**, *2*, 488-494

[4] Wiseman, T., Williston, S., Brandts, J. F., Lin, L. N. Rapid measurement of binding constants and heats of binding using a new titration calorimeter. *Anal. Biochem.* **1989**, *179*, 131–137.

[5] Freire, E., Schon, A., Velazquez-Campoy, A. Isothermal titration calorimetry: general formalism using binding polynomials. *Methods Enzymol*. **2009**, *455*, 127–155.

[6] Kumaraswamy, S., Tobias, R. Label-free kinetic analysis of an antibody-antigen interaction using biolayer interferometry. *Methods Mol Biol.* **2015***, 1278,* 165-182.

[7] Schiraldi, C., Di Lernia, I., Giuliano, M., Generoso, M., D'Agostino, A., De Rosa, M. Evaluation of a high temperature immobilised enzyme reactor for production of non-reducing oligosaccharides. *J. Ind. Microbiol. Biotechnol*., **2003**, *30*, 302–307.

[8] Matsuda, T., Watanabe, K., Kamitanaka, T., Harada, T., Nakamura, K. Biocatalytic reduction of ketones by a semi-continuous flow process using supercritical carbon dioxide. *Chem. Commun*., **2003**, 1198–1199,

[9] Tan, A. W. I., Fischbach, M., Huebner, H., Buchholz, R., Hummel, W., Daussmann, T., Wandrey, C., Liese, A. Synthesis of enantiopure (5*R*)-hydroxyhexane-2-one with immobilised whole cells of *Lactobacillus kefiri. Appl. Microbiol. Biotechnol*., **2006**, *71*, 289–293.

[10] Zajkoska, P., Rebroš, M., Rosenberg, M. Biocatalysis with immobilized Escherichia coli. *Appl. Microbiol. Biotechnol*. **2013**, *97*, 1441–1455.

[11] Syga, L., Spakman, D., Punter, C. M., Poolman, B. Method for immobilization of living and synthetic cells for high resolution imaging and single particle tracking. *Nat. Sci. Rep*. **2018**, *8*, 13789.

[12] Britton, J., Dyer, R. P., Majumdar, S., Raston, C. L., Weiss, G. A. Ten-Minute Protein Purification and Surface Tethering for Continuous-Flow Biocatalysis. *Angew. Chem. Int. Ed*. **2017**, *56*, 2296-2301.

[13] Kotzsch, A., Vernet, E., Hammarström, M., Berthelsen, J., Weigelt, J., Gräslund, S., Sundström, M. A secretory system for bacterial production of high-profile protein targets, *Prot. Sci*. **2010**, *20*, 597-609.

[14] Qian, Z. G., Xia, X. X., Choi, J. H., Lee, S. Y. Proteome-Based Identification of Fusion Partner for High-Level Extracellular Production of Recombinant Proteins in Escherichia coli. *Biotechnol. Bioeng*, **2008**, *101*, 587-601.

[15] Gupta, S., Adlakha, N., Yazdani, S. S. Efficient extracellular secretion of an endoglucanase and a β-glucosidase in E. coli. *Protein Expr. Purif*. **2013**, *88*, 20-25.

[16] Le, Y., Wang, H. High-level soluble expression of a thermostable xylanase from thermophilic fungus Thermomyces lanuginosus in Escherichia coli via fusion with OsmY protein. *Protein Expr. Purif*. **2014**, *99*, 1-5.

[17] Chen, R. R. Permeability issues in whole-cell bioprocesses and cellular membrane engineering. *Appl. Microbiol. Biotechnol.* **2007**, *74*, 730–738.

[18] Perez-Pardo, M. A., Ali, S., Balasundaram, B., Mannall, G. J., Baganz, F., Bracewell D. G. Assessment of the Manufacturability of Escherichia coli High Cell Density Fermentations. *Biotechnol. Prog.,* **2011**, *27*, 1488-1496.

[19] Patel, T. M., Park, A. A. Banta, S. Genetic Manipulation of Outer Membrane Permeability: Generating Porous Heterogeneous Catalyst Analogs in Escherichia coli. *ACS Synth. Biol*. **2014**, *3*, 848-854.

[20] Williams, D. C., Van Frank, R. M., Muth, W. L., Burnett, J. P. Cytoplasmic inclusion bodies in Escherichia coli producing biosynthetic human insulin proteins. *Science*, **1982**, *215*, 687–689.

[21] Freedman, R. B., Wetzel R. Protein engineering. *Curr. Opin. Biotechnol*. **1992**, *3*, 323–325.

[22] Chrunyk, B.A., Evans, J., Lillquist, J., Young, P., Wetzel, R. Inclusion body formation and protein stability in sequence variants of interleukin-1 beta. *J. Biol. Chem*. **1993**, *268*, 18053–18061.

[23] Vallejo, L. F., Rinas, U. Strategies for the recovery of active proteins through refolding of bacterial inclusion body proteins. *Microb. Cell Fact.* **2004**, *3*, 11, 1-12.

[24] Singh, A., Upadhyay, V., Upadhyay, A. K., Singh, S. M., Panda, A. K. Protein recovery from inclusion bodies of Escherichia coli using mild solubilization process. *Microb. Cell Fact.* **2015**, *14*, 41, 1-10.

[25] Tsumoto, K., Ejima, D., Kumagai, I., Arakawa, T. Practical considerations in refolding proteins from inclusion bodies. Protein Expression Purif. **2003**, *28*, 1–8.

[26] Yuan, T. Z., Ormonde, C. F. G., Kudlacek, S. T., Kunche, S., Smith, J. N., Brown, W. A., Pugliese, K. M., Olsen, T. J., Iftikhar, M., Raston, C. L., Weiss, G. A. Shear stress-mediated refolding of proteins from aggregates and inclusion bodies. *ChemBioChem*. **2015**, *16,* 393-396.

[27] Britton, J., Smith, J. N., Raston, C. L., Weiss, G. A. Protein folding using a vortex fluidic device. *Methods Mol. Biol.* **2017,** *1586*, 211-220.

6.5. Supporting Information

6.5.1. E. coli Cell Immobilisation for Continuous-Flow Phage Propagation

An aliquot of SS320 cells were streaked onto an agar plate supplemented with 15μg/mL tetracycline and incubated at 37°C for 12h. A single colony was used to inoculate 30mL of LB media supplemented with 15μg/mL tetracycline and grown at 37°C for 18h. The culture is centrifuged at 1450g and resuspended in PBS buffer (pH 7.2). The culture was diluted 1 in 12 prior to measuring optical density at 600nm.

Each resin (1.0g) was washed, with vortexing (as a distinctly different process to use of the VFD), with 2mL of ddH_2O three times. Resins 3 and 4 were functionalised with 2.5% glutaraldehyde (final concentration of 2.0%) and shaken at 25°C for 1 hour. These resins were washed, with vortexing, with 2mL of PBS buffer (pH 7.0) three times. To each resin suspended in 1mL of buffer, 2mL of the SS320 cells suspension, described above, was added. A control solution of 2mL cells suspension and 1mL buffer was used. Each cell-resin suspension was slowly stirred at 4°C for 18h. The cell suspensions (2mL) are removed and OD_{600} measured. The resins were washed with 2mL of buffer, vortexed, and the solution removed and OD_{600} measured. This was repeated two more times. The amount of SS320 cells immobilised was determined by calculating the difference between the amount of cells in the starting solution and the amount of cells removed and washed from the resins, where 1.0 = 8.0 x 10^8 cells/mL. No change in the negative control was observed. This protocol was performed in triplicate (Figure 6.5).

6.5.2. Extracellular Protein Expression for Continuous-Flow Protein Production

Construction of OsmY-eGFP and OsmY-AS pET28 Expression Construct:

The gene encoding for OsmY was cloned from the pCDB180 vector and into a pET28 vector containing the gene encoding AS or eGFP using Gibson Assembly. The following PCR parameters and oligonucleotides (integrated DNA Technologies) were used to amplify the OsmY gene with overhangs complimentary to the pET28 vectors. PCR reaction mixture (25μL) contains Herculase ii DNA polymerase (New England Biolabs), following the manufacturer's instructions, and buffer (5× diluted final concentration, New England Biolabs), dNTPs (0.5mM each final concentration, New England Biolabs), primers (33ng each final concentration, Integrated DNA Technologies), and AS pET28 (50ng) vector as the template DNA. PCR reaction was as follows: one cycle at 95°C for five min, 25 cycles at 95°C for one min, 50°C for one min, 72°C for three min, and one cycle at 72°C for five min. The below primers were used.

Forward: 5'- CTTTAAGAAGGAGATATACCATGACTATGACAAGACTGAAG -3'. Reverse: 5'- GATGATGATGCATGTGTGCGCTCTTAGTTTTCAGATCATTTTTAACGC-3'. The pET28 vector backbone, containing the protein to be expressed, was cloned using an annealing temperature of 50 °C. The below primers were used.

Forward: 5'- CTGAAAACTAAGAGCGCACACATGCATCATCATCATCATCACG -3'. Reverse: 5'- CAGTCTTGTCATAGTCATGGTATATCTCCTTCTTAAAG -3'.

The PCR products were extracted from a 1% agarose gel using a Zymoclean Gel DNA Recovery Kit. The following Gibson Assembly reaction mixture was used: 10 ng of Fab PCR

product, 10 ng of pET28 PCR product, 2μL of NEBuilder ® HiFi DNA Assembly Master Mix (NEB), and autoclaved ddH2O to a total volume of 4μL. The reaction mixture was incubated at 50°C for 1h, and stored at 4°C. The reaction product was transformed into *E. coli* Nova blue cells and plated on an agar plate supplemented with kanamycin (40μg/mL), followed by incubation at 37°C for 18h. A single colony is used to inoculate 5 mL of 2YT supplemented with kanamycin (40μg/mL), and grown at 37 °C for 18h. The DNA plasmid is isolated, purified and sequenced by Genewiz.

Expression and Purification:

The below protocol was used for the expression of OsmY-eGFP and OsmY-AS in *E. coli*. The OsmY-eGFP or OsmY-AS pET28 constructs were transformed *via* heat shock into *E.coli* BL21 (DE3) cells and transferred to a LB agar plate containing 40 μg/mL of kanamycin, and incubated at 37°C for 14h. A seed culture was prepared by inoculating a single colony into 25mL of LB media with 40μg/mL of kanamycin and shaken (220 rpm) in a 125mL baffled flask at 37°C for 14h. The expression culture was prepared by inoculating 125mL of LB media with 40μg/mL of kanamycin with 1.5mL of seed culture into and shaking at 220rpm at 37°C in 500mL baffled flask. When the culture reached an OD_{600} of 0.6-0.7 the cells were induced with 0.5mM IPTG. The induced expression culture was incubated by shaking at 220rpm for 24 h at 25 or 30°C. The cells and expression media were separated and collected by centrifugation. The cells were resuspended and sonication in 25mL lysis buffer (50mM Na_2HPO_4, 300mM NaCl, 10mM imidazole, pH 8.0, 10mM BME, 100μL HALT protease inhibitor). The expression media was purified using nickel affinity chromatography using a gravity column containing charged (with 100mM $NiSO_4$) and equilibrated IMAC resin (2g, Purolite). The

following buffers were used to purify: lysis buffer (50mL), wash buffer (50mM Na_2HPO_4, 300mM NaCl, pH 8.0, 40mM imidazole, 10mM BME), and elution buffer (60mL collected as three fractions, 50mM Na_2HPO_4, 300mM NaCl, 250mM imidazole, pH 8.0, 10mM BME). Fractions containing purified protein, identified by SDS-PAGE (Figure 6.7).